ELECTROCHEMICAL STUDIES OF SELF-ASSEMBLED MONOLAYER USING SMALL AROMATIC DISULFIDES AND THIOLS ON POLYCRYSTALLINE GOLD, SILVER AND COPPER SURFACES

A THESIS

SUBMITTED TO THE

UNIVERSITY OF POONA

FOR THE DEGREE OF

DOCTOR OF PHILOSOPHY

IN

CHEMISTRY

BY

KRISANU BANDYOPADHYAY

Physical and Materials Chemistry Division

National Chemical Laboratory

Pune - 411 008

June 1998

DEDICATED TO MA AND BABA

DECLARATION

I hereby declare that the thesis entitled "**Electrochemical Studies of Self-assembled Monolayer using Small Aromatic Disulfides and Thiols on Polycrystalline Gold, Silver and Copper Surfaces**" submitted for Ph. D. degree to the University of Poona has been carried out at National Chemical Laboratory, under the supervision of Dr. K. Vijayamohanan. The work is original and has not been submitted in part or full by me for any degree or diploma to this or any other University.

Krisanu Bandyopadhyay

Date: 2.6.98

(Krisanu Bandyopadhyay)

Physical and Materials Chemistry Division
National Chemical Laboratory
Pune-411 008.

NCL

Dr. K. Vijayamohanan
Scientist

Physical & Materials Chemistry Division
National Chemical Laboratory
Pune - 411 008. INDIA
Phone: (0212)-336451 Extn: 2270
Res: (0212)-234307
Fax: (0212)-337044
Email: viji@ems.ncl.res.in

CERTIFICATE

This is to certify that the work incorporated in the thesis entitled "**Electrochemical Studies of Self-assembled Monolayer using Small Aromatic Disulfides and Thiols on Polycrystalline Gold, Silver and Copper Surfaces**" submitted by Krisanu Bandyopadhyay was carried out by him under my supervision at the National Chemical Laboratory, Pune. Material that has been obtained from other sources is duly acknowledged in the thesis.

2 June 1998
Date

(K. Vijayamohanan)
Research Guide

ACKNOWLEDGMENT

I take this opportunity to express a deep sense of gratitude to my mentor ***Dr. K. Vijayamohanan*** for introducing me to the fascinating area of Self-assembled monolayers. His competent guidance, stimulus, continuous encouragement and constructive criticism not only motivated me but also instilled a sense of confidence in me. The work presented in this thesis would not have been accomplished without his unfailing attention and relentless adherence to the finer scientific strictures.

I would like to express my profound gratitude to Dr. P. Ganguly, head, Physical and Material Chemistry Division, for his constant encouragement throughout the study. I would also like to acknowledge my deepest gratitude to Dr. B. D. Kulkarni, Dr. Murali Shastry and Dr. T. Pradeep for providing me valuable guidance at different stages of the work.

I am deeply indebted to Dr. Anil Kumar for his immense patience in listening to my problems and for being a constant source of encouragement. I would also like to thank Dr. P. A. Joy, Dr. K. Sreedhar, Dr. I. S. Mulla and Dr. Amitabha Sarkar for their stimulating discussions.

The warm and friendly atmosphere created by my colleagues Dr. M. P. Vinod, Varsha, Dr. Sushma Pethkar, Dr. Rahul Patil, Aslam, Wahida is greatly appreciated. They made working in the lab enjoyable. I specially thank Vinod for his various help and encouragement in the difficult times.

I would also like to thank Souravda, Sanjoyda, Debasishda, Sukhenda, Sanjibda, Soumenda (SS and Hz), Tapanda, Tomalda, Manasda, Bishuda, Rashidulda, Dipakda, Partha, Tanya, Bindu, Subarna, Sunil, Anil, Surojit, Radha, Rajesh, Swamy, Sachin, Jayaprakash, Mahua, Priyo, Raja, Bikash, Anjan, Subho, Saptarshi, Aditya, Debasish (Hz), Maji, Laha, Manna, Karuna and all friends in NCL campus and OLD and NEW HOSTEL for making my stay in Pune memorable.

I would like to record my special appreciation for the cheerful company of my old friends, Shruti and Sundar.

Thanks are also due to Koshi, Daore, Punekar for their day to day help in laboratory and office work.

Help from Dr. Sainkar and Dr. (Mrs.) Mitra in taking SEM and XRD Measurements is gratefully acknowledged.

Finally, I would like to thank the Director, NCL, for providing infrastructural facilities and permitting me to present this work in the form of a thesis. I am thankful to UGC, New Delhi for financial assistance.

I am at a loss of words in acknowledging my parents and all members of my family and inlaws for providing me immense support, believing and

understanding me and the pride they took in my achievements. I would specially like to thank ma and baba for making me what I am today.

Last but not the least, I would like to thank my wife and best friend Debu, for being there always by my side. Without her I would not have been able to achieve anything. Her optimistic approach and the confidence she had in my ability was a constant source of courage and support. Thank you Debu, for everything.

Krisanu Bandyopadhyay.

Contents

Chapter 1

Introduction

This introductory chapter discusses an overview of the area of self-assembled monolayer (SAM) of alkanethiols/disulfides on gold, silver and copper surfaces. This chapter also gives the major objectives and overall organization of the present investigation.

1.1. Importance of Ultrathin Organic Films:

Preparation and characterization of ordered ultrathin organic films of molecular level thickness (few nm to several hundred nm) has recently attracted considerable interest for its technological and fundamental significance. For example, the possibility of controlling order at the molecular level has triggered several innovative applications ranging from molecular electronics to tribology.[1] Similarly, the unique ability of these monolayers to serve as a precision spacer between the electrodes and a redox couple (either attached or freely diffusing) has been utilized to unravel several fundamental questions related to long-range electron-transfer in biological systems including the predictions of Marcus model of electron transfer.[2] In addition, the similarities of these ultrathin films with lipid bilayer membranes have encouraged the application of these dimensional (2-D) structure as model systems to investigate a host of biological processes such as bioenergetics of photosynthesis and protein adsorption.[3]

Ultrathin organic films on different surface are generally formed by either a forced interfacial transfer of floating organic molecules on an air-liquid interface (Langmuir-Blodgett-LB) or by the spontaneous adsorption of molecules from solution (self-assembled monolayer-SAM). In the former technique, long chain amphiphilic molecules are forced to order on a liquid subphase by slowly increasing the surface pressure and then transferring these monolayers to a solid substrate, often several times to form multilayers of ultrathin organic films. In contrast, the latter technique involves the spontaneous adsorption of some multifunctional molecules from aqueous or nonaqueous solutions on few selected surfaces. Organic thin films prepared by both these techniques have shown considerable technological promise during the last few years. The relative advantages and disadvantages of these two principle methods are briefly summarized in Table 1.1.

1.2. Self-Assembled Monolayer (SAM):

The term 'self-assembly' involves the arrangement of atoms, molecules or even aggregate of molecules into ordered functional entities without the intervention of man-kind towards an energetically stable form.[4] Formation of self-assembled monolayer

Table 1.1.

Comparison of Self-Assembly and Langmuir-Blodgett Techniques for the Formation of Ultrathin Organic Films

Features	Self-Assembly Technique	LB-Technique
(1) Formation process	Simple, near equilibrium procedure.	Nonequilibrium procedure.
(2) Driving force	Strong and specific chemisorption between an adsorbate and a substrate.	Physisorption (either van der Waals or hydrogen bonding).
(3) Types of ordering	Precise molecular control at the solid/liquid interface.	Precise molecular control at the liquid/air interface.
(4) Thermal and chemical stability	Better thermal, physical and mechanical stability.	Less thermal stability; Structural changes during the transfer process.
(5) Selection of molecules	Wide range of organic species can be incorporated.	Restricted to long chain amphiphiles; difficult to generate surface exposing polar functional groups.
(6) Substrate	Only selected surfaces.	Any substrate can be used.
(7) Film formation control	Kinetics of monolayer formation is important.	Transfer process is important.
(8) Molecular arrangement	Molecules are organized during monolayer formation.	Molecules are preorganized at liquid/air interface before transfer.
(9) Solubility restriction	Restricted by solubility of the molecules.	No such solubility restriction.
(10) Types of molecules	Specific functional group required.	Any amphiphilic molecule.

(SAM) is essentially an organization of molecules at the solid-liquid interface induced by strong chemisorption between the substrate and the head group. The main objective is to attain the capability of assembling individual molecules into highly ordered architectures for obtaining a desired function.

The apparent origin of self-assembled monolayers can be attributed to Zisman's[5] work in 1946, where he prepared monomolecular layer of a surfactant by adsorption onto a clean metal surface but the primary emphasis was on the relationship between wetting angle and molecular structure. This was followed by a few isolated studies about the chemisorption of similar molecules on different metal surface until 1983, when Nuzzo and Allara[6] showed that organosulfur compounds like dialkyl disulfides (RS-SR) can form oriented and highly ordered monolayers on gold surfaces from dilute solutions. Followed by this discovery, it was found that, sulfur compounds like long chain alkane thiols can also form highly organized assemblies on gold surface. Since then, a large number of substrates and organic molecules have been investigated although monolayers of long chain alkane thiolates[7] and disulfides[8] on noble metal surfaces constitute one of the most well studied and thoroughly characterized system.

1.3. Classification of SAM:

Depending on the functional groups and substrates, several molecules can form SAM and typical examples are illustrated in Table 1.2. Accordingly, different classification schemes are possible on the basis of both molecules and substrates. The simplest type is on the basis of nature of bonding of the headgroup to the surface as illustrated by the strong chemisorption of RSH on Au on one hand and alkyltrichlorosilane on hydroxylated surface via long range force (i.e. physisorption)[11] on the other hand. Depending on the nature of organic molecules, we can classify these as monolayers of fatty acids, monolayer of organosulfur derivatives, monolayer of all organic adsorbates, multilayer of diphosphonate, monolayer of bifunctional molecules etc. From an electrochemistry perspective, SAM can be classified into two types: the redox inactive SAM (e.g. RSH on Au) and the redox active SAM (e.g. pendent redox group containing organo sulfur compound on Au). Further classifications are also

Table 1.2.

Different Substrates and Molecules generally used for SAM Formation

Molecule	Substrate used for SAM	References
Thiols, Sulfides, Disulfides	Gold (polycrystalline, single crystal or colloidal gold particles), Copper, Silver, Platinum, Mercury, Iron, Nanosized γ-Fe_2O_3 particles, InP and high temperature super conductor surfaces	9
Alkane selenols and diselenides	Gold	9p,q
Carboxylic acids	Metal oxides like Al_2O_3 and Ag_2O	10
Alkylchlorosilanes, Alkylalkoxysilanes, Alkylaminosilanes	Oxide surfaces, Glass, Mica, Zinc selenide, gold, Pt, Ge, HOPG	11
Alkyl amines	High temperature super conductor surfaces	12
Phosphine, Isonitriles, Phosphonates	Gold, Metal-phosphonate surface	13
Thiols	GaAs, CdSe , CdS	14
Olefins, and Isonitriles	Platinum surface, graphite	15

possible on the basis of substrates (metal or semiconductor), structure of substrates (single crystal or polycrystalline), orientation of the substrates and functional groups. Most of the classifications are not rigid as the primary objective is the convenience of grouping together few systems for structural investigation.

The chemisorbed SAM can further be divided into two forms depending on whether a superlattice is formed on the surface (alkanethiolates on Au surface)[7] or not. In the covalent type, extensive chemisorption driven reconstruction on the surface can occur as observed for alkanethiol adsorption on Ag surface.[14d] Ionic form of bonding can occur in the chemisorption of carboxylic acids on basic oxide surfaces[10] where carboxylate ion salt is formed.

1.4. Preparation of Self-Assembled Monolayer:

The spontaneous adsorption of the molecules on a clean substrate can be achieved in two different ways as discussed below:

1.4.1. Solution State:

The most convenient and extensively used SAM preparation methodology is from solution. In a typical formation procedure, substrates are immersed in a milimolar solution of the desired molecule in a solvent such as ethanol, n-hexane etc. based on its solubility. The time of monolayer formation varies from several minutes to hours depending on the system under study. The longer incubation period generally allows the molecular film to assemble in a crystalline-like solid phase and also provides the possibility for the desorption of physisorbed and chemisorbed contaminants from the gold surface into the solution. The substrates are taken out from the solution, washed several times with the same solvent and then dried; sometimes annealing is conducted to get better organization.

Another method of SAM formation is to use the electric field to help monolayer formation.[16] For example, SAM has been formed from a millimolar solution of thiol dissolved in 0.5 M ethanolic KOH under potential control where equilibrium monolayer forms by holding the applied voltage at an appropriate potential. Nevertheless, the structural and interfacial properties are similar to those of usual SAM from solution phase without the application of any external field.

1.4.2. Vapor Phase:

Unlike the above case where, the solvent plays an important role, the preparation and characterization of SAM in vapor phase has been reported only in rare cases. For example Crooks group[17] has prepared by passing a 10% saturated n-alkanethiol vapor (mixed with N_2) over the Au (111) substrate for several hours at a low flow rate (0.5 L/min) and the comparison with SAM from solution indicates similar structures and packing densities. Nevertheless, these vapor phase deposited SAMs are poor mass-

transfer barriers than that from solution phase, especially when the molecule contains a long hydrocarbon chain.

1.5. Important Parameters Affecting SAM Formation:

1.5.1. Effect of Substrate:

Substrate plays a crucial role in the formation of a monolayer. In most cases, evaporated gold film [(111) crystallographic orientation] on glass, mica or single crystal silicon are used with a buffer coating of chromium or titanium for better adhesion. Gold is mostly used for SAM formation due to its reasonable inertness in ambient conditions compared to copper and silver, so that manipulation can be possible with lesser contamination. The ability of Au, Ag and Cu to chemisorb thiol/disulfide may be explained on the basis of their general nobleness, reactivity and the interaction of s-state of the adsorbate with the metal d-state. For example, self-consistent density functional calculation of hydrogen-metal surface interactions clearly illustrate that the antibonding states just above *d* band are especially filled for these metals.[18]

Generally, a gold surface is hydrophilic in high vacuum preparation chamber,[19] although, it can strongly adsorb organic molecules from air as well as from solutions to render the surface permanently hydrophobic.[19] Moreover, it is known that, gold does not have stable oxide on the surface[20] so that surface can be cleaned simply by removing the physically and chemically adsorbed contaminants. Substrate cleanliness, structure and orientation of the gold surface has significant influence on monolayer formation along with the nature of the cleaning procedure.[21] Nevertheless, extensive cleaning with sulfochromic acid for long time may generate oxides species and cathodic pretreatments may be necessary to eliminate these oxides species.[22]

The other metals like silver and copper used for self-assembly are more reactive and hence prone to easy oxidation in air. Similarly, prolonged immersion of Ag and Cu substrates in alkanethiol solution leads to the formation of interfacial metal sulfides which can adversely influence the monolayer structure and quality.[23]

1.5.2. Effect of Solvent:

In most of the preparation procedures of SAM, ethanol is used as the preferred solvent perhaps, due to low cost, low toxicity, easy availability in high purity and low tendency to be incorporated into the monolayer. Other solvents like, heptane,[21] acetonitrile,[24] cyclohexane,[25] n-hexane,[25] and dimethyl formamide[24] are also used occasionally considering the solubilities of the compounds. The work of Bain *et. al.*[7d] has compared the influence of solvent on SAM formation by taking a mixture of $HS(CH_2)_{10}OH$ and $HS(CH_2)_{10}CH_3$ in protic (ethanol), aprotic (acetonitrile) and nonpolar (isooctane) solvents, and the composition and structure of monolayer is found to changed significantly. The structure of the monolayer-liquid interface is controlled by the intermolecular bonding. (e.g. hydrogen bonding with solvent and terminal -OH group of tail) and hydrophobicity of the solvent. Different investigations show that solvent trapping can occur during monolayer formation in certain specific cases,[7b] while it is absent for the other cases.[7d] It is suggested that, solvent incorporation can be possible if there is a geometrical matching of the solvent and component of the film, or some specific interactions like hydrogen bonding are present between the tail groups and the solvent, and the extent of solvent trapping is been found to vary drastically with the nature of the solvent.[7d] Moreover, solvents can play a crucial role in governing the kinetics of formation.[26] Solvents with poor solubility property provides strong driving force for adsorption and the resultant monolayer is likely to be composed of both physisorbed and chemisorbed material.[27] It has been demonstrated that a better solvent for the adsorbate can lead to a SAM with higher density of defect sites which is exemplified by the fact that the monolayer from dichloromethane contains more defects than that from ethanol.[28] Moreover, the hydrophobicity of the solvent dictates the stability of n-alkanethiolate monolayer on Ag(111).[29] Dielectric constant, viscosity etc. may play an important role but more studies are needed to understand the role of solvent in SAM formation.

1.5.3. Nature of the Molecules:

Alkyl chain plays a key role in the formation of SAMs as long chain alkanethiols are adsorbed preferably over the short chains ones[7a] and, the change in chain length is

expected to affect the kinetics as well as the quality of monolayer. Investigations related to the effect of chain length on monolayer properties for a series of n-alkane thiols show that for long-chain thiols monolayers are arranged in a crystalline like environment and as chain length decreases, the intrachain as well as the interchain interaction energy decreases.[7b] In effect, the coverage decreases, and molecules residing on low energy surface sites are likely to be thermally desorbed. Heterogeneous electron transfer at the monolayer modified electrode shows that current decreases rapidly with chain length as expected for nonadiabatic electron transfer.[7f] Other than long chain alkane thiols, rigid rod like,[30] conjugated,[31] and purely aromatic thiols[32] have also been employed for SAM formation. Although a high density of packing is observed for these molecules, the packing density as well as the rate of formation of SAM is slower compared to n-alkanethiols.[30a]

1.5.4. Concentration:

Most of the studies indicate that, for the formation of equilibrium monolayer, a 1 mM solution of the organosulfur compound is sufficient[1a] and, for more concentrated solutions, the time required for monolayer formation gets reduced[36] except for cases where, multilayer formation adversely affects the organization. The relation between the coverage and the concentration of the solution can be understood in terms of the solubility of the compound and the adsorption isotherm. If the adsorbed species is in equilibrium with the solution species, then,

$$RSH\ (soln) + [Au] = RS\text{-}Au + \tfrac{1}{2}\ H_2 \qquad (1.1)$$

and we can define the equilibrium constant as

$$K_{eq} = [RS\text{-}Au]\ [H_2]^{1/2} / [RSH] \qquad (1.2)$$

Several methods including the use of radiotracers (^{35}S) and QCM experiments[25,34] establish that, the alkane thiolate/Au system exhibit a measurable equilibrium between the adsorbed thiolate and the free species in solution ($\Delta G_{ads} \sim -5$ Kcal/mole). This equilibrium is established with a very a short time (<1 min) following the

thiol introduction. The rate of equilibrium attainment is a strong function of concentration and the calculated value of K_{eq} varies from 10^3 - 10^5 M^{-1} for octadecanethiol (ODT) in n-hexane corresponding to a ΔG_{ads} of -4.4 to -5.6 Kcal/mole.[25] The variation of fractional coverage as a function of concentration of the molecule is represented as:[25]

$$\theta_s = c / c + (1/K_{eq}) \qquad (1.3)$$

where θ_s is the steady state coverage. Concentration variation from 3×10^{-6} to 3×10^{-4} M gives a θ of 0.04 to 0.82 which illustrates the importance of concentration control during the monolayer formation.[25]

1.5.5. Temperature:

Temperature is another important variable which can control the molecular conformations and physical properties of SAM during formation stage. Temperature control is specially significant as several investigations have shown that SAMs possess limiting mobility leading to rearrangement at elevated temperature. For example, it has been reported that better ordering of the monolayer can be achieved by lowering the formation temperature.[35] The accumulation of gauche conformation especially at the hydrocarbon region can play a central role in defining the stability and complex order-order and order-disorder phase transitions that are likely to occur on monolayer assemblies with variation of temperature. Helium diffraction experiments and molecular simulation studies have recently verified these temperature induced structural changes.[36]

1.6. Characterization Techniques for SAM:

Over the last few years, the application of a wide variety of characterization techniques have yielded several valuable information regarding the structural, kinetic, thermodynamic and mechanistic aspects of the self-assembled monolayers. Figure 1.1. shows the various techniques used to characterize different parts of SAM structure. These methods should preferably have no damaging interactions and yet must reveal subtle features such as the conformation and orientation of functional groups with depth

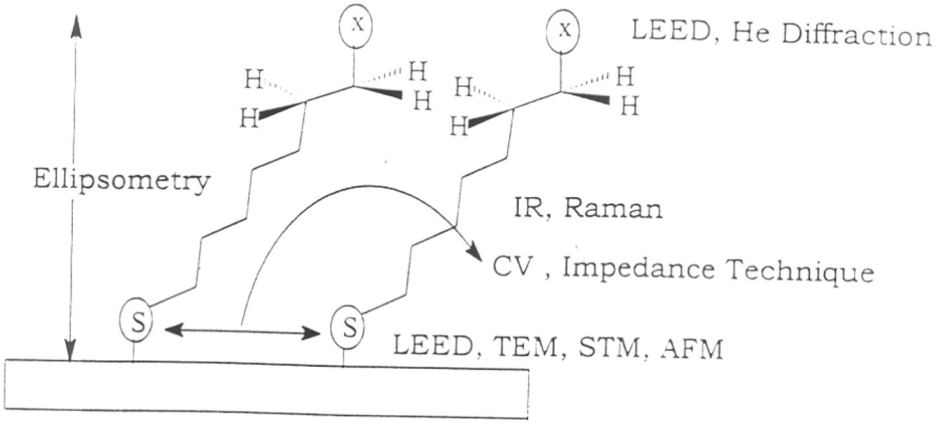

Figure 1.1. Various techniques used to characterize different parts of Self-assembled monolayer (SAM) structure. Here S is the sulfur atom bonded to surface and x is terminal functional group.

profiling. More importantly, since the applications of some of these techniques require the specific environment such as monolayer/solution or monolayer/UHV interface, the possibility of reorganization due to the change in environment is to be considered during the analysis. With the advent of highly sensitive *in situ* analytical techniques some of these limitations are eliminated and generally different complimentary surface analysis techniques are necessary to investigate the surface regions with submicron dimension. Thus, any single method of characterization is unable to provide the complete insight and the application of various characterization tools are hence essential. Some of the most useful analytical techniques for characterization of SAM are presented below.

1.6.1. Ellipsometry:

Ellipsometry is a common optical technique for the determination of film thickness and refractive index of monolayer and multilayer films by measuring the change of state of polarization of light upon reflection from a surface. When a polarized light beam interacts with a surface at some angle, it is resolved into its parallel (s-polarized) and perpendicular (p-polarized) components. The presence of a monolayer changes the ratio ψ of the s and p components as well as their phase difference Δ. Both ψ and Δ can be used to find the optical thickness of the monolayer and the optical constant of the substrates assuming that the monolayer is nonabsorbing and effectively isotropic. More significantly, an accurate value of the refractive index should be used in order to estimate the proper thickness. Elliipsometry has been extensively used for the characterization of different SAMs and a typical illustration includes the SAM of ODT on gold using the refractive index (n_f) value of 1.5.[7a]

1.6.2. X-Ray Photoelectron Spectroscopy:

X-ray photoelectron spectroscopy (XPS or ESCA) is a surface analytical tool where, a sample is exposed to monochromatic X-ray and the properties of inner-shell electrons are probed. According to the photoelectric effect, when a material is exposed to electromagnetic radiation of sufficiently short wavelength, (high photon energy), the

emission of electrons is observed. If ν is the frequency of photon, the kinetic energy of estimated electron (E_{kin}) is given by,

$$E_{kin} = h\nu - E_B \qquad (1.4)$$

where, E_B is the binding energy (ionization energy) of the electron (s, p etc.) in the atom which, being a function of the valence state of the atom, can give valuable structural informations. XPS is one of the most powerful tools to study SAM formation as it can give significant information about the nature of the chemical state of elements at the surface and to explore the changes occurred to the substrate atoms upon adsorption. For example, the Au $4f_{7/2}$ shows a single peak at 84 eV binding energy, suggesting the absence of any chemical changes of the bulk substrate atom. Similarly, the Ag $3d_{5/2}$ occurring at 386.2 eV shows the similarity of bulk Ag atoms. More significantly, the S 2p region may show single peak around 164 eV, or shifted to lower values corresponding to normal thiolate (Au^+S^-) binding energy of ~162.eV.[37]

Study of photoelectron spectroscopy as a function of the take off angle (i.e. angle dependent XPS) offers an excellent way of atom distribution in a film, as well as an additional tool for film thickness estimation. Finally, ESCA can also be used for analyzing the surface functionality and its concentration, especially for mixed monolayers. Nevertheless, in all these applications the limitations such as beam induced damage on the monolayer and carbon contamination from XPS chamber are to be kept in mind during the analysis of the XPS results.

1.6.3. Electrochemical Quartz Crystal Microbalance:

Quartz crystal microbalance (QCM) has proved to be a very useful tool for investigating the adsorption kinetics of SAMs. Although, it has been used for many decades as mass sensors in vacuum and gas phase experiments (for thickness monitor), its application to solution was found to be highly successful only recently to monitor interfacial mass change. The resonance frequency of the QCM depends on mass loading as per the Sauerbrey equation, [38]

$$\Delta f = -2\Delta m n f_o^2/(A\sqrt{(\mu_q \rho_q)} \qquad (1.5)$$

where, Δf represents the change in the oscillation frequency linearly related to the mass change Δm; A is the area of the electrode, f_o is the oscillation frequency of the fundamental mode of the QCM, μ_q is the shear modulus of the quartz (= 2.947 x 10^{11} g cm^{-1} s^{-2}), and ρ_q is the density of quartz (= 2.648 g cm^{-3}). Since the equation was originally designed for gas phase measurements, its application to *in situ* solution needs caution. For example, apart from the mass loading (Δm), several additional factors such as viscous damping, surface stress, energy disruption by nonshere couplings etc. can also affect its oscillation frequency. In addition, the monolayer has to be considered as a rigid film. Finally the variation in surface roughness of substrates can induce mechanical stress and along with all these deviations, there can be a continuous drift due to change in surface/ solvent interaction. As a consequence of these complex processes, the frequency shift can not be directly related to the absolute mass change and hence correction by using blank experiments (i.e. quartz crystal in the same environment without the adsorbing molecule) is an essential prerequisite for reliable kinetic information of monolayer formation. The technique can be especially useful to coupled with both controlled-potential and controlled-current experiments where, only one side of the crystal can serve both as a part of the QCM oscillator circuit and as a working electrode. [39]

1.6.4. Fourier Transform Infrared Spectroscopy:

Infrared spectroscopy is a general tool for the study of ultrathin organic films, specially their orientation and packing. Detailed information about the orientation of hydrocarbon chains and other functional groups can, in principle, be obtained with polarized light, since the adsorption in the vicinity of a molecular vibration frequency is dictated in general by the relative orientation of the electric field and the dipole transition moment. Nevertheless, the main difficulty is the low signal corresponding to a small amount (monolayer generally means less than 10^{14} molecules/cm^2) and hence the use of attenuated total reflection (ATR) and grazing-angle (GA) methods are essential. For

example, a quantitative analysis of the IR data indicates the optimum tilt angle as 30° for ODT monolayer on gold. The utility of this technique to quantitatively probe the composition and the spatial arrangement of monolayer assembly in an unmatched manner, has been illustrated in several recent investigation. [40]

1.6.5. Surface-Enhanced Raman Spectroscopy (SERS):

Raman spectroscopy usually involves the excitation of a sample with monochromatic light. The photons exchange energy with the sample and are scattered with a change in wave length as a consequence of loss or gain in energy. This process, known as Raman effect provides much qualitative information about the sample from the characteristic changes in the energy of the scattered photons. SERS is a type of Raman spectroscopy which shows an enhancement of the intensities of signal for the molecule adsorbed on selected roughened and reflective metal surfaces. The mechanism of this enhancement can be explained by electromagnetic and molecular/chemical enhancement theory. In effect, SERS has proven to be a sensitive and powerful probe of surface and *in situ* interfacial processes with interesting applications.

One important advantage of Raman spectra over IR is that it can detect the symmetrical bond (like S-S) which makes this technique increasingly attractive in the area of SAM.[41] Raman spectra is especially promising to investigate SAMs since it is sensitive to the internal and local molecular structure, as well as the chemical nature of the molecule. However, its use has been limited due to the weakness of the Raman scattering cross section, and the unusually enhancement of the scattering (by an order of 10^2-10^6) makes SERS an important tool to characterize the monolayer surface. The disappearance of the S-H or S-S stretching upon adsorption can confirm the adsorption path and the downshift of the frequencies due to metal-adsorbate charge transfer and adsorption induced spectral broadening can provide valuable information about the nature of adsorbing molecule. More importantly, in situ SERS can be performed in temperature-dependent and potential-dependent modes to provide information about the monolayer in varied experimental conditions. Although SERS is proves to be an effective technique for studying the packing effects on peak positions, investigation of electron

transfer and other surface reaction on thin organic films, it is not useful for the quantitative study of molecular orientation. Moreover, this technique is only applicable to rough and highly reflective metal surfaces.

1.6.6. Scanning Tunneling Microscopy (STM) and Atomic Force Microscopy (AFM):

Both scanning probe microscopes (STM and AFM) offer unique capability of probing the individual arrangement of atoms to map the surface with routine single atom resolution. STM as well as AFM have been used extensively to image SAM structures in vacuum, air, and liquid environments revealing the presence of pits or pinholes and even manipulating the monolayer by the interaction of the probe tip.[1a]

In a STM measurement, an atomically sharp metallic tip (e.g. tungsten) is brought very close (≤ 10Å) to the surface and on application of a small potential difference (~1V) between the surface and the tip, the generated tunneling current is monitored during scanning of the tip on the surface. The STM experiment can be done in either (1) constant current or (2) constant height mode. In the former, the tip height is adjusted maintaining a constant current and the image is obtained as a map of height of the tip with the lateral coordinates. In the latter case, height is kept constant while the current is recorded as a function of the x, y coordinate. The samples for STM should have few desirable criteria such as (1) good electrical conductivity, (2) atomically flat surface and (3) limited surface mobility.The imaging of organic films by STM can be difficult due to their low electrical conductivity and consequently, AFM has gained more importance since it can image both conducting as well as non-conducting films with similar resolution. In a typical AFM measurement, the sample is scanned with a stationary tip mounted on a spring so that the atoms in the tip interact with those on the surface and the resulting attractive or repulsive forces can be monitored.

Although both STM and AFM are widely used to characterize SAMs, the reproducibility of the image have to be verified to avoid scratches and the possibility of the tip penetrating into the organic film is to be kept in mind. Often multiple imaging and change of tip materials are necessary to eliminate tip-induced artifacts.

1.6.7. Contact angle measurement:

The macroscopic wetting properties of the surface can be studied by placing a small drop of liquid onto a flat, solid surface and by following the behavior of the same. The shape of the liquid drop will be affected by the free energy of the surface which forms an angle with the surface, known as the contact angle. This contact angle is a function of the surface free energy and is defined by the Young-Dupré equation [42] ($\gamma_{lv}\cos\theta = \gamma_{sl} - \gamma_{sv}$), where θ is the contact angle (defined as the angle between the tangent to the droplet and the surface, measured with a goniometer), γ is the interfacial free energy per area and subscripts lv, sv, sl refer to liquid-vapor, solid-vapor, and solid liquid interfaces respectively.

It was Langmuir, who first pointed out that the properties of the monomolecular film as measured by their contact angle, depends "apparently as much on the character of the underlying solid (substrates) as upon the nature of the molecule".[43] For example, when a liquid wets the surface completely and spreads over the surface at a rate depending on the liquid viscosity and the solid roughness, the contact angle is close to zero; on the other hand, when the liquid does not wet the surface, it has a finite contact angle. It is frequently found that the contact angle measured when a drop advances on a solid surface is different from that measured when the drop recedes (i.e. hysteresis). Although impurities can be a potential source of hysteresis, irreproducibility in surface tension due to local change in surface roughness can also be an important parameter. The usefulness of contact angle measurements to characterize SAM has been pioneered by Whitesides' group[44] using different liquids like water, hexadecane etc. demonstrating that it is possible to control the wetting properties of surface by SAM. Moreover, contact angle measurement can be used to evaluate surface-free energy and uniformity in order to get information on the surface order using various specific liquids.

1.6.8. Electrochemical Impedance measurement:

Among electrochemical techniques useful for studying SAM, the impedance method based on the measurement of the response of the electrochemical cell to a small amplitude alternating potential can give valuable information about surface

coverage, dielectric constant and electron-transfer behavior of the pinholes. The response is often analyzed by the complex impedance presentation and results are interpreted in terms of an equivalent electrical circuit.

With the help of appropriate double layer model (primitive Helmholtz parallel plate model, Goay-Chapmann model, Stern model etc.)[45] both faradaic and nonfaradaic process at the Au/SAM/electrolyte interface can be investigated to estimate several important parameters such as double layer capacitance, ohmic resistance, surface coverage etc. For example bare Au (111) on mica gives 17.5 $\mu F/cm^2$ as the double layer capacitance[46] and a monolayer of $SH\text{-}(CH_2)_{17}CH_3$ changes it to 1.2 $\mu F/cm^2$.[7a] The differential capacitance should decrease as film thickness increases and film permeability decreases. The use of externally added redox couple such as ferrocene, $Fe(CN)_6^{3-/4-}$ or $Ru(NH_3)_6^{2+/3+}$ can be valuable to study the distribution of pinholes by focusing attention on the mass-transfer component at low frequency.[47] Diffusion of ions from the bulk can take place at a finite rate and thus gives rise to an impedance to current flow through the electrode system at low frequencies which is known as Warburg impedance. In the simple equivalent circuit model for electrode-electrolyte interface, this diffusion impedance is in series with the charge-transfer resistance and both are generally considered to be in parallel with the double layer capacitance. Equivalent circuit description of the monolayer-solution interface provides the way to determine the double layer structure, estimation of surface coverage, double layer capacitance, dielectric constant of the monolayer and heterogeneous electron transfer rate constant of the redox species at the monolayer coated electrodes. The main limitation is the model-dependence of the calculated parameters as all the values can be misleading if incorrect equivalent circuit is selected.

1.6.9. Cyclic voltammerty:

Cyclic voltammetry is one of the most valuable techniques to study the barrier properties of SAMs. It is a simple technique where the potential is varied linearly with time between two fixed values with a definite sweep rate and the resulting current response is plotted against the applied potential. This technique has significant applications in the area of SAM as voltammetric data can provide a means to evaluate

monolayer energetic and monolayer coverage using appropriate solvents and supporting electrolytes.[48] The potential use of this technique to elucidate the response of the surface bound redox species and barrier properties of monolayers to ionic species in solution are illustrated by ferrocene thiol on Au.[49] It also provides a ready means to estimate the double layer capacitance as well the defect (pinhole) distribution in the monolayer.[7a] The surface coverage determination of SAM from cyclic voltammetric results are not straight forward although the integration of redox waves associated with surface-confined species has been used extensively as means for finding adsorbed surface-coverage for redox-active monolayer film.[49] Accuracy of such a method is highly dependent on the structure of the monolayer and the ability for charge compensating ions to access the adsorbate species that are being oxidized or reduced. Potential-dependent reorganization, solvent trapping, reductive desorption beyond -1.3 V vs Ag/AgCl reference electrode in alkaline KOH solution[50] etc. may be important in the analysis of CV data and blank experiments are necessary to define the potential window for investigations. Use of external redox couple can be very valuable to estimate surface coverage, pinhole distribution etc.

Chronoamperometry, chronopotentiometry and chronocoulometry are some of the other related electrochemical techniques useful for investigating the adsorption kinetics and mechanism of SAM formation. For example, the nucleation and growth of monolayer formation can be studied using chronoamperometric experiments where the shape of the I-t transients gives valuable clues. It is observed from chronoamperometric measurements that reductive removal of butanethiol monolayer in alkaline KOH[51] follows a nucleation and growth mechanism.[51]

Besides the techniques described above, several special characterization techniques such as He-, electron-, and neutron- diffraction, surface plasmon spectroscopy (SPS),[52] secondary ionization mass spectroscopy (SIMS),[53] matrix-assisted laser desorption/ionization mass spectrometry (MALDI-MS),[54] sum frequency generation[55] interfacial force microscopy (IFM),[56] surface potential measurement etc.[57] have been applied for the investigation of SAMs to get valuable informations.

1.7. Structure, Kinetics and Mechanism of SAM Formation:

As a result of the extensive application of above techniques a comprehensive picture has been emerged about the structure, kinetics and mechanism of SAM.

1.7.1. Structure of SAM:

Generally the structure of self-assembled monolayer can be divided into three parts namely (1) the bonding of the headgroup to the substrate, (2) the alkyl chains and (3) the order and orientation of the tailgroups. The headgroup provides exothermic chemisorption (~ 40 kcal/mole) on the substrate surface which results in apparent pinning of the headgroup. The nature of the bonding may be purely covalent, polar or ionic depending on the specific headgroup-substrate interactions. Once these molecules are on the surface via chemisorption, the close packing can start via the interchain van der Waals interaction (<10 Kcal/mole). Starting with simple methyl group, the terminal functionality can be a wide range of groups such as -OH, -Cl, $-NH_2$ etc.

Extensive studies using STM,[48] AFM and both high and low energy electron diffraction (LEED)[47] suggest that the monolayer forms a $(\sqrt{3} \times \sqrt{3})R30°$ overlayer structure. The symmetry of sulfur atoms in monolayer of docosanethiol on (111) gold is hexagonal with S-S spacing 0.497 nm and calculated area per molecule is 2.14 nm^2. This spacing is close to the spacing between the next nearest gold atoms on the (111) gold surface (0.499 nm). The spacing between the adjacent sulfur atom is nearly three times than that of the van der Waals diameter of sulfur atom (0.185 nm), thus sulfur-sulfur interaction is believed to be minimum. Moreover, this distance is also greater than the distance of closest approach of alkyl chains (0.424 nm) (Figure 1.2a). In comparison, it is suggested[50] that short chain alkane thiols like butane thiol and hexane thiol show growth of ordered domains having a unit cell of $p \times \sqrt{3}$ ($8 \leq p \leq 10$).

Ab-initio calculations on geometry optimization of -SH and CH_3S- group on Au (111) show the -SH groups to be placed on the three fold hollow site in order to have an equilibrium geometry with a linear Au(111)-S-H angle.[61] It is found that the hollow equilibrium site is 6.03 Kcal/mole more stable than on-top configuration and two types of bonding modes (sp^3 and sp) are possible. These two modes of chemisorption are

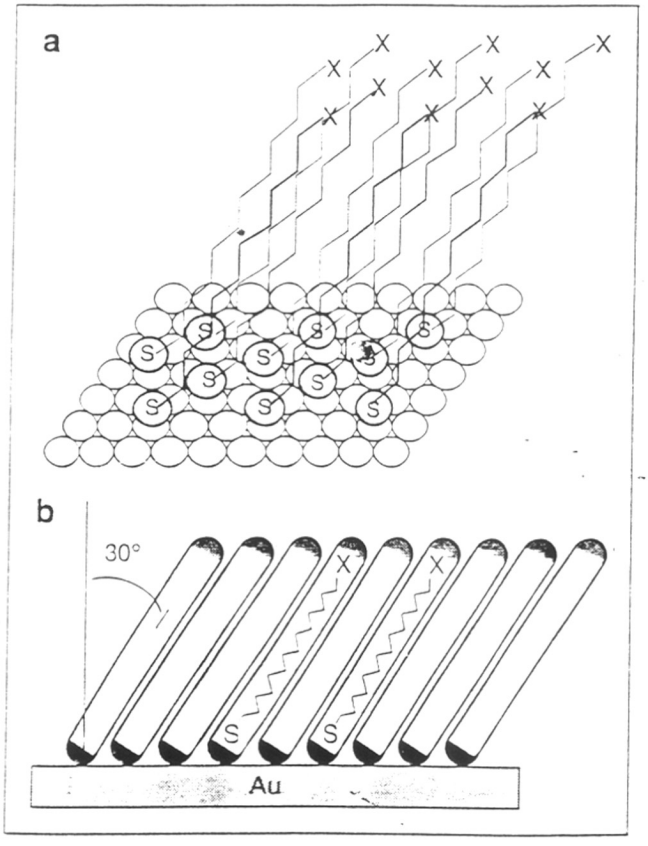

Figure 1.2. Self-assembled monolayer (SAM) of alkanethiolates on gold surface. (a) The sulfur atoms (S) are coordinated to the hollow three-fold sites of the gold (111) surface to form a ($\sqrt{3}$ x $\sqrt{3}$)R30° overlayer structure. Gold atom are (open circles) are arranged in a hexagonal relationship. (b) the alkyl chains are close packed and tilted ~ 30° from the normal to the surface. (Adopted from reference 128)

separated by very small energy barrier; amounting to 2.5 kcal/mole,[61] and therefore, can easily cross from one form to another.

The above structural model of Au/SAM could be further confirmed by the extensive results of IR spectroscopic studies. For example, from the width and position of the asymmetric CH_2 stretching vibrations, heptadecane and octadecane thiol monolayers are found to possess fully extended chains which reside in a crystalline-like environment.[40] The tilting of these chains with respect to surface normal can be understood from the relative intensities of the asymmetric and orthogonal asymmetric stretching vibrations of the polymethylene chain.[40] A quantitative analysis of both the infrared[40,62] and Raman spectroscopy[41d] suggest that the optimum tilt angle is 25 - 30° (Figure 1.2b). Molecular dynamics (MD) calculation shows that chains are tilted towards the next nearest neighbour[61] which is independent of chain length ($9 \leq n \leq 21$) or chain terminal group.[64] The twist angle β is measured to be nearly 52° for long chain alkane thiols and implies that the gold surface-sulfur-carbon bond angle is nearly 120°.[54a] This value is close to the optimum for an sp^2 hybridized sulfur atom. The actual tilt and twist angles of chains are directed by metal-sulfur bond. MD simulations further suggest that, monolayer is densely packed at 300 K with few gauche defects, concentrated near the chain terminal. [63]

One of the salient features of the above picture is the possibility of limited mobility of the molecules. STM studies show that, island structure formed during SAM formation by alkane thiol on evaporated gold surface exhibit macroscopic shape changes over a period of minutes and it has been concluded that, these shape changes are associated with mobile defects in the gold surface and that the Au-S bond is labile.[66] Migration of thiolates between neighboring hollow sites is required to remove defects from the organization. Actually, migration can be possible through the on-top or the bridge sites. It is possible that the thiolate which is chemically bonded to the on-top site (neutral gold-thiolate molecule) can move to a hollow site leaving a defect and STM studies suggest that some pinholes in the monolayer can be observed following this mechanism.[67] These pinholes are shown to disappear with annealing of the monolayers at 373 K.[64,67]

1.7.2. Mechanism of SAM Formation:

The chemisorption of alkane thiols/disulfides on Au(0) leads to the Au(I) thiolate (RS^-) species on the surface.[68,69] The monolayer formation mechanism in case of alkane thiol on Au(0) involves the formation of RS^-Au^+ species via the elimination of the -SH hydrogen, but the mechanism of removal of proton is not clear. Possibilities are that, this proton is lost as H_2 involving electrochemical step or via a reductive elimination reaction;

$$RSH + Au \Leftrightarrow RS\text{-}Au + \tfrac{1}{2} H_2 \qquad (1.7)$$

or as H_2O. No S-H stretching frequency (2600 cm^{-1}) is observed in either IR[70] or Raman spectrum[41d] of n-alkaline thiol adsorption on Au, as a supporting evidence for this type of a mechanism. In addition, Laser Desorption Fourier Transform Mass Spectroscopy confirms the nature of the species, as significant quantities of molecular thiolate negative ions are shown to desorb from the surface.[71]

The possible mechanism of SAM formation from dialkyl disulfide with Au(I) is a simple oxidative addition of S-S bond to the gold surface.

$$RS\text{-}SR + Au^0_n \Rightarrow 2\, RS^-Au^+ . Au_{n-2}{}^0 \qquad (1.8)$$

However, all the proposed mechanisms point to the fact that, monolayer formed from both alkane thiol and dialkyl disulfides are identical with the same gold-thiolate species on the surface as confirmed by the extensive XPS results.[72] In addition, the cleavage of S-S bond from dialkyldisulfide during the oxidative addition to the gold substrate is confirmed by the results of the temperature programmed desorption (TPD).[73] Moreover, fourier transform mass spectrometry,[70] electrochemistry [71] as well as Raman spectroscopy[41c,.d,48b] provide convincing evidence to show that the thiolate is the adsorbing species.

The generally accepted thiolate bonding structure for the adsorption of thiol/disulfide on Au has been contradicted in a X-ray diffraction study[74] where the S-S distance in the equilibrium structure of the monolayer is found to be much shorter (0.22 NM) suggesting the existence of a S-S bond. More recent studies using TDS show that,

alkanethiols desorb from gold surface as dimers where, two desorption peaks are observed at low and high temperature.[75] To resolve the problem of S-S bond cleavage, unsymmetrical disulfides have been used for SAM formation and there is a strong evidence for phase separated domains at elevated temperature.[76] These studies provide confirmatory evidence for the cleavage of S-S bond in disulfide during the monolayer formation subsequent formation of gold-thiolate species.

A recent ultrahigh vacuum STM study provides[77] a detailed molecular scale picture of the mechanism of SAM formation on clean single crystal Au(111). The monolayer formation follows a two-step process which begins with the condensation of crystalline islands. At a very low coverage, thiol forms a highly mobile lattice-gas phase while, above a critical value of surface coverage, stripped-phase islands are formed which contain surface aligned molecule. When a saturation coverage of stripped phase is attained, surface undergo lateral pressure induced solid-solid phase transition by nucleation of high density islands and at the last step this high density island starts growing until surface reaches saturation. In a similar manner, monolayer formation mechanism of alkanethiol on Ag(111) revealed from electrochemical investigations[78] suggest that atleast two energetically distinct chemical steps are present for the oxidative adsorption of short chain ($n<7$) alkanethiolates. In contrast, for longer chainlength ($n>7$), only single step has been observed, suggesting more structurally ordered and energetically favored molecular organization.

Inspite of extensive studies on SAM of n-alkane thiols/disulfides on Au(111) and polycrystalline gold, there are still inadequate and contradicting arguments regarding the headgroup-substrate interaction and about the actual nature of the species present on the surface after monolayer formation.[74]

1.7.3. Kinetics of SAM formation:

Monolayer formation kinetics of alkanethiol on Au surface has been studied from dilute (~1 mM) solution. In this case, a two-step adsorption kinetics has been observed with a very fast initial step (few minutes), and a second step of diffusion controlled first-order process, which strongly depends on thiol concentration as per the Langmuir

isotherm. The second step can be viewed as surface crystallization leading to the transfer of disordered alkyl chains into crystalline two dimensional unit cells.[7b] The main features are chain disorder (like gauche defect), chain-chain interaction (van deer Waals', dipole-dipole etc.) in the monolayer and limited surface mobility of the chains. The kinetics has also been found to be strongly dependent on alkyl chain length, solvent and the concentration of thiols as demonstrated by the adsorption rate constant (k_d) of 2.2 x 10^{-3} and 7.4 x 10^{-4} cm/s for octadecanethiol and octanethiol respectively on Au surface. The corresponding desorption rate constants are significantly lower (i.e 1.5 x 10^{-10} and 3.8 x 10^{-10} cm/s respectively)[25] suggesting their equilibrium stability (K_{eq} = 10^6); higher solution concentration and longer alkyl chains show faster kinetics probably due to the increased van der Waals interactions.

The above model of two step adsorption process was supported by the results of second harmonic generation (SHG)[79] and near edge X-absorption fine structure (NEXAFS).[80] Monolayer formation kinetics has also been followed by a number of *in-situ* characterization techniques though all of them are not in agreement with each other. In most of the studies a two step process is observed [81] although examples of single step[25, 82] and three-step[81a,b] processes as revealed by QCM and surface plasmon resonance spectroscopy (SPRS). The discrepancy could be understood in terms of the presence of a bulky group in the chain, where, the previously observed two steps can couple together.[83]

1.7.4. Stability of Self-Assembled Monolayer:

The stability of SAM has been studied in a wide variety of investigations. Since it is well understood that the Au-S interaction is not fully covalent, some loss of molecules can be expected when it is in contact with alkane thiol solutions.[84] Moreover, self-exchange of labeled (^{35}S) to unlabeled C_{18} thiol in hexane[34] as well as on exposure to electroactive SAMs in pure solvent[85] are known to be independent of thiol concentration, a significant amount of thiol remaining unexchanged over a large period of time. Exposure of thiol monolayer to piranha solution and UV-radiation also causes extensive damage to the monolayer surface.[34]

Electrochemical stability studies of SAM under the application of external electric field indicates that the potential window for voltammetry (i.e. the region of ideal poarizable behavior) gradually increases with the increase in chain length. The double layer capacitance of the electrode modified by shorter chain monolayer is found to increase slowly with continuous cycling unlike for the long chain thiols.[7a,f] In an AFM study of SAM of C_{18} thiol,[86] the monolayer is found to be stable over a wide range of potential with the possibility of film break down at negative potentials depending on the amount of oxygen dissolved in the solution. In an alkaline solution (pH >11), removal of thiol monolayer is possible via both one electron oxidative and three electron reductive desorption of alkane thiol.[87] A recent *in-situ* vibrational spectroscopic study [88] shows that, the oxidative removal of thiol is slow and occurs in multiple steps involving upto eleven electrons per molecule.

Thermal stability studies using XPS show a loss of sulfur from hexadecane thiolate monolayer in a temperature range of 443 - 503 K,[8b] and further studies using TPD indicate that the desorption of methane thiolate SAM on gold surface occurs at 493 K.[8a] Additional evidence for this comes from the mass spectroscopic studies on 2-methylpropane thiolate monolayer, where a maximum desorption at ~ 473 K is found to happen,[89] as is also confirmed by the use of radiolabeled ODT. Several STM/XPS studies also reveal the excitation of S-Au or S-C bond within temperature ultimately leading to molecular desorption or surface decomposition.[90] These studies further suggest that, there is no major structural change if alkane thiol SAM is annealed to 325 K, while monolayer annealed above 350 K exhibits significant structural changes. Vacuum annealing of the sample has shown melting transition above 350 K with complete decomposition at 575 K for dodecanethiol monolayer.[90e] On the other hand, air annealing [90c,d,91] at 375 K for 20 hours shows the decomposition of surface thiol which upon continuation, forms disordered regions due to oxidized thiols and on prolonged heating desorption of these sulfonates take place as is indicated by XPS studies. The combined evidence from these diverse techniques unambiguously prove the thermal stability of RSH/Au SAM upto 473 K.

1.7.5. Electrochemistry of SAMs:

SAM formation is one of the simplest approaches to modify the electrode surface and all the applications of modified electrodes including the fabrication of chiral electrodes can be achieved following this simple methodology.[9w] The success of this methodology depends mainly on the ability to manipulate both the structure and the composition of the monolayer organization to accomplish the precise control of the electrode response at molecular level. These organized assemblies can broadly be classified into electroinactive and electroactive depending on the redoxactive groups present in the chain although thiol itself is redox active in alkaline media.

Electrochemical reactions of thiols and disulfides in both aqueous and nonaqueous media on different electrode surfaces (Hg, Pt and Au) are well known.[92] In aqueous solution of pH greater than pK_a, generally RS^- is formed while for pH< pK_a, RSH prefers to exist. The equilibrium potential (E^0) corresponding to the reaction,

$$RSH = RS^- + H^+ \qquad (1.9)$$

varies from -0.53 to -0.71 V vs NHE, depending on the pK_a values in the range of 9 - 12.[25] The RSH oxidation to disulfides in aqueous media is generally quasi reversible although irreversible behavior has been observed as molecular weight increases, for instance from butanethiol to 1-decane thiol. When pH is greater than Pk_a, the half wave potential ($E_{½}$) values are found to be independent of pH. For example, differential pulse polarography and other electrochemical techniques (linear sweep voltammetry and coulometry) at Hg electrode in aqueous 0.2 M NaOH solution with thiol concentration varying from 10^{-7} to 10^{-4} M show a quasireversible behavior at a constant $E_{½}$ value of 0.76V vs SCE.[92] Dimerization and disproportionation on Hg surface have also been observed in several polarographic studies and irregular surface waves have been occationally attributed to adsorption.[92] These electrochemical reactions in aqueous media have important effect on monolayer stability. Since the Pk_a value of most of the thiols vary from 8 - 11,[25] the SAM electrodes can undergoes reductive desorption in alkaline solution as:[34]

$$RS\text{-}Au + e = RS^- + Au \qquad E^o = -0.88\ V\ vs\ NHE \qquad (1.10)$$

Similar desorption reactions have also been reported on Ag(111) and indeed two separate voltammetric waves have been observed at low coverage, which merges to a single reversible wave as coverage approaches unity.[78]

Reduction of RSH in non aqueous media (DMF) is known to give rise to the anion as:

$$RSH + e = RS^- + \tfrac{1}{2} H_2 \qquad (1.11)$$

where, both platinum and murcury have been employed as electrodes.[92] Similarly, disulfide can also get reduced as RS^- first,

$$RS\text{-}SR + 2e = RS^- \qquad E^0 = -0.35\ V\ vs\ NHE \qquad (1.12)$$

followed by reductive adsorption,

$$2RS^- + Au = RSSRAu + 2e \qquad E^0 = -0.88\ V\ vs\ NHE \qquad (1.13)^{34}$$

1.7.5.1. Electroinactive SAM:

The electroinactive character of the alkanethiol SAM is related to the solvent, supporting electrolyte and the potential window used for the measurements. In most of the solvents used for electrochemical characterization of SAM, thiol monolayer has been found to be stable in a limited potential range (section 1.7.4). In aqueous system, the pH of the solution and pK_a of the thiol control this window as illustrated by different studies of oxidative adsorption and reductive desorption in alkaline solutions leading to the break down of the assemblies.[58]

Alkanethiol monolayers on gold provide high quality barriers for both electron and ion transfer processes and this ability of passivation of electrode surface and the

consequent inhibition of ion permeation is increased with increase in alkanethiol chain length. Electrochemical studies related to the monolayer of long-chain alkane thiols with different surface functionalities suggest the importance of steric and electrostatic interaction between the functional group at the chain end in determining packing of chains which will lead to the change in barrier properties.[93] For example, extremely compact and defect-free monolayer formed using ω-hydroxyalkanethiols has been employed as a valuable tool to probe the dynamics of electron transfer between solution-phase redox couples.[94] The current has been found to decrease exponentially with monolayer thickness according to the equation from Marcus electron-transfer theory:

$$i = i^{'} e^{-\beta d} \qquad (1.14)$$

where, β is the electron tunneling constant (~ 0.9 per methelene unit of alkane thiol), $i^{'}$ is the current in the absence of monolayer and d is the thickness. The ability of these monolayers to effectively block the electrochemical reactivity of redox probes in solution can suitably be used to measure very large heterogeneous electron transfer rate constants.[47] For example, studies on different electroinactive thiolate films like capacitive, fully covered, and partially covered gold suggest electron transfer through the film as well as at the defect sites.[95] These assemblies can behave as nanoporous electrodes which can discriminate the diffusion of redox probes depending upon their size and nature. The study related to double layer effects at uncharged self-assembled monolayer shows that the kinetics of heterogeneous electron-transfer at the monolayer/solution interface depends both on the charge of the reactant and the composition of the monolayer.[94a]

1.7.5.2. Electroactive SAM:

The molecule for SAM formation can be selected in such a way that a pendant redox group is present, which can act as a signature, keeping a variable distance from the electrode surface. Functionalities like ferrocenyl,[96] biotinyl,[97] 2,2'-bipyridyl,[98] tetrathiafulvalenecarboxylate,[99] tetraphenylporphyrin[100]and ferrocenylazobenzene[101] are

incorporated which are important for engineering surface properties as well as for further chemical reactions. This procedure produces reasonably spatially isolated ferrocenyl and ruthenium pentammine groups that appear to exhibit well-defined separation distance between the redox group to test the Marcus theroy of electron transfer.[102] The well-defined molecular thin film can be formed from the coadsorption of ferrocene (electroactive) and methyl (inert) terminated long chain thiols on gold electrodes, where the concentration of the electroactive group is so small (~<25%) that it is homogeneously dispersed and behaves as ideal independent one-electron redox species. Using this strategy, both the forward and reverse electron transfer rates are measured over a large range of potentials.[96c] It is shown that rate constant can be obtained using Laviron formalism where the ferrocene group is placed at a fixed distance from the electrode surface. On the other hand, surface coverage of these electroactive SAM can be easily estimated by integrating the area under surface confined wave, and in favorable cases, we get all the diagnostic features of reversible surface waves.[48a]

1.8. Applications of SAM:

Monomolecular films prepared by self-assembly technique are attractive for several exciting applications due to the possibility of engineering the surfaces at the molecular level. The chemical properties can be fine tuned by selecting different types of terminal functional groups and a large variety of flexibility in SAM structure, formation and manipulation can be utilized to evaluate modern theories of wetting, tribology, adhesion, molecular recognition and related phenomena. More significantly, the close similarity of the structure of SAM with biomembranes (e.g. bilayer lipid membranes) enables to use them as model system to study ion transport as demonstrated by the electron transfer through the immobilized proteins on the surface. Some of the recent applications of SAMs are described below.

1.8.1. Support for Protein Adsorption:

The organic interfaces prepared by the self-assembly of long-chain alkane thiol on gold are suitable model systems for the study of protein adsorption at the interface.

For example, the efficiency of chemical separation of many closely related biomolecules and pharmaceuticals are often limited by the unwanted electrostatic interaction with the surfaces and the mixed SAM of octadecyl and methyl chains organized into a 2D cross-linked network on the chromatographic silica surfaces is found to be very good for separation. Similarly, different types of ω-functionalized long chain alkanethiols on gold are found to be very useful to study the interactions of proteins on membrane surfaces[106]and the amount of protein adsorption can be controlled by varying the monolayer composition and hydrophobicity. The adsorption of several proteins on SAMs that contain different functionality (e.g. alkyl, perfluoroalkyl, amide, ester, alcohol, nitrile, carboxylic acid, phosphonic acid, boric acid, amine, heterocyclic groups) has been found to correlate well with the hydrophobicity of the surfaces. However, some of the proteins get denatured after the irreversible adsorption and further work is in progress to avoid these limitations.

1.8.2. Patterning of Surfaces:

The self-assembled monolayer surface has been used extensively for patterning to provide new approaches for two and three dimensional, quasiplanar, mesoscale structures. The fact that SAMs are stable under various conditions makes them ideal for patterning of surfaces as demonstrated recently by Whitesides' group.[106] There are various methods available, like e-beam writing,[107] photolithography,[108] microcontact printing using an elastomeric stamp,[109] microwriting,[110] micromachining,[111] photooxidation,[112] electrochemical reduction,[113] and exposure to electrons, atoms or X-rays,[114] which provide decomposition of SAMs in patterns. These patterned surfaces can be applied in planar microdevice fabrication, fabricating microelectrodes in electron and scanning probe microscopes, in producing environmentally sensitive diffraction gratings etc. [115]

1.8.3. Materials Synthesis through Biomineralization:

Biomineralization can be defined as a process that involves the controlled nucleation and growth of ceramics from solutions, often in the host matrix provided by an

organism. SAMs can be used to develop practical processing schemes mimicking biomineralization as, manipulation of surface engineering can be extremely useful for controlling crystal phase morphology, growth habit, orientation and even chirality. For example SAM has been used to prepare both tetragonal ZrO_2 nanocryatallites (< 10 nm) and Y_2O_3-doped zirconia at low temperatures. The high degree of physical and chemical stability of SAMs and use of wide range of characterization techniques to determine the relationship between organic and inorganic phases make these systems an ideal support to carry out nucleation and growth of various solid materials.[116] Consequently, a number of studies have been performed on the growth of inorganic crystals on SAMs, using both solution and vapor phase methods[117] through biomimetic processing.[118] This impact on material processing has created renewed interests in the studies of surface nucleation and growth in biological systems.

1.8.4. Corrosion Protection:

The highly organized monomolecular films formed from alkanethiol/disulfides on various metal surfaces has successfully demonstrated their ability of corrosion inhibition. The resistance of these films towards molecular oxygen and ion permeation is the primary reason and several studies relating to the corrosion protection of highly reactive metals like Cu[119] are available in different media. For example, SAM of alkane thiol on polycrystalline copper has been found to be well protected in both aqueous Na_2SO_4 and NaCl solutions and their protection abilities are found to be better in comparison with normal inhibitors such as mecaptobenzotriazole and benzotriazole. The SAMs on Ag and Au also show excellent passivation properties and recent applications of scanning probe techniques has enabled to understand the fundamental mechanism of corrosion and its prevention.[119f, 120b,c,d, 121] Nevertheless, more studies are necessary to demonstrate the validity of these findings and also to get better SAM films that prevent aqueous and atmospheric corrosion of various electronic devices.

1.8.5. Molecular Recognition:

The stability, uniform surface structure and relative ease of varying the functionality make SAMs particularly suitable towards developing applications in the area of chemical sensors.[122] For example, several electrochemical sensors,[123] surface acoustic wave devices,[124] piezoelectric devices[125] and bio-sensors[126] have been demonstrated with different SAM surfaces and even fabrication of simple ion-selective electrodes are possible with a high degree of selectivity.[127] The self-assembled monolayers of alkanethiols on gold are probably one of the best currently available surfaces for accomplishing the functionalization and patterning necessary for fabricating biosensors along with several advantages such as flexibility and stability.[128] A convenient way of tailoring surfaces in the molecular level is the inclusion of some well-known receptor molecules in the monolayer to use as a support for molecular recognition at the surface through the formation of inclusion complexes by host-guest interaction.[129]

1.8.6. Two Dimensional Organization of Nanoparticle:

Self-assembled monolayer finds an exciting application in the area of nanotechnology, where, nanoscale clusters can be easily organized to impart stability. For example, SAMs with suitably tailored terminal functionality have been widely used to covalently bind colloidal particles of metal and semiconductors.[130] The site selective synthesis of different nanoclusters has been demonstrated recently by various SAMs and this general method seems to be a promising alternative to the organization of cluster by Langmuir-Blodgett[131] and chemical insertion techniques.[132]

Alkane thiol monolayers on Au-clusters[133] opens a new concept about self-assembled monolayers. These systems can be viewed as self-assembled monolayer formation in three dimension (3D-SAM)[134] and it is possible that the character of alkane chain ordering on the periphery of the nanoparticle (or metal clusters) may exhibit intrinsic differences due to surface curvature. This field has gained significant interest with major contributions by Brust et al.[133] where, the stabilization of Au colloids are achieved with chemisorbed C12 alkane-thiols. Comparison of the 3D SAM to the

classical 2D SAM[1] using results from techniques like solution and solid state ^{1}H and ^{13}C NMR spectroscopy, elemental analysis, differential scanning calorimetry (DSC), thermogravimetry (TGA) and diffusion-ordered NMR spectroscopy (DOSY)[135] show that the packing density of the alkane thiolate chains bonded to the Au cluster surface (62-68 %) is nearly twice to that found on flat Au (111) (33%). There has been significant concentration (10-25 %) of chain end gauche defects in case of 3D SAM which is absent in 2D monolayers.[136]

Apart from the applications discussed above, self-assembled multilayer films are gaining particular importance for their potential application in nonlinear optics and molecular electronics, even though these types of multilayer films have been considerably less investigated. Recent examples of multilayer synthesis include the use of strong ionic interaction between zirconium ion and organic phosphonate[137] or that of Cu^{2+} with carboxylic acid and thiol[138] to build up successive multilayers. SAMs are also applied for controlling the wetting, adhesion and lubricating properties of the surfaces of various metallic and oxide surface structure.

1.9. Objectives and the Structure of the Present study:

It is quite clear from the foregoing critical review of the area of SAM of thiols/disulfides on coinage metals that studies related to the organization of small aromatic compounds are still rare. Most of the studies are concerned with long chain molecules, which are known to form well-ordered, oriented and highly compact molecular assemblies. Hence, it will be interesting to study SAM formation from disulfides/thiols of relatively small dimension without the ordering influence of a hydrophobic, hydrocarbon chain. More significantly, by selecting organosulfur compounds with planar π-system, the influence of the aromatic ring on SAM formation can be evaluated. The main objectives of the work embodied in this thesis are set out in this perspective as described below.

The primary objectives of the present study are: (a), understanding the organization of small (~7Å) aromatic disulfides/thiols on Au, Ag and Cu surfaces and hence the differences in organization using different characterization techniques; (b), to

understand the influence of the rigid ring systems on SAM formation which constrains the sulfur to a particular geometry (geometrical constraint); (c), comparing the kinetics and structural characterization of SAMs obtained from a rigid and flexible system for evaluating the influence of structural rigidity on SAM formation; (d), introducing new compounds like small aromatic diselenides for SAM formation and comparison of the results with similar disulfides; (e), to understand the effect of the anionic surfactant on SAM formation kinetics as well as on the equilibrium structure from long chain thiols to small aromatic disulfides; (f), to investigate the potential applications of small aromatic bi-functional thiols in two dimensional organization of metal clusters; (g), to understand the corrosion resistance capabilities of these small disulfides, and finally (h), to investigate the application of the funtionalized interface of SAM for solid sate materials synthesis.

The present thesis contains five chapters. In chapter 1, a general introduction of molecular self-assembly, supramolecular organization and their importance and relevance to the materials science is presented. This chapter deals with an overview of the area of selfassembled mono(multi)layer with a primary emphasis on thiols/disulfides based system on Au, Ag and Cu surfaces. This chapter discusses the recent understanding and developments of SAM with special focus on certain new overlapping and emerging fields.

In chapter 2, a comparatively small (~7Å) aromatic disulfides namely naphthalene disulfide (NDS) is used for SAM formation on Au, Ag and Cu surfaces. Monolayer formed on polycrystalline Au surface has been characterized by different characterization techniques like XPS, cyclic voltammetry, impedance measurement with redox active probe and STM. Kinetics of monolayer formation has also been studied. Monolayer formation of the same on Ag and Cu surfaces has been followed by capacitance and XPS measurements and the results are compared with that of monolayer on Au.

Chapter 3, deals with studies related to understanding the effect of geometric constraints on SAM formation. The molecule discussed in the previous chapter has a characteristic structure as the rigid naphthalene ring constrains the two sulfurs to a

particular geometry. This aspect has been highlighted and another disulfide, without any structural rigidity but with similar molecular dimension, namely diphenyl disulfide (DDS) has been used for SAM formation. Monolayer thus formed has been characterized by different techniques and the results are compared to understand the effect of the structural constraint. In this context, a similar type of compound with Se-Se head group is introduced for SAM formation. This study shows significant difference in organization for NDS and DDS. Moreover, it is suggested that diselenides like disulfides are capable of forming SAM with similar efficiency.

Chapter 4 contains the study of the effect of surfactant on monolayer formation kinetics and structure of long-chain thiol as well as small aromatic disulfides. This study shows that SAMs obtained in presence of surfactant are different in structure with the presence of distributed surfactant patches and difference in the kinetics of monolayer formation.

Chapter 5 deals with three different applications of these SAMs of small aromatic thiols/disulfides. The corrosion protection of Cu is performed by using SAM of two disulfide monolayers and the results are compared with the corrosion protection efficiency of octadecylthiol (ODT). These results indicate high corrosion resistance power of the two disulfides and are comparable to C_{18} thiol for DDS monolayer.

Another application is that, the SAMs of small bi-functional molecules with -SH and -COOH in two different ends are used to form monolayer on Au and Al surfaces. The resulting monolayer can effectively be applied to organize metal nanoclusters. It is demonstrated that the molecule will have different orientation in the two metal surfaces. Moreover, the surface with -SH functionality only are capable of organizing the cluster.

In the last application, a small aromatic dithiol has been used to functionalize the metal surface to be used for the synthesis of crystalline, monoclinic zirconia at room temperature. It has been demonstrated that, SAM provides new methodologies for synthesizing thin films of advanced materials with unique physical and chemical properties.

These results clearly suggest that small aromatic disulfides and thiols are capable of forming well-ordered monolayer with high surface coverage although,

geometric constraints can affect equilibrium organization. While these developments are promising, more work on similar monolayer assemblies, are required to understand the organization of small aromatic thiol and disulfide for realizing the complete potential for applications.

1.10 . Reference:

1. (a) Ulman, A. *An Introduction to Ultrathin Organic Films: From Langmuir-Blodgett to Self-Assembly,* Academic Press, INC, 1991, (b) Dubois, L. H.; Nuzzo, R. G. *Annu. Rev. Phys. Chem.* **1992**, *43*, 437, (c) Ulman, A. *Chem. Rev.* **1996**, *96*, 1533, (d) Bain, C. D.; Whitesides, G. M. *Angew. Chem. Int. Ed. Engl.* **1989**, *28*, 506, (e) Swalen, J. D.; Allara, D. L.; Andrade, J. D.; Chandross, E. A.; Garoff, S.; Israelachvili, J.; McCarthy, T. J.; Murray, R.; Pease, R. F.; Rabolt, J. F.; Wynne, K. J.; Yu, H. *Langmuir* **1987**, *3*, 932.

2. Marcus, R. A. *J. Chem. Phys.* **1965**, 43, 679.

3. Sigal, G. B.; Mrksich, M.; Whitesides. G. M. *J. Am. Chem. Soc.* **1998**, *120*, 3464.

4. Fecilla, P.; Dixon, R. P.; Slobodkin, G.; Alvi, D. S.; Waldeck, D.H.; Hamilton, A. D. *J. Am. Chem. Soc.* **1990**, *112*, 9408,

5. Bigelow, W. C.; Pickett, D. L.; Zisman, W. A. *J. Colloid Interface. Sci.* **1946**, *1*, 513.

6. Nuzzo, R. G.; Allara, D. L. *J. Am. Chem. Soc.* **1983**, *105*, 4481.

7. (a) Porter, M. D.; Bright, T. B.; Allara, D. L.; Chidsey, C. E. D. *J. Am. Chem. Soc.* **1987**, *109*, 3559, (b) Bain, C. D.; Troughton, E. B.; Tao, Y-T.; Evall, J.; Whitesides, G. M.; Nuzzo, R. G. *J. Am. Chem. Soc.* **1989**, *111*, 321, (c) Bain, C. D.; Whitesides, G. M. *J. Am. Chem. Soc.* **1989**, *111*, 7164, (d) Bain, C. D.; Evall, J.; Whitesides, G. M. *J. Am. Chem. Soc.* **1989**, *111*, 7155, (e) Bain, C. D.; Biebuyck, H. A.; Whitesides, G. M. *Langmuir* **1989**, *5*, 723, (f) Miller, C.; Cuendet, P.; Grätzel, M. *J. Phys. Chem.* **1991**, *95*, 877, (g) Folkers, J. P.; Laibinis, P. E.; Whitesides, G. M. *Langmuir* **1992**, *8*, 1330.

8. (a) Nuzzo, R. G.; Zegarski, B. R.; Dubois, L. H. *J. Am. Chem. Soc.* **1987**, *109*, 733, (b) Nuzzo, R. G.; Fusco, F. A.; Allara, D. L. *J. Am. Chem. Soc.* **1987**, *109*, 2358, (c) Offord, D. A.; Jhon, C. M.; Griffin, J. H. *Langmuir* **1994**, *10*, 761.

9. (a) Troughton, E. B.; Bain, C. D.; Whitesides, G. M.; Allara, D. L.; Porter, M. D. *Langmuir* **1988**, *4*, 365, (b) Kartz, E.; ItzhakC. D.; Whitesides, G. M.; Allara, D. L.; Porter, M. D. *Langmuir* **1988**, *4*, 365, (c) Sabatani, E.; Cohen-Boulakia, J.; Bruening, M.; Rubinstein, I . *Langmuir* **1993**, 9, 2974, (d) Bryant, M. A.; Joa, S. L.; Pemberton, J. E. *Langmuir* **1992**, *8*, 753, (e) Hill, W.; Wehling, B. *J. Phys. Chem.* **1993**, *97*, 9451, (f) Li, T. T. -T.; Liu, H. Y.; Weaver, M. J. *J. Am. Chem. Soc.* **1984**, *106*, 1233, (g) Kartz, E.; ItzhakC. D.; Whitesides, G. M.; Allara, D. L.; Porter, M. D. *Langmuir* **1988**, *4*, 365, (h) Cooper, J. M.; Greenough, K. R.; McNeil, C. J. *J. Electroanal. Chem.* **1984**, *347*, 267, (i) Uvdal, K.; Bodö, P.; Liedberg, B. *J. Colloid Interf. Sci.* **1992**, *149*, 162, (j) Ihs, A.; Uvdal, K.; Liedberg, B. *Langmuir* **1993**, *9*, 733, (k) Arndt, Th.; Schupp, H.; Schepp, W. *LThin Solid Films* **1989**, *178*, 319, (l) Mielczarski, J. A.; Yoon, R. H.; *Langmuir* **1991**, *7*, 101. (m) Edwards, T. R. G.; Cunnane, V. J.; Persons, R.; Gani, D. *J. Chem. Soc. Chem. Commun.* **1989**, 1041, (n) Arduengo, A. J.; Moran, J. R.; Rodriguez-Paradu, J.; Ward, M. D. *J. Am. Chem. Soc.* **1990**, *112*, 6153, (o) Ihs, A.; Uvdal, K.; Liedberg, B. *Langmuir* **1993**, *9*, 733, (p) Samanat, M. G.; Broen, C. A.; Gordon, J. G. *Langmuir* **1992**, *8*, 1615, (q) Dishner, M. H.; Hemminger, J. C.; Feher, F. J. *Langmuir* **1997**, *13*, 4788. (r) Demoz, A.; Harrison, D. J.; *Langmuir* **1993**, *9*, 1046. (s) Muskal, N.; Turyan, I.; Shurky, A.; Mandler, D.; *J. Am. Chem. Soc.* **1995**, *117*, 1147. (c) Stratmann, M. *Adv. Mater.* **1990**, *2*, 191. (t) Liu, Q.; Xu, Z. *Langmuir* **1995**, *11*, 4617. (u) Brust, M.; Walker, M.;Bethell, D.;

Schiffrin, D.J.; Whyman, R. *J. Chem. Soc. Chem. Commum.* **1994**, 804. (v) Gu, Y.; Lin, B.; Smentkowski, V. S.; Waldeck, D. H. *Langmuir* **1995**, *11*, 1849. (W) Muskal, N.; Turyan, I.; Shurky, A.; Mandler, D. *J. Am. Chem. Soc.* **1995**, *117*, 1147.

10. (a) Allara, D. L.; Nuzzo, R. G. *Langmuir* **1985**, *1*, 45. (b) Allara, D. L.; Nuzzo, R. G. *Langmuir* **1985**, *1*, 52. (c) Ogawa, H.; Chihera, T.; Taya, K. *J. Am. Chem. Soc.* **1985**, *107*, 1365. (d) Tao, Y.-T. *J. Am. Chem. Soc.* **1993**, *115*, 4350. (e) Thomson, W. R.; Pemberton, J. E. *Langmuir* **1995**, *11*, 1720. (e) Tao, Y.-T.; Lee, M.-T.; Chang, S. -C. *J. Am. Chem. Soc.* **1993**, *115*, 9547.

11. (a) Sagiv, J. *J. Am. Chem. Soc.* **1980**, *102*, 92. (b) Tilman, N.; Ulman, A.; Schildkraut, J. S.; Penner, T. L. *J. Am. Chem. Soc.* **1988**, *110*, 6136. (c) Gun, J.; Sagiv, J. *J. Colloid Interface. Sci.* **1986**, *112*, 457. (d) Gun, J.; Iscovici, R.; Sagiv, J. *J. Colloid Interface. Sci.* **1984**, *1o1*, 201. (e) Kessel, C. R.; Granick, S. *Langmuir* **1991**, *7*, 532. (f) Finklea, H. O.; Roninson, L. R.; Blackburn, A.; Richter, B.; Allara, D. L.; Bright, T. *Langmuir* **1986**, *2*, 239.

12. Chen, K.; Mirkin, C. A.; Lo, R. -K.; Zhao, J.; McDevitt, J. T. *J. Am. Chem. Soc.* **1995**, *117*, 6374.

13. Lee, H.; Kepley, L. J.; Hong, H. -G.; Akhter, S.; Mallouk, T. E. *J. Phys. Chem.* **1988**, *92*, 2597.

14. (a) Sheen, C. W.; Shi, J.-X.; Martensson, J.; Parikh, A. N.; Allara, D. L. *J. Am. Chem. Soc.* **1992**, *114*, 1514. (b) Natan, M. J.; Thackeray, J. W.; Wrighton, M. S. *J. Phys. Chem.* **1986**, *90*, 4089. (c) Laibinis, P. E.; Whitesides, G. M.; *J. Am. Chem. Soc.* **1992**, *114*, 1990. (d) Laibinis, P. E.; Whitesides, G. M.; Allara, D. L.; Tao, Y.-T.; Parikh, A. N.; Nuzzo, R. G. *J. Am. Chem. Soc.* **1991**, *113*, 7152.

15. (a) Lee, T. R.; Laibinis, P. E.; Folkers, J. P.; Whitesides, G. M.; *Pure Appl. Chem.* **1991**, *63*, 821. (b) Gui, J. Y.; Stern, D. A.; Frank, D. G.; Lu, F.; Zapien, D. C.; Hubbard, A. T. *Langmuir* **1991**, *7*, 955. (c) Lane, R. F.; Hubbard, A. T. *J. Phys. Chem.* **1973**, *77*, 1401. (d) Lane, R. F.; Hubbard, A. T. *J. Phys. Chem.* **1973**, *77*, 1411. (e) Hickman, J. J.; Zou, C.; Ofer, D.; Harvey, P. D.; Wrighton, M. S.; Laibinis, P. E.; Bain, C. D.; Whitesides, G. M.; *J. Am. Chem. Soc.* **1989**, *111*, 7271. (f) Hickman, J. J.; Laibinis, P. E.; Auerbach, D. I.; Zou, C.; Gardner, T. J.; Whitesides, G. M.; Wrighton, M. S. *Langmuir* **1992**, *8*, 357.

16. (a) Weisshaar, D. E.; Lamp, B. D.; Porter, M. D. *L J. Am. Chem. Soc.* **1992**, *114*, 5860. (b) Willicut, R. J.; McCarley, R. L. *Langmuir* **1995**, *11*, 296. (c) Sayre, C. N.; Collard, D. M. *Langmuir* **1995**, *11*, 302.

17. (a) Chailapakul, O.; Sun, Li.; Xu, C.; Crooks, R. M. *J. Am. Chem. Soc.* **1993**, *115*, 12459. (b) Thomas, R. C.; Sun, Li.; Crooks, R. M.; Ricco, A. J. *Langmuir* **1991**, *7*, 620.

18. Hammer, B.; Nørskov, J. K. *Nature* **1995**, *376*, 238.

19. Smith, T. *J. Colloid Interface Sci.* **1980**, *75*, 51.

20. Somorjai, G. A.; *Chemistry in Two Dimensions - Surfaces*; Cornell University Press: Ithaca, New York, 1982.

21. Peterlinz, K . A.; Georgiadis, R. *Langmuir* **1996**, *12*, 4731.

22. Guo, L. -H.; Facci, J. S.; McLendon, G.; Mosher, R. *Langmuir* **1994**, *10*, 4588.

23. Laibinis, P. E.; Whitesides, G. M.; Allara, D. L.; Tao, Y.-T.; Parikh, A. N.; Nuzzo, R. G. *J. Am. Chem. Soc.* **1991**, *113*, 7152.

24. Schneider, T. W.; Buttry, D. A.; *J. Am. Chem. Soc.* **1993**, *115*, 12391.

25. Karpovich, D. S.; Blanchard, G. J. *Langmuir* **1994**, *10*, 3315.

26. Bensebaa, F.; Voicu, R.; Huron, L.; Ellis, T. H. *Langmuir* **1997**, *13*, 5335.

27. Castner, D. G.; Hinds, K.; Grainger, D. W. *Langmuir* **1996**, *12*, 5083.

28. Zener, R. W.; Sita, L. R. *Langmuir* **1997**, *13*, 2973.

29. Hatchett, D. W.; Uibel, R. H.; Stevenson, K. J. Harris, J. M.; White, H. S. *J. Am. Chem. Soc.* **1998**, *120*, 1062.

30. (a) Kwan, W. S. V.; Atanasoska, L.; Miller, L. L. *Langmuir.* **1991**, *7*, 1419. (b) Kwan, W. S. V.; Cammarata, V.; Miller, L. L.; Hill, M. G.; Mann, K. R. *Langmuir.* **1992**, *8*, 3003. (c) Sabatani, E.; Cohen-Boulakia, J.; Bruening, M.; Rubinstein, I. *Langmuir.* **1993**, *9*, 2974. (d) Dhirani, A.; Zener, R. W.; Hsung, R. P.; Guyot-Sionnest, P.; Sita, L. R. *J. Am. Chem. Soc.* **1996**, *118*, 3319.

31. (a) Chang, S. C.; Chao, I.; Tao, Y. *J. Am. Chem. Soc.* **1994**, *116*, 6792. (b) Tour, J. M.; Jones, L.; Pearson, D. L.; Lamba, J. J. S.; Burgin, T. P.; Whitesides, G. M.; Allara, D. L.; Parikh, A. N.; Atre, S. V. *J. Am. Chem. Soc.* **1995**, *117*, 9529.

32. Hutchison, J. E.; Postlethwaite, T. A.; Murray, R. W. *Langmuir.* **1993**, *9*, 3277.

33. Ulman, A.; Tillman, N. *Langmuir.* **1989**, *5*, 1418.

34. Schlenoff, J. B.; Li, M.; Ly, H. *J. Am. Chem. Soc.* **1995**, *117*, 12528.

35. (a) Dubois, L. H.; Zegarski, B. R.; *J. Electron Spectrosc. Rel. Phenom.* **1990**, *54/55*, 1143. (b) Nuzzo, R. G.; Korenic, K. M.; Dubois, L. H. *J. Chem. Phys.* **1990**, *93*, 767.

36. (a) Hautmann, J.; Klein, M. I. *J. Chem. Phys.* **1990**, *93*, 7483.(b) Hautmann, J.; Klein, M. I. *J. Chem. Soc. Farady Trans.* **1991**, *87*, 2031.

37. Castner, D. G.; Hinds, K.; Grainger, D. W. *Langmuir* **1996**, *12*, 5083.

38. Sauerbrey, G. Z. *Z. Phys.* **1959**, *155,* 206.

39. Buttry, D. A.; Ward, M. D. *Chem. Rev.* **1992**, *92,* 1355.

40. Nuzzo, R. G.; Dubois, L. H.; Allara, D. L. *J. Am. Chem. Soc.* **1990**, *112,* 558.

41. (a) Dorf, C. J.; Herschbach, D. R. *J. Phys. Chem.* **1982**, *86,* 3277. (b) Sandroff, C. J.; Garoff, S.; Leung, K. P. *Chem. Phys. Lett.* **1983**, *96,* 547. (c) Bryant, M. A.; Pemberton, J. E. *J. Am. Chem. Soc.* **1991**, *113,* 3629. (d) Bryant, M. A.; Pemberton, J. E. *J. Am. Chem. Soc.* **1991**, *113,* 8284.

42. Young, T. In *Miscellaneous Works;* Peacock, G., Edt. Murry: London, 1855; Vol 1, P. 418.

43. Langmuir, I. *Trans Faraday Soc.* **1920**, *15*, 62.

44. (a) Abbott, N. L.; Gorman, C. B.; Whitesides, G. M. *Langmuir* **1995**, *11*, 16. (b) Floker, J. P.; Laibinis, P. E.; Whitesides, G. M. *Langmuir* **1992**, *8*, 1330. (c) Bain, C. D.; Whitesides, G. M. *Langmuir* **1989**, *5*, 1370.

45. Bard, A. J. Faulkner, L. R. In *Electrochemical methods:Fundamentals and Applications*, John wiley & Sons, New York: 1980, chapter 12.

46. Caldwell, W. B.; campbell, D. J.; Chen, K.; Herr, B. R.; Mirkin, C. A.; Malik, A.; Durbin, M. k.; Dutta, P.; Huang, K. G. *J. Am. Chem. Soc.* **1995**, *117*, 6071.

47. (a) Sabatani, E.; Rubinstein, I.; Maoz, R.; Sagiv, J. *J. Electroanal. Chem.* **1987**, *219*, 365. (b) Sabatani, E.; Rubinstein, I. *J. Phys. Chem.* **1987**, *91*, 6663.

48. (a) Uosaki, K.; Sato, Y.; Kita, H. *Langmuir* **1991**, *7*, 1510. (b) Groat, K. A.; Creager, S. E. *Langmuir* **1993**, *9*, 3668. (c) French, M.; Creager, S. E. *Langmuir* **1998**, *14*, 2129.

49. Gardner, T. J.; Frisbie, C. D.; Wrighton, M. S. *J. Am. Chem. Soc.* **1995**, *117*, 6937.

50. Walczak, M. M.; Popenoe, D. D.; Deinhammer, R. S.; Lamp, B. D.; Chung, C.; Porter, M. D. *Langmuir* **1991**, *7*, 2687.

51. Yang, D.- F.; Morin, M. *J. Electroanal Chem.* **1997**, *429*, 1.

52. Caruso, F.; Serizawa, T.; Furlong, D. N.; Okhata, Y. *Langmuir* **1995**, *11*, 1546.

53. Hutt, D. A.; Copper, E.; Leggett, G. J. *J. Phys. Chem. B* **1998**, *102*, 174.

54. Mauradian, S.; Nelson, C. M.; Smith, L. M. *J.Am.Chem.Soc.* **1996**, *118*, 8639.

55. Hines, M. A.; Todd, J. A.; Guyot-Sionnest, P. *Langmuir* **1995**, *11*, 493.

56. Joyct, S. A.; Thomas, R. C.; Houston, J. E.; Michalske, T. A.; Crooks, R. M. *Phys. Rev. Lett* **1992**, *68*, 2790.

57. Evans, S. D.; Ulman, A. *Chem. Phys. Lett* **1990**, *170*, 462.

58. (a) Widrig, C. A.; Alves, C. A.; Porter, M. D.; *J. Am. Chem. Soc.* **1991**, *113*, 2805. (b) Widrig, C. A.; Chung, C.; Porter, M. D.; *J. Electroanal. Chem.* **1991**, *310*, 335.

59. (a) Strong, L.; Whitesides, G. M. *Langmuir* **1988**, *4*, 546 (b) Chidsey, C. E. D.; Loiacono, D. N. *Langmuir* **1990**, *6*, 682. (c) Dubois, L. H.; Zegarski, B. R.; Nuzzo, R. G. *J. Chem. Phys.***1993**, *98*, 678.

60. Poirier, G. E.; Tarlov, M. J.; Rushneier, H. E. *Langmuir.* **1994**, *10*, 3383.

61. Sellers, H.; Ulman, A.; Shnidman, Y.; Eilers, J. E. *J. Am. Chem. Soc.* **1993**, *115*, 9389.

62. Parikh, A. N.; Allara, D. L. *J. Chem . Phys.* **1982**, *96*, 927.

63. (a) Hautman, J.; Klein, M. L.; *J. Chem. Phys.* **1989**, *91*, 4994. (b) Hautman, J.; Klein, M. L. *J. Chem. Phys.* **1990**, *93*, 7483.

64. Bucher, J. -P.; Santesson, L.; Kern, K. *Langmuir.* **1994**, *10*, 979.

65. Sabatani, E.; Cohen-Boulakia, J.; Bruening, M.; Rubinstein, I. *Langmuir* **1993**, *9*, 2974.

66. McCarley, R. L.; Dunaway, D. J.; Willicut, R. J. *Langmuir.* **1993**, *9*, 2775.

67. Schönenberger, C.; Sondag-Huethorst, J. A. M.; Jorritsma, J.; Fokkink, L. G. J. *Langmuir* **1994**, *10*, 611.

68. Poirier, G. E.; Tarlov, M. J. *Langmuir.* **1994**, *10*, 2859.

69. Biebuyck, H. A.; Bain, C. D.; Whitesides, G. M. *Langmuir* **1994**, *10*, 1825.

70. Nuzzo, R. G.; Dubois, L. H.; Allara, D. L. *J. Am. Chem. Soc* **1990**, *112*, 558.

71. Li, Y.; Huang, J.; McIver, R. T.; Jr., Hemminger, J. C. *J. Am. Chem. Soc.* **1992**, *114*, 2428.

72. Walczak, M. W.; Chung, C.; Stole, S. M.; Widrig, C. A.; Porter, M. D. *J. Am. Chem. Soc.* **1991**, *113*, 2370.

73. Bain, C. D.; Biebuyck, H. A.; Whitesides, G. M. *Langmuir* **1989**, *5*, 723.

74. Fenter, P.; Eberhardt, A.; Eisenberger, P. *Science* 1994, 266, 1216.

75. NIshida, N.; Hara, M.; Sasabe, H.; Knoll, W. *Jpn. J. Appl. Phys.* **1996**, *35*, L799.

76. Ishida, T.; Yamamoto, S.; Mizutani, W.; Motomatsu, M.; Tokumoto, H.; Hokari, H.; Azehara, H.; Fujihira, M. *Langmuir* **1997**, *13*, 3261.

77. Poirer, G. E.; Pylant, E. D. *Science* **1996**, *272*, 1145.

78. Hatchett, D. W.; Uibel, R. H.; Stevenson, K. J.; Harris, J. M.; White, H. S. *J. Am. Chem. Soc.* **1998**, *120*, 1062.

79. Buck, M.; Grunze, M.; Eisert, F.; Fisher, J,; Träger, F. *J. Vac. Sci. Technol. A* **1992**, *10*, 926.

80. Hähner, G.; Wöll, Ch.; Buck, M.; Grunze, M. *Langmuir* **1993**, *9*, 1955.

81. (a) Peterlinz, K. A.; Georgiadias, R. *Langmuir* **1996**, *12*, 4731. (b) Debono, R. F.; Lucks, G. D.; Manna, D. D.; Krull, U. J. *Can. J. Chem.* **1996**, *74*, 677. (c) Fruböse, Ch.; Dolhofer, K. *J. Chem. Soc. Faraday Trans.* **1995**, *91*, 1949.

82. (a) Pan, W.; Durning, C. J.; Turro, N. J. *Langmuir* **1996**, *12*, 4469, (b) Schneider, T. W.; Buttry, D. A. *J. Am. Chem. Soc.* **1993**, *115*, 12391.

83. Evans, S. D.; Urankar, E.; Ulman, A.; Ferris, N. *J. Am. Chem. Soc.* **1991**, *113*, 4121.

84. Hickman, J. J.; Ofer, D.; Zou, C.; Wrighton, M. S.; Laibinis, P. E.; Whitesides, G. M. *J. Am. Chem. Soc.* **1991**, *113*, 1128.

85. (a) Collard, D. M.; Fox, M. A. *Langmuir* **1991**, *7*, 1192. (b) Groat, K. A.; Creager, S. E.; *Langmuir* **1993**, *9*, 3668. (c) Ravenscroft, M. S.; Finklea, H. O. *J. Phys. Chem.* **1994**, *98*, 3843. (d) Curtain, L. S.; Peck, S. R.; Tender, L. M.; Murray, R. W.; Rowe, G. K.; Creager, S. E. *Anal. Chem.* **1993**, *65*, 368.

86. Pan, J.; Tao, N.; Lindsay, S. M. *Langmuir* **1993**, *9*, 1556.

87. (a) Yang, D. -F.; Wilde, C. P.; Morin, M. *Langmuir* **1996**, *12*, 6570. (b) Yang, D.-F.; Wilde, C. P.; Morin, M. *Langmuir* **1997**, *13*, 243. JEC 1991, 310, 335.

88. Yang, D. -Y.; Al-Mazai, H.; Morin, M. *J. Phys. Chem. B* **1997**, *101*, 1158.

89. Jaffey, D. M.; Madix, R. J.; *J. Am. Chem. Soc.* **1994**, *116*, 3012.

90. (a) Bucher, J.-P.; Santesson, L.; Kern. K. *Langmuir* **1994**, *10*, 979. (b) Cavalleri, O.; Hirstein, A.; Kern, K. *Surf. Sci.* **1995**, *340*, L960. (c) Delamarche, E.; Michel, B.; Biebuyck, H. A.; Gerber, C. *Adv. Mater.* **1996**, *8*, 719. (d) Delamarche, E.; Michel, B.; *Thin Solid Films* **1996**, *273*, 54. (e) Camillone, N. et. al. *J. Chem. Phys.* **1994**, *101*, 11031.

91. Delamarche. E.; Michel, B.; Kang, H.; Gerber, Ch. *Langmuir* **1994**, *10*, 4103.

92. J. Q. Chambers In *Encyclopedia of Electrochemistry of the Organic Elements (organic section)*; Eds. Bard, A. J.; Lund, H. Vol XII, Marcel Dekker, Inc. New York and Basel, 1978, Chapter XII-3.

93. Chidsey, C. E. D.; Loiacono, D. N. *Langmuir* **1990**, *6*, 682

94. (a) Becka, A. M.; Miller, C. J. *J. Phys. Chem.* **1993**, *97*, 6233. (b) Miller, C. J.; Grädzel, M. *J. Phys. Chem.* **1991**, *95*, 5225. (c) Becka, A. M.; Miller, C. J. *J. Phys. Chem.* **1992**, *96*, 2657. (d) Terrettaz, S.; Becka, A. M.; Traub, M. J.; Fettinger, J. C.; Miller, C. J. *J. Phys. Chem.* **1995**, *99*, 11216. (e) Sinniah, K.; Cheng, J.; Terrettaz, S.; Reutt-Robey, J.; Miller, C. J. *J. Phys. Chem.* **1995**, *99*, 1500. (f) Cheng, J.; Saghi-Sjabo, G.; Tossell, J. A.; Miller, C. J. *J. Am. Chem. Soc.* **1996**, *118*, 680.

95. Nahir, T. M.; Bowden, E. F. *Electrochim. Acta* **1994**, *39*, 2347.

96. (a) Chidsey, C. E. D.; Bertozzi, C. R.; Putvinski, T. M.; Mujsce, A. M. *J. Am.. Chem. Soc.* **1990**, *112*, 4301. (b) Uosaki, K.; Sato Y.; Kita, H. *Langmuir* **1991**, *7*, 1510. (c) Chidsey, C. E. D. *Science* **1991**, *251*, 919. (d) Rowe, G. K.; Creager, S. E. *Langmuir* **1994**, *10*, 1186.

97. (a) Spinke, J.; Liley, M.; Guder, H.-J.; Angermaier, L.; Knoll, W. *Langmuir* **1993**, *9*, 1821. (b) Spinke, J.; Liley, M; Schmitt, F.-J.; Guder, H.-J.; Angermaier, L.; Knoll, W. *J. Chem. Phys.* **1993**, *99*, 7012. (c) Häussling, L.; Michel, B.; Ringsdorf, H.; Rohrer, H. *Angew Chem. Int. Ed. Engl.* **1991**, *30*, 679.

98. Obeng, Y. S.; Bard, A. J. *Langmuir* **1991**, *7*, 195.

99. Yip, C. M.; Ward, M. D. *Langmuir* **1994**, *10*, 549.

100.(a) Zak, J.; Yuan, H.; Woo, K.; Porter, M. D. *Langmuir* **1993**, *9*, 2772. (b) Hutchinson, J. E.; Postlethwaite, T. A.; Murray, R. W. *Langmuir* **1993**, *9*, 3277.

101. Herr, B. R.; Mirkin, C. A.; *J. Am. Chem. Soc.* **1994**, *116*, 1157.

102. (a) Finklea, H. O.; Hanshew, A. A. *J. Am. Chem. Soc.* **1992**, *114*, 3173. (b) Chidsey, C. E. D.; Putvinski, T. M. *J. Am. Chem. Soc.* **1992**, *114*, 8771.

103. Chidsey, C. E. D. *Science* **1991**, *251*, 919.

104. Laviron, E. *J. Electroanal Chem.* **1979**, *101*, 19.

105. Wirth, M. J.; Fairbank, R. W. P.; Fatunmbi, H. O. *Science* **1997**, *275*, 44.

106.(a) Prime, K. L.; Whitesides, G. M. *Science* **1991**, *252*, 1164. (b) *Angew. Chem.Int. Ed. Engl.* **1994**, *33*, 871. (c) *J. Am. Chem. Soc.* **1994**, *116*, 2225. (d) *Science* **1997**, *275*, 44. (e) *Langmuir* **1997**, *13*, 5559. (f) *J. Electroanal. Chem.* **1995**, *394*, 149. (g) *J. Chem. Soc., Faraday Trans.* **1997**, *93*, 1367. (h) *J. Am. Chem. Soc.* **1998**, *120*, 225.

107.(a) Sondag-Huethorst, J. A.; van Helleputte, H. R.; Fokkink, L. G. *Appl. Phys. Lett.* **1994**, *64*, 285. (b) Marrian, C. R.; Perkins, F. K.; Brandow, S. L.; Koloski, T. S.; Dobisz, E. A.; Calvert, J. M. *Appl. Phys. Lett.* **1994**, *64*, 390.

108.(a) Wollman, E. W.; Kang, D.; Frisbie, C. D.; Lorkovic, I. M.; Wrighton, M. S. *J. Am. Chem. Soc.* **1994**, *116*, 4395. (b) Rozsnyai, L. F.; Wrighton, M. S. *J. Am. Chem. Soc.* **1994**, *116*, 5993. (c) Huang, J. Y.; Dahlgren, D. A.; Hemminger, J. C. *Langmuir* **1994**, *10*, 626.

109.(a) Kumar, A.; Whitesides, G. M. *Appl. Phys. Lett.* **1993**, *63*, 2002. (b) Kumar, A.; Whitesides, G. M. *Science* **1994**, *263*, 60. (c) *Appl. Phys. Lett.* **1997**, *70*, 7. (d) *Appl. Phys. Lett.* **1997**, *70*, 2464.

110. Kumar, A.; Biebuyck, H. A.; Abbott, N. L.; Whitesides, G. M. *J. Am. Chem. Soc.* **1992**, *114*, 9188.

111. (a) Abbott, N. L.; Kumar, A.; Whitesides, G. M. *Chem. Mater.* **1994**, *6*, 596. (b) Abbott, N. L.; Whitesides, G. M. *Langmuir* **1994**, *10*, 1493. (c) Abbott, N. L.; Whitesides, G. M.; Racz, L. M.; Szekely, J. *J. Am. Chem. Soc.* **1994**, *116*, 290.

112. Tarlov, M. J.; Burgess, D. R.; Gillen, G. *J. Am. Chem. Soc.* **1993**, *115*, 5305.

113. Abott, N. L.; Gorman, C. B.; Whitesides, G. M. *Langmuir* **1995**, *11*, 16.

114. (a) Scoer, J. K.; Ross, C. B.; Crooks, R. M.; Corbitt, T. S.; Hampden-Smith, M. J. *Langmuir* **1994**, *10*, 615. (b) Ross, C. B.; Sun, L.; Crooks, R. M. *Langmuir* **1994**, *9*, 632. (c) Tiberio, R. C.; Craighead, H. G.; Lercel, M.; Lau, T.; Sheen, C. W.; Allara, D. L. *Appl. Phys. Lett.* **1993**, *10*, 476.

115. Kumar, A.; Abbott, N. L.; Kim, E.; Biebuyck, H. A.; Whitesides, G. M. *Acc. Chem. Res.* **1995**, *28*, 219 and references there in).

116. Bunker, B. C.; Rieke, P. C.; Tarasevich, B. J.; Campbell, A. A.; Fryxell, G. E.; Graff, G. L.; Song, L.; Liu, J.; Virden, J. W.; McVay, G. L. *Science* **1994**, *264*, 48.

117. (a) Meldrum, F. C.; Flath, J.; Knoll, W. *Langmuir* **1997**, *13*, 2033. (b) Kumar, A.; Biebuyck, H. A.; Whitesides, G. M. *Langmuir* **1994**, *10*, 1498. (c) Dressick, W. J.; Dulcey, C. S.; Georger, J. H.; Calvert, J. M. *Chem. Mater.* **1993**, *5*, 148. (d) Dunaway, D. J.; McCarley, R. L. *Langmuir* **1994**, *10*, 3598. (e) Smith, E. L.; Alves, C. A.; Anderagg, J. W.; Porter, M. D. *Langmuir* **1992**, *8*, 2707.

118. Agarwal, M.; De Guire, M. R.; Heuer, H. *J. Am. Ceram. Soc.* **1997**, *80*, 2967.

119. (a) Laibinis, P. E.; Whitesides, G. M. *J. Am. Chem. Soc.* **1992**, *114*, 9022. (b) Yamamoto, Y.; Nishihara, H.; Aramaki, K. *J. Electrochem. Soc.* **1993**, *140*, 436. (c) Itoh, M.; Nishihara, H.; Aramaki, K. *J. Electrochem. Soc.* **1995**, *142*, 3696. (d)

Haneda, R.; Nishihara, H.; Aramaki. K. *J. Electrochem. Soc.* **1997**, *144*, 1216. (e) Feng, Y.; Teo, W.-K.; Siow, K.-S.; Gao, Z.; Tan, K.-L.; Hsieh, A.-K. *J. Electrochem. Soc.* **1997**, *144*, 55. (f) Zamborini, F. P.; Campbell, J. K.; Crooks, R. M. *Langmuir* **1998**, *14*, 640.

120. (a) McCarley, R. L.; Bard, A. J. *J. Phys. Chem.* **1989**, *62*, 7410. (b) Sawaguchi, T.; Yamada, T.; Okinaka, Y.; Itaya, K. *J. Phys. Chem.* **1995**, *99*, 14155. (c) Sun, L.; Crooks, R. M.; *Langmuir* **1993**, *9*. 1951. (d) Zamborini, F. P.; Crooks, R. M. *Langmuir* **1997**, *13*, 122.

121. Scherer, J.; Vogt, M. R.; Magnussen. O. M.; Behm, R. J. *Langmuir* **1997**, *13*, 7045.

122. Duan, C.; Meyerhoff, M. E. *Anal. Chem.* **1994**, *66*, 1369.

123. (a) Hickman, J.J.; Ofer, D.; Laibinis, P. E.; Whitesides, G. M.; Wrighton, M. S. *Science* **1991**, *252*, 688, (b) Rojoa, M. T.; Kaifer, A. E. *J. Am.Chem.Soc.* **1995**, *117*, 5883.

124. Thomas, R. C.; Sun, Li.; Crooks, R. M. *Langmuir* **1991**, *7*, 620.

125. Schierbaum, K. D.; Weiss, T.;ThodenvanVelzen. E. U.; Engbersen, J. E. J.; Reinnoudt, D. N.; Gopel, W. *Science* **1994**, *265*, 1413.

126. (a) Willner, I.; Riklin, A. *Anal. Chem.* **1994**, *66*, 1535. (b) Creager, S. E.; Olsen, K. G.; *Anal. Chem. Acta* **1995**, *307*, 277.(c) Jung, S. -K.; Wilson, G. S. *Anal. Chem.* **1996**, *68*, 591.

127. (a) Turyan, I.; Mandler, D. *Anal. Chem.* **1997**, *69*, 894. (b) Rubinstein, I.; Steinberg, S.; Tor, Y.; Shanzer, A.; Sagiv, J. *Nature* **1988**, *332*, 426. (c) Turyan, I.; Mandler, D. *Anal. Chem.* **1994**, *66*, 58.

128. Whitesides, G. M. *Tibtech* **1995**, *13*, 228.

129. (a) Rojas, T. M.; Königer, R.; Stoddart, J. F.; Kaifer, A. E. *J. Am. Chem. Soc.* **1995**, *117*, 336. (b) *Angew. Chem.Int. Ed. Engl.* **1995**, *34*, 235. (c) *Science* **1994**, *265*, 1413. (d) Henke, C.; Steinem, C.; janshoff, A.; Steffan, G.; Luftmann, H.; Sieber, M.; Galla, H.-J. *Anal. Chem.* **1996**, *68*, 3158.

130. (a) Doron, A.; Katz, E.; Willner, I., *Langmuir*, **1995**, *11*, 1313. (b) Chumanov, G.; Sokolov, K.; Gregory, B.W.; Cotton, T.M., *J.Phys.Chem.*, **1995**, *99*, 9466. (c) Grabar, K.C.; Freeman, R.G.; Hommer, M.B.; Natan, M.J., *Anal. Chem.*, **1995**, *67*, 735. (d) Grabar, K.C.; Allion, K.J.; Baker, B.E.; Bright, R.M.; Brown, K.R.; Freeman, R.G.; Fox, A.P.; Keating, C.D.; Musick, M.D.; Natan, M. J. *Langmuir* **1996**, *12*, 2353. (e) Colvin, V.L.; Goldstein, A.N.; Alivisatos, A. P. *J. Am.Chem. Soc.*, **1992**, *114*, 5221. (f) Colvin, V.L.; Alivisatos, A.P.; Tobin, J. G., *Phys.Rev.Lett.*, **1991**, *66*, 2786.

131. (a) Zhao, X.K.; Zhu, S.; Fendler, J.H. *Langmuir* **1991**, *7*, 520. (b) Yi, K.C.; Horvolgyi, Z.; Fendler, J.H. *J.Phys.Chem.* **1994**, *98*, 3872.

132.(a) Urquhart, R.S.; Furlong, D.N.; Gegenbach, T.; Geddes, N.J.; Grieser, F. *Langmuir* **1995**, *11*, 1127. (b) Zylberaijch, C.; Ruadel-Teixier, A.; Barraud, A. *Synth.Met.* **1988**, *27*, B609.

133.Brust, M.; Walker, M.; Bethell, D.; Schriffin, D. J.; Whyman, R. *J. Chem. Soc., Chem. Commun.* **1994**, 801.

134.Terril, R. H.; Postlethwaite, T. A.; Chen, C.-H, Poon, C.-D.; Terzis, A.; Chen, A.; Hutchison, J. E.; Clark, M. R.; Wignall, G.; Londono, J. D.; Superfine, R.; Falvo, M.; Jonson, C. S.Jr.; Samulski, E. T.; Murray, R. W. *J. Am. Chem. Soc.* **1995**, *117*, 12537.

135. (a) Badia, A.; Demers, L.; Dickinson, L.; Morin, F. G.; Lennox, R. B.; Reven, L. *J. Am. Chem. Soc.* **1997**, *119*, 11104. (b) Ingram, R. S.; Hostetler, M. J.; Murray, R. W.; Schaaff, T. G.; Khoury, J. T.; Whetten, R. L.; Bigioni, T. P.; Guthrie, D. K.; First, P. N. *J. Am. Chem. Soc.* **1997**, *119*, 9279. (c) Hostetler, M. J.; Wingate, J. E.; Zhong, C.-J.; Harris, J. E.; Vachet, R. W.; Clark, M. R.; Londono, J. D.; Green, S. J.; Stokes, J. J.; Wignall, G. D.; Glish, G. L.; Porter, M. D.; Evans, N. D.; Murray, R. W. *Langmuir* **1998**, *14*, 17 and references there in.

136. Hostetler, M. J.; Stokes, J. J.; Murray, R. W. *Langmuir* **1996**, *12*, 3604.

137. (a) Lee, H.; Kepley, L. J.; Hong, H.-G.; Mallouk, T. E. *J. Am. Chem. Soc.* **1988**, *110*, 618. (b) Putvinski, T. M.; Schilling, M. L.; Katz, H. E.; Chidsey, C. E. D.; Mujsce, A. M.; Emerson, A. B. *Langmuir* **1990**, *6*, 1567. (c) Katz, H. E.; Scheller, G.; Putvinski, T. M.; Schilling, M. L.; Wilson, W. L.; Chidsey, C. E. D. *Science* **1991**, *254*, 1485.

138. (a) Evans, S. D.; Ulman, A.; Goppert-Berarducci, K. E.; Gerenser, L. J. *J. Am. Chem. Soc.* **1991**, *113*, 5866. (b) Freeman, T. L.; Evans, S. D.; Ulman, A. *Langmuir* **1995**, *11*, 4411. (c) Evans, S. D.; Flynn, T. M.; Ulman, A. *Langmuir* **1995**, *11*, 3811. (d) Brust, M.; Blass, P. M.; Bard, A. J. *Langmuir* **1997**, *13*, 5602.

Chapter 2

Self-Assembled Monolayer of NaphthaleneDisulfide on Polycrystalline Gold, Silver and Copper Surfaces

---

This chapter deals with the study of self-assembled monolayer formation of naphthalenedisulfide (NDS) on polycrystalline gold surface. The monolayer structure and ion permeation behavior are characterized by using ellipsometry, X-ray photoelectron spectroscopy (XPS), electrochemistry and Scanning tunneling microscopy (STM). XPS studies show the presence of two different sulfur environments in the monolayer with a binding energy difference of 6.3 eV, while electrochemical measurements indicate an unusual loss of redox activity during voltammetric cycling. The rate constant of a fast redox couple like $Fe(CN)_6^{3-/4-}$ has been decreased from 2.6×10^{-2} to 9.4×10^{-4} cm/s due to the partial barrier provided by the monolayer rather than a complete blocking of electron transfer. The STM image further confirms the presence of defects (as pinhole) on the monolayer surface in agreement with the residual current observed in voltammograms.

---

* A portion of this chapter has appeared recently in *Langmuir* **1997**, *13*, 866 and another part has been accepted in *J. Electroanal. Chem.* (1998, in press)

2.1. Introduction:

Preparation and characterization of structurally well defined organic monolayers on solid surfaces by self-assembly has attracted much attention in recent years.[1] Such assemblies could provide a means to control the chemical and physical properties of interfaces for a variety of heterogeneous phenomena including catalysis,[2] corrosion,[3] lubrication[4] and adhesion.[5] Although linear alkanethiols are the most widely studied and well characterized class of compounds known to form self-assembled monolayers (SAMs), organodisulfide compounds were the first members used for this type of monolayer formation on polycrystalline gold surfaces.[6] It is interesting to study the self-assembly of disulfide compounds of relatively small molecules not containing the ordering influence of a "*hydrophobic*" hydrocarbon chain[7] as is the molecule used in this study. More significantly, by selecting disulfides with planar π-systems such as naphthalene, the influence of the aromatic ring that constrains the sulfur to a particular geometry on SAM formation can be studied. In addition, the experimental results obtained on these systems are expected to verify the prediction of Ulman and Scaringe[8] that, for self-assembly, *amphifunctionality* of the SAM forming molecule is more integral to monolayer formation than *amphiphilicity*. Several disulfide compounds have been investigated to date[9] and it has generally been believed that, during the formation of SAMs dissociative chemisorption takes place leading to the formation of two identical Au-S bonds (the thiolate bond).[10]

The present chapter deals with the study of self-assembled monolayer formation of NDS on polycrystalline gold surface and its characterization by ellipsometry, XPS, electrochemistry and STM. Earlier XPS reports regarding the SAM formation of disulfides on Au have identified only one type of sulfur signal, even for cyclic disulfides.[9b] Contrary to these results, in this chapter, a strong evidence for two distinct sulfur species from the NDS SAM on Au is presented. Similar types of sulfur signals have been observed for SAMs of *n*-alkane thiols on Cu and Ag surfaces, with different binding energies (BEs) very close to that observed in this study. One possible explanation for the different sulfurs observed could be due to inequivalent bonding

sites (three-fold vs quasi-bridge coordination).[11] Considering the inherent rigidity imparted by the aromatic ring on the sulfurs, the XPS results mentioned here are novel and extremely interesting as the disulfide molecule of this study (the two sulfurs are constrained to be ~2.4 Å apart), could serve as a valuable tool to study the effect of geometric constraint on SAM formation. This may also provide new information through control experiments on single crystal Au (111) surface on the issue of whether organothiols and disulfides bind as thiolates or disulfides. In addition, double layer capacitance and cyclic voltammetric measurements have been included to confirm the monolayer formation and redox activity respectively of the surface bound disulfide molecule.

2.2. Experimental:

2.2.1. Materials

NDS was prepared by the reported procedure[12] and its purity was found to be 99.99% by GC-Mass and NMR studies. Double distilled water was passed through Milli-Q system to get deionized highly pure water (R = 18 M Ω cm) and was used through out. Tetrabutylammonium tetrafluoroborate, KF, $K_3Fe(CN)_6$, $K_4Fe(CN)_6$ all were received from Aldrich and were used as received. All solvents were of reagent grade and were distilled following usual procedure before using.

2.2.2. Preparation of Substrates

The gold substrates were prepared by thermal evaporation onto clean glass substrate under high vacuum conditions (pressure better than 10^{-6} torr) in an Edward E 306 coating unit. Before deposition, glass substrates were cut into required size to use as electrode substrate. Visible contaminants were removed by wiping with tissue paper followed by chemical cleaning by immersion in 1:4 H_2O_2/concentrated H_2SO_4 (piranha) at 70°C for about 30 minutes, rinsed with double distilled water and blown dry in a stream of Ar. The glass slides were then placed in an oven at 105°C for about 10-15 minutes. Substrates cleaned by this procedure were transformed to the vacuum

evaporator for gold deposition. A 5 nm thick chromium buffer layer was used to improve the adhesion of the Au film. This procedure produced polycrystalline Au film with strong (111) texture. All substrates were stored in polypropylene containers.

2.2.3. Preparation of Monolayer

The freshly evaporated gold coated glass samples were cleaned through repeated 30 sec exposure to 323 K sulfochromic acid (saturated $K_2Cr_2O_7$ in concentrated H_2SO_4) and to 3% HF. Extensive rinsing of the substrates with de-ionized water (Milli-Q system) followed each of these exposures. Extensive pretreatment is likely to leave the gold surface oxidized which can not be removed by water rinsing. The cleaning with sulfochromic acid was performed for a few seconds, which is sufficient to remove the organic impurities but provides inadequate exposure to form oxide layer. The reproducible surface properties of gold electrodes were checked by taking cyclic voltammogram with bare gold in aqueous solution of $Fe(CN)_6^{3-/4-}$ couple or in 0.1 M KOH to get a similar response reported in the literature.[13] After three such cycles, the electrodes were immediately transferred into a deaerated 1 mM solution of the compound in acetonitrile. The exposure time was typically two hours and no attempt was made to exclude the dissolved oxygen from solution. The substrates were removed after specified monolayer formation time and rinsed with the solvent and absolute ethanol, then dried in a stream of highly pure argon.

2.2.4. Ellipsometric Measurement

Ellipsometry measurements were made on the SAMs using a Gaertner L 119 null ellipsometer operated in the PCSA (polarizer-compensator-substrate-analyzer) mode. The light source was a He-Ne laser (λ = 632.8 nm) operated at 5 mV. For the calculation of film thickness and refractive index, the dielectric function of the bare Au substrate was determined by ellipsometry. The calculations were performed using an application written in Mathcad for a simple one layer model.[14] Considering a value of l.6 for the refractive index n, (a value of 1.5 is applicable in the case of alkane disulfides/thiols;[9b] benzene, an aromatic compound has n = 1.6), the film thickness was

estimated to be ~ 7 Å. This value is in good agreement with the molecular dimension obtained from a space filling model. Using the same procedure and a refractive index of 1.5, ellipsometric thickness measurement of octadecanethiol (ODT) on the same Au surface estimated thickness value of ~ 2.5 nm which is in excellent agreement with the reported ones.[15]

2.2.5. X-ray Photoelectron Spectroscopy:

XPS measurements were performed on the SAMs using a VG Scientific ESCA 3 MK II spectrometer operated at a pressure of better than 10^{-9} Torr. The different core level spectra were recorded using Mg Kα radiation (hν = 1253.6 eV) with the X-ray source operated at a power of 400 W and at an electron takeoff angle (ETOA, defined as the angle between electron emission direction and surface parallel) of 54°. The time interval between preparation of the SAM and mounting in the XPS chamber was typically 2 hours (due to the intermediate characterization time involved in ellipsometry). The core level spectra of the C 1s, Au 4f, O 1s and S 2p orbitals were recorded at an overall instrumental resolution of ~ 1 eV. A large window general scan did not show the presence of any impurities. The background subtraction was done by the Shirley method.[16] The alignment of the binding energy (BE) was done using the Au 4f binding energy of 84 eV as reference. The X-ray flux was kept low to reduce beam-induced damage (electron power 70W).

2.2.6. Electrochemical Characterization

Impedance and cyclic voltammetric measurements were performed using a three-electrode cell comprising of a gold coated glass as the working electrode, a large area platinum flag counter electrode and a saturated calomel reference electrode (SCE). Cyclic voltammetry and impedance measurements were carried out with a PAR 283 potentiostat/galvanostat and a PAR 5012 lock-in amplifier interfaced with a computer. Impedance measurements were performed at 5 mV rms at the formal potential of the redox couple and readings were taken at 5 discrete frequencies per decade. Automatic data acquisition was carried out using EG&G M 388 software and a

commercially available program EQUIVALENT CIRCUIT written by B. A. Boukamp (University of Twente) was used to analyze the impedance data which determined the parameters of the assumed equivalent circuit by a weighted nonlinear regression procedure. It is difficult to extract charge-transfer resistance (R_{ct}) from impedance plot when well-defined semicircle is not obtained in the higher frequency range. Depending on the individual case non-linear fitting can be tried to get the desired parameter. It is not tried to obtain the R_{ct} value of bare gold electrode in the solution of $Fe(CN)_6^{3-/4-}$ couple, since the electron-transfer of the redox couple is very fast. It is calculated indirectly by taking the value of rate constant as 2.6×10^{-2} cm/s.[17] Impedance response of respective monolayer modified electrodes were analyzed with commercially available impedance software using non-linear regression procedure to obtain the respective R_{ct} values. The quality of the fit can be estimated by the χ^2 (chi-squared) value, which was found to be less than 10^{-5} confirming a reasonably good fit and these values were used in subsequent calculations. Cyclic voltammetry was performed in a solution containing only one oxidation state of the redox couple like 1 mM of $K_3Fe(CN)_6$ in 0.1 M KF. Solutions used for impedance measurements always contained equal concentrations of the oxidized and reduced form of redox couple like 5 mM of both $K_3Fe(CN)_6$ and $K_4Fe(CN)_6$ in 0.5 M of KF in a frequency range of 100 KHz to 0.1 Hz. All experiments were carried out at room temperature (298 ± 0.1 K). Double layer capacitance were calculated from impedance response by taking in 0.1 M KF and extrapolating the linear portions of the plots of log(absolute impedance) vs log (ω) = 0. Double layer capacitance of the disulfide treated Au electrodes were measured from cyclic voltammograms performed from -100 mV to + 500 mV in 0.1 M KF solution at a scan rate of 500 mV/s. The current from the positive and negative scan direction at + 200 mV was summed and divided by twice the scan rate and normalized by the actual area of the electrode to obtain the reported capacitance. The surface roughness factor (R = actual/geometrical surface area) of the Au was determined according to standard literature procedure where the charge required to cathodically reduce the oxide layer was used for the calculation.[18]

2.2.7. Scanning Tunneling Microscopy

The samples (bare gold as well as gold with the SAM of NDS) were investigated by Nanoscope-II (Digital instruments Inc., CA) STM at room temperature in air. The tunneling tips used were mechanically cut Pt-Ir (80:20) probes and no sample treatment was performed prior to STM imaging in a constant height mode. Typical image acquisition times were 150-200 seconds per image and the images consisted of 400 scan lines and 400 pixels each. Sample bias voltages were varied from -300 mV to 800 mV with set point currents of 0.2 nA. The apparatus was enclosed in an air tight box for reducing the noise due to air turbulence and simple low pass filtering was used to remove high frequency noise before recording the final images. To ensure that the data collected were representative of the particular film surface morphology, multiple images were taken. Although continuous rescanning of an area did not change the image significantly, Pt-Ir tips were frequently changed in order to eliminate any tip-surface artifacts.

2.3. Results and Discussion:

2.3.1. X-ray photoelectron spectroscopy

In order to determine the S 2p BEs as accurately as possible, a non-linear least squares fit of the data has been performed using two Gaussian pairs consisting of the spin-orbit components separated by 1.15 eV[19] (Figure 2.1). Based on the fits, we find that there are two species of sulfurs separated by a difference in binding energy of 6.3 eV. The lower BE peak at 162.8 eV agrees well with that reported in literature for chemisorbed disulfide sulfur species on Au.[9a] For comparison purpose, XPS measurements have also been performed on the bulk powder sample of the present disulfide compound, although the S 2p spectrum (Figure 2.2) shows only a single S 2p component with a BE of 163.7 eV which is typical of an undissociated disulfide.[9a] It is well known that the difference in binding energies of the dissociated and undissociated sulfurs in such compounds is ~ 2 eV.[9a] However, the shift of 6.3 eV observed by us, negates the possibility of an undissociated sulfur component and hence rules out the possibility of multilayer formation. Although, two types of XPS signals can arise in

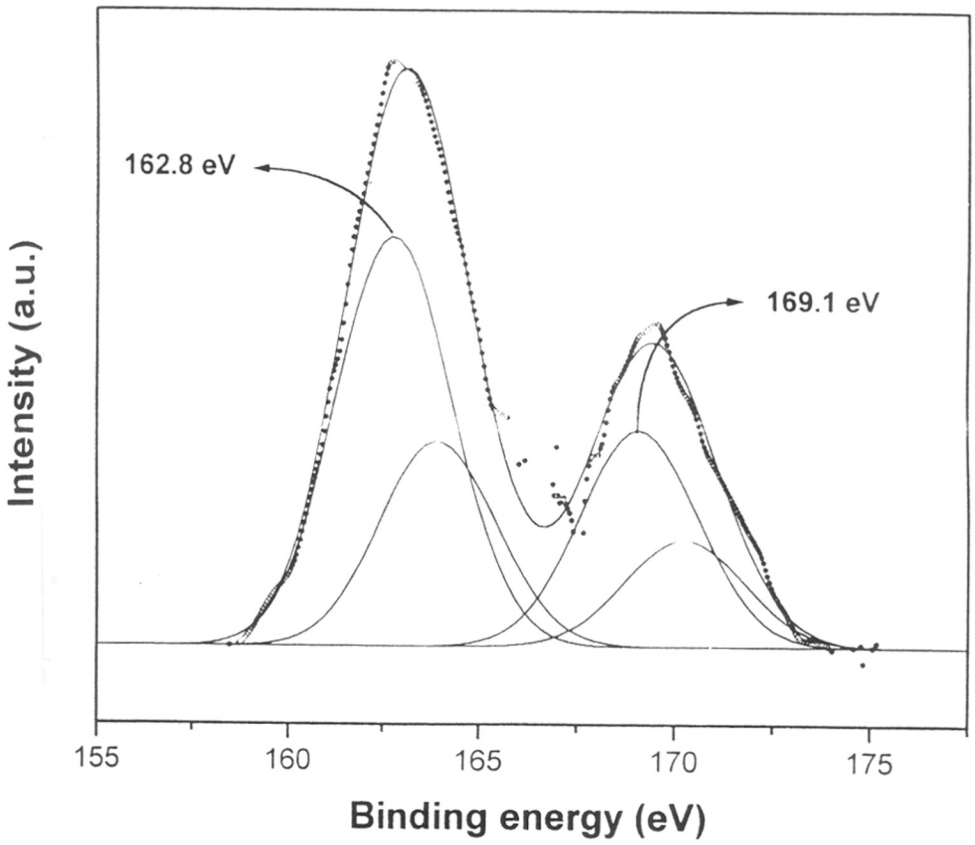

Figure 2.1. XPS spectrum showing the S 2p core level region of the NDS monolayer on gold together with the non-linear least square Gaussian fits with spin-orbit splitting of 1.15 eV.

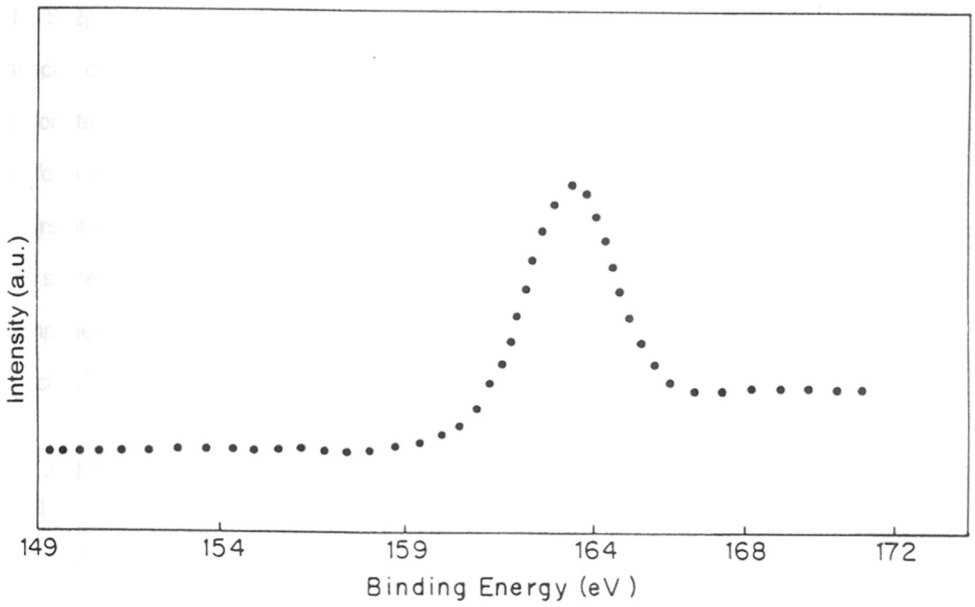

Figure 2.2. XPS spectrum showing the S 2p core level region of NDS in powder form.

principle due to inequivalent bonding sites (namely Au three fold hollow site and Au bridge site)[11] on the gold surface, it is believed that the observed BE difference is too large to account for this explanation. This belief is motivated by the fact that such shifts are characteristic of sulfur coordination with a highly electronegative element such as oxygen.[20] Different coordination to the Au surface can affect the measured BEs through differences in screening which is expected to be much smaller than that observed. We therefore assign the high BE S 2p component at 169.1 eV to a *sulfonate* moiety.[19] The S : O ratio as determined from the core level peak areas corrected for ionization cross section variation is 1 : 4.5 which is fairly close to the expected ratio of 1 : 3 and strengthens our assignment of the high BE S 2p signal. This large BE shift in the S 2p signal observed in this case is similar to that reported for the S 2p XPS spectra of octadecane thiolate monolayers on Ag and Cu.[19] However, the formation of sulfonate species on Cu and Ag surfaces were observed only in samples exposed to air for a couple of weeks whereas we see evidence for this species even after only two hours of exposure to air. For comparison, the XPS spectrum of ODT is also taken on the same surface (figure not shown) where the S 2p spectrum shows only a single component with a binding energy of ~ 162.4 eV, which is typical of Au-S thiolate species.[19]

2.3.2. Electrochemistry of the Compound in Solution and in Adsorbed State.

Cyclic voltammetry is an effective technique to demonstrate the structural integrity and ease of electron transfer across the thin barrier formed by SAMs. The observed redox activity of the disulfide compound is due to the one electron oxidation of the cyclic disulfide to form a stable radical cation (an aromatic dithiolylium cation).[21] The cyclic voltammogram of the compound in acetonitrle/0.1 M Bu_4NBF_4 with a platinum disk as working electrode in Figure 2.3 exhibits a reversible oxidation/reduction wave at $E_{1/2}$ = + 0.79 V vs SCE (ΔEp = 70 mV , i_{pa}/i_{pc} = 1). The expected normal two electron reduction of disulfide leading to the S-S bond cleavage is noted to be absent here. In the monoanion of the compound of this study, sulfur atoms are retained within the bonding distance of the rigid naphthalene backbone and further

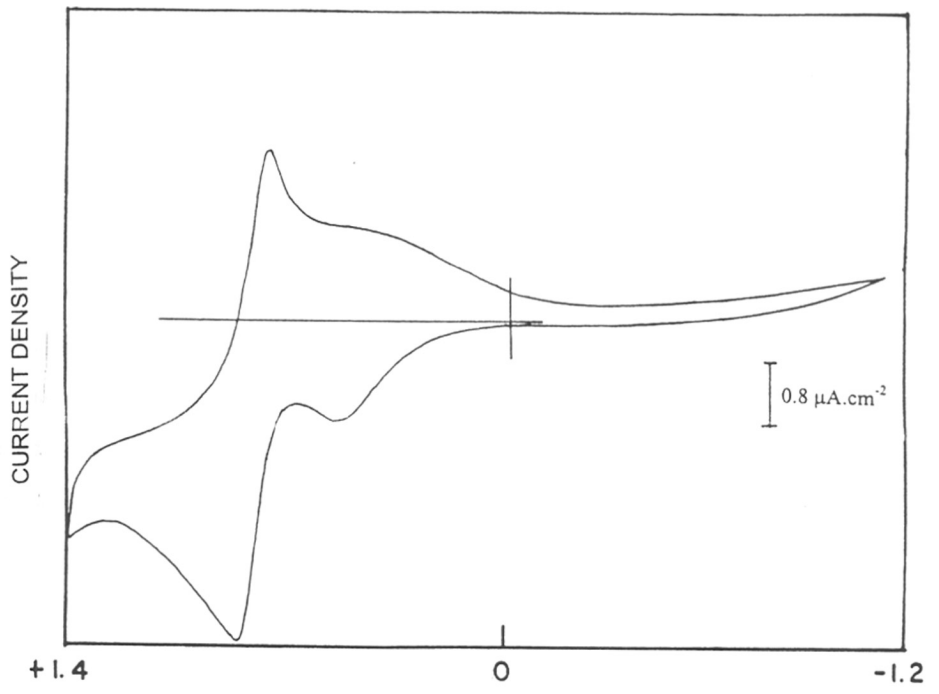

Figure 2.3. Cyclic voltammogram of NDS (10^{-3} M) in acetonitrile with 0.1 M tetrabutyl ammonium tetrafluoroborate as supporting electrolyte and platinum disk as working electrode. Scan rate is 200 mV/s.

reduction is made difficult by electronic repulsion.[22] The anodic as well as the cathodic peaks in the voltammogram are not symmetric in nature indicating the possibility of strong adsorptive interactions of both oxidized and reduced species. In addition, a response similar to the surface confined species is also indicated by the symmetrical reversible peak around $E_{1/2}$ = + 0.50 V and the broadness suggests a decrease in the rate of the heterogeneous electron transfer.

An estimation of the double layer capacitance provides an additional means to examine the uniformity and compactness of SAMs as well as its permeability to simple ionic species. Double layer capacitance is measured from cyclic voltammetry[23] in 0.1 M KF solution at + 200 mV with a scan rate of 500 mV/sec. Prior to the measurement of capacitance, the roughness factor of the gold substrates are measured to be 1.8 to 2 using the reported procedure.[18] The roughness factor of the substrates is high compared to the commonly observed value (1.2) for evaporated gold films. In the present case the gold film has not been annealed after evaporation which may be one of the reasons for high roughness factor. These values are used throughout the study to calculate the differential capacitance values. A decrease in the double-layer capacitance value from 20.78 $\mu F/cm^2$ (for bare gold) to 14.58 $\mu F/cm^2$ (gold coated with monolayer) indicates that the separation of charge between the electrolyte solution and gold substrate has increased and/or polarizability of the intervening medium has decreased. It is well known that for an electrochemical double layer, the differential capacity decreases with an increasing separation between the electrode surface and the plane of closest approach of the ionic charges.[15] In comparison, a double layer capacitance value of 1.4 $\mu F/cm^2$ is obtained for ODT on same substrate which is in good agreement with the literature value[15]. The reduction in the double layer capacitance upon SAM formation is less for the present molecule compared to ODT and this could be attributed to smaller molecular dimension for NDS. Figure 2.4 shows a plot of electrode potential against the double layer capacitance values for bare gold, NDS and ODT modified gold electrodes. A potential dependence of capacitance can be observed similar to that for bare gold. However, the maxima corresponding to the

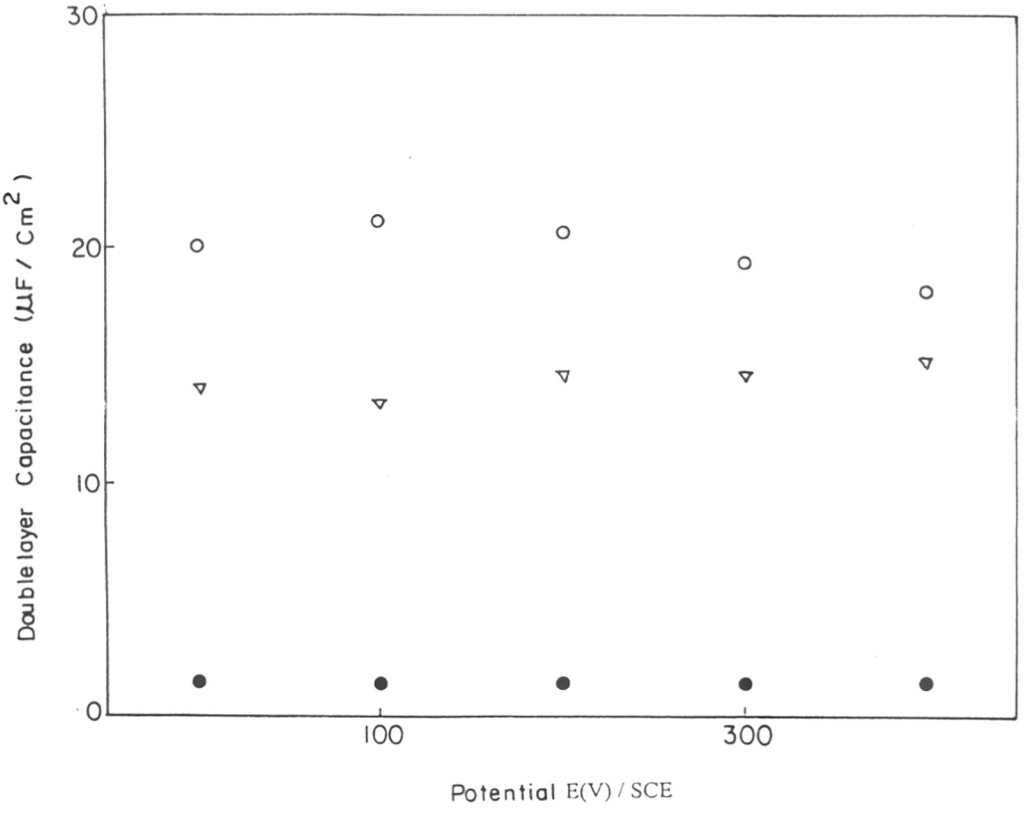

Figure 2.4. Electrode capacitance measurement from cyclic voltammograms at several potentials;(O) bare gold electrode; (▽) NDS modified Au electrode; (●) ODT modified Au electrode; in 0.1 M KF solution.

potential of zero charge (PZC) is not clear for NDS SAM on gold unlike the case for bare gold.

A comparison of the voltammograms taken with platinum disk electrode in Figure 2.3 with that taken on a gold coated glass in 0.1 M tetrabutylammonium tetra fluoroborate in acetonitrile after forming the self-assembly (Figure 2.5), indicates interesting changes in redox behavior of the compound. Although the reduction peak is observed at similar (+ 0.75 V for platinum and + 0.74 V for SAM on Au) potential, the oxidation peak for SAM on Au has shifted by 700 mV to the anodic side. The peak to peak separation (ΔE_p) observed for a completely reversible one electron process in the case of platinum becomes unusually large (800 mV) for the SAM. This large separation of the peak potential, in this case, is an indication of the slow redox kinetics of the compound after the formation of SAM. This is in contrast to the ideal case of surface confinement generally observed for redox active SAMs on Au electrodes.[23] More interestingly, the peak current observed for the SAM on Au decreases exponentially with the number of cycles, and totally vanishes by the end of 7th cycle. This decrease is more for the anodic peak than for the cathodic, presumably indicating greater tendency of desorption for the oxidized species. A small shift is also observed in the peak potential both for the anodic and cathodic waves towards more negative potentials during cycling (there is apparently 100 mV and 40 mV difference in peak potential between first and second cycle for anodic and cathodic waves respectively). Some of these unique features of the voltammograms are observed for the first time in the case of a self-organizing disulfide molecule.

2.3.3. Heterogeneous Electron Transfer at the Monolayer modified Electrode:

The redox behavior of a reversible couple can be effectively used to probe the compactness and sensitivity of the monolayer.[15,24] For example, the cyclic voltammetric response of a diffusion limited process at the monolayer coated electrode depends on the presence of pinholes in the monolayer.[25] Consequently, the efficiency of the monolayer can be estimated by following the kinetics of the redox probe as expressed by the peak to peak separation (ΔE_p).[26] The increase in ΔE_p values

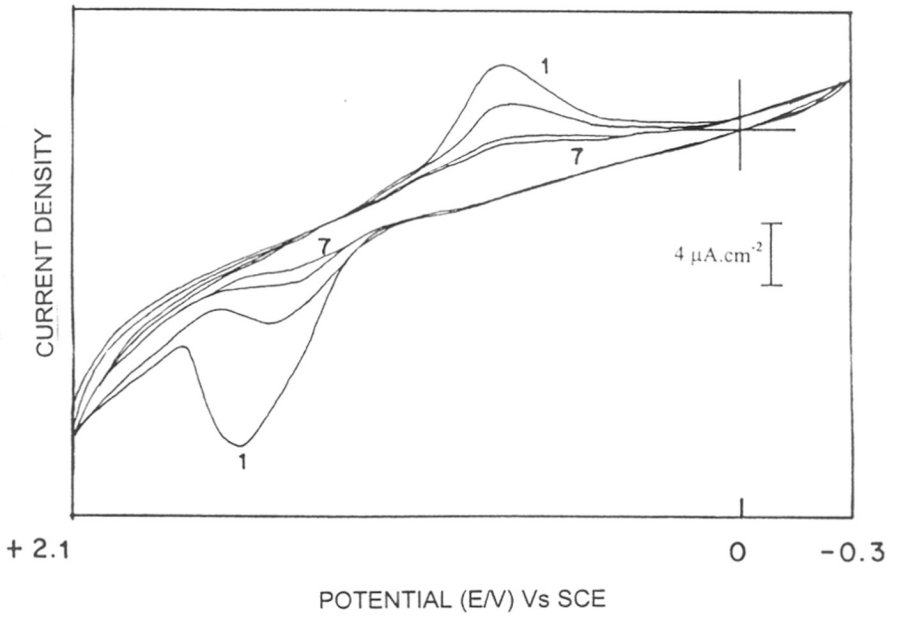

Figure 2.5. Cyclic voltammogram with Au coated glass, modified with the SAM of NDS in acetonitrile with 0.1 M tetrabutyl ammonium tetrafluoborate as supporting electrolyte. Scan rate is 200 mV/s.

observed with a monolayer coated electrode is a measure of the kinetic hindrance exerted by the monolayer on the electron transfer process assuming that the uncompensated resistance has not changed.

Figure 2.6 shows the changes in the cyclic voltammogram of naphthalene disulfide modified gold electrode in 1 mM aqueous $K_3Fe(CN)_6$ with variable modification times. The voltammograms show a progressive increase in ΔE_p values from bare gold (Figure 2.6a) to the electrode modified by NDS for longer time. The electrode modified by two hours immersion showed a large shift in the ΔE_p values. There was no further change in the ΔE_p value for an electrode dipped for more than 2 hours, which independently confirmed the typical time required for the formation of monolayer as obtained from QCM results. Voltammogram taken with the electrode modified for 2 hours (Figure 2.6c) shows no clear redox response except the nonfaradaic, sloping background current. This clearly indicates that, within 2 hours the electrode surface is covered with a compact monolayer causing a barrier to electron transfer. In addition, the comparison of the time dependent cyclic voltammograms indicate that there are some defect sites (pinholes) through which the probe molecule can penetrate completely or partially and the sloping current observed is mostly due to these pinholes present in the monolayer. With the progress of the monolayer formation, the peaks due to the redox probe become continuously broadened, presumably due to the decrease in the rate of electron transfer of $Fe(CN)_6^{3-/4-}$ on the monolayer coated electrode. With complete formation of the monolayer, electron-transfer is totally blocked which can be attributed to the formation of close packed monolayer assemblies.

2.3.4. Impedance analysis

The impedance method is based on the measurement of the response of electrochemical cell to a small amplitude alternating potential. The response is often analyzed by the complex impedance presentation and results are interpreted in terms of an equivalent electrical circuit. According to Randles' equivalent circuit,[27] two frequency regions can be distinguished to understand the change in faradaic

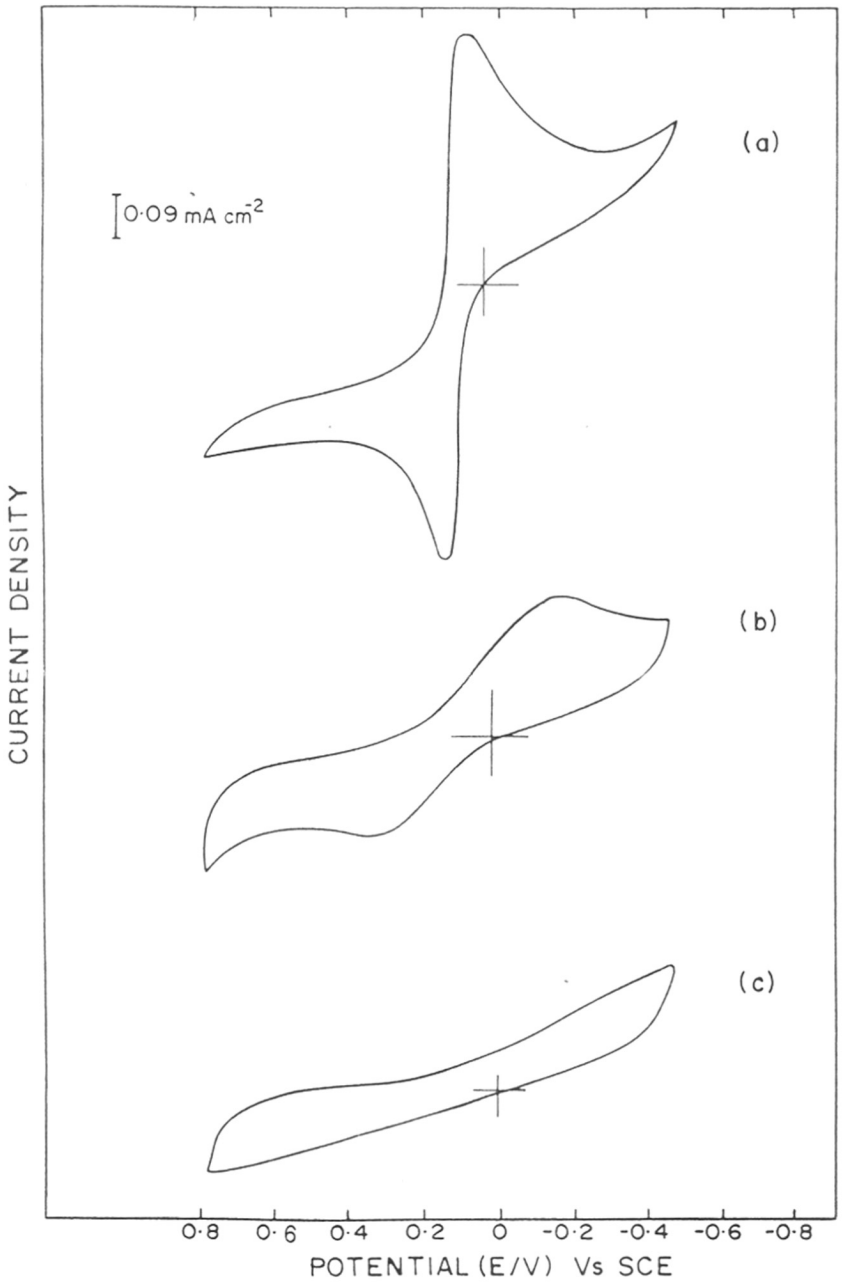

Figure 2.6. Cyclic voltammograms of $K_3Fe(CN)_6$ in 0.1 M KCl with (a) bare gold electrode; (b) gold electrode derivatized with NDS monolayer for 1 hour; (c) gold electrode derivatized with NDS monolayer for 2 hours. Scan rate is 200 mV/s.

impedance due to the presence of electroactive species in electrode/SAM/electrolyte interface. In the low frequency region, mass transfer via diffusion has to be taken into account, whereas, the microarray behavior of the pinholes within the passivating monolayer disturb the $\omega^{-1/2}$ dependence of Warburg impedance.[28] The deviation from semi-infinite diffusion[27] is due to the defects or pinholes in the monolayer which are far apart from each other. In this type of a situation, the overlap of diffusion layer is not achieved and spherical diffusion seems to be valid.[29] We focused our attention on the more interesting part of the spectrum at higher frequencies where the electrode reaction is purely kinetic controlled and heterogeneous charge transfer resistance R_{ct} is expected to increase due to the inhibition of the electron transfer by the monolayer present on the electrode surface.[30] From this increase in the charge transfer resistance one can calculate the approximate coverage of the gold electrode (θ),[31] assuming that the current is due to the defects within the monolayer:

$$\theta = 1 - [R_{ct}/R_{ct}'] \qquad (2.1)$$

where R_{ct} indicates the charge transfer resistance of pure gold electrode and R_{ct}' the corresponding term of the passivated electrode covered by NDS. The value of R_{ct} is calculated as 20.46 Ω cm^2 using Equation 2.2:

$$R_{ct} = R\,T / n\,F\,i_o \qquad (2.2)$$

and exchange current:

$$i_o = n\,F\,A\,k_o\,c_o^{(1-\alpha)}\,c_r^{\alpha} \qquad (2.3)$$

where c_o is the concentration of $[Fe(CN)_6]^{3-}$ and c_r is the concentration of $[Fe(CN)_6]^{4-}$. A, R, T and F denote as usual, the electrode area, the gas constant, temperature and Faraday's constant respectively. The transfer coefficient α is taken to be 0.5 and the electron transfer rate k_o at a bare gold electrode as 0.026 cm/s.[14]

A comparison of the complex impedance plots of bare gold and monolayer coated gold in Figures 2.7 - 2.9 show the effect of adsorbed NDS monolayer on the ac response of gold electrodes. It is known that at higher frequency the diameter of the semicircle corresponds to the R_{ct} of the monolayer coated electrode.[31] The charge transfer resistance with the monolayer covered electrodes are found to be greater than the R_{ct} measured at bare gold electrode due to the inhibition of electron transfer rate. For example, from the analysis of the spectra shown in Figures 2.8 and 2.9, the charge transfer resistance of 320 Ω cm^2 and 568 Ω cm^2 respectively are obtained and the corresponding electrode coverage values are estimated to be 93.5% and 99.6%. In comparison, the semicircle measured at the bare electrode is poorly defined presumably due to fast electrode reactions.

An approximate determination of the monolayer dielectric constant is also possible with a few additional assumptions. For example, if the measured total double layer capacitance is assumed to be a parallel combination of two capacitors,[31]

$$C_{total} = C_{dl} + C_m = C^{o}_{gold} (1-\theta) + C_{ns}\, \theta \qquad (2.4)$$

where C_{dl} is the capacitance at pinholes and C_m is the capacitance across the monolayer itself. C^{o}_{gold} is the capacitance of pure gold electrode and C_{ns} is the capacitance of a complete NDS monolayer assuming 100% coverage. In general, capacitance is determined by dielectric permittivity, the thickness of the adsorbed layer and packing density of the molecule and these parameters have to be determined separately. Other than the capacitance C, independent measurement of the thickness and the electrode coverage are necessary to evaluate the dielectric permittivity of the adsorbed NDS monolayer. In our case the capacitance of the bare gold is evaluated from the complex impedance plot obtained for the bare gold (Figure 2.7) and C_{total} from the corresponding impedance plot of monolayer covered electrode for 2 hours dipping (Figure 2.9). The surface coverage (θ) was determined by impedance analysis, making use of the electroactive probes $Fe(CN)_6^{3-/4-}$. These ions tend to penetrate through the defects of the monolayer, therefore impedance measurements yield the information

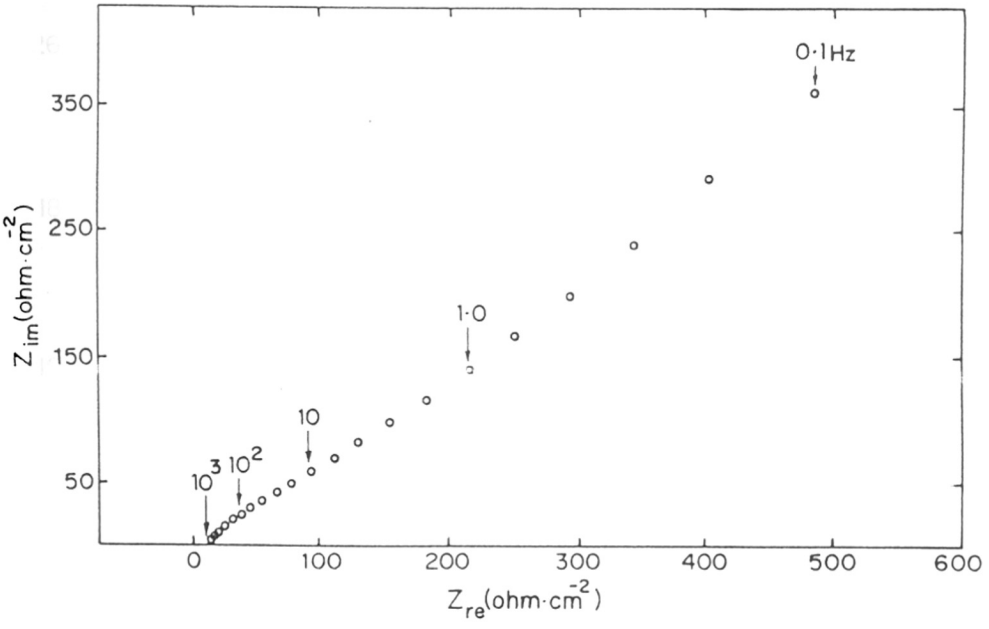

Figure 2.7. Complex impedance plots at 0.22V vs SCE for bare gold electrode for 5 mM $K_3Fe(CN)_6$ + 5 mM $K_4Fe(CN)_6$ in 0.5 M aqueous KF solution; Geometric area 0.54 cm^2; Frequency range used is 100 KHz to 100 mHz with a signal amplitude of 5 mV rms at 5 steps per decade.

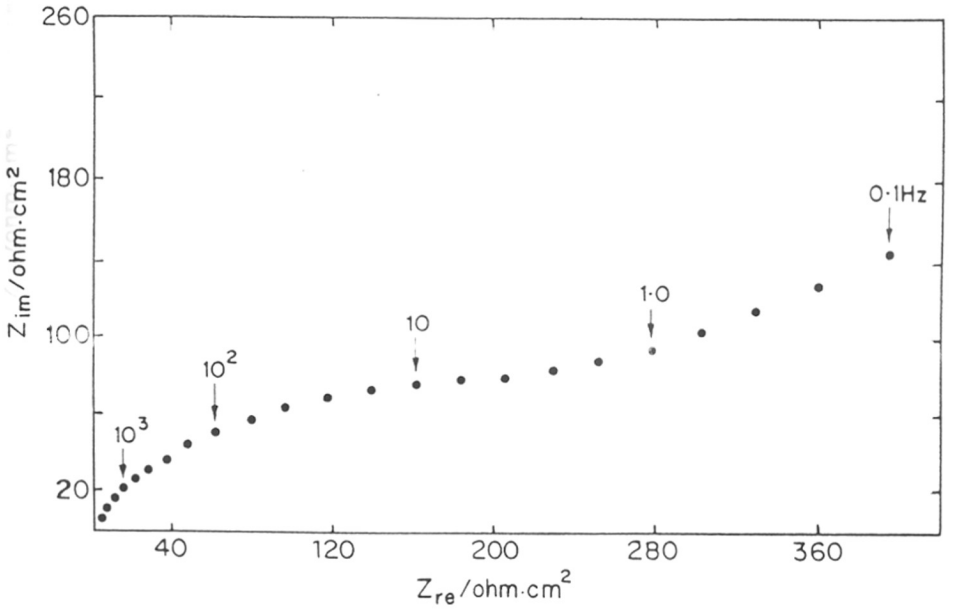

Figure 2.8. Complex impedance plots at 0.22V vs SCE for gold electrode derivatized with NDS monolayer for 1 hour for 5 mM $K_3Fe(CN)_6$ + 5 mM $K_4Fe(CN)_6$ in 0.5 M aqueous KF solution; Geometric area 0.54 cm^2; Frequency range used is 100 KHz to 100 mHz with a signal amplitude of 5 mV rms at 5 steps per decade.

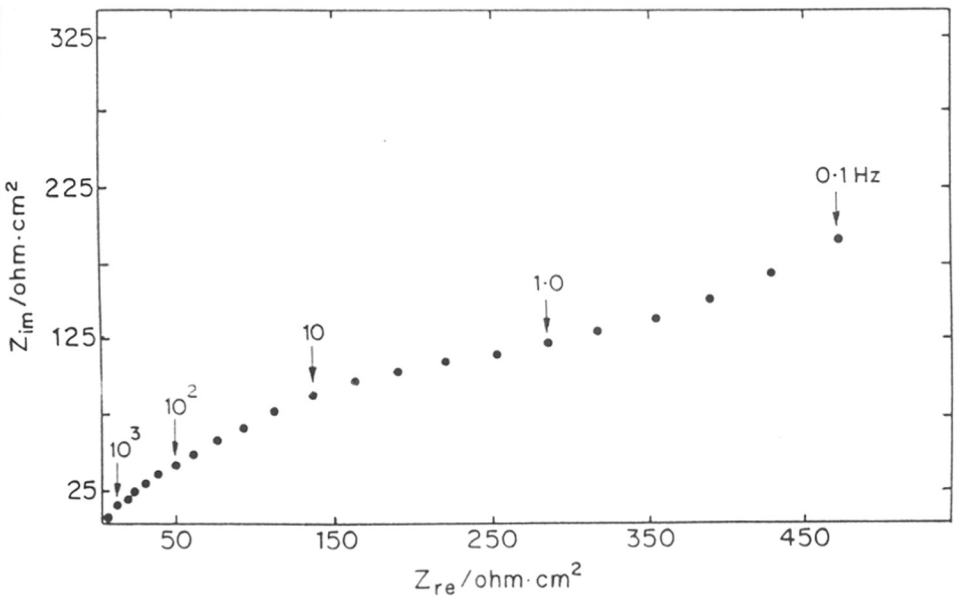

Figure 2.9. Complex impedance plots at 0.22V vs SCE for gold electrode derivatized with NDS monolayer for 2 hours for 5 mM $K_3Fe(CN)_6$ + 5 mM $K_4Fe(CN)_6$ in 0.5 M aqueous KF solution; Geometric area 0.54 cm^2; Frequency range used is 100 KHz to 100 mHz with a signal amplitude of 5 mV rms at 5 steps per decade.

about uncovered surface fraction which can be derived from Equation 2.1. With a calculated surface coverage of 99.6% and measured final capacitance of 14.9 $\mu F/cm^2$, one can calculate C_{ns} from Equation 2.4, which gives reliable data for the defect free monolayer capacitance. This C_{ns} can be used to calculate the dielectric permittivity of the monolayer film (ε_{ns}) by using Equation 2.5:

$$\varepsilon_{ns} = [C_{ns}\, d] / \varepsilon_O \qquad (2.5)$$

where, d is the monolayer thickness (~ 0.7 nm) obtained from space filling model and ε_o is the permittivity of the free space (= 8.85×10^{-12} C^2 N^{-1} m^2). The value obtained is 11.7 which is high compared with the value of alkane thiols (ε = 2.1 - 2.5)[1] indicating a more hydrophilic nature of the monolayer.

The rate constant of $Fe(CN)_6^{3-/4-}$ couple can be calculated on the bare and SAM covered electrode from the impedance plot since the monolayer behaves as a microelectrode assembly leading to an expected decrease in the rate constant.[27] Thus from Equation 2.6, for one electron first order reaction with $c_o = c_r = c$ and for unit geometric area:

$$R_{ct} = R\,T / j_o\,F \qquad (2.6)$$

and:

$$j_o = (1-\theta)\,F\,k_o\,c \qquad (2.7)$$

$$j_o = F\,k_{app}\,c \qquad (2.8)$$

Where:

$$k_{app} = k_o\,(1-\theta) \qquad (2.9)$$

Combination of Equations 2.6 and 2.8 gives

$$k_{app} = R\,T / F^2\,R_{ct}\,c \qquad (2.10)$$

Thus k_{app} is calculated to be 9.3×10^{-5} cm/sec from R_{ct} in Figure 2.8. Using k_{app} value and θ equal to 0.96, the actual rate constant for the $Fe(CN)_6^{3-/4-}$ couple is estimated to be 2.3×10^{-2} cm/s (from Equation 2.9) which is in agreement with the literature value[29] and is listed in Table 2.1 along with the other parameters obtained from the impedance analysis.

Table 2.1

Different Parameters Obtained For NDS SAM on Gold Electrode From Impedance Measurements

Charge transfer resistance (R_{ct})/ Ω cm^2	567.7[a]
Apparent electrode coverage (θ)/%	99.6
Double layer capacitance (C)/ μF/cm^2	14.9[b]
Defect free monolayer capacitance (C_{ns})/μF/cm^2	14.8
Monolayer dielectric constant (ε_{ns})	11.7
Apparent rate constant of $Fe(CN)_6^{3-/4-}$ couple (k_{app})/cm sec^{-1}	9.3×10^{-5}
Actual rate constant of $Fe(CN)_6^{3-/4-}$ couple (k_0)/cm sec^{-1}	2.3×10^{-2}

[a] R_{ct}, the charge transfer resistance at a bare gold electrode, was calculated to be 20.46 Ωcm^2 using Equations 2.2 and 2.3. [b] The measured double layer capacitance value of bare gold was 25.36 μF/ cm^2.

2.3.5. Scanning Tunneling Microscopy

STM has been used extensively to obtain nanoscopic structure of SAMs to a high degree of accuracy,[32] and the understanding of the molecular level structure of the organized monolayer correlates well with the conclusions drawn from the electrochemical experiments regarding the compactness and nature of the organization.[33] For example, Figure 2.10 shows a typical three dimensional perspective view of 300 x 300 nm STM image of bare gold surface (a) and gold surface after monolayer formation for the specified incubation time (b). The bright regions correspond to higher surface areas while the dark regions depict the lower regions on the surface. Since single crystal gold surfaces are not used in this study, the bare

(a)

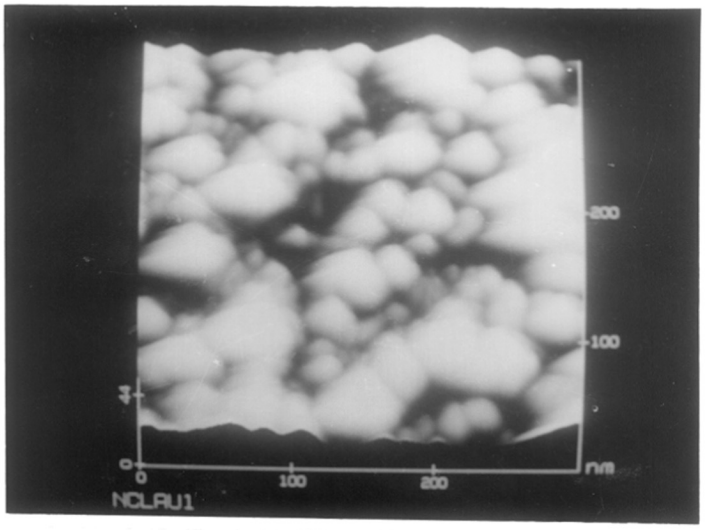

(b)

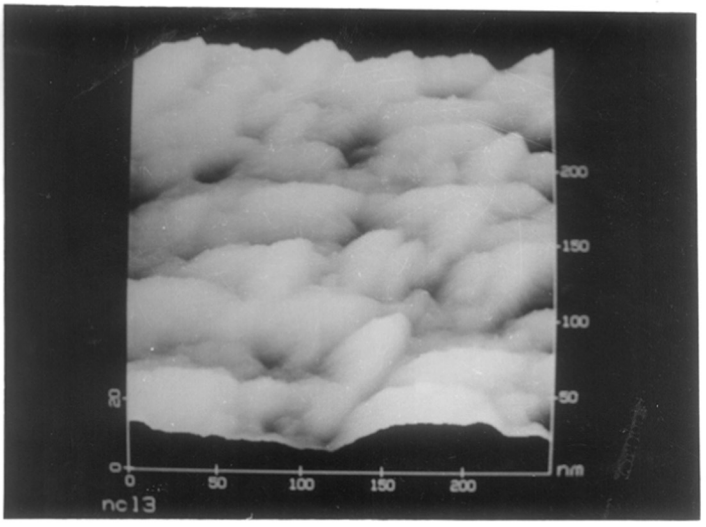

Figure 2.10 STM 3D image of a 300 x 300 nm area of (a) bare gold surface showing the granular structure; (b) gold surface with naphthalene disulfide SAM (time of derivatization ~ 2 hours). The drastic change in surface morphology is clearly due to the monolayer formation.

surface (Figure 2.10a) clearly indicates that the surface is granular (with grain size ~ 20 nm) which may be attributed to polycrystallinity of the gold film. Despite the granular nature, the surface of gold appears to be relatively smooth. In comparison, Figure 2.10b shows the 3D STM image of the monolayer coated gold in which the granular structure of the bare gold is totally absent after monolayer formation. The height of the disulfide layer varied from 1.0 - 1.2 nm as obtained from the image which is consistent with the monolayer dimension. The monolayer is not fully compact as pinholes are clearly visible in the image. The presence of these pinholes can explain the reduced surface coverage and residual electron transfer rates obtained in the case of impedance and cyclic voltammetric experiments. Here STM has been used only for purely qualitative understanding of the monolayer formation as a single crystal gold surface was not used to enable the quantitative estimation of structure. Comparison of the STM images of bare gold and monolayer coated gold clearly show that a nearly closed packed monolayer with dispersed pinholes is formed with NDS molecule.

2.4. Comparison of Self-Assembled Monolayer of NDS Formed on Polycrystalline Gold, Silver and Copper Surfaces:

2.4.1. X-ray photoelectron spectroscopy:

A comparative investigation of the monolayer formation of NDS on Au, Ag and Cu surfaces is important since it can provide useful information regarding the nature of organization and structure of the monolayer with the change in substrate. Since it is known that the above mentioned three metals have their nearest neighbor spacing in (111) plane similar (2.56 Å, 2.89 Å and 2.88 Å for Cu, Ag and Au respectively),[34] it can be expected that monolayer on these three coinage metal substrates will be similar. However, the adsorption process becomes complicated considering different oxidation tendencies of these metals on exposure to laboratory conditions. For example, it is known that the surface of copper oxidizes more rapidly and is capable of adsorbing impurities from the environment at an ambient condition. Similarly silver is also oxidized on exposure to atmosphere but the oxidation is less extensive than that of copper. However, one or two monolayers of silver oxide can always be present on the

silver surface. Gold, on the other hand, is unreactive and reproducible surfaces can easily be possible. Moreover, length of exposure time of substrate to adsorbate solution can also be a key parameter in determining the equilibrium monolayer structure.

Figures 2.1, 2.11 and 2.12 show the representative S 2p XPS spectra of the monolayer of NDS on Au, Ag and Cu surfaces respectively. In all the cases, two components are observed at the higher and lower binding energy compared to the single component for the compound itself (Figure 2.2). The lower binding energy species is well within the range expected for a surface-thiolate[35] species which implicates a dissociative mode of adsorption of S-S on all three substrates while the higher binding energy component corresponds to the oxidized species of sulfur head group (like sulfonate, sulfate etc.).[35] This can be possible due to the X-ray induced damage of the monolayer.[36] It is known that monolayer of small molecules can have a disordered organization leading to a substantial amount of X-ray damage.[35] The spectra observed for Cu-substrate is significantly different than that of gold and silver. In the former case, both the components are broad, suggesting that more than one type sulfur species is present possibly due to beam induced damage.[36] In contrast, the spectra on Au and Ag are well-defined and have narrow linewidth indicating single species for each component. Although, for all the substrates, the NDS monolayer undergoes X-ray induced damage, it is more for Cu-surface. This difference can be attributed to the structure of the substrate i.e. the presence of the oxide layer which leads to the heterogeneity of the surface[19] resulting in the different organization of the monolayers.

It is important to note from the intensities of O 1s core level region (binding energy ~535 eV), that a significant quantity of oxide is present on the copper surface. On the other hand, the residual oxide content of the monolayer on silver is very low which is the main reason for the difference in the structure of the monolayer on these two substrates. The broad line width in the S 2p level spectrum for copper may be due to the compositional heterogeneity of the surface due to the presence of oxide. The most likely phase present is a hydrous Cu_2O and it is known to adsorb the

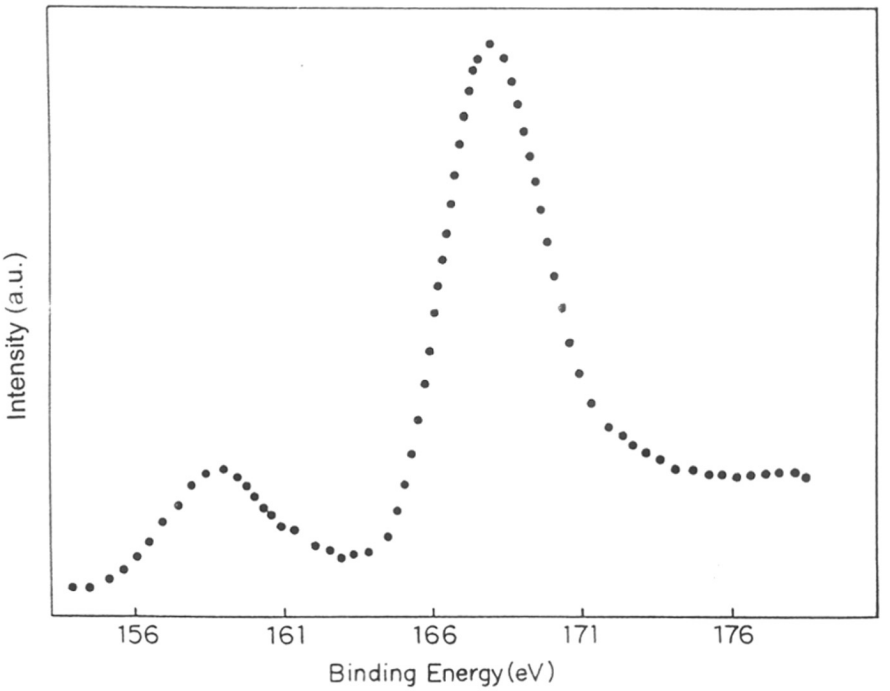

Figure 2.11. XPS spectrum showing the S 2p core level region of the NDS monolayer on silver.

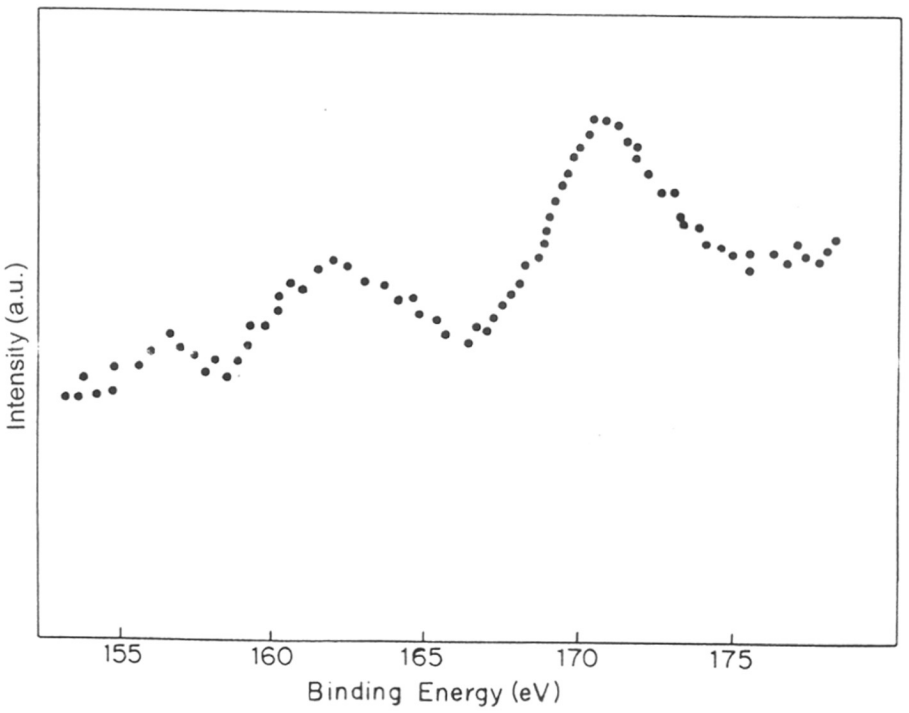

Figure 2.12. XPS spectrum showing the S 2p core level region of the NDS monolayer on copper.

environmental contaminants as well as CO_2 as carbonate.[19] This will retard the adsorption of NDS to a high coverage. It is known from other studies of CH_3SH and CH_3SSCH_3 adsorption on clean Cu (111) surfaces under UHV conditions[37] that, the surface species generated from thiol or disulfides is a surface thiolate. This is in agreement with the results obtained for ODT adsorbed on Cu. XPS data strongly suggest that the major sulfur species is a thiolate in the present case. Although the silver surface can also contain oxide when exposed to ambient condition, the core level spectra shows negligible oxide on the surface upon monolayer formation. The line width of the S 2p spectrum indicates single component species in the higher as well as lower binding energy region. This strongly suggests that monolayer on Ag is better organized and suffer less beam induced damage.

The formation of organized assemblies of disulfides on Au, Ag and Cu surface can be considered to be dominated by the energy associated with adsorbate-substrate interactions which thus control the major structural features of the entire assemblies. Moreover, the presence of oxide on the surface can play a crucial role in controlling the organization. The XPS results presented in the foregoing section clearly demonstrate the common feature that the species binding to surface is in the form of thiolate for all the three metals. The results also suggest that the NDS monolayer on Au and Ag have a comparable structure which is different from the more reactive Cu surfaces. This is primarily due to the more reactive nature of copper leading to heterogeneous surface. Monolayer in this case suffers a significant amount of beam induced damage which also suggests comparatively disordered structure of NDS SAM on Cu. It is also observed that prolong immersion of Ag and Cu surface leads to the formation of corresponding sulfides at the interface. Hence, it emerges that, the monolayer on Au is most stable followed by Ag with Cu being the least stable one.

2.4.2. Impedance Measurement Without any Redox Probe in Solution:

The monolayer formation of NDS on Au, Ag and Cu surfaces have also been characterized by impedance measurements. Due to the reactivity of Cu and Ag towards oxidation, impedance measurements are carried out in 0.1M KF solution which

may not get specifically adsorbed on the respective surfaces. Double layer capacitance values have been measured for NDS SAM on different metal surfaces to elucidate the differences in organization. Figures 2.13 - 2.15 show the variation of total impedance with frequency for different metals with NDS monolayer along with the respective response of the bare electrode. In case of all the metal surfaces, capacitance values are decreased for monolayer coated electrodes suggesting the formation of organized assembly (Table 2.2). Indeed the measured decrease in the double layer capacitance for Au is comparable to that obtained by earlier cyclic voltammetric response. For Cu, the decrease is more pronounced compared to the others which may be a combined effect of monolayer formation for the presence of oxides on the surface as also indicated by the earlier XPS results. Finally, the organization of molecules on Au and Ag surfaces are comparable as is evident from the values of their doublelayer capacitance and is supported by the XPS results.

Table 2.2

Comparison of the Double layer Capacitance and Binding Energies of S 2p Core level from Impedance and XPS Measurements respectively of NDS SAM on Au, Ag and Cu Surfaces

Substrate	Double layer capacitance[a] ($\mu F/cm^2$)	Binding energy (eV)[b]	
Au	14.20 (20)[c]	162.8	169.1
Ag	12.00 (76.7)	159	168
Cu	5.26 (54.6)	159	167.5

[a]Calculated from Impedance response in 0.1 (M) KF. [b]S 2p binding energy of powder NDS is 163.7 eV. [c]Number indicated in parentheses are corresponding doublelayer capacitance values for respective bare substrate in 0.1 M KF.

2.4.3. Cyclic Voltammetric Study:

Cyclic voltammetric response of NDS monolayer on different metal surfaces are also useful for confirming the above differences in organization. Figures 2.16 - 2.18

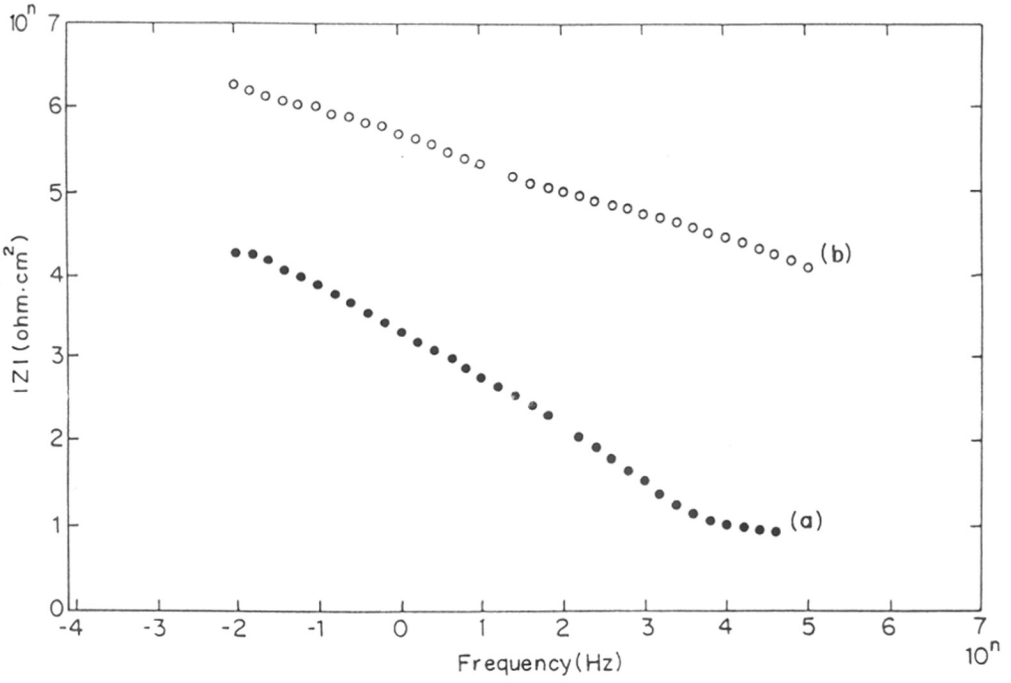

Figure 2.13. Superimposed plot of total impedance with frequency at a range of 100 KHz to 100 mHz with 5 mV rms signal of (a) bare gold and (b) NDS monolayer modified gold in 0.1 M KF solution.

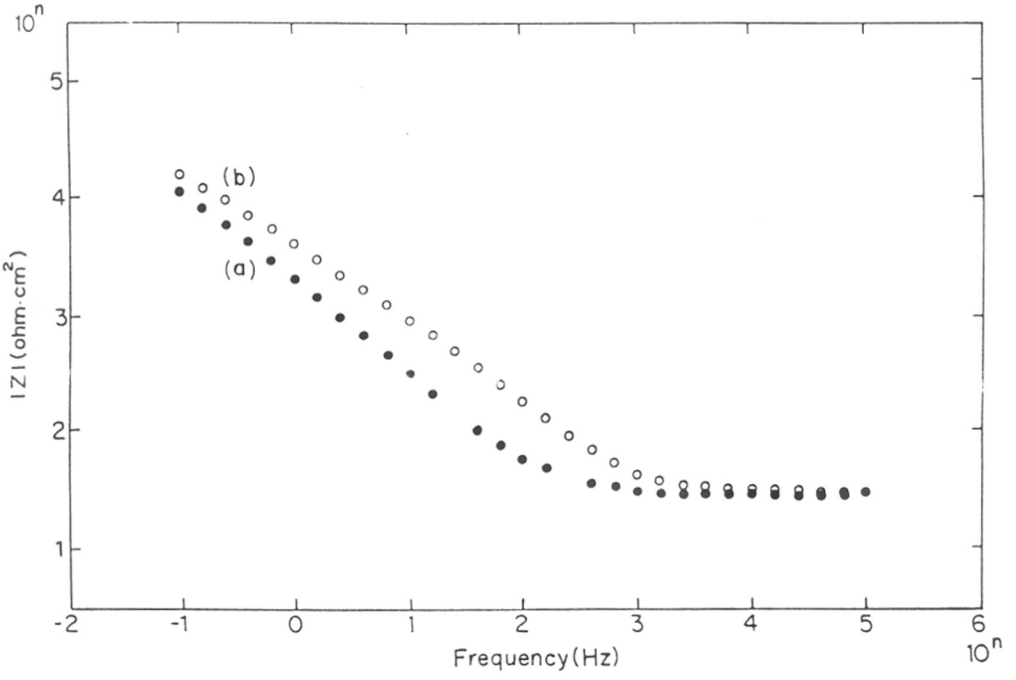

Figure 2.14. Superimposed plot of total impedance with frequency at a range of 100 KHz to 100 mHz with 5 mV rms signal of (a) bare silver and (b) NDS monolayer modified silver in 0.1 M KF solution.

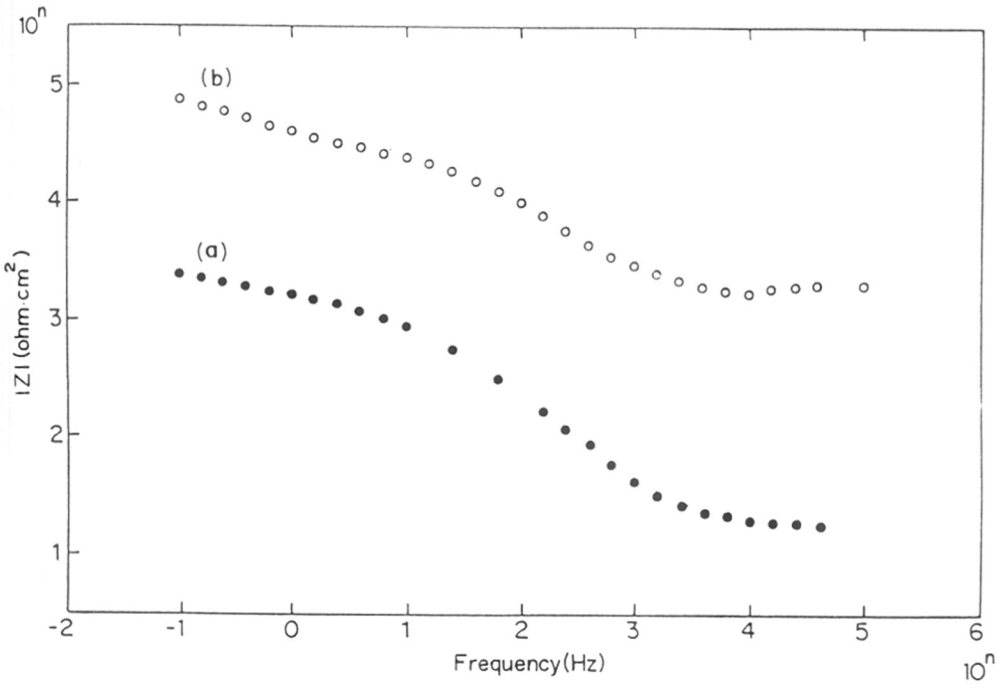

Figure 2.15. Superimposed plot of total impedance with frequency at a range of 100 KHz to 100 mHz with 5 mV rms signal of (a) bare copper and (b) NDS monolayer modified copper in 0.1 M KF solution.

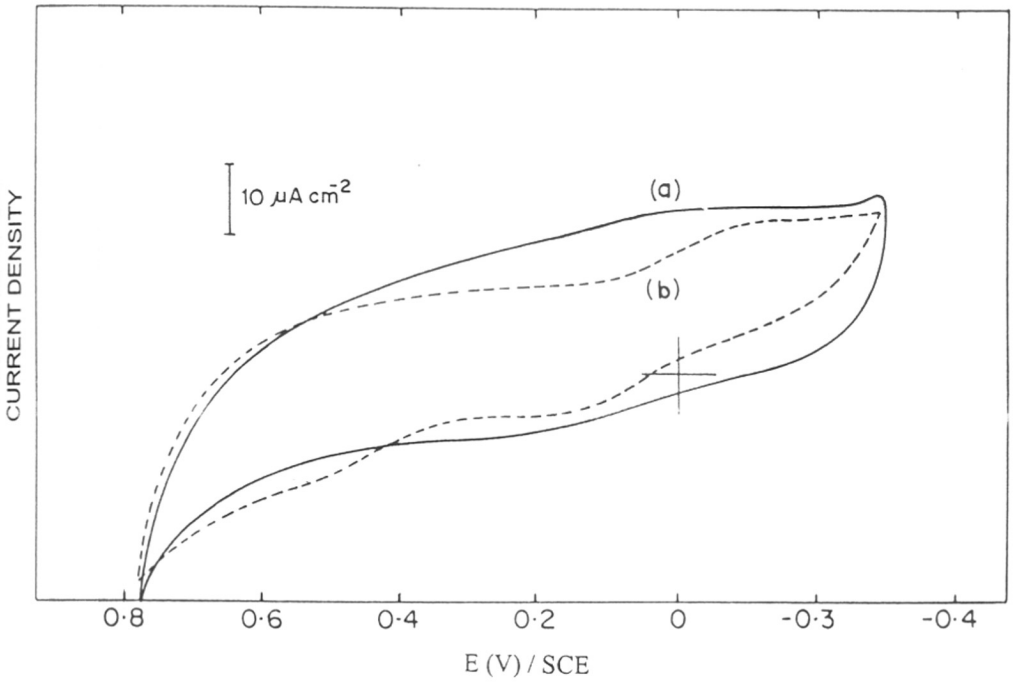

Figure 2.16. Superimposed cyclic voltammograms of (a) bare gold and (b) NDS monolayer modified gold in 0.1 M KF solution with a scan rate of 200 mV/s.

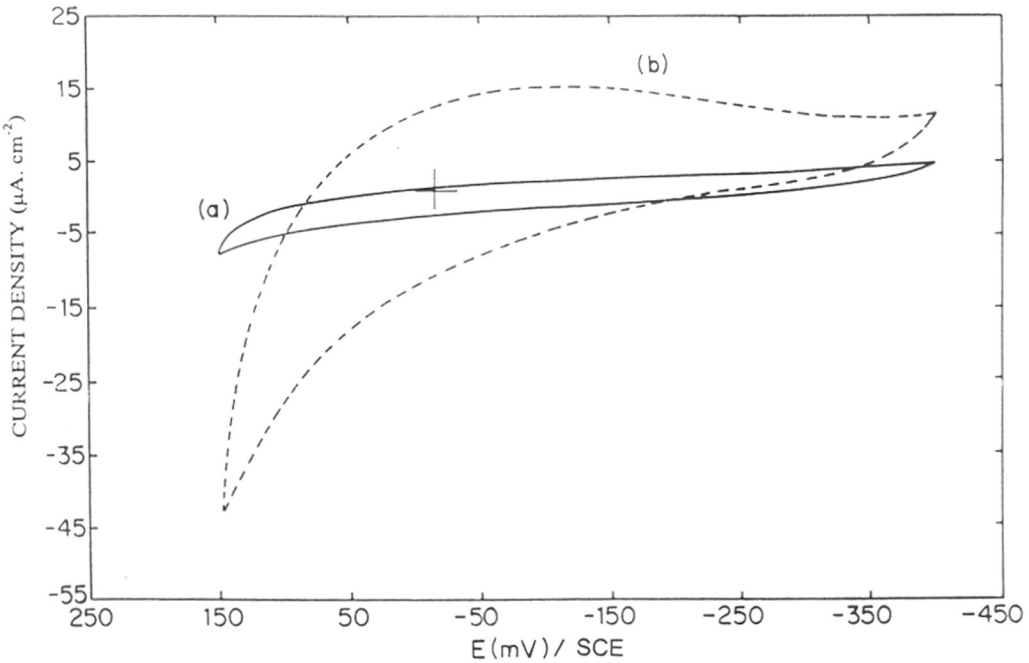

Figure 2.17. Superimposed cyclic voltammograms of (a) bare silver and (b) NDS monolayer modified silver in 0.1 M KF solution with a scan rate of 200 mV/s

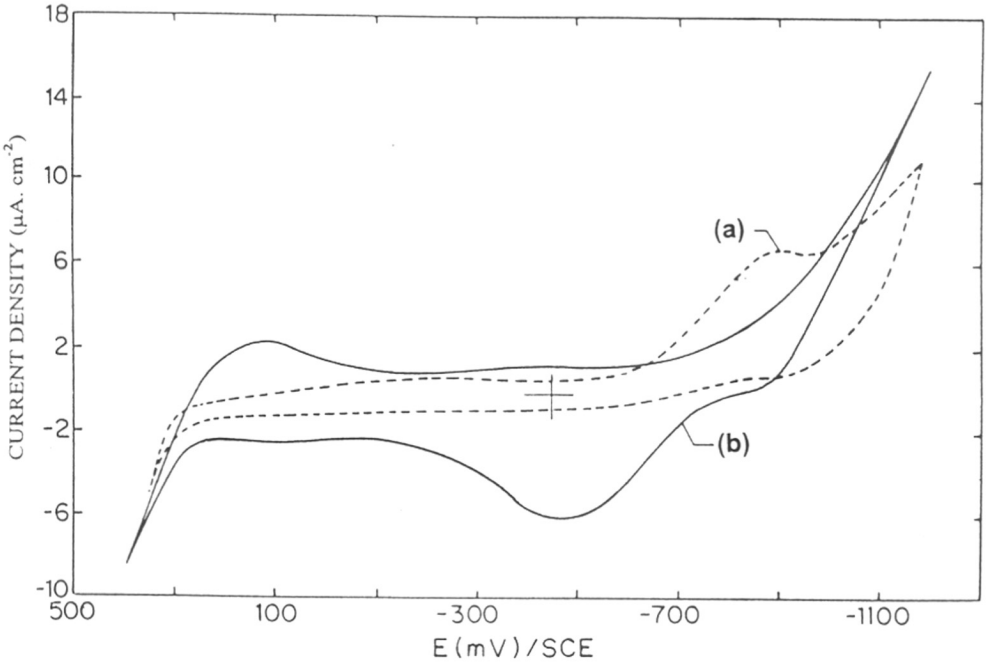

Figure 2.18. Superimposed cyclic voltammograms of (a) bare copper and (b) NDS monolayer modified copper in 0.1 M KF solution with a scan rate of 200 mV/s.

show the cyclic voltammograms of respective bare and monolayer coated surfaces in 0.1M KF solution. As expected on the basis of the above discussions, the response of the Au electrode is different from that of Cu and Ag. In the former case, the expected decrease in the nonfaradaic current is evident upon monolayer formation. In contrast, increase for Cu and Ag surfaces suggesting the possibility of a chemical reaction at the interface. This is relevant, since, it is known that metal sulfides can get easily formed on prolonged exposure to the derivatized solution. Therefore, it is reasonable to believe that, NDS can form a well-defined monolayer on gold surface, unlike for Ag and Cu.

2.5. Conclusion:

Cyclic voltammetric results together with ellipsometric and XPS studies clearly indicate the formation of a spontaneous molecular assembly of NDS with two types of sulfur moieties on Au. Electrochemical impedance analysis and STM show a high degree of surface coverage (99.6%) on gold despite the lack of the ordering influence of the hydrophobic chain. Comparison of monolayer formation of NDS on Au, Ag and Cu surfaces by XPS, impedance and cyclic voltammetry demonstrates that, the monolayer on Ag and Cu surfaces are not well-organized, possibly due to their relatively fast tendency of oxidation in ambient conditions.

2.6. References:

1. Ulman, A. *"An introduction to Ultrathin organic films from Langmuir-Blodgett to Self-assembly"*; Academic press: San Diego, CA, 1991.

2. Durand, R.R.; Bencosme, C.S.; Collman, J.P.; Anson, F.C. *J. Am. Chem. Soc.* **1983**, *105*, 2710.

3. Notoya, T.; Poling, Q. W. *Corrosion* **1979**, *35*, 193.

4. Bowden, F. P.; Tabor, D. *"The Friction and Lubrication of Solids"*, Oxford University press. London 1968.

5. Kaelble, D. H. *"Physical chemistry of Adhesion"*, Wiley-Interscience; New York, 1971.

6. Nuzzo, R. G.; Allara, D. L. *J. Am. Chem. Soc.* **1983**, *105*, 4481.

7. Israelachvili, J. N. *"Intermolecular and Surface forces"* Academic press, New York 1985.

8. Ullman, A.; Scaringe, R.P. *Langmuir* **1992**, *8*, 894.

9. (a) Nuzzo, R. G.; Zegarski, B.R.; Dubois, L. H. *J. Am. Chem. Soc.* **1987**, *109*, 733. (b) Nuzzo, R. G.; Fusco, F. A.; Allara, D. L. *J. Am. Chem. Soc.* **1987**, *109*, 2358. (c) Offord, D. A.; Jhon, C .M.; Griffin, J. H. *Langmuir* **1994**, *10*, 761.

10. Whitesides, G. M.; Laibinis, P. E. *Langmuir* **1990**, *6*, 87.

11. Fenter, P.; Eberhardt, A.; Eisenberger, P. *Science* **1994**, *266*, 1216.

12. Gamage, S. A.; Smith, R. A. J. *Tetrahedron* **1990**, *46*, 2111.

13. Hamlein, A.; Sottomayer, M.J.; Silva, F.; Chang, S.-C.; Weaver, M. J. *J. Electroanal. Chem.* **1990**, *295*, 291.

14. Mathcad is a commercial mathematical software package from Mathsoft Inc. The application for ellipsometry, ELLIP. MCD by M.S is available from the Mathsoft public domain on the Internet.

15. Porter, M. D.; Thomas, B. B.; Allara, D. L.; Chidsey. E.D. *J. Am. Chem. Soc.* **1987**, *109*, 3559.

16. Shirley, D. A. *Phys. Rev. B* **1972**, *5*, 4709.

17. Sabatani, E.; Cohen-Boulakia, J.; Bruening, M.; Rubinstein, I. *Langmuir* **1993**, *9*, 2974.

18. Oesch, U.; Janata, J. *Electrochimica Acta.* **1983**, *28*, 1237.

19. Laibinis, P. E.; Whitesides G. M.; Allara, D. L. ; Tao Y-T; Parikh, A. N.; Nuzzo, R. G. *J. Am. Chem. Soc.* **1991**, *113*, 7152.

20. Gray, R.C.; Hercules, D.M. *J.Electron Spectrosc.* **1977**, *12*, 37.

21. Chambers, J. Q. in *Encyclopedia of electrochemistry of the elements*, vol XII; Bard, A. J., Lund, H., Eds.; Marcel Dekker Inc: New York and Basel, p 403, 406.

22. Zweig, A.; Hoffmann, A. K. *J. Org. Chem.* **1965**, *30*, 3997.

23. Miller, C.; Cuendet, P.; Gratzel, M. *J. Phys. Chem.* **1991**, *95*, 877.

24. (a) Hickman, J. J.; Ofer, D.; Laibinis, P. E.; Whitesides, G. M.; Wrighton, M. S. *Science* **1991**, *252*, 688. (b) Collard, D. M.; Fox, M. A. *Langmuir* **1991**, *7*, 1192. (c) Chidsey, C. E. D.; Bertozzi, C. R.; Putvinski, T. M.; Mujsce, A. M. *J. Am. Chem. Soc.* **1990**, *112*, 4301. (d) Bunding Lee, K. A. *Langmuir* **1990**, *6*, 709.

25. Chailapakul, O.; Crooks, R. M. *Langmuir* **1995,** *11*, 1329.

26. Finklea, H.O.; Avery, S.; Lynch, M.; Furtsch, T. *Langmuir* **1987**, *3*, 409.

27. Sluyters-Rehbach; Sluyters, J. H. in *Electroanalytical Chemistry*, Ed. A. J. Bard, Dekker, New York, Vol 4, 1970.

28. Finklea, H. O.; Sinder, D. A.; Fedyk, J.; Sabatani, E.; Gaini, Y.; Rubinstein, I. *Langmuir* **1993**, *9*, 3660.

29. Tokuda, K.; Gueshi, T.; Matsuda, H. *J. Electroanal. Chem.* **1979**, *102*, 41.

30. Amatore, C.; Saveant, J. M.; Tessier, D. *J. Electroanal. Chem.* **1983**, *147*, 39.

31. Sabatani, E.; Rubinstein, I.; Maoz, R.; Sagiv, J. *J. Electroanal. Chem.* **1987**, *219*, 365.

32. (a) Kim, Y.; Bard, A. J. *Langmuir* **1992**, *8*, 1096. (b) Sprik, M.; Delamarche E.; Michel, B. *Langmuir* **1994**, *10*, 4116.

33. Chailapakul, O.; Sun, Li.; Xu, C.; Crooks, R. M. *J. Am. Chem. Soc.* **1993**, *115*, 12459.

34. Kittel, C. *Solid State Physics*, 5th ed.; Wiley: New York, 1976; P 32.

35. Castner, D. G.; Hinds, K.; Grainger, D. W. *Langmuir* **1996**, *12*, 5083.

36. Colvin, V. L.; Goldstein, A. N.; Alivisatos, A. P. *J. Am. Chem. Soc.* **1992**, *114*, 5221.

37. Bao, S.; McConville, C. F.; Woofruff, D. P. *Surf. Sci.* **1987**, *187*, 133.

Chapter 3

A Comparative Study of the Molecular Organization of Naphthalenedisulfide, Diphenyldisulfide and Diphenyldiselenide on Gold: Effect of Geometrical Constraints and Difference in Substrate-Headgroup Interactions

---

The self-assembled monolayer formation capability of naphthalenedisulfide (NDS), diphenyldisulfide (DDS) and diphenyldiselenide (DDSe) has been investigated using X-ray photoelectron spectroscopy (XPS), quartz crystal microbalance (QCM), surface enhanced Raman spectroscopy (SERS) and electrochemical measurements like cyclic voltammetry and impedance techniques. All the results strongly demonstrate the effect of *geometrical constraints* and change in *substrate-headgroup interaction* in controlling the microscopic structure and highlight the importance of intramolecular conformational changes in regulating the monolayer packing-density.

---

* A portion of this work have been published in:
Langmuir **1998**, *14*, 625 and another part is accepted in *Langmuir* **1998** (*in press*)

3.1. Introduction:

Recently, the formation and characterization of self-assembled monolayers (SAMs) have gained intense research activity[1] as it has been shown to be a versatile technique for surface modification with a number of applications such as chemical sensors, non-linear optical materials, high density memory devices and photo-patterning methodology.[2] Although, a wide variety of substrates and functional groups are known to form SAMs, the thiol/disulfide monolayer on Au has received considerable attention due to simplicity and ease of preparation.[1]

The bonding pattern in both thiols and disulfides is the same except for an oxidative dissociation of the S-S bond for disulfides. While the nature of the surface attachment is believed to involve a Au-thiolate interaction,[3] the possibility of thiolate group dimerization to form disulfides on gold surfaces has also been recently considered.[4] Most of the data obtained from different techniques are consistent with a $(\sqrt{3} \times \sqrt{3})R30°$ overlayer structure (Scheme 3.1a) during the chemisorption of thiols and disulfides on Au (111) surfaces.[5] In such a model, each sulfur head group may rest over a three-fold hollow site on the underlying Au (111) surface. However, recent reports using helium diffraction[6] on long chain alkane thiols adsorbed on Au (111) surface clearly demonstrate that for a chain-chain separation of 0.5 nm, a $c(4\sqrt{3} \times 2\sqrt{3})R30°$ superlattice is formed rather than a simple $(\sqrt{3} \times \sqrt{3})R30°$ structure. Detailed calculations confirm that the three-fold hollow sites on the Au (111) surface is the more stable binding site and chemisorption is epitaxial.[7]

In contrast, selenol/diselenide monolayers have not received enough attention despite their promising utility for a variety of applications such as photoresists, photocatalysts, preparation of semiconductor quantum dots, photo induced electron transfer systems etc.[8] In the first report of SAM formation of selenium compound, docosaneselenol has been found to form SAM on gold surface as characterized by surface x-ray diffraction.[9] It has been concluded that the organoselenium monolayer is less ordered than the monolayer derived from the corresponding thiols/disulfides. On the contrary, a very recent STM investigation[10] on monolayer formation of DDSe on Au (111) shows that the arylselenium monolayer is more strongly chemisorbed than the

(a)

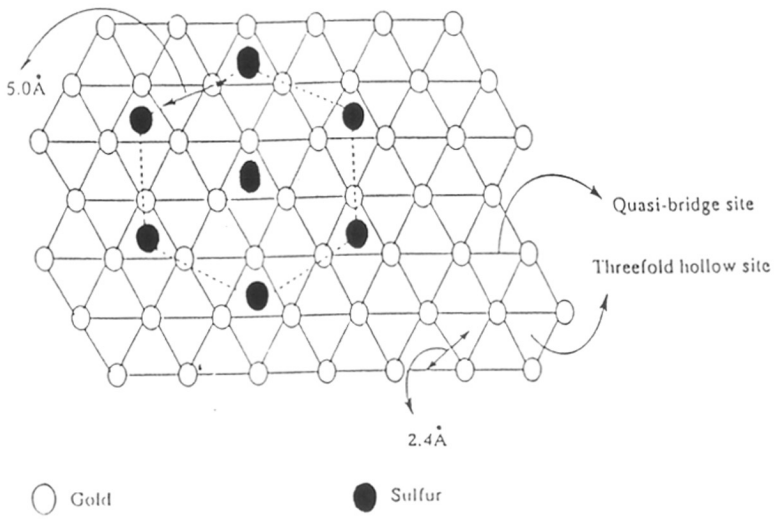

(b)

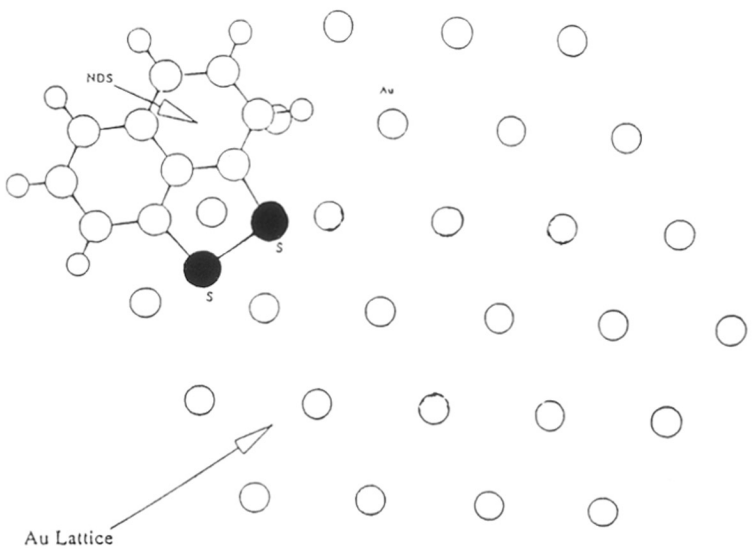

Scheme 3.1. (a) Atomic view of Au(111) plane with the bonding mode of sulfur atoms for thiols/disulfides. (b) Simulated view of adsorbed NDS molecule on Au (111) surface with one sulfur at three fold hollow site and other at the bridge site.

arylsulfur analogue. A $(3\sqrt{3} \times 2\sqrt{3})R30°$ structure has been formed as a result of benzeneselenol adsorption and the structure is also similar to DDSe monolayer on Au.

In this chapter, the earlier studies of monolayer formation of NDS in chapter 2 are compared with similar results of DDS and DDSe on the basis of structural rigidity and substrate-headgroup interaction. The main emphasis is the understanding of the role played by the fused naphthalene ring, which places a constraint on the S-S distance in NDS, on the monolayer quality (in terms of molecular packing and ion permeation) with DDS and DDSe not facing such a constraint. More specifically, in case of NDS, the two sulfur atoms must retain the bonding distance of 2.4 Å (i.e. the actual S-S distance in the present aryl disulfide)[11] even if normal dissociative chemisorption takes place unless a S-C bond is broken (Scheme 3.2a). On the other hand, for DDS and DDSe, dissociation of the S-S or Se-Se bond gives rise to two separate molecules (Scheme 3.2b) as observed in the case of long chain alkane disulfides. Keeping these facts in mind, it is unlikely that both the sulfur atoms in the NDS molecule will be able to occupy the normal 3-fold hollow sites as has been proposed for long chain alkane thiols/disulfides adsorbed on gold.[5] The inherent rigidity in the molecule may direct the other sulfur to coordinate to a *quasi-bridge site* (the distance between one 3-fold hollow and bridge site is equal to 2.4 Å, as indicated in Scheme 3.1a), which is comparable to the S-S distance in case of NDS (Scheme 3.2a) on the gold surface and is energetically unfavorable. This situation can be seen from the simulation of NDS molecule on Au surface in Scheme 3.1b. In contrast, both DDS and DDSe are free from such structural constraints and can form a normal overlayer with a S-S distance of 5 Å, which is the distance between the two three fold hollow sites on the Au (111) surface[5] (Scheme 3.1a). More significantly, a comparison of the monolayer formation ability of the disulfides/diselenides may provide valuable information about the relative degree of organization with the change in substrate-head group interaction considering the more facile dissociative nature of the Se-Se bond.[8]

The present chapter deals with the comparative ability of SAM formation of NDS, DDS, and DDSe on polycrystalline gold using QCM, SERS, XPS and electrochemistry. These techniques are selected on their well proven ability to

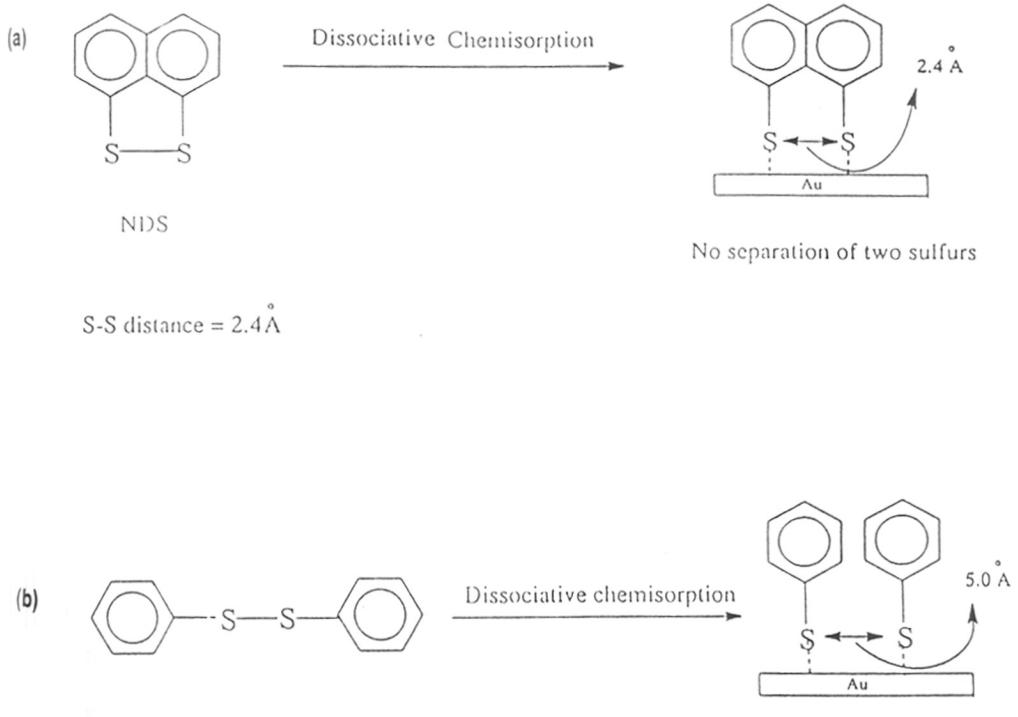

Dissosiation mode of two disulfides on gold surface during SAM formation

Scheme 3.2 Possible dissociation modes of two disulfides and the corresponding distance between the two sulfur atoms on gold surface during SAM formation.

effectively unravel the molecular level understanding of the SAM structure and the degree of organization. For example, since Raman spectroscopy can give an intense band for S-S and Se-Se stretching, unlike the case for IR, valuable information could be obtained about the fate of disulfide or diselenide bond during the monolayer formation. Moreover, the relative orientation with respect to steric constraints can also be commented from the SERS results as in the case of NDS where the presence of a rigid naphthalene ring can force two sulfur atoms to a fixed distance. This type of a structural constraint is not present for DDS or DDSe, which can lead to the understanding of the effect of structural difference on the mode of organization. In addition, it is of considerable interest to observe the effect of change in the head group from S-S to Se-Se on the binding mode and structure of the monolayer.

3.2. Experimental:

3.2.1. Materials:

Vacuum deposited gold substrates with a chromium-buffer layer were prepared by previously discussed procedure in chapter 2 (section 2.2.1). DDS, DDSe, $K_3Fe(CN)_6$, and $K_4Fe(CN)_6$ were purchased from Aldrich and were used as received. The monolayer formation time was typically 24 hours for all the three molecules to form an equilibrium molecular organization as demonstrated by reproducible SERS and electrochemical responses.

3.2.2. Quartz crystal Microgravimetric (QCM) Measurement:

QCM measurements were performed on an Edwards FTM5 microbalance. A 6 MHz AT cut quartz crystal was used with the microbalance having a resolution of the order of ± 1 Hz. This translates into a mass resolution of 12.1 ng/cm^2 which for common SAM forming molecules is well within the monolayer coverage range. Frequency changes were converted to mass loading using the Sauerbrey formula.[12] All measurements were performed *ex-situ* after thorough washing and drying of the crystal prior to frequency measurements. Before the experiments, the crystals were cleaned

with piranha solution, (see chapter 2, section 2.2.2) rinsed with ethanol and finally with the solvent used. The frequency change due to adsorption was converted directly to mass and plotted with time. One of the major limitations of the *ex situ* QCM measurement arises due to the possible drift which causes a gradual shift in the base line. To overcome this difficulty and to obtain reliable results, blank experiments were performed with solvent alone. This blank experiments to some extent, provided the inherent drift of the system. These QCM experiments were conducted with the same solvent which was indicated by a minor mass change (~ 8 ng) compared to the mass change due to the monolayer formation from respective disulfides and diselenide and this background correction was utilized for all the QCM data.

3.2.3. SERS :

For SERS measurements, an oxidized aluminum foil of 20 μm thickness made by heating it in air at 873 K for five hours, was sputter coated with about 200 nm gold or silver of 99.9% purity in an Edwards sputter coater. The films prepared by this method were shown to be excellent substrates for SERS work although the films showed corrugations in the sub-micrometer scale in scanning electron microscopy (SEM). All SERS measurements on these surfaces gave excellent spectra as the intensities were reproducible from batch to batch under identical conditions. Raman spectra were recorded with a Bruker IFS 66V FT-IR spectrometer with a FRA 106 Raman accessory. Nd-YAG laser of 1064 nm was used as the primary excitation source. A laser power of 70 mW was used. Each spectrum was an average of 500 scans and the acquisition took nearly 30 minutes. The temperature dependent measurements were conducted with a locally built heater with a programmable temperature controller.

The details of the XPS and electrochemical measurements used in this chapter are described in chapter 2 (sections 2.2.5 and 2.2.6 respectively).

3.3. Results and Discussion:

3.3.1. QCM:

QCM is considered to be an ideal tool for investigating the adsorption processes due to its high sensitivity (± 0.1 ng) towards mass change. The Sauerbrey formula,[12] which relates the frequency change on mass loading can be used to determine the approximate mass of the species adsorbed on the QCM crystal surface. When gold coated quartz crystal was exposed to 10^{-3} M solution of the respective disulfides and diselenide in acetonitrile, such mass change with time is indicated in Figures 3.1 - 3.3. The mass increase seems to attain a plateau value at about 150, 200 and 292 ng/cm^2 for monolayers of NDS, DDS and DDSe respectively after subtracting the minor mass change (8 ng) from blank experiments with only the solvent. Although three curves are similar in nature, the one corresponding to DDS is quite steep suggesting a faster adsorption rate than NDS or DDSe. Among the latter two cases, DDSe adsorbs in lesser time than NDS even if the equilibrium mass uptake is possible for all molecules within 2 hours of time. Furthermore, a comparison of the mass uptake suggests a more closely packed molecular assembly for DDSe and DDS than NDS. This could be explained due to the ease of relaxation during bond breaking for DDSe and DDS while for NDS, the fused ring may impose constraints for lateral movement and a lesser interaction affinity of DDSe than the corresponding disulfides. These results underline the importance of intramolecular conformational changes in controlling the monolayer packing density.

3.3.2. Double layer Capacitance Measurements:

The differential capacity for an electrical double layer is known to decrease with increasing separation between the electrode surface and the plane of closest approach for the ionic charges.[13] Hence, double layer capacitance studies can provide additional insight into the average structure of the self-organized assemblies. The simple parallel plate capacitance model of the electrode-electrolyte interface has shown to be successful in case of electrodes derivatized with long chain alkanethiol monolayers.[14]

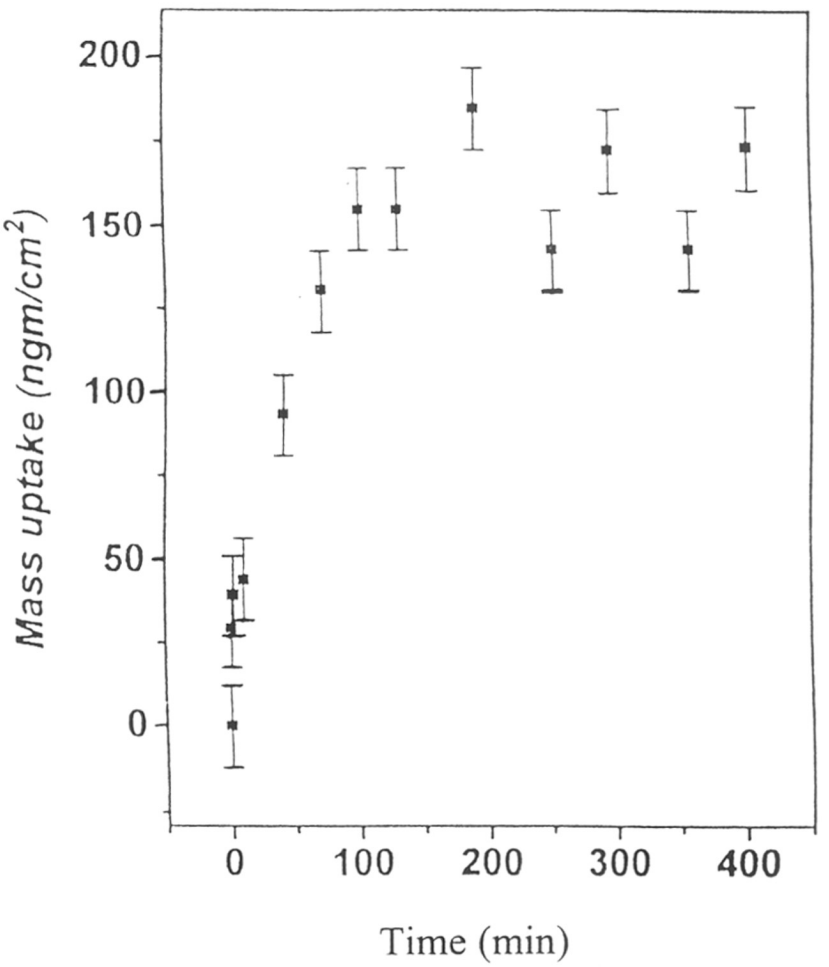

Figure 3.1. Variation of the mass uptake with time for a gold coated 6 MHz AT cut quartz crystal during the SAM formation using 1 mM of NDS in acetonitrile.

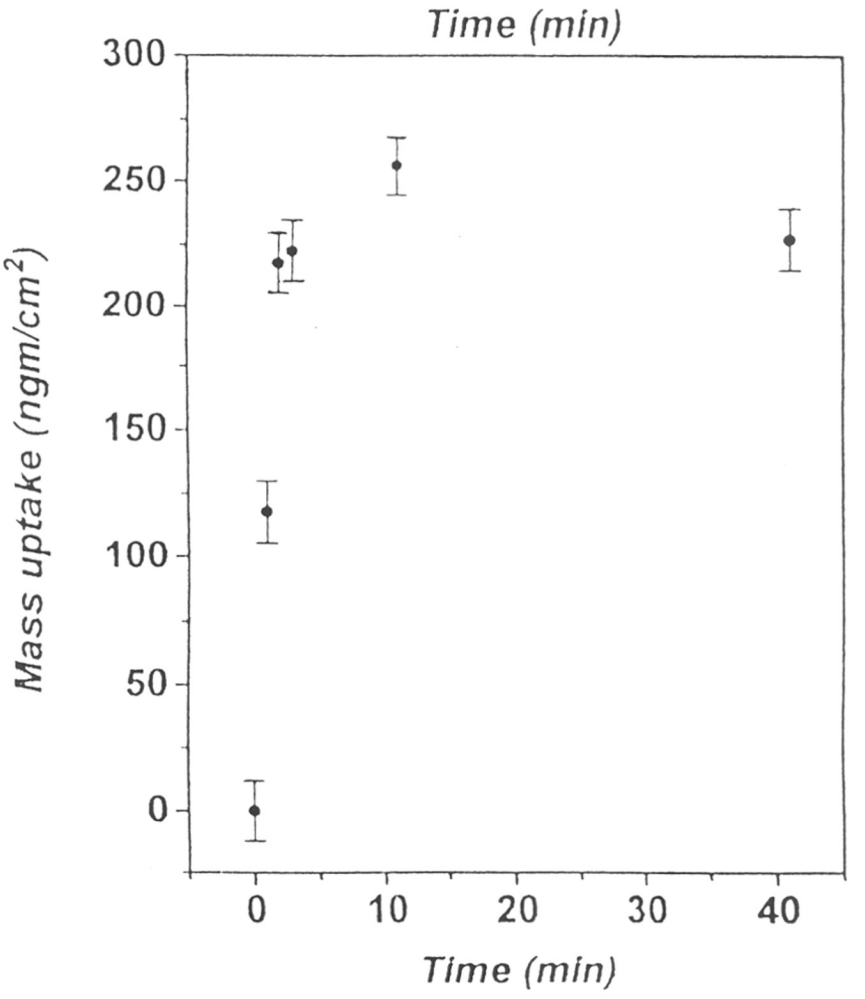

Figure 3.2. Variation of the mass uptake with time for a gold coated 6 MHz AT cut quartz crystal during the SAM formation using 1 mM of DDS in acetonitrile.

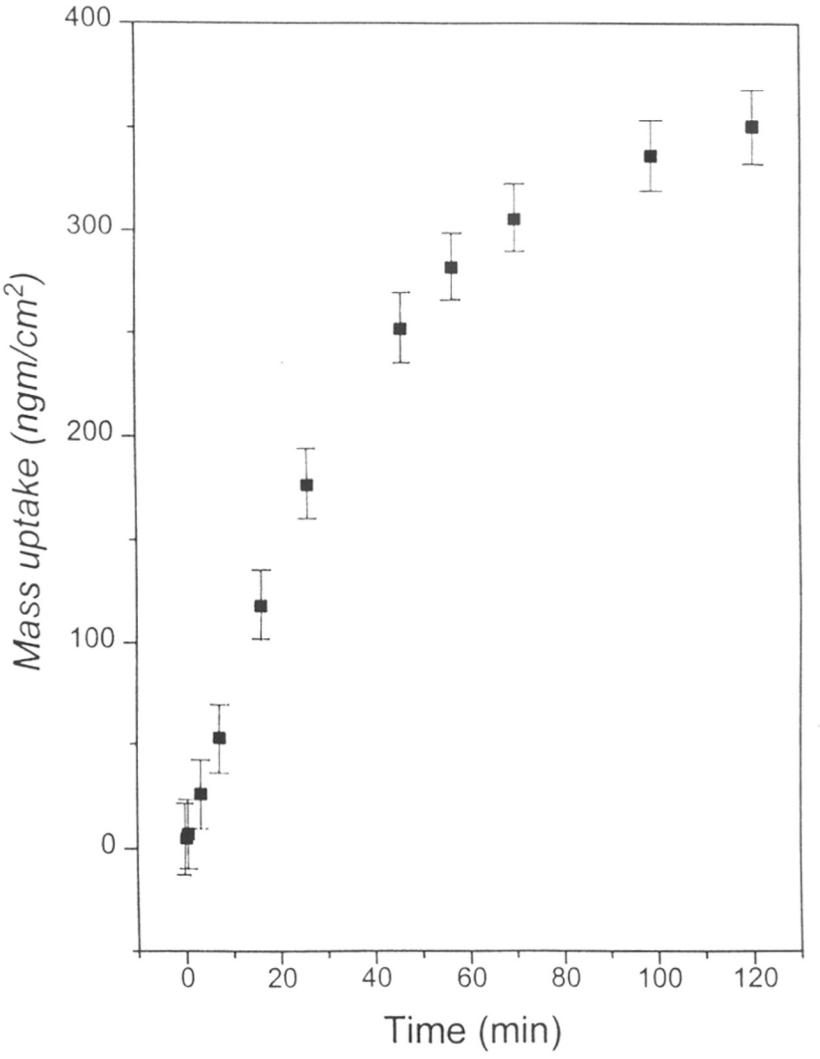

Figure 3.3. Variation of the mass uptake with time for a gold coated 6 MHz AT cut quartz crystal during the SAM formation using 1 mM of DDSe in acetonitrile.

Figure 3.4 shows a plot of differential capacitance in a limited range versus applied potential in 0.1 M KF solution (pH = 7) for bare gold and gold electrodes modified with NDS, DDS and DDSe monolayers. These double layer capacitance values are obtained from cyclic voltammetric data at a scan rate of 500 mV/s as discussed in chapter 2 (section 2.2.6). The double layer capacitance value of ODT is also included for comparison. This value is found to be ~ 21 $\mu F/cm^2$ for bare gold, which is in good agreement with the available data.[15] The roughness factor of the substrates are measured to be 1.8 - 2.0 as mentioned in chapter 2 (section 2.3.2) and these values are used throughout the study to calculate the differential capacitance. Our capacitance measurements at several potentials demonstrate that DDSe, DDS and NDS are chemisorbed on the gold surface as manifested from the decrease in double layer capacitance compared to that of bare gold. As the differential capacitance is extremely sensitive to the interfacial composition, these changes can commonly be used to evaluate the extent of monolayer formation and quality. The measured capacitance values are higher for both the disulfides and the diselenide than those reported for compact monolayers of long chain alkanethiols like ODT.[14a] The higher values may be a combined effect of the presence of pinholes in the monolayer or due to the smaller molecular dimensions of the disulfides/diselenide with delocalized π-electrons. However, it should be noted that, the observed double layer capacitance values are reasonably close to the values reported in the literature[16] for such small aromatic molecules. Among the three molecules, the double layer capacitance values are gradually increased from DDS to NDS suggesting a greater compactness and presence of less pinholes in the former monolayer. The values of double layer capacitance for DDSe indicates the poor molecular organization with the change in the head-group from S-S to Se-Se. Monolayer formed from NDS shows most disordered organization compared to the isostructural disulfide/diselenide pointing towards the importance of structural rigidity in controlling the degree of ordering in the monolayers.

3.3.3. Solution Electrochemistry:

To understand the redox activity of these molecules in solution, cyclic voltammograms have been taken in acetonitrile with 0.1 M tetrabutylammonium

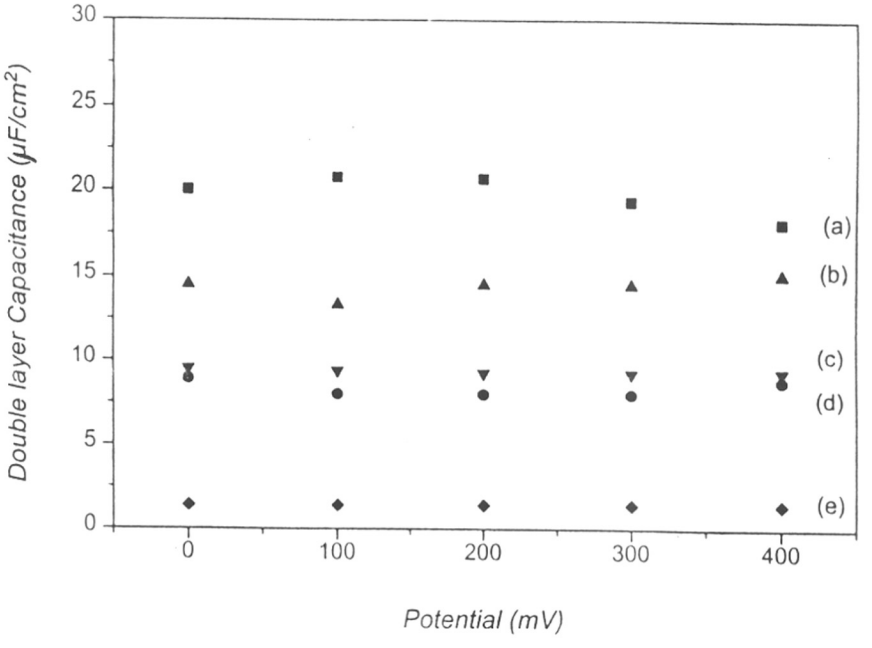

Figure 3.4. Variation of double layer capacitance values with potential for (a) bare gold; (b) NDS; (c) DDSe; (d) DDS and (e) ODT modified gold electrode in 0.1 M aqueous KF. Double layer capacitance of the respective electrodes are measured from cyclic voltammetry measurements as discussed in the text.

tetrafluoroborate as supporting electrolyte using a platinum electrode at a representative scan rate of 200 mV/s. Figure 3.5 shows a superimposed cyclic voltammogram of all the three relevant molecules. The voltammetric response on DDS and DDSe are similar in nature, where, DDSe (Figure 3.5a), shows an irreversible oxidation peak at + 1.4 V vs SCE corresponding to the formation of $C_6H_5Se^+$ from the Se-Se cleavage along with a cathodic peak at + 0.26 V. The latter cathodic peak may probably be attributed to the reduction of H^+ in the media since the electrochemical behavior of diselenide is very similar to its sulfur analogue.[17] However, in case of the corresponding disulfide, DDS, (Figure 3.5b) the oxidation peak potential is much higher (~ + 1.6 V), suggesting a comparatively easy dissociation of the Se-Se over S-S bond. The observed redox activity of NDS (Figure 3.5c) is completely different from the above discussed disulfide and diselenide. The observed one electron oxidation of the cyclic disulfide is due to the formation of a stable radical cation (an aromatic dithiolylium cation).[18] The cyclic voltammogram of the compound exhibits a reversible oxidation/reduction wave at $E_{1/2}$ = + 0.79 V vs SCE. The expected two electron reduction of disulfide leading to the S-S bond cleavage is noted to be absent here. Presumably, in the monoanion, sulfur atoms are retained within the bonding distance of the rigid naphthalene backbone and further reduction is made difficult by electronic repulsion.[18] The anodic as well as the cathodic peaks in the voltammogram are not symmetric in nature indicating the possibility of strong adsorptive interactions of both oxidized and reduced species. In addition, a response similar to surface confined species is also indicated by the symmetrical reversible peak around $E_{1/2}$ = + 0.50 V and the broadness suggests a decrease in the rate of the heterogeneous electron transfer.

3.3.4. Surface Enhanced Raman Spectroscopy:

Figures 3.6 - 3.8 show the resonance Raman spectra of NDS, DDS and DDSe compounds respectively in powder form and their monolayers on Au. The spectral region of 400-650 cm^{-1} in normal Raman spectra of the powdered samples are specially interesting as S-S stretching frequency lies in this region for different disulfide compounds. This region also contains number of bands other than ν(S-S) stretching

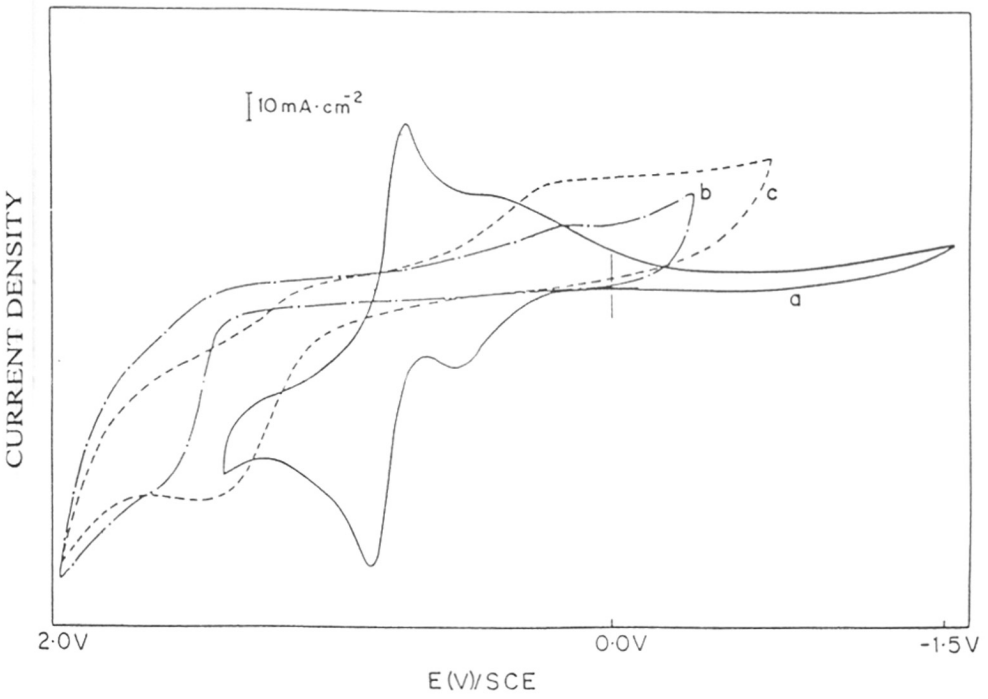

Figure 3.5. Superimposed cyclic voltammogram of 1 mM (a) NDS; (b) DDS and (c) DDSe in acetonitrile with 0.1 M tetrabutyl ammonium tetrafluoroborate as supporting electrolyte at a scan rate of 200 mV/s. Platinum disk and SCE are used as working and reference electrodes respectively.

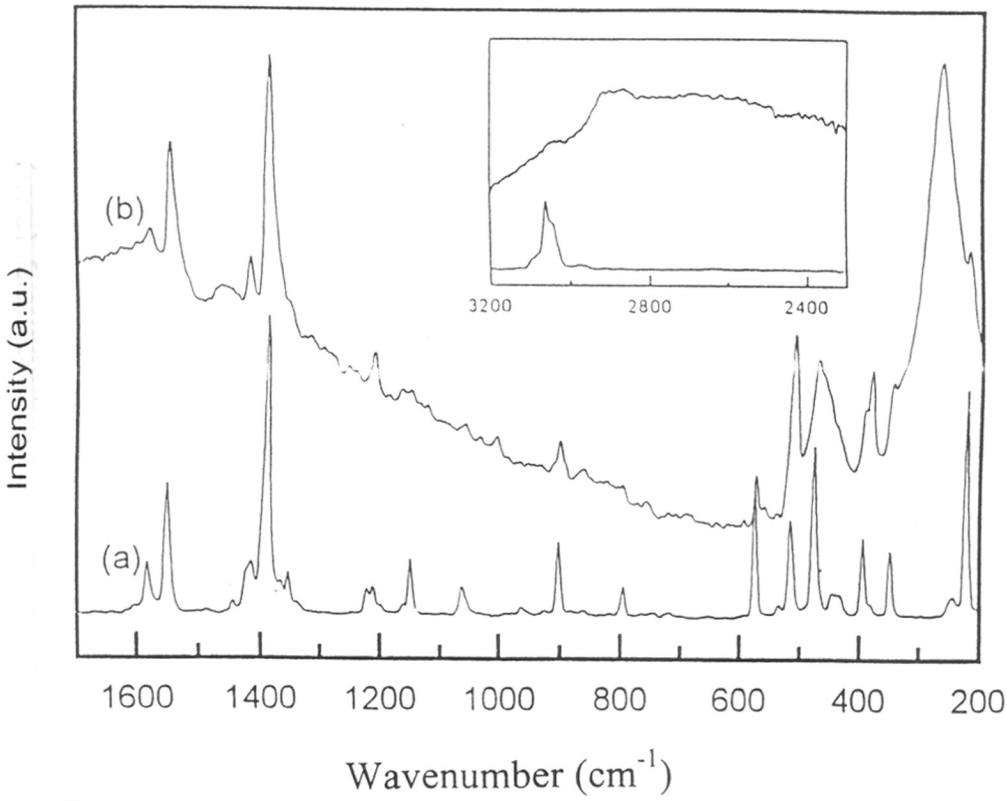

Figure 3.6. The (a) normal Raman of NDS in powder form and the (b) SER spectra of its monolayer on Au. The C-H stretching region of the respective system is shown in the inset. Spectrum has been taken on an oxidized aluminium foil sputter coated with ~ 200 nm gold.

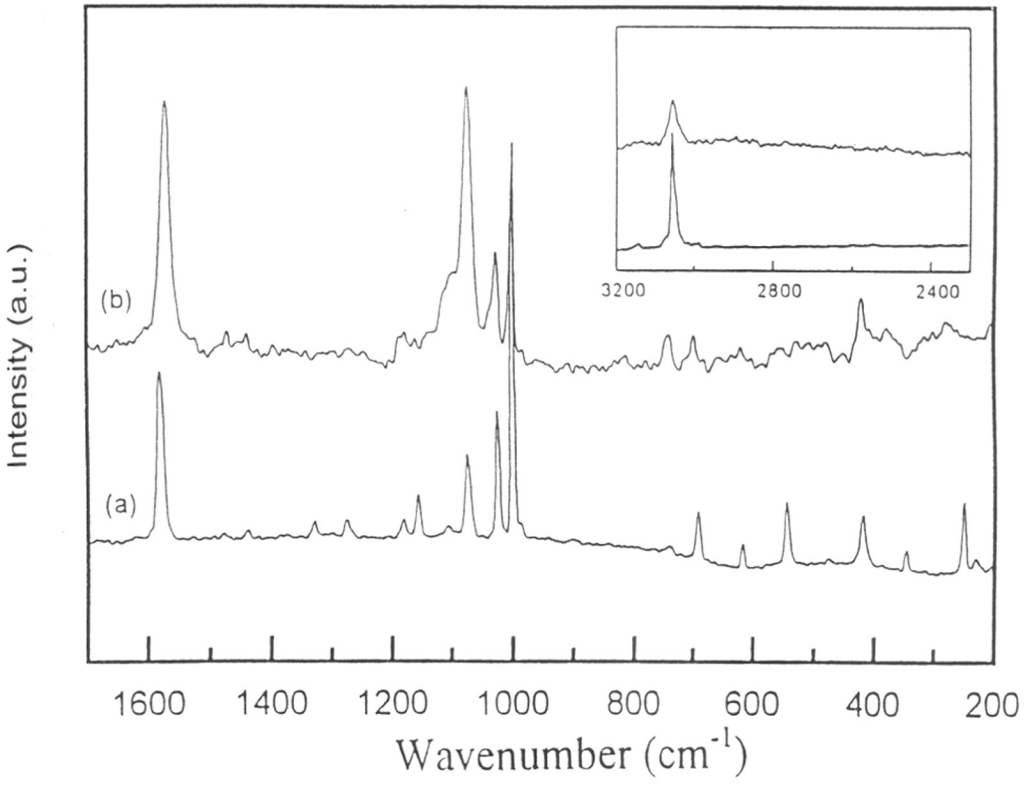

Figure 3.7. The (a) normal Raman of DDS in powder form and the (b) SER spectra of its monolayer on Au. The C-H stretching region of the respective system is shown in the inset. Spectrum has been taken on an oxidized aluminium foil sputter coated with ~ 200 nm gold.

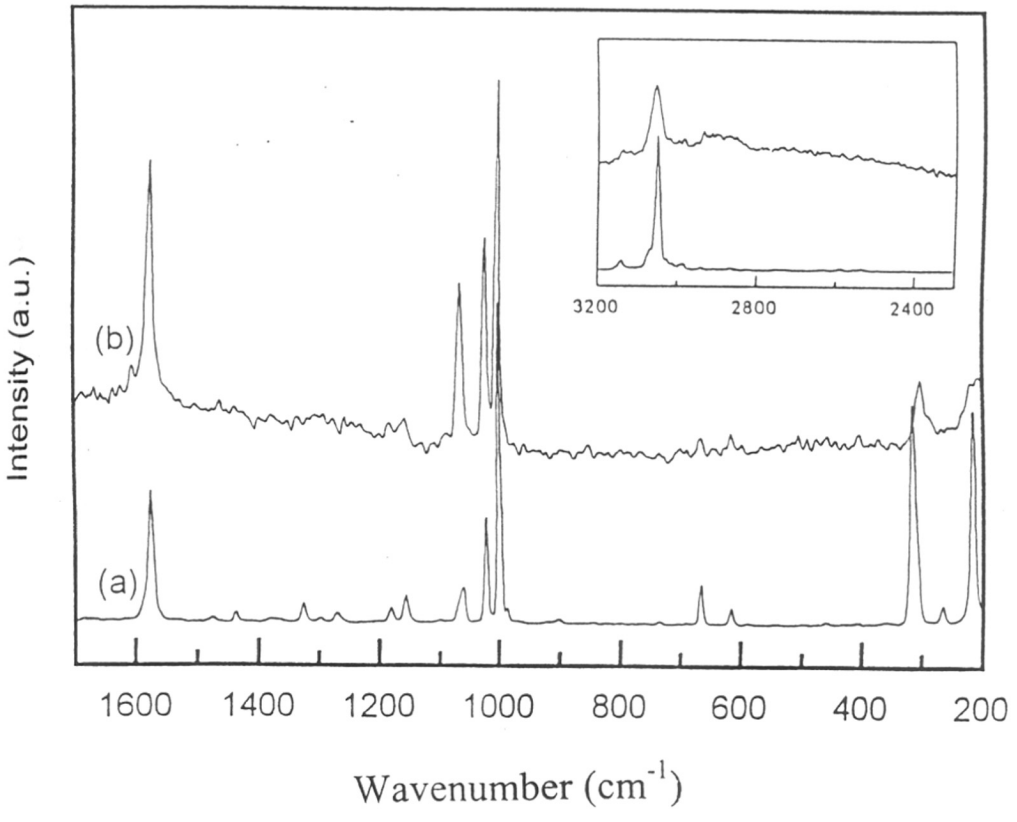

Figure 3.8. The (a) normal Raman of DDSe in powder form and the (b) SER spectra of its monolayer on Au. The C-H stretching region of the respective system is shown in the inset. Spectrum has been taken on an oxidized aluminium foil sputter coated with ~ 200 nm gold.

possibly due to the crystal field effect.[19] On the other hand, the strong Se-Se stretching vibration is known to fall in the region 330-290 cm^{-1}. The S-S stretch has been observed at 572 cm^{-1} and 542 cm^{-1} for NDS and DDS respectively, and that of the Se-Se at 310 cm^{-1} for DDSe. The features observed at 416, 692, 1000, 1020, 1070, and 1572 cm^{-1} are characteristic of the benzenethiol group (C_6H_5S-),[20] observed both for bulk as well as monolayer of DDS, DDSe and NDS, excepting some difference in the last one due to the presence of the naphthalene ring. It is known that, for a benzene system, the major peaks are ring stretch doublet near 1600 cm^{-1}, ring in plane bending at 618 cm^{-1}, in-plane C-H deformation at 1028 cm^{-1} and in-plane ring deformation[21] at 995 cm^{-1}. In comparison, the SER spectrum of NDS, DDS and DDSe after adsorption on the gold surface reveal several interesting features. Firstly, it is known that disulfides can form self-assembled monolayer by an oxidative dissociation of the S-S bond and the absence of the band at 542 cm^{-1} for DDS confirms the dissociative mode of monolayer formation.[22] In addition, the other bands due to benzene ring are shifted to lower energy due to adsorption. Down-shift of bands due to adsorption is characteristic of monolayer formation. The extent of shift is not large indicating negligible π-interaction. In contrast, for NDS, a band is seen at 568 cm^{-1} suggesting the presence of undissociated S-S bonds in the adsorbed molecule. This difference in the Raman spectra is specially significant as the probable origin of this mode can be understood in terms of the restrictions imposed by the rigid naphthalene ring, which can hold the two sulfurs within a bonding distance. The spectrum for DDSe after adsorption on Au surface shows a band around 301 cm^{-1} indicating the possibility of the undissociated Se-Se bond. On the other hand, behavior of DDSe is somewhat surprising considering the lower binding energy of Se-Se than that of S-S.

The SER spectra of these systems in the C-H stretching region gives important information on the orientation of the adsorbed species. It has been well established that the vibrations parallel to the surface are enhanced only to a lesser extent in SERS.[23] When the benzene ring lies flat on the surface, the component of the polarisability tensor normal to the surface due to C-H vibrations will be small, leading to a weak C-H stretching band. However, in case of all the molecules, the C-H stretching

region (the inset of Figure 3.6 - 3.8) shows peaks. Additional peaks are also observed due to combination bands in the case of NDS. This would suggest that the molecules are "sticking up" on the surface.

Figures 3.9 - 3.11 show the variable temperature SER spectra of DDSe, DDS and NDS respectively after adsorption on the Au surface in order to demonstrate the comparative thermal stability of the respective monolayers. The variation of spectral features after heating the respective samples in air starting from room temperature clearly shows that the intensity of major bands are totally lost at 348 K for NDS while for DDSe and DDS this happens at 423 K and 448 K respectively. This trend unambiguously suggests that, DDS monolayer on gold is thermally most stable followed by the monolayers of DDSe and NDS. This order of thermal stability can be explained on the basis of the structure of the molecules and substrate-head group interaction.

To be specific, the structure of the NDS molecule is different from the other two as the sulfurs are bound at a definite distance due to the constraint offered by the rigid naphthalene ring (Scheme 3.2a) which would hinder both the sulfur atoms from occupying the three-fold hollow site - the normal mode of bonding observed for sulfur in SAMs[5] (Scheme 3.1a). On the other hand, this type of a constraint is absent for DDS and DDSe. In addition, sulfur and selenium can have different energy of interaction with Au surface thus explaining the different thermal stability. Evaporated gold will preferentially form (111) islands and the three-fold hollow sites are at a distance of 2.885 Å on such a surface. This would make it impossible for both the sulfurs of NDS to occupy the preferred binding sites. For both the sulfurs to bind the surface keeping the S-S bond intact, both the hollow and on-top (or bridge) sites have to take part in the bonding.

3.3.5. XPS Measurements:

XPS shown in Figures 3.12 - 3.14 (the S 2p and Se 3p binding energy values for NDS, DDS and DDSe are listed in Table 3.1) also indicate the difference in the nature of the monolayer for these three molecules on Au surface. In DDS, the S 2p

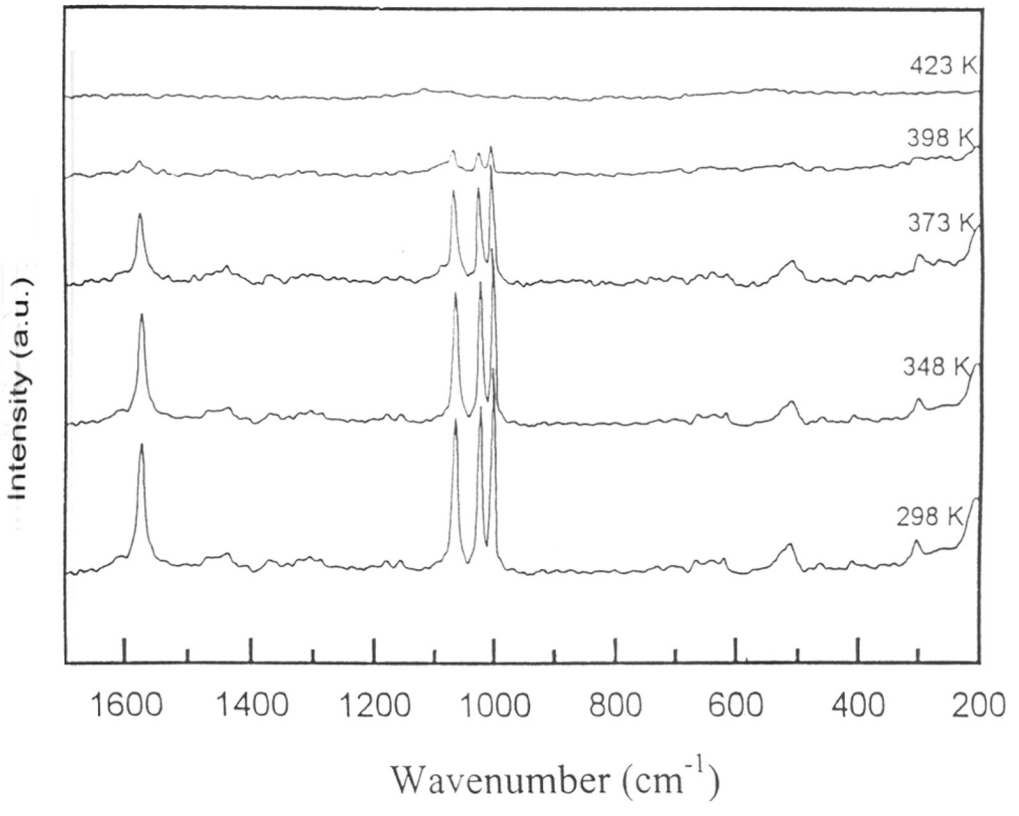

Figure 3.9. The temperature dependent SER spectra of DDSe on Au. The temperatures are indicated.

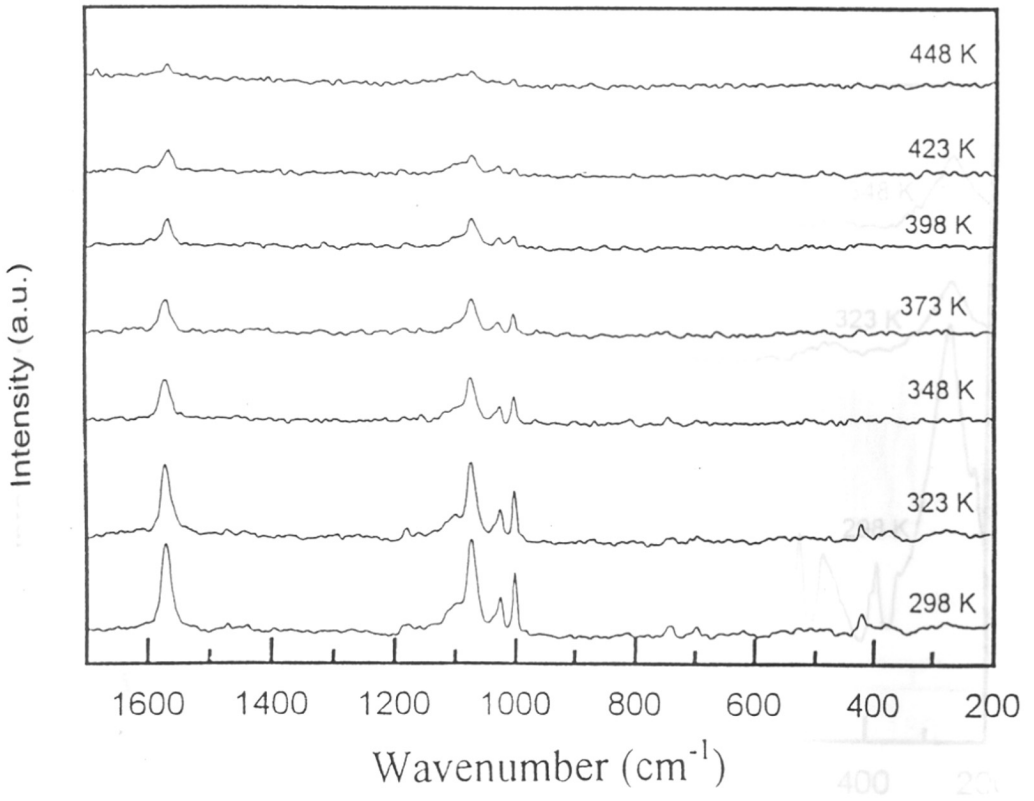

Figure 3.10. The temperature dependent SER spectra of DDS on Au. The temperatures are indicated.

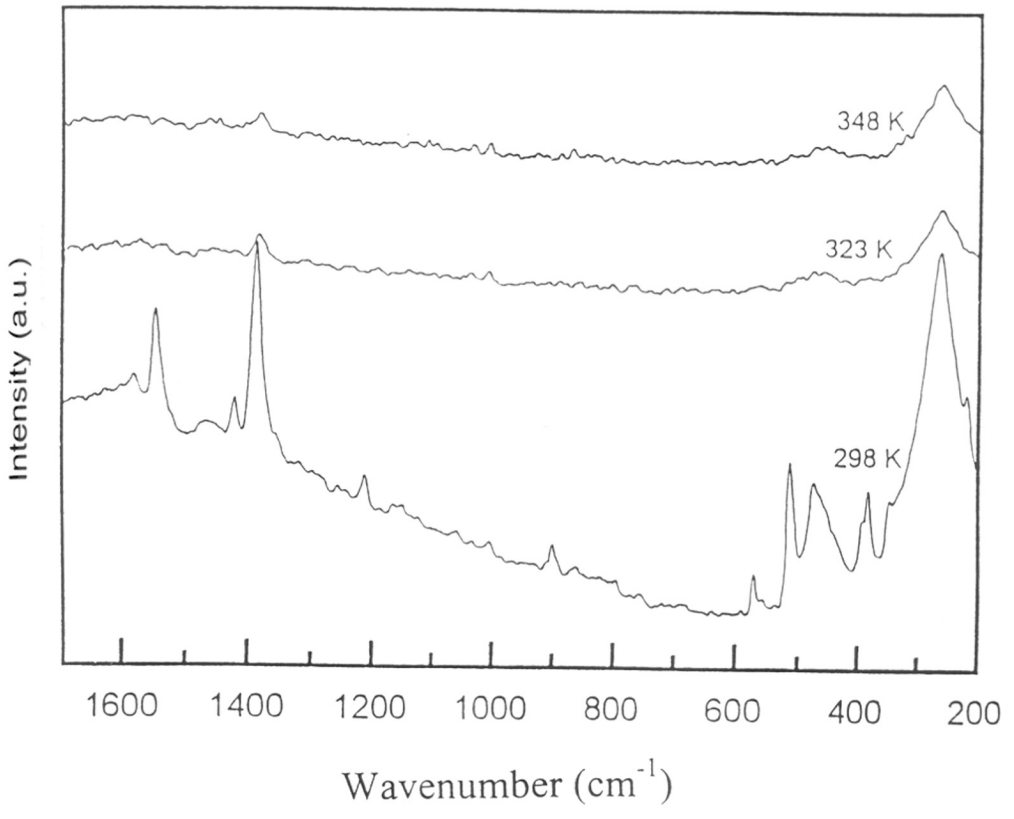

Figure 3.11. The temperature dependent SER spectra of NDS on Au. The temperatures are indicated.

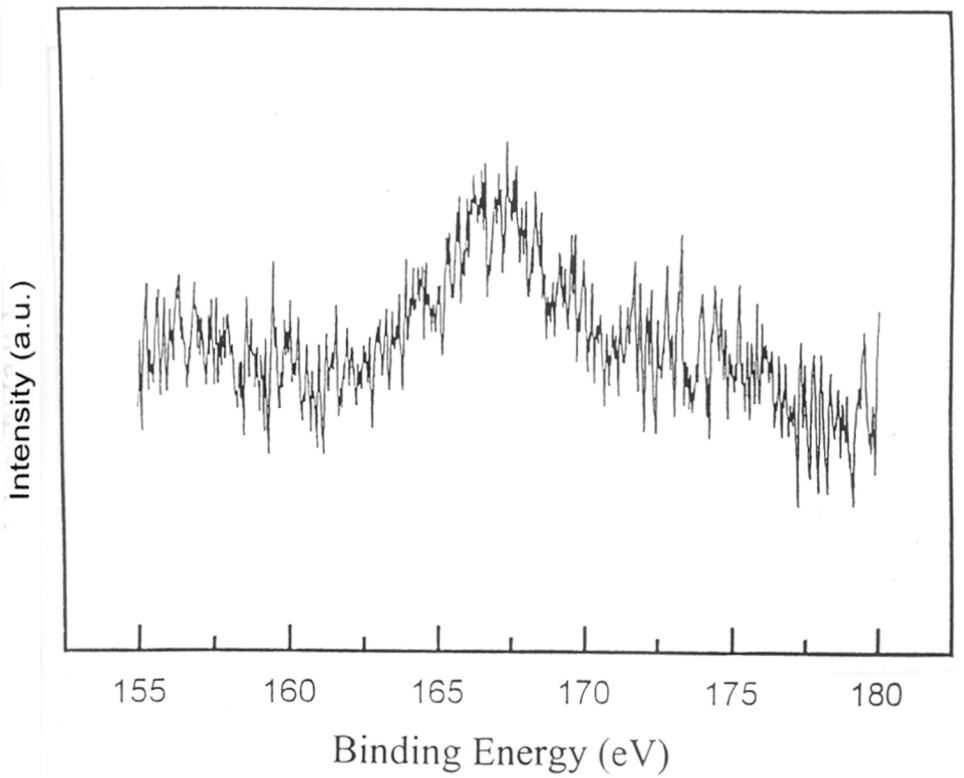

Figure 3.12. Mg Kα induced XPS spectrum showing the S 2p core level region of the NDS monolayer on gold. The spectra are not subjected to a peak fitting analysis since there can be more than one beam induced (damaged) products.

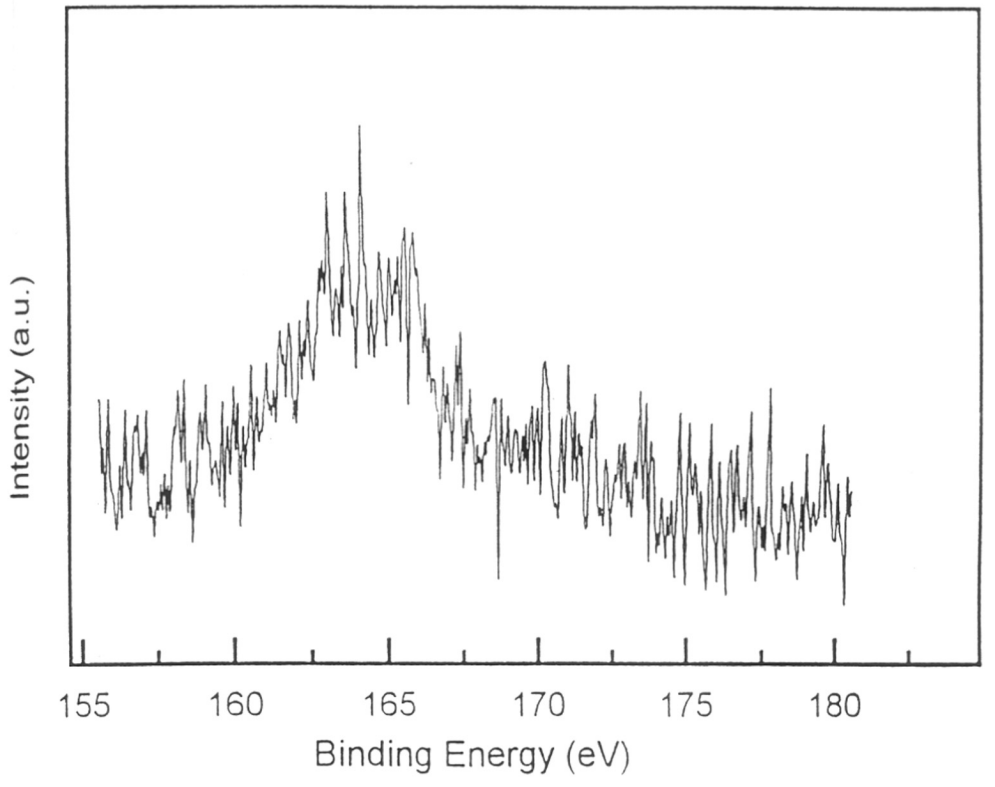

Figure 3.13. Mg Kα induced XPS spectrum showing the S 2p core level region of the DDS monolayer on gold. The spectra are not subjected to a peak fitting analysis since there can be more than one beam induced (damaged) products.

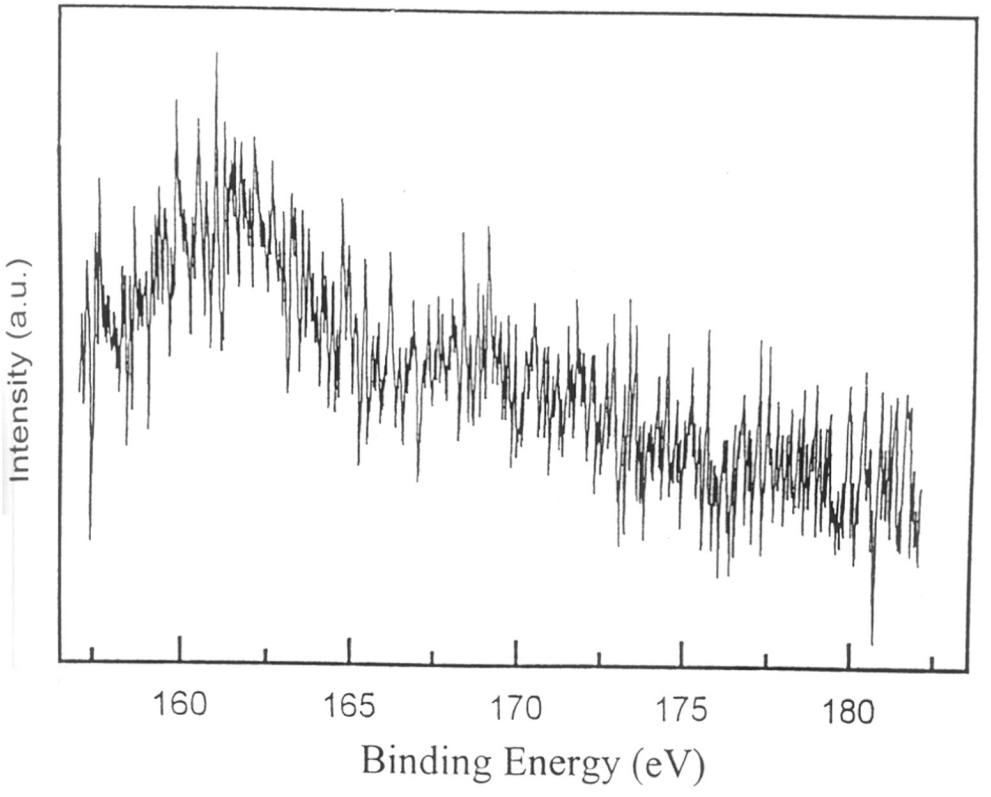

Figure 3.14. Mg Kα induced XPS spectrum showing the Se 3p core level region of the DDSe monolayer on gold. The spectra are not subjected to a peak fitting analysis since there can be more than one beam induced (damaged) products.

Table 3.1

Different Parameters Obtained From XPS, Impedance and SERS Measurements For NDS, DDS and DDSe SAMs on Gold Surface

Different parameters	NDS	DDS	DDSe
Charge transfer resistance, R_{ct} (Ω cm^2)	567	1300	1100
Apparent electrode coverage, θ (%)	99.6	99.8	99
Double layer capacitance*, C (μF/cm^2)	14.9	8.03	9.4
Defect free monolayer capacitance, C_s (μF/cm^2)	14.8	7.9	9.28
Monolayer dielectric constant, ε	11.7	6.23	7.3
Apparent rate constant for $Fe(CN)_6^{3-/4-}$ couple, k_{app} (cm/s)	9.3×10^{-5}	4.1×10^{-5}	4.83×10^{-5}
Diffusion coefficient, D (cm^2/s)	1.2×10^{-7}	1.6×10^{-8}	4.0×10^{-8}
Binding Energy (eV)	S_{2p} 167.2 169.1	S_{2p} 163.5 165.4	Se_{3p} 161.5 167
Monolayer stability temperature (K)	348	448	423

* The double layer capacitance of bare gold is 21 μF/cm^2 and that of ODT modified gold is 1.4 μF/cm^2.

peaks appear at 163.5 and 165.4 eV, the former being similar in intensity. We attribute the former to the thiolate[24] (RS^-) and the latter to the X-ray beam induced damage. The peaks are, however, broad and therefore, beam induced damage cannot be ruled out. Beam induced oxidative damage in small organic thiol monolayers are well known in the literature leading to the formation of sulfonate or sulfate species.[25] In DDSe, however, the beam induced damage is not clearly visible. The peaks at 161.5 is similar to the surface Au-Se (taking the similar binding energy shift for disulfides/thiols on Au-S bond formation) and at 168.7 eV is a result of oxidation product of corresponding selenium. Although there are two distinct kinds of seleniums in the monolayer (if only one is binding), they both are expected to appear within 1 eV B.E. Since the Se-Se bond is retained in the monolayer, both the atoms are expected to have more or less similar charges. In NDS, the peak is well-defined and has a substantially higher B.E and we attribute it to the beam induced damage. It may be noted that the beam induced oxidation is more feasible for disordered monolayer structure.[26] Therefore, the lower intensity of higher binding energy component for DDS monolayer suggests a more compact and the ordered monolayer structure compared to NDS. This conclusion from the XPS investigation is in excellent agreement with the order of thermal stability observed in the temperature dependent SER spectra.

3.3.6. Heterogeneous Electron Transfer at the Monolayer Modified Electrode with External Redox Probe:

It is known that, SAM in most of the cases, provides an effective barrier for the electron transfer of the redox probes in solution and the extent of hindrance to ion permeation helps to understand the distribution of the defect density over the monolayer. Moreover, the barrier properties can give a direct microscopic evidence of the extent of molecular organization. The superimposed cyclic voltammetric response of $Fe(CN)_6^{4-/3-}$ couple at bare gold, NDS, DDS and DDSe monolayer modified electrodes in Figure 3.15 (a, b, c and d) show that in both the modified electrodes the reversible response of the redox couple is not seen although a drastic reduction of the nonfaradaic current is distinct compared to the bare gold electrode. Further, among the three cases the decrease in charging current is more for the DDS modified electrode

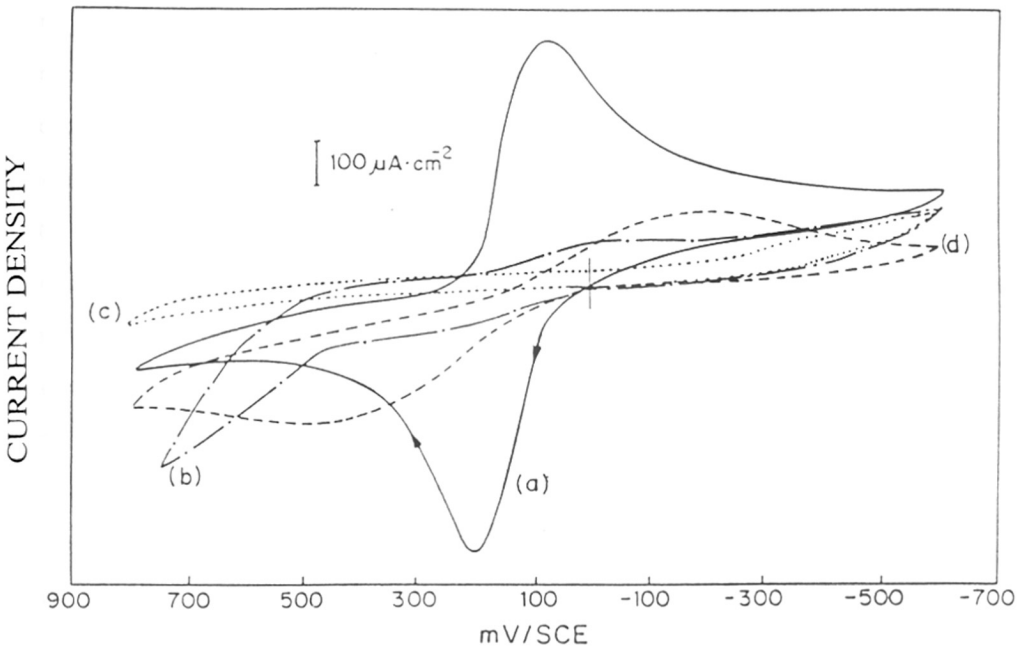

Figure 3.15. Superimposed cyclic voltammogram of 1 mM $K_3Fe(CN)_6$ in 0.1 M KF at (a) bare gold (b) NDS (c) DDS and (d) DDSe modified gold electrodes after two hours of dipping in 1 mM solution of the respective compounds in acetonitrile at a scan rate of 200 mV/s.

suggesting that the monolayer obtained from DDS is more compact (i.e., with a smaller number of pinholes) than NDS and DDSe monolayers. More specifically, the electron transfer kinetics has become slower due to the barrier produced by the monolayers as evident from the increase in ΔE_p value from ~70 mV to ~644.5 mV. Interestingly, unlike the case of long chain thiol/disulfides, here the redox activity is not totally suppressed by the monolayer. Actually, long chain thiols/disulfides are reported to form a compact monolayer, free of measurable pinholes, which provides substantial barrier to electron transfer and strong resistance to ion penetration. The faradaic current observed at these monolayer modified electrodes is believed to be due to electron tunneling through the long alkyl chain. On the contrary, a monolayer having a number of pinholes can show a different current-potential response depending on the distribution of the defects in the monolayer. If the pinholes are close enough so that the diffusion layers are overlapping to each other, then, a current response similar to a linear diffusion is observed. On the other hand, a current response similar to a radial diffusion will be observed if the defects are small in number so that they do not overlap and hence act as an array of individual electrodes.[14c] Voltammograms taken with NDS and DDSe modified gold electrode indicate that the current is controlled primarily by linear diffusion as evident from the increase in peak current with scan rate in contrary to the response obtained for the DDS monolayer. The shape of the voltammograms also provides additional support for this mode of electron transfer and further suggests that the monolayer do not completely block the electron transfer as these small molecules provide only a partial barrier. Moreover, the π-electrons present in the molecule can further help the electron transfer across the monolayer due to extended conjugation.

3.3.7. Impedance Measurements:

A comparison of the total impedance plots of bare (Figure 2.7 in chapter 2) and NDS (Figure 2.9 in chapter 2), DDS and DDSe (Figures 3.16 and 3.17 respectively) monolayer coated gold electrode shows the effect of different adsorbed monolayer. It is known that the diameter of this semicircle is a measure of the R_{ct} which is greater than

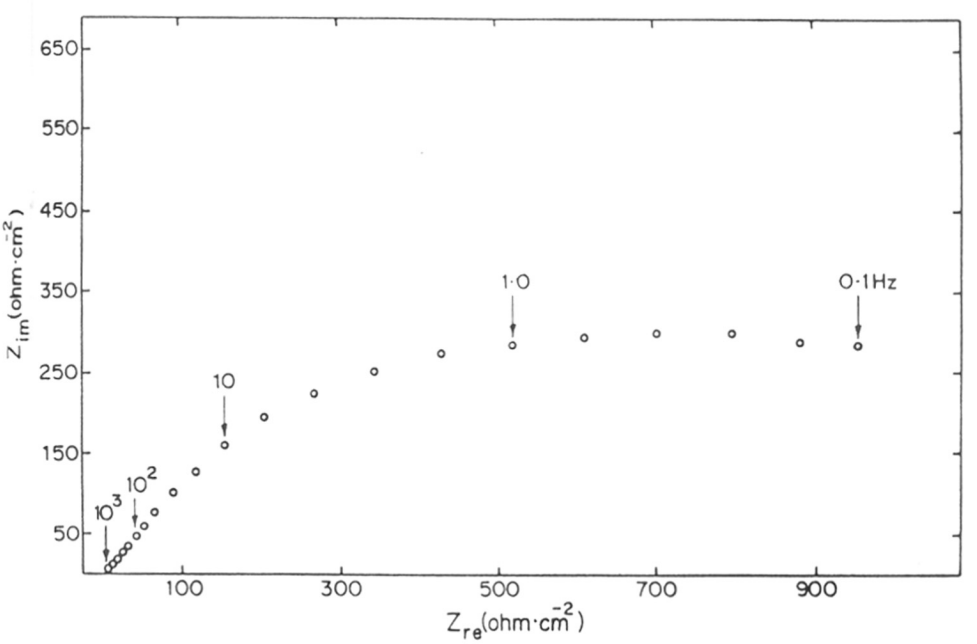

Figure 3.16. Complex impedance plots at a dc bias of 0.22 V vs SCE in 5 mM $K_3Fe(CN)_6$ + 5mM $K_4Fe(CN)_6$ in 0.5 M aqueous KF solution for gold electrode derivatized with DDS monolayer for 2 hours. Frequency range used is 100 KHz to 100 mHz with a 5 mV rms signal at 5 steps per decade.

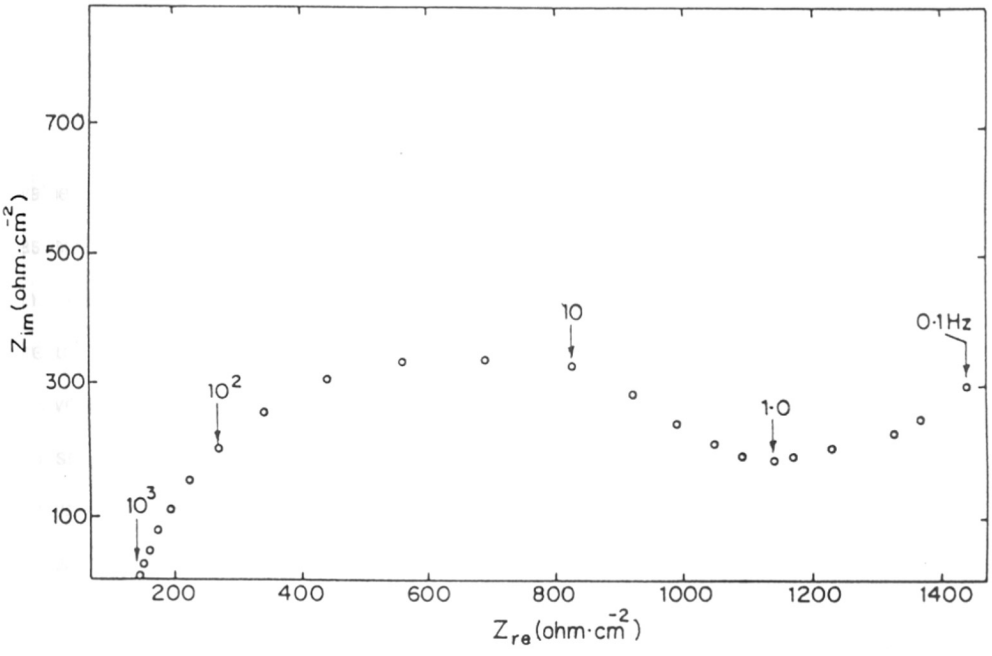

Figure 3.17. Complex impedance plots at a dc bias of 0.22 V vs SCE in 5 mM $K_3Fe(CN)_6$ + 5mM $K_4Fe(CN)_6$ in 0.5 M aqueous KF solution for gold electrode derivatized with DDSe monolayer for 2 hours. Frequency range used is 100 KHz to 100 mHz with a 5 mV rms signal at 5 steps per decade.

the corresponding R_{ct} measured at bare gold electrode due to the inhibition of electron transfer rate.[27] From this increase in the charge transfer resistance, one can calculate the approximate coverage of the gold electrode[28] from Equation 2.1 (chapter 2, section 2.3.4). Moreover, this semicircle is indicative of a parallel RC equivalent circuit for the electrode impedance. From a semicircle fit (using a nonlinear least square program) of the spectra shown in Figures 2.9, 3.16 and 3.17, charge transfer resistance for NDS, DDS and DDSe monolayer coated gold electrode are obtained along with the corresponding coverage values as listed in Table 3.1. These compare well with the available values of alkane thiols and disulfides monolayer indicating similar extent of monolayer formation.[29]

The above value of R_{ct} can also be used to estimate the apparent rate constant value of $Fe(CN)_6^{4-/3-}$ couple at the monolayer modified electrode since the monolayer assemblies provide a barrier for electron transfer leading to an expected decrease in the rate constant.[29] Since, impedance can give a considerable separation in frequencies between the kinetic semicircle and diffusion limited region, it allows convenient evaluation of kinetic parameters with the possible interference from mass transport. Under these conditions the charge transfer resistance R_{ct} can be calculated by using Equation 3.1, from the diameter of the semicircle at higher frequencies, assuming $c_{ox} = c_{red} = c$, unit geometry and one electron first order reaction:

$$R_{ct} = R\,T / [F^2(1-\theta)\,k_0\,c] = R\,T / [F^2\,k_{app}\,c] \qquad \textbf{(3.1)}$$

where θ is the surface coverage by the monolayer and $(1-\theta)$ corresponding to the total fraction of pinholes. k_0 and k_{app} are the real and apparent standard heterogeneous rate constant respectively. Thus k_{app} is calculated to be 9.37×10^{-5}, 4.83×10^{-5} and 4.09×10^{-5} cm/s for $Fe(CN)_6^{4-/3-}$ couple at NDS, DDSe and DDS monolayer modified electrodes using R_{ct} value from Figures 2.9, 3.16 and 3.17. A comparison of these measured apparent rate constants (Table 3.1) indicates that, at both the monolayer

modified electrodes, the rate constant of the redox couple has been decreased by three orders of magnitude (rate constant of the redox couple at the bare gold electrode is 2.6 x 10^{-2} cm/s).[16] This reduction is expected as the organized assemblies form a barrier for electron transfer at the electrode-electrolyte interface and the amount of decrease in the rate constant can be correlated with the degree of compactness. Interestingly, the rate constant of the redox couple calculated at the DDS modified electrode is smaller than that for NDS and DDSe case suggesting a more compact and organized SAM structure in the former case.

The impedance response of the monolayer coated electrode can be explained as an array of microelectrodes and related theory has been developed by Finklea *et al.*[29a] For a total defect area (pinholes) of less than 0.1, both real and imaginary part of the faradaic impedance can be related to frequency (as $\omega^{-1/2}$). From this formulation, it is evident that, high frequency domain of faradaic impedance is less affected due to the nonuniformity of the defects as a result of uneven size and spacing of the pinholes. Consequently, this portion can be analyzed to obtain the surface coverage (θ) under the assumption of (i) θ is very large to form $1-\theta = 0.1$, (ii) electrolyte contains equal concentration of oxidized and reduced form of the redox couple and (iii) equal diffusion coefficients. At higher frequencies corresponding to nearly isolated diffusion profiles for each microelectrode, following expressions should be used.

$$Z_f' = [R_{ct}/1-\theta\ ] + [\sigma/\sqrt{\omega}] + [\sigma/\ (1-\theta)\sqrt{\omega}] \qquad (3.2)$$

$$Z_f'' = [\sigma/\sqrt{\omega}] + [\sigma/\ (1-\theta)\sqrt{\omega}] \qquad (3.3)$$

Similarly at low frequency,

$$Z_f' = [R_{ct}/1-\theta\ ] + [\sigma/\sqrt{\omega}] + [\sigma R_a(0.72/D)^{1/4}/1-\theta] \qquad (3.4)$$

$$Z_f'' = [\sigma/\sqrt{\omega}] \qquad (3.5)$$

where R_{ct} is the charge transfer resistance, θ is the coverage, σ is the Warburg coefficient, ω is the frequency, D is the diffusion coefficient, R_a is the radius of the pinhole, Z_f' and Z_f'' are the real and imaginary components of the faradaic impedance respectively. The essential requirement of the above set of equations is that the diffusion layers of the individual microelectrodes do not strongly overlap. In Figure 3.18 (a, b and c), the real part of the faradaic impedance (Z_{re}) has been plotted as a function of $\omega^{-1/2}$ after subtracting the solution resistance and interfacial capacitance from the measured total impedance. The values for the uncompensated resistance and capacitance are obtained from the impedance data corresponding to highest frequency. The faradaic impedance plot shows features similar to those of a microarray electrode. The simulated behavior for ideal microarray electrode indicates two nearly linear domain at high and low frequencies[29a] although the curves obtained by us resemble more to a monotonically increasing function with $\omega^{-1/2}$. This deviation from the ideal microarray behavior may be due to the nonuniform distribution of pinholes on the monolayer surface. The slope of the Z_f' vs $\omega^{-1/2}$ at higher frequency region can give approximate estimate of surface coverage of the NDS, DDSe and DDS monolayer using known values of Warburg coefficient (σ).[29a] The value of σ can be obtained experimentally using a bare electrode in the same solution. Analysis of Figure 3.18 yields θ as 0.995, 0.997 and 0.993 for NDS, DDS and DDSe (Table 3.1) respectively which qualitatively confirm to the greater compactness of DDS compared to the other two monolayers.

The analysis of the Z_f' vs $\omega^{-1/2}$ plot at lower frequency for all the monolayer shows that the slope of the curve is decreased as $\omega^{-1/2}$ is increased (with bare gold remaining constant; not shown in figure). The Warburg coefficient (σ) calculated from the curve corresponding to each monolayer is always greater than that obtained for a bare gold electrode in the same solution. Values of σ calculated in the lower frequency region gives 216, 375 and 594 ohm $cm^2/s^{1/2}$ respectively for NDS, DDSe and DDS monolayers while that of bare gold is 39.5 ohm $cm^2/s^{1/2}$. The increase in the apparent value of the Warburg coefficient for monolayer coated electrodes suggest a lower diffusion coefficient or that the pinholes are distributed in patches over the surface

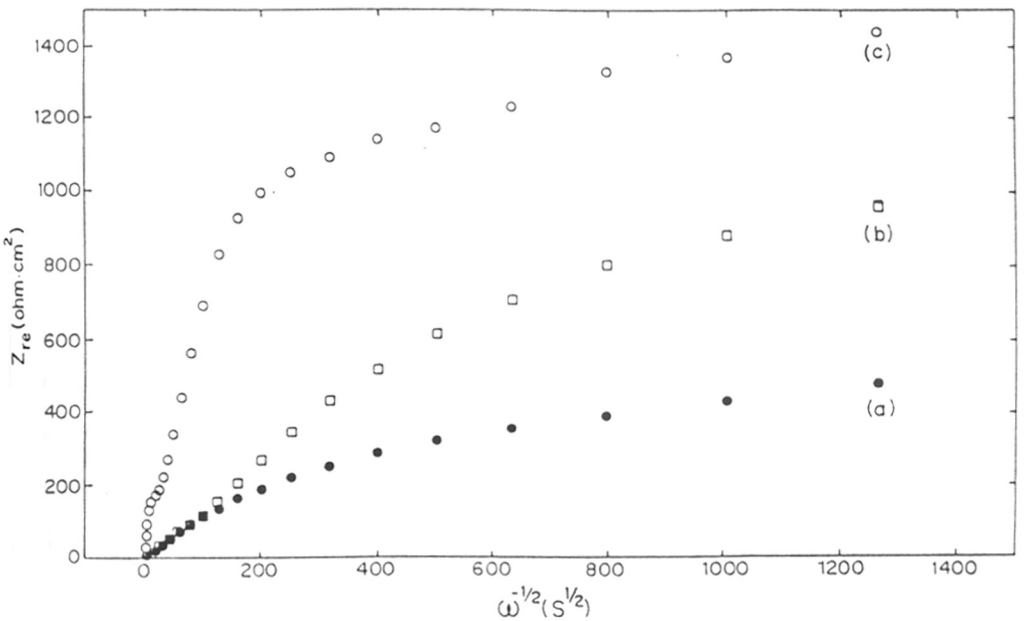

Figure 3.18. Superimposed plot of the real part of faradaic impedance (Z_{re}) vs $\omega^{-1/2}$ in 5 mM $K_3Fe(CN)_6$ + $K_4Fe(CN)_6$ in 0.5 M aqueous KF solution for (a) NDS monolayer; (b) DDS monolayer and (c) DDSe monolayer on Au electrode.

instead of being uniformly distributed or perhaps both.[29a] Assuming equal values of diffusion coefficients for both the oxidized and reduced species, the corresponding diffusion coefficients for bare gold (3.62×10^{-6} cm^2/s) and NDS, DDS and DDSe modified gold electrodes are calculated to be 1.2×10^{-7}, 1.6×10^{-8} and 4.0×10^{-8} cm^2/s respectively.[30] The diffusion coefficient of the bare gold electrode is in excellent agreement with the known diffusion coefficient of aqueous solution of $Fe(CN)_6^{4-/3-}$ from different independent experimental measurements.[31] An order of magnitude reduction in the diffusion coefficient value from NDS to DDS and DDSe is especially significant since the monolayer formed from DDS and DDSe allows slower ion permeation compared to the NDS monolayer indicating more compact monolayer formation in the former.

An approximate determination of the monolayer dielectric constant is possible from the impedance results with a few additional assumptions,[32] as shown in chapter 2 (section 2.3.4, Equation 2.4). The doublelayer capacitance value of the defect free monolayer values (C_s) (listed in Table 3.1 along with the other parameters obtained from impedance and XPS measurements on NDS, DDS and DDSe monolayer modified electrode) obtained for all the monolayers can be used to calculate the dielectric permittivity of the monolayer film (ε_{ns}) by using Equation 2.5 (section 2.3.4, chapter 2). The dielectric permittivity values obtained are 11.7, 6.3 and 7.3 for NDS, DDS and DDSe monolayers respectively, which are in fairly good agreement with those obtained by Rubinstein *et al*[16] for similar compound (*p*-biphenyl mercaptan and *p*-terphenyl mercaptan). Nevertheless, they are significantly high compared to the values reported for pure benzene (2.28) and naphthalene (2.52)[33] revealing the importance of geometric constraints.

3.4. Conclusion:

It emerges from QCM, SERS, XPS and electrochemical investigations of SAMs of NDS, DDS and DDSe on Au surface that, molecular geometry as well as substrate-headgroup interaction holds a key role in determining the monolayer organization and stability. From all the data, it is clearly evident that, monolayer obtained from DDS is

highly organized, provide an effective barrier for electron transfer and undergoes less beam-induced damage. Higher thermal stability of the DDS monolayer is also evident from the temperature dependent SERS investigation. These results can be substantiated on the basis of the strained structure of the molecule and the difference in substrate head-group interaction. The facile S-S cleavage in DDS is the principal reason for the stability of the monolayer. Structurally similar DDSe also forms a monolayer which is quite stable, unlike the case of NDS which forms thermally most unstable and less ordered monolayer, presumably due to the inherent structural rigidity on two sulfurs by naphthalene group. In the present investigation the most interesting result is the evidence of S-S bond cleavage in DDS upon monolayer formation in contrast to that of DDSe and NDS where retention of the S-S and Se-Se bond is observed.

3.5. References:

1. Ulman, A. *Chem.Rev.* **1996**, *96*, 1533.

2. (a) Hickman, J. J.; Ofer, D.; Laibinis, P. E.; Whitesides, G. M. Science **1991**, *252*, 688. (b) Mirkin, C. A.; Ratner, M. A. *Annu. Rev. Phys. Chem.* **1992**, *43*, 719. (c) Li, D.; Ratner, M. A.; Marks, T. J.; Znang, C. H.; Yang, J.; Wong, G. K. *J. Am. Chem. Soc.* **1990**, *112*, 7389. (d) Wollman, E. W.; Kang, D.; Frisbie, C. D.; Larcovic, T. M.; Wrighton, M. S. *J. Am. Chem. Soc.* **1994**, *116*, 4395. (e) Tariov, M. J.; Jr. Burgess, D. R. F.; Gillen, G. *J. Am. Chem. Soc.* **1993**, *115*, 5305. (f) Kawanishi, Y.; Tamaki, T.; Sakuragi, M.; Seki, T.; Swuzki, Y.; Ichimura, K. *Langmuir* **1992**, *8*, 2601.

3. Ulman, A. *An Introduction to ultrathin organic films from Langmuir-Blodgett to Self-assembly;* Academic Press: San Diego, CA, 1991.

4. Fenter, P.; Eberhardt, A.; Eisenberger, P. *Science* **1994**, *266*, 1216.

5. Strong, L.; Whitesides, G. M. *Langmuir* **1988**, *4*, 546.

6. Camillone, N.; Chidsey, C.E.D.; Liu, G. L.; Scoles, G. *J. Chem. Phys.* **1993**, *98*, 3503.

7. Sellers, H.; Ulman, A.; Shnidman, Y.; Eilers, J. E. *J. Am. Chem. Soc.* **1993**, *115*, 9389.

8. Patai, S.; Rappoport, Z. *Organic Selenium and Tellurium Compounds;* John Wiley & Sons: New York, 1986; Vol.1.

9. Samant, M. G.; Brown, C. A.; Gordon, J. G.,II *Langmuir* **1992**, *8*, 1615.

10. Dishner, M. H.; Hemminger, J. G.; Feher, F. J. *Langmuir* **1997**, *13*, 4788.

11. Zweig, A.; Hoffmann, K. *J. Org. Chem.* **1965**, *30*, 3997.

12. Sauerbrey, G. *Z. Phys.* **1959**, *155*, 206.

13 Delahay, P. *Double layer and electrode kinetics,* Interscience publishers, 1965.

14. (a) Porter, M. D. Thomas, B. B.; Allara,D.L.; Chidsey,C. E. D. *J. Am. Chem. Soc.* **1987**, *109*, 3559. (b) Miller, C.; Cudent, P.; Grätzel, M. *J. Phys. Chem.* **1991**, *95*, 877. (c) Sabatani, E.; Rubinstein, I. *J. Phys. Chem.* **1987**, *91*, 6663.

15. Angerstein-Kozlowska, A.; Conway, B. E.; Hamelin, A.; Stoicoviciu, I. *J. Electroan al. Chem.* **1987**, *228*, 429.

16. Sabatani, E.; Cohen-boulakia, J.; Bruening, M.; Rubinstein, I. *Langmuir* **1993**, *9*, 2974.

17. Morris, M. D.; Gregory, L. K. In *Encyclopedia of Electrochemistry of Elements.* Bard, A. J.; Lund, H.; Eds.; Marcel and Dekker Inc. New York and Brasel, 1979; Vol XIII p. 67, 68.

18. Chambers, J. Q. in *Encyclopedia of Electrochemistry of the elements*, vol XII; Bard, A. J., Lund, H., Eds.; Marcel Dekker Inc: New York and Basel, p 403, 406.

19. Van Wart, H. E.; Scherage, H. A. *J. Phys. Chem.* **1976**, *8*, 1823.

20. Scott, P. W.; McCullough. J. P.; Hubbard, W. N.; Messerly, J. F.; Hossenlopp. I. A.; Frow, F. R.; Waddington, J. *J. Am. Chem.Soc.* **1956**, *78*, 5463.

21. Scrader, B. *Angew. Chem. Int. Ed. Engl.* **1973**, *12*, 884.

22. Sandroff, C. J.; Herschbach, D. R. *J. Phys. Chem.* **1982**, *86*, 3277.

23. (a) Geo, X.; Davies, J. P.; Weaver, M. J. J. Phys. Chem. **1990**, 94, 6858. (b) Lee, T. G.; Kim, K.; Kim, M. S. *J. Raman Spectrosc.* **1991**, 22, 339. (c) Kwon, C. K.; Kim, M. S.; Kim, K. *J. Raman Spectrosc.* **1989**, 20, 575. (d) Lee, S. B.; Kim, K.; Kim, M. S. *J. Raman Spectrosc.* **1991**, 22, 811.

24. (a) Bain, C. D.; Troughton, E. B.; Tao, Y.-T.; Evall, J.; Whitesides, G. M.; Nuzzo, R. G. *J. Am. Chem. Soc.* **1989**, 111, 321. (b) Bain, C. D.; Evall, J.; Whitesides, G. M. *J. Am. Chem. Soc.* **1989,** 111, 7155.

25. Colvin, V. L.; Goldstein, A. N.; Alivisatos, A. P. *J. Am. Chem. Soc.* **1992**, 114, 5221.

26. Castner, D. G.; Hinds, K.; Grainger, D. W. *Langmuir* **1996**, *12*, 5083.

27. Whitman, R. M.; Wipf, D. O. In *Electroanalytical Chemistry:* Bard, A. J. Ed; Dekker, Newyork, 1989; Vol 15.

28. Sabatani, E.; Rubenstein, I. *J. Electroanal. Chem.* **1987**, *219*, 365.

29. (a) Finklea, H. O.; Snider, D. A.; Fedyk, J.; Sabatani, E.; Gafni, Y.; Rubenstein. I. *Langmuir*, **1993**, *9*, 3660. (b) Henke, C.; Steinem, C.; Jaushoff, A.; Steffan, G.; Luftmann, H.; Sieber, M.; Galla, H, -J. *Anal. Chem.* **1996**, *68*, 3158.

30. This is strictly not true since bare gold offers linear semi infinite diffusion condition while both modified electrodes offer a microarray diffusional condition and this change in diffusion geometry does not allow such a comparison.

31. Sawyer, D. T.; Roberts, J. L., Jr. *Experimental Electrochemistry for Chemists*; Wiley: New york, 1974; P 77.

32. Sabatani, E.; Rubinstein, I. *J. Phys. Chem.* **1987**, *91,* 6663.

33. *CRC Handbook of Chemistry and Physics,* 64 ed; West, R., Ed.; CRC press: Boca Raton, FL, 1984.

Chapter 4

Effect of Co-adsorbed Surfactant on the Structure of Self-Assembled Monolayer of Thiol on Polycrystalline Gold

---

The structure and formation-kinetics of SAM of long chain alkane thiol in the presence and absence of an anionic surfactant like sodiumdodecylsulfate (SDS) has been studied using impedance, cyclic voltammetric and QCM measurements. The comparison of these results, especially the ionic permeability of the monolayer suggests a composite monolayer when both the surfactant and thiol molecules are cooperatively adsorbed to form distinct surfactant patches. This is further substantiated by the voltammetric and impedance measurements with redox probe in solution. The kinetics of monolayer formation by QCM shows a phase transition from simple to composite monolayer. Impedance measurements indicate similar effect of surfactant on the monolayer structure of 1-pentanethiol (1-PT), NDS, and DDS suggesting a general mechanism.

---

* A paper based on this chapter has been accepted in *J. Colloid Interface Sci.* (1998).

4.1. Introduction:

Self-assembled monolayers (SAMs) have been effectively used in recent years to modify clean metal surfaces like that of Au, Ag and Cu into a well-defined organic surface.[1] The method depends on immersing a clean metal surface in a dilute solution of thiols or disulfides to produce an organized structure at the metal/solution interface. Such monolayers have been found to be extremely useful for a variety of applications ranging from catalysis to corrosion protection[2] as illustrated in chapter 1. During the past few years, a substantial amount of work has been done to understand the structure, kinetics, mechanism and stability of SAMs of disulfides and thiols on gold surface.[3] It emerges that, a dynamic and reversible adsorption process is primarily responsible for attaining equilibrium surface coverage with maximum packing density and the essential structure of SAMs of disulfides and thiols are same.[4]

Considering the lipophilic nature of the SAM forming molecules and that the stability of SAM owes much to the interchain van der Waals' interaction, the SAM forming molecule could very well interact with other surfactant molecules present in solution. Since micelles are dynamic aggregates of amphiphilic molecules possessing well-defined regions of hydrophobic and hydrophilic character, their presence is expected to profoundly influence the SAM formation due to possible coulombic and van der Waals' interactions with alkane thiol molecules. More importantly, the microscopic order provided to the solution by micelles may induce or hinder molecular self-assembly depending on the nature (anionic, cationic, non-ionic or zwitterionic) and concentration (i.e. above and below the critical micelle concentration (cmc)) of the surfactant molecules along with other parameters like temperature, pressure and solvent.

Although recently Krause and coworkers[5] have recognized the influence of non-specific adsorption of the surfactant from the aqueous phase on the methyl terminated SAM, their experiments were conducted with preformed SAM before allowing any surfactant interaction. It is much more important to understand the effect of surfactant molecules on the architecture of the organized assemblies during SAM formation since the advantages of using a microheterogeneous system could be exploited favorably to alter the kinetics of SAM formation especially due to the well recognized catalytic ability

of micelles. In addition, by selecting suitable surfactant molecules capable of order-promoting interactions, their structural similarity could be used to study competitive adsorption with different functional groups.

In the present chapter, we investigate the effect of coadsorbed anionic surfactants such as SDS on the SAM formation dynamics and structure. This type of studies on mixed thiol-surfactant SAM is important in terms of the current controversy over the air-oxidation of thiol SAMs which is believed to form sulfonates, just like the SDS molecules.[6] Moreover, these materials may have potential use in motor fuels and lubricants to remove the detrimental effect of ice formation and can be used as coating on the walls of carburetor to prevent the irreversible solid organic deposits.[7] The results of electrochemical techniques (impedance and cyclic voltammetry) and also *in-situ* QCM measurements are compared to show that the surface coverage and microscopic structures are different for SAMs on gold surface formed from ODT, 1-PT, NDS and DDS in the presence and absence of anionic surfactant.

4.2. Experimental:

4.2.1. Materials:

The gold film used in this study were prepared by vacuum deposition (pressure better than 10^{-6} torr) on conventionally cleaned glass substrates with Cr-buffer layer as discussed in detail in chapter 2 (section 2.2.1). SDS purchased from Aldrich was used without any further purification. In all the cases, substrates were kept for 12 hours for the formation of equilibrium monolayer. The substrates were then removed, rinsed with solvent, and deionized water and finally dried in a stream of Ar. The monolayers were formed from surfactant, mixture of surfactant and C_{18}-thiol and C_{18}-thiol solution (25 ml), each containing 15 ml ethanol and 10 ml water. In solutions containing SDS alone, the concentration of surfactant was 1.4×10^{-2} M while that of C_{18}-thiol was 10^{-3} M. In case of mixture of SDS and thiol, similar concentration of the components were used for meaningful comparison. The concentration of surfactant was well-above the cmc value (8.1×10^{-3} M)[8] and thiol concentration was sufficient to form well-defined organized

assemblies. ODT was obtained from Aldrich and was used to form SAM from ethanolic solution in the absence of surfactant.

4.2.2. QCM:

Monolayer formation kinetics was followed by *in situ* QCM measurements on an Elchema electrochemical nanobalance (with 0.1 Hz resolution) interfaced with a computer. Vacuum deposited 10 MHz Au coated quartz crystals (0.2 cm^2 exposed area) were used for all experiments at a constant temperature of 298 ± 0.1 K. Before the experiments, crystals were cleaned with piranha solution, (chapter2, section 2.2.2) rinsed with ethanol and finally with the solvent used. For the initial stabilization of QCM frequency, the solvent was introduced in the experimental vessel followed by measured small aliquot of high concentration solution of the compound by syringe to get the final desired concentration. The frequency change due to adsorption was converted directly to mass and were plotted with time. The results of the *in situ* QCM measurements are only semiquantitative in many cases mainly due to the capacitive and colligative effect of the solvents and adlayers, as, several factors are responsible for affecting oscillation frequency of a quartz crystal other than mass loading.[3f,9] The blank QCM experiments were performed as discussed in chapter 3 (section 3.2.2).

The details of the electrochemical measurements discussed in this chapter are identical to that given in chapter 2 (section 2.2 6).

4.3. Results and Discussion:

Figure 4.1 shows the complex faradaic impedance plot (after subtraction of the nonfaradaic component) of gold electrode modified in surfactant solution alone for 24 hours. The semicircle obtained at higher frequencies is indicative of a parallel RC combination of the equivalent circuit for the electrode impedance.[10] The electron transfer rate for $Fe(CN)_6^{3-/4-}$ couple is inhibited due to the formation of surfactant monolayer at the electrode surface as manifested by the increase in the charge transfer resistance (R_{ct}) compared to bare gold electrode not shown here since the detailed description is available in chapter 2. Approximate surface coverage is estimated to be 98% from the

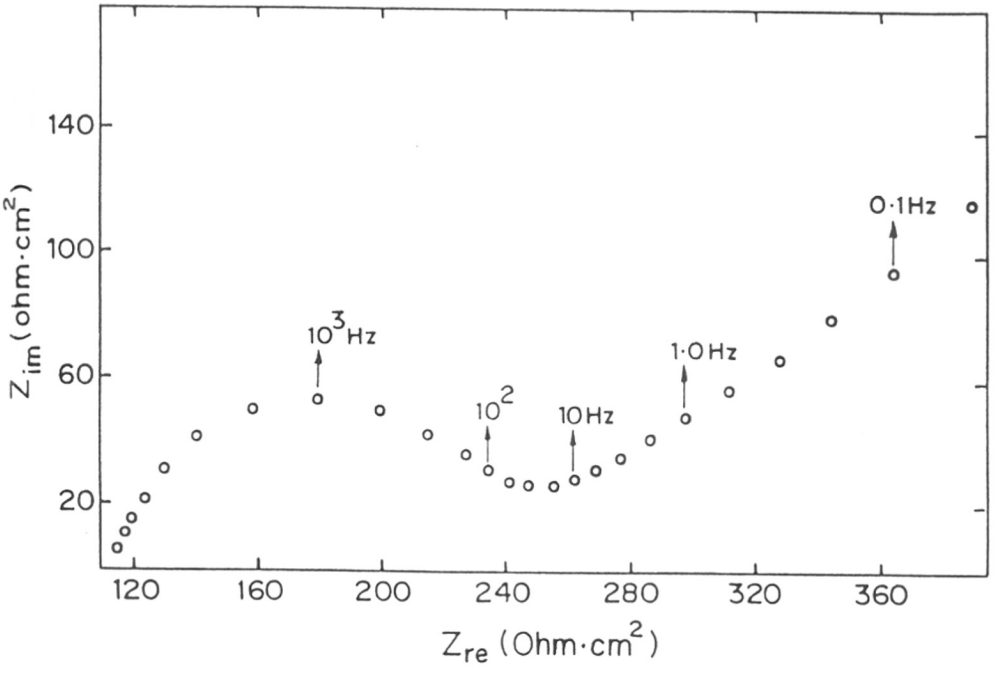

Figure 4.1. Faradaic impedance plot at the formal potential of the $Fe(CN)_6^{3-/4-}$ redox couple (0.22 V) vs SCE for gold electrode modified with SDS monolayer. Geometric area of all the electrodes are same (0.54 cm^2). Frequency range is 100 KHz to 100 mHz and the signal is 5 mV rms.

measured R_{ct} value[11] at the surfactant modified electrode taking R_{ct} at bare gold[12] to be 2.04 Ω cm^2. In the lower frequency range, there is a prominent Warburg diffusion part from which the calculation of diffusion coefficient gives a value of 5.91 x 10^{-7} cm^2/s. Double layer capacitance value is also decreased to 11 $\mu F/cm^2$ as compared to 25 $\mu F/cm^2$ for bare gold electrode.

Figure 4.2 shows complex faradaic impedance plane plot for gold electrode modified with SAM of C_{18} thiol, formed in the presence of the surfactant. In this case, an approximate surface coverage of 99.4% is obtained for the R_{ct} value, compared to the case of surfactant alone and interestingly, the monolayer is not perfectly blocking unlike the case of normal SAM using C_{18}-thiol. The diffusion coefficient obtained from the Warburg part compared to the case of surfactant alone is still lower (1.30 x 10^{-9} cm^2/s) and the double layer capacitance value amounts to 6.7 $\mu F/cm^2$. These observations clearly demonstrate that the monolayer is formed with greater compactness as compared to the surfactant adsorption, where multilayers are known to form during the physisorption of surfactant.[13] The thiol monolayer in presence of surfactant is not perfect (due to the presence of pinholes) and diffusion of the electroactive species through these defects is still possible.

On the other hand, Figure 4.3 shows gold electrode modified with ODT monolayer in absence of any surfactant indicating nearly a defect free system. The impedance features of the thiol monolayer has already been studied[14] and unlike the two previous cases, here the lower frequency Warburg component is found to be absent. The presence of a nearly perfect semicircle at higher frequencies indicate that the electron transfer is under kinetic control. A surface coverage value of 99.9% and a capacitance value of 1.4 $\mu F/cm^2$, thus substantiates the formation of a compact thiol monolayer, in agreement with the results of several available studies.[14a,15] Furthermore, a comparison of the time constant (RC) of the surface layer calculated from the higher frequency semicircle (i.e. 0.083 s for C_{18}-thiol layer to 0.026 s for the composite layer and finally to 0.0015 s for the SDS surfactant layer) reflects similar trends to R_{ct} change corresponding to the composition of the mixed monolayer. The apparent rate constants calculated from the R_{ct} values of the redox couple for different monolayer modified

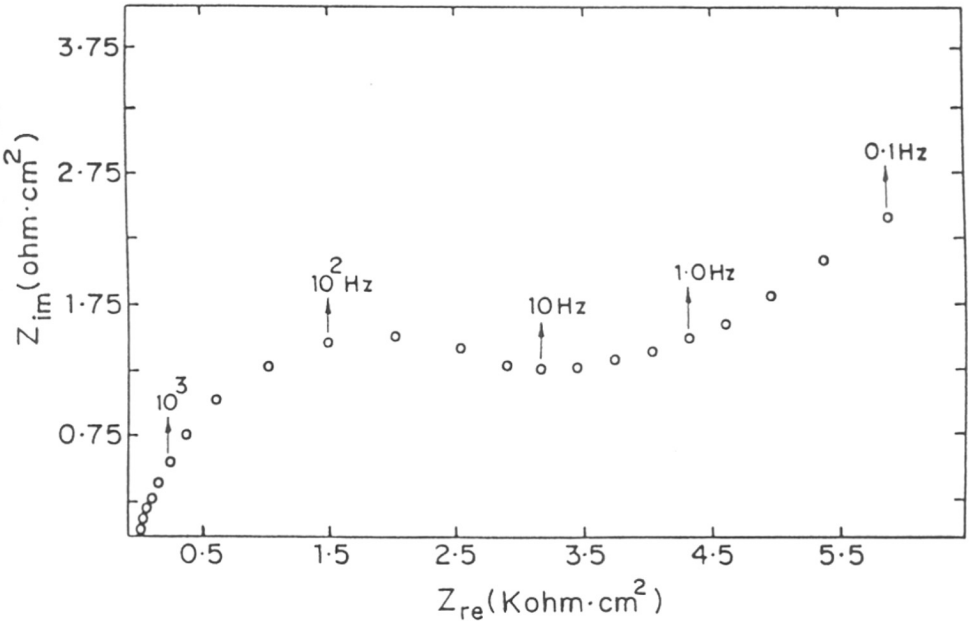

Figure 4.2. Faradaic impedance plot at the formal potential of the $Fe(CN)_6^{3-/4-}$ redox couple (0.22 V) vs SCE for gold electrode derivatized with SDS + C_{18} thiol. Geometric area of all the electrodes are same (0.54 cm^2). Frequency range is 100 KHz to 100 mHz and the signal is 5 mV rms.

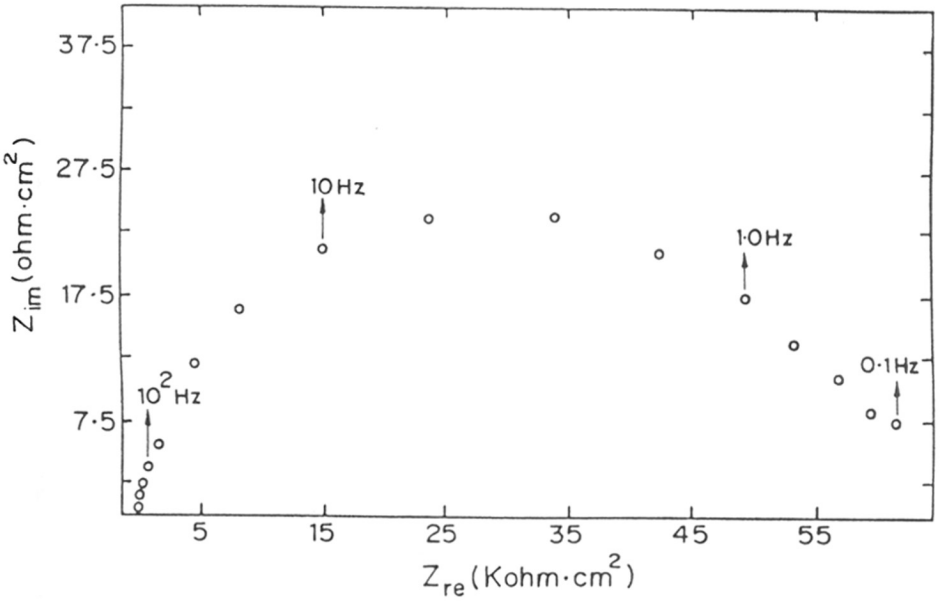

Figure 4.3. Faradaic impedance plot at the formal potential of the $Fe(CN)_6^{3-/4-}$ redox couple (0.22 V) vs SCE for gold electrode with C_{18} thiol alone in 0.5 M aqueous KF solution. Geometric area of all the electrodes are same (0.54 cm^2). Frequency range is 100 KHz to 100 mHz and the signal is 5 mV rms.

electrodes show a gradual decrease in the values (3.8×10^{-4} for SDS, 1.3×10^{-5} for a mixture of SDS and C_{18}-thiol and 8.9×10^{-7} cm/s for thiol alone) suggesting less compact monolayer formation in presence of SDS.

Comparison of the cyclic voltammograms of $Fe(CN)_6^{3-/4-}$ couple in Figure 4.4 at gold electrode modified with surfactant alone (a), surfactant and thiol (b) and thiol alone (c) shows a gradual decrease in current response indicating more and more suppression of the redox process. The electrode modified with surfactant alone shows a sloping background current with no clear redox response of $K_3Fe(CN)_6$. The shape of the voltammogram indicates high ohmic drop and the monolayer formed on the gold surface is inefficient to block the electron transfer completely compared to a passivated case of SAM with thiols. There is probably strong electrostatic repulsion between the SDS head group and $Fe(CN)_6^{4-/3-}$ couple and this can also contribute to the blocking behavior. The residual current may be due to the defect structure of the surfactant monolayer. In comparison, the monolayer of C_{18}-SH obtained in the presence of surfactant shows 90% decrease in the current while the monolayer with thiol alone shows 99.5% as compared to the case of surfactant alone. This gradual decrease in current response is indicative of a more compact monolayer assembly with less pinholes. The current obtained at the thiol coated electrode is totally capacitive and tunneling mechanism of electron transfer, is presumably valid.[15]

QCM can be an effective technique to understand any change in the kinetics of monolayer formation with the presence and absence of surfactant molecules. The frequency shift due to the variation of viscosity and density upon addition of thiol and surfactant are assumed to be negligible. Figure 4.5 shows a superimposed plot of mass uptake vs time obtained form *in situ* QCM measurements for all the cases under consideration. The monolayer formation from C_{18}-thiols on gold surface are known to follow Langmuir adsorption isotherm and the coverage variation with time has been discussed by several investigators.[3f,16] If we consider the cases of individual monolayer formation from thiol and surfactant separately, the kinetics of monolayer formation is much faster for C_{18}-thiol due to an energetically favorable interaction of thiol-gold compared to surfactant-gold interaction. Interestingly, the monolayer formation from the

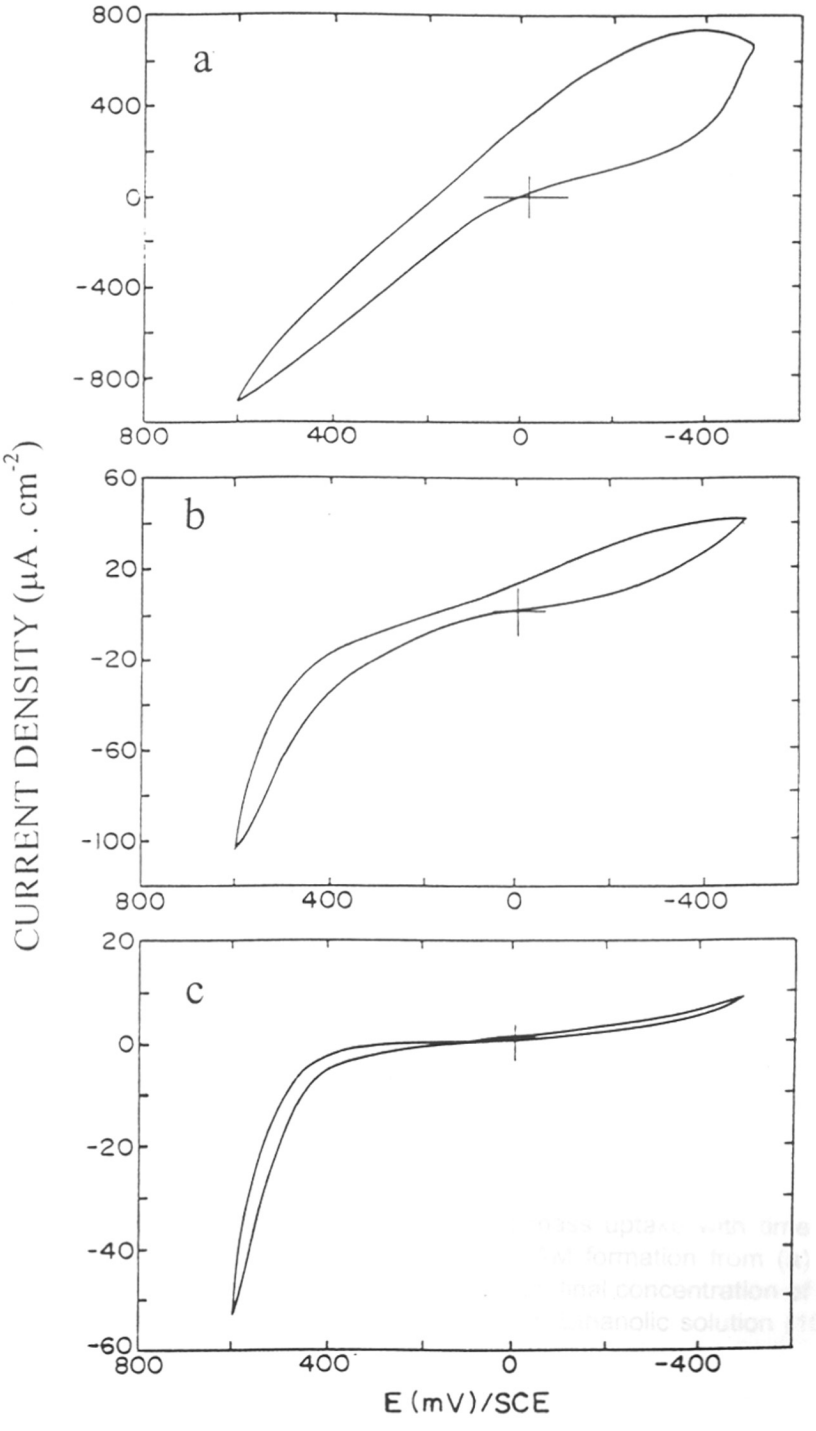

Figure 4.4. Cyclic voltammogram of 10^{-3} M $K_3Fe(CN)_6$ in 0.1 M KF at the gold electrode modified with (a) Surfactant (SDS) alone (b) surfactant + C_{18} thiol (c) C_{18}-thiol alone with scan rate of 200 mV/s. Electrode area (0.35 cm^2) is same for all the cases.

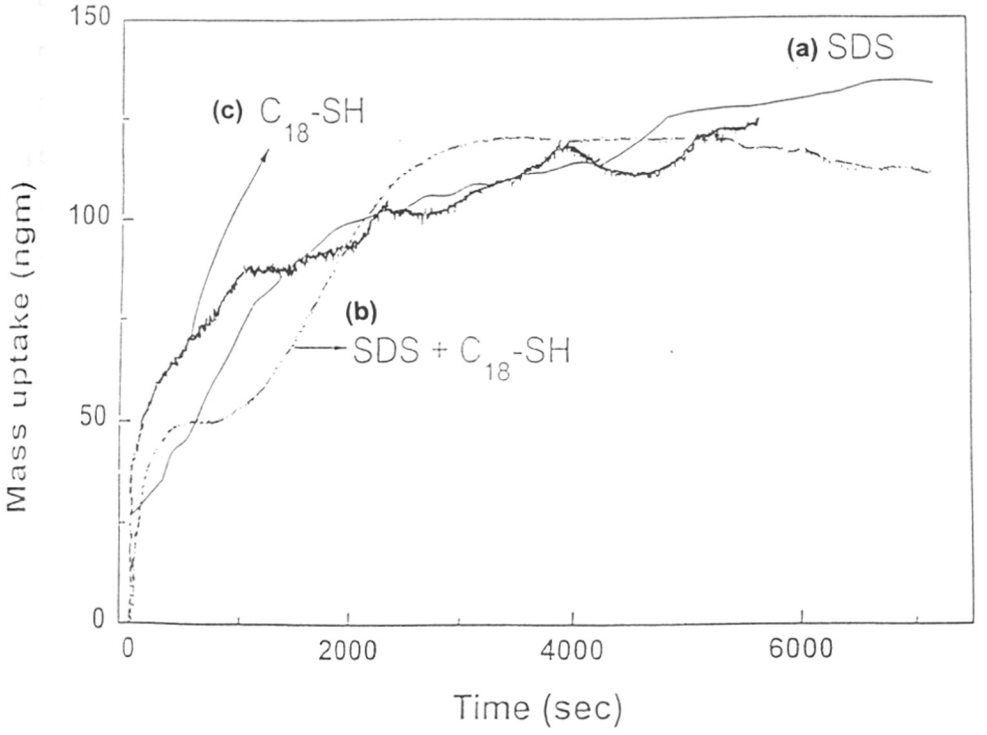

Figure 4.5. Superimposed plot of variation of mass uptake with time for a Au coated 10 MHz AT cut quartz crystal during SAM formation from (a) aqueous (10^{-2} M) solution of SDS alone (b) SDS + C_{18} thiol (final concentration of SDS and C_{18} thiols are 10^{-2} M and 10^{-3} M respectively) (c) Ethanolic solution (10^{-3} M) of C_{18}-thiol alone.

solution containing both thiols and SDS shows a two step process towards equilibrium with an initial rapid monolayer growth (mass uptake up to a coverage of 0.44) followed by a slow step of adsorption with a steeper slope than that predicted on the basis of Langmuir kinetics. At this particular value of coverage, it is also possible to have a phase transition from a simple and compact thiol monolayer to a composite (i.e., thiol and surfactant) monolayer with the associated change in kinetics. This composite monolayer is also found to be more stable compared to the individual cases of adsorption since mass variation in the solution environment due to temperature and/or convective motion are less. The faster approach towards equilibrium coverage in the time scale of two hours is probably due to a cooperative adsorption compared to the competitive adsorption process in the initial time scale of first few minutes. It is also possible to estimate roughly the respective adsorption rate constant in the above three cases (neglecting the initial transition in the composite case) of QCM response. The application of a Langmuir adsorption kinetic model[3f] indicates two orders of magnitude reduction in the rate constant value from pure thiol monolayer to composite monolayer. This observed trend in the adsorption rate constants strongly demonstrate that the presence of surfactant has significantly retarded the normal thiol adsorption.

The results obtained in the two cases (i.e. monolayer formation with surfactant and thiol alone) are straight forward. The structural aspect and dynamics of SAM formation with thiol on gold is well-studied[3a,16] and similarly, the adsorption of surfactant as well as the structure of the aggregate on metal or solid surfaces have been thoroughly investigated[13,17] establishing electrostatic attraction between the substrate and headgroup of the ionic surfactant along with the lateral attractive interaction between the hydrocarbon chains as the driving force. A recent AFM study[17a] has confirmed the possible surfactant aggregation in half-cylindrical or full-cylindrical configuration depending on the nature of substrate. More specifically, AFM image of SDS adsorption on Au shows half cylindrical mode of aggregation of surfactants on the surface with tails parallel to the gold symmetry axis[17a] and physisorption of the tail group has been proven to be the dominating factor. This mode of surfactant aggregation will naturally allow more access of the redox molecule to the electrode surface[17a] compared to a normal flat

monolayer or bilayer. Consequently, this can explain the large residual faradaic current obtained in the cyclic voltammogram and the prominent Warburg part of the impedance at the SDS monolayer coated electrode. Thus the results of SAM formation with C_{18}-thiol and surfactant individually indicate a nearly perfect (with less pinholes) molecular organization as discussed by Finklea *et al*[14a] for thiols and a uniform half-cylinder or full cylinder mode of aggregation for surfactant adsorption.[17a]

The most important and interesting situation is the case of monolayer formation of thiol in presence of the surfactant molecules. In this case, surfactant aggregation and micelle formation can affect the monolayer formation kinetics of thiols and there can be a complex behavior of adsorption on the metal surface. Since SAM formation is driven by pure chemisorption of the headgroup to substrate (thiolate moiety), involving strong interaction between sulfur and gold surface than the case of surfactant physisorption, we may not expect any competitive adsorption due to the large difference between the binding affinities. Due to this, initially thiol will get adsorbed on the surface. However, the presence of aggregates and micelles can reduce the diffusional mode of mass transfer to the Au surface, since, it is known that surfactants like SDS can adsorb strongly on a hydrophobic SAM surface to form a bilayer structure by interchain penetration.[18] The observed double layer capacitance change is not in agreement with this increase of the dielectric thickness, as, in this mode of adsorption a strong decrease in double layer capacitance is expected from thiol modified surface[5]. In contrast, we obtain a double layer capacitance value which is higher than that for a normal SAM coated surface and this along with the evidence from impedance plot (a prominent Warburg component at lower frequency region) indicate a cooperative adsorptive nature. Also, the results of cyclic voltammetry using these mixed monolayer coated electrode in presence of redox probe indicate a higher faradaic current compared to normal thiol monolayer, substantiating the drastic change of the actual structure in comparison with the individual case. Therefore, we tend to believe that the surfactant molecules are aggregated as patches and are distributed (as microarray) throughout the thiol monolayer. The lability of the Au-S bond[19] can allow a slow surfactant adsorption on initially organized C_{18} SAM. This model can effectively explain the large residual current obtained in cyclic

voltammogram and diffusion component observed in impedance response with redox probe for this mixed monolayer. This is also in complete agreement with the QCM results indicating that monolayer obtained from thiol-surfactant system is a composite one due to the cooperative adsorption of both surfactant and thiol molecules.

Impedance measurements have been carried out on monolayers of NDS, DDS and 1-PT formed in the presence and absence of SDS using $Fe(CN)_6^{3-/4-}$ as redox probe. Figures 4.6 - 4.8 show the superimposed impedance plot of the respective monolayers prepared in the presence and absence of SDS. The corresponding R_{ct} values as well as the apparent rate constant of the redox probe (calculated following the same procedure as discussed in chapter 2 (section 2.3.4) at different monolayer modified electrode, formed in the presence and absence of SDS, obtained from different plots are listed in Table 4.1. It is evident that, R_{ct} values for the monolayer formed in the

Table 4.1

Charge tranfer resistance (R_{ct}) obtained for gold electrode modified with 1-PT, NDS and DDS molecules from impedance measurements in presence and absence of SDS using $Fe(CN)_6^{3-/4-}$ couple as redox probe

Monolayers	R_{ct} value ($ohm.cm^2$)		Rate constant of $Fe(CN)_6^{3-/4-}$ couple (cm/s)	
	in presence of SDS	in absence of SDS	in presence of SDS	in absence of SDS
1-PT	616	3500	8.6×10^{-5}	1.5×10^{-5}
NDS	656	700	8.1×10^{-5}	7.5×10^{-5}
DDS	567	960	9.3×10^{-5}	5.5×10^{-5}

presence of SDS are always lower than the corresponding values in the absence of SDS, perhaps due to decrease in surface coverage in the presence of the surfactant. Moreover, decrease in the values of apparent rate constant shows that, the monolayer formed in the absence of SDS provides better barrier to the elctron transfer. Considering the individual impedance responses of the monolayer, for 1-PT, a broad depressed

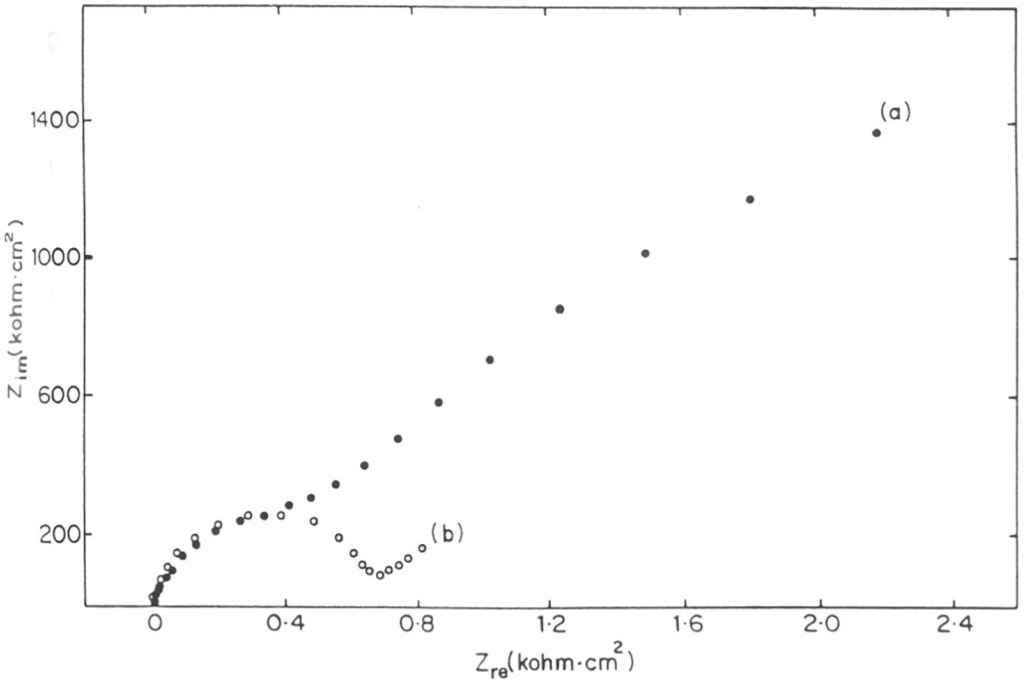

Figure 4.6. Superimposed impedance plot at the formal potential of the $Fe(CN)_6^{3-/4-}$ redox couple (0.22 V) in 0.5 M KF solution vs SCE for gold electrode modified with (a) NDS monolayer formed in absence of SDS. (b) NDS monolayer formed in presence of SDS in. Geometric area of all the electrodes are same (0.54 cm^2). Frequency range is 100 KHz to 100 mHz with a 5 mV rms signal.

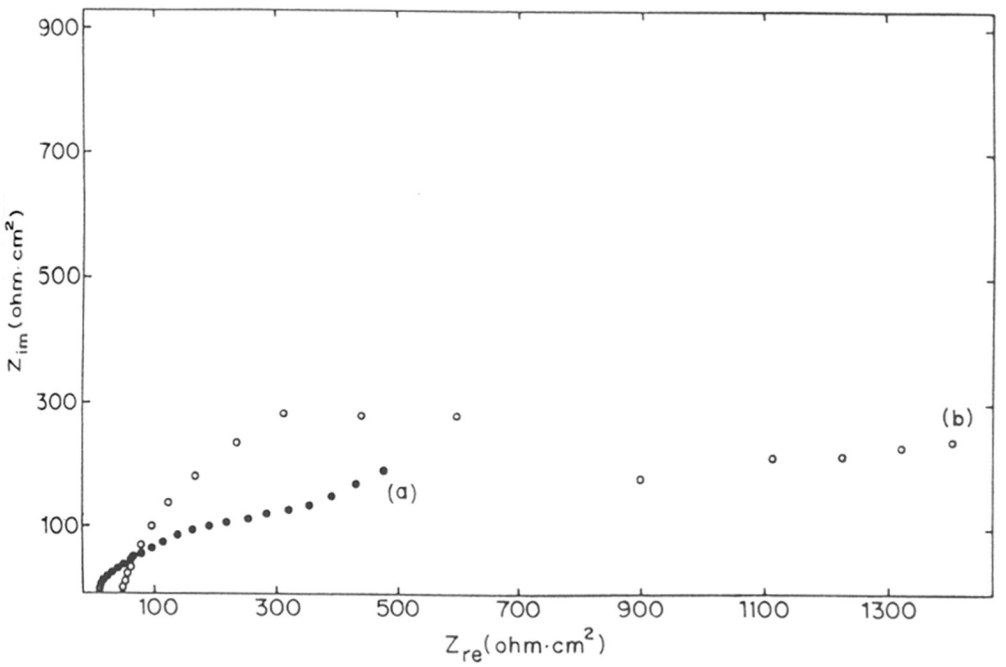

Figure 4.7. Superimposed impedance plot at the formal potential of the $Fe(CN)_6^{3-/4-}$ redox couple (0.22 V) in 0.5 M KF solution vs SCE for gold electrode modified with (a) DDS monolayer formed in absence of SDS. (b) DDS monolayer formed in presence of SDS. Geometric area of all the electrodes are same (0.54 cm^2). Frequency range is 100 KHz to 100 mHz with a 5 mV rms signal.

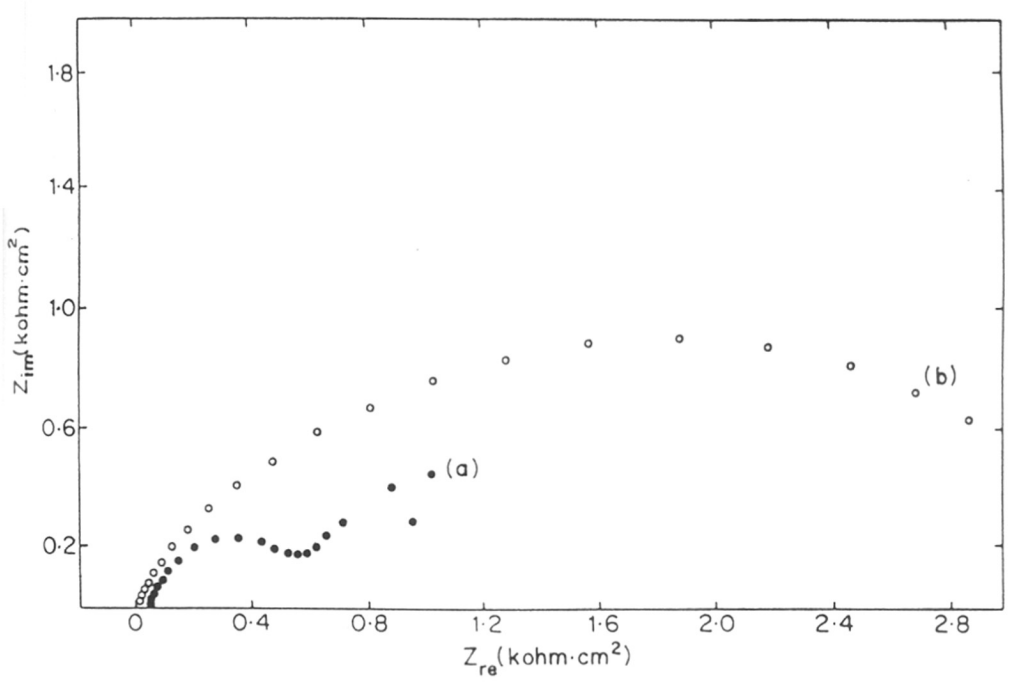

Figure 4.8. Superimposed impedance plot at the formal potential of the $Fe(CN)_6^{3-/4-}$ redox couple (0.22 V) in 0.5 M KF solution vs SCE for gold electrode modified with (a) 1-PT monolayer formed in absence of SDS. (b) 1-PT monolayer formed in presence of SDS. Geometric area of all the electrodes are same (0.54 cm^2). Frequency range is 100 KHz to 100 mHz with a 5 mV rms signal.

semicircle is obtained with no diffusion limited part in the absence of SDS. On the other hand, when monolayer is formed in presence of SDS, a comparatively smaller semicircle is obtained along with a prominent Warburg impedance part. The same trend is observed for DDS. Impedance response of NDS in the presence of surfactant shows an ill-defined semicircle at higher frequencies with a large contribution from diffusional impedance. In contrast, a well-defined semicircle is evident for the monolayer prepared in the absence of surfactant with a negligible contribution from the diffusional impedance. All these above results strongly suggest a better organization in the monolayer structure in the absence of the surfactant. Moreover, the prominent diffusional impedance part observed in all the impedance response of monolayers prepared in the presence of surfactant indicate more defects (as pinholes or surfactant patches) which allow a ready permeation of the redox species. The effect of surfactant is not so prominent in the present case as in long chain thiols. This presumably is due to the lesser chain-chain interaction between surfactant and the adsorbed molecule.

Clearly, several questions remain regarding the fundamental mechanism underlying similarities and differences in the adsorption of surfactant and thiol molecules, the actual interaction of surfactant with thiol during SAM formation and also the molecular level view of SAM obtained in the presence of surfactant. Although the present study clearly establishes that the extent of organization is distorted by the cooperative adsorption of anionic surfactant like SDS, one could speculate the possibility of using cationic and non-ionic surfactants to understand their effect on equilibrium organization. Moreover, a potentially interesting proposition is to use both thiols and surfactant molecules to build multilayers and nanostructures where the micellar aggregations could be used to trap transition metal ions or even big colloidal particles at the center.

4.4. Conclusion:

The self-assembled monolayer formed in the presence of surfactant has a different structure as compared to a normal one and the presence of SDS in adsorption medium leads to poor quality of SAM due to the composite nature of the monolayer.

From electrochemical and *in-situ* QCM measurements it emerges that the surfactant molecules are distributed as patches in the mixed thiol-surfactant monolayer. The kinetics of adsorption show interesting deviation from individual cases as indicated by the results of the QCM measurements and a deeper understanding of the mixed molecular level structure of the monolayer requires surface characterization techniques such as surface probe microscopy.

4.5. References:

1. (a) Ulman, A. *An Introduction to Ultrathin organic films from Langmuir-Blodgett to Self-assembly;* Academic Press: San Diego, CA, 1991. (b) Ulman, A. *Chem. Rev.* **1996**, *96*, 1533.

2. (a) Durand, R. R.; Bencosme, C. S.; Collman, J. P.; Anson, F. C. *J. Am. Chem. Soc.* **1983**, *105*, 2710. (b) Notoya, T.; Poling, Q. W. *Corrosion* **1979**, *35*, 193. (c) Laibinis, P. E.; Whitesides, G. M. *J. Am. Chem. Soc.* **1992**, *114*, 9022.

3. (a) Strong, L.; Whitesides, G. M. *Langmuir* **1988**, *4*, 546. (b) Camillone, N.; Chidsey, C. E. D.; Liu, G. L.; Scoles, G. *J. Chem. Phys.* **1993**, *98*, 3503. (c) Fenter, P.; Eberhardt, A.; Eisenberger. P. *Science* **1994**, *266*, 1216. (d) McCarley, R. L.; Kim, Y.-T.; Bard, A. J. *J. Phys. Chem.* **1993**, *97*, 211. (e) McCarley, R. L.; Dunaway, D. J.; Willicut, R. J. *Langmuir* **1993**, *9*, 2775. (f) Karpovich, D. S.; Blanchard, G. J. *Langmuir* **1994**, *10*, 3315. (g) Poirier, G. E.; Pylant, E. D. *Science* **1996**, 272, 1145. (h) Schlenoff, J. B.; Li, M.; Ly, H. *J. Am. Chem. Soc.***1995**, *117*, 12528. (i) Porter, M. D.; Bright, T. B.; Allara, D. L.; Chidsey, C. E. D. *J. Am. Chem. Soc.* **1987**, *109*, 3559.

4. Bain, C. D.; Biebuyck, H. A.; Whitesides, G. M. *Langmuir* **1989**, *5*, 723.

5. Krause, C.; Mirsky, V. M.; Heckmann, K. D. *Langmuir* **1996**, *12*, 6059.

6. Castner, D. G.; Hinds, K.; Grainger, D. W.; *Langmuir* **1996**, *12*, 5083.

7. J. P. Wallquier in *Petroleum refining* Ed. Editions Technip, Paris 1995, page 346.

8. Fendler, J. H.; Fendler, E. J. in *Catalysis in Micellar and Macromolecular systems*: Academic press, New York, 1975.

9. (a) Yang, M.; Thompson, M. *Langmuir* **1993**, *9*, 802. (b) Yang, M.; Thompson, M.; *Langmuir* **1993**, *9*, 1990.

10. Sluyters-Rebbach, M.; Sluyters, J. H. in *Electroanalytical Chemistry*, Volume 4, Dekker, New York, 1970.

11. (a) Sabatani, E.; Rubinstein, I.; Maoz, R.; Sagiv, J. *J. Electroanal. Chem.* **1987**, *219*, 365. (b)Sabatani, E.; Cohen-Boulakia, J.; Bruening, M.; Rubinstein, I. *Langmuir* **1993**, *9*, 2974.

12. Charge transfer resistance at bare gold can be calculated for one electron process by using the equation $R_{ct} = RT/F^2Ak_0c$ and taking electron-transfer rate constant (k_0) at a bare gold electrode to be 2.6×10^{-2} cm/s.[8b] R, T, F, A, c are the usual gas constant, temperature, Faraday constant, area of the electrode surface and concentration of the redox species in solution respectively.

13. (a) Li, J.; Kaifer, A. E. *Langmuir* **1993**, *9*, 591. (b) Suga, K.; Bradley, M.; Rusling, J. F. *Langmuir* **1993**, *9*, 3063. (c) Sun, S.; Birke, R. L.; Lombardi, J. R. *J. Phys. Chem.* **1990**, *94*, 2005.

14. (a) Finklea, H. O.; Snider, D. A.; Fedyk, J.; Sabatani, E.; Gafni, Y.; Rubinstein, I. *Langmuir* **1993**, *9*, 3660. (b) Nahir, T. M.; Bowden, E. F. *Electrochimica Acta.* **1994**, *39*, 2347.

15. (a) Porter, M. D.; Bright, T. B.; Allara, D. L.; Chidsey, C. E. D. *J. Am. Chem. Soc.* **1987**, *109*, 3559. (b) Miller, C.; Cuendet, P.; Grätzel, M. *J. Phys. Chem.* **1991**, *95*, 877.

16. (a) Bensebaa, F.; Voicu, R.; Huron, L.; Eills, T. H. *Langmuir* **1997**, *13*, 5335. (b) Sondag-Huethorst, J. A. M.; Schönenberger, C.; Fokkink, L. G. J. *J. Phys. Chem.* **1994**, *98*, 6826. (c) Pan, W.; Durning, C. J.; Turro, N. J. *Langmuir* **1996**, *12*, 4469. (d) Bucher, J. P.; Santesson, L., Kern, K. *Langmuir* **1994**, *10*, 979.

17. (a) Jaschke, M.; Butt, H. -J.; Gaub, H. E.; Manne, S. *Langmuir* **1997**, *13*, 1381. (b) Soderlind, E.; Stilbs, P. *J. Colloid Interface Sci.* **1991**, *143*, 586. (c) Wangnerud, P.; Olofsson, G. *J. Colloid Interface Sci.* **1992**, *144*, 392.

18. Hu, K.; Bard, A. J. *Langmuir* **1997**, *13*, 5418.

19. McCarley, R. L.; Dunaway, D. J.; Willicut, R. J. *Langmuir* **1993**, *9*, 2775.

Chapter 5

Some Selected Applications of Self-Assembled Monolayers of Small Aromatic Thiols and Disulfides

---

This chapter deals with three specific applications of SAM of small aromatic disulfides and thiols: (1) corrosion protection of copper, (2) two dimensional organization of metal cluster from solution and (3) solid materials synthesis using the functionalized interface of SAM. A high degree of protection efficiency is observed for Cu in aqueous solution considering the smaller dimension of these molecules compared to long chain thiols. Monolayer with suitable pendant functional groups are capable of organizing metal clusters from solution as illustrated by a bifunctional molecule. Lastly, application of SAM for solid state synthesis has been illustrated using two dimensional reaction of surface functional groups with solution species leading to the formation of microcrystalline zirconia at the interface.

---

* A part of this study has been published in *Langmuir* **1997**, *13*, 5244 and another part has been accepted in *J. Am. Ceram. Soc.* (1998)

5.1. Introduction:

Self-Assembled monolayer (SAM) formation provides an elegant way to form well-defined organic assemblies with a wide range of surface functionalities.[1] These monolayer assemblies are being effectively used as a platform to build up multilayers, patterning of surfaces, nanolithography and molecular recognition etc.[2] In most of these applications long chain thiols/disulfides are used as these have been characterized and studied exhaustively.[3] On the other hand, monolayer formation from small aromatic thiols/disulfides and their characterization are extremely important to understand the difference in organization and structure of these assemblies. In this chapter, monolayers from small aromatic thiols and disulfides are used to explore some of the possible applications like, (1) corrosion protection of Cu, (2) two dimensional organization of metal clusters from solution and (3) formation of microcrystalline materials.

Previous studies show that n-alkanethiols and ω-substituted alkanethiols form densely packed oriented monolayer assemblies on polycrystalline Cu surface,[4] and consequently, it was found from XPS investigation[4c] that, alkanethiol SAMs can protect the underlying copper surfaces from air oxidation. Further confirmation comes from an electrochemical study indicating a moderate protection ability of these films against copper corrosion in aerated 0.5 M Na_2SO_4 solution.[5] Moreover, investigations related to Cu-corrosion covered by long-chain alkane thiols demonstrate that SAMs can provide a high protection ability by inhibiting the oxide growth in water.[6] Similarly, application of dodecanethiol SAM to prevent corrosion of Cu in 0.5 M NaCl solution suggests that, the sample pre-treatment prior to thiol adsorption had a strong influence on the structure and properties of the monolayer and hence to the protection abilities.[7] The first part of the present chapter deals with studies of the molecular assemblies from NDS and DDS for protection against copper corrosion in 0.5 M aerated Na_2SO_4 solution and the results are compared with those for ODT monolayer. The difference in protection efficiency between these two disulfides of comparable dimension has been rationalized on the basis of their structure.

Covalent linkage of colloidal metal/semiconductor particles to SAMs of bifunctional molecules[8] or to polymer films with suitably grafted pendant groups[9] appears

to be a promising route for obtaining ordered colloidal films. In particular, exhaustive studies on the use of various functional groups in polymers for the adsorption of colloidal metal particles have been done, and it is shown to be a promising route to obtain metal films of well-defined surface roughness.[9a] The second part of the present chapter deals with the organization of a bifunctional molecule 4-carboxythiophenol (4-ATP) containing a thiol and a carboxylate group at either end of the *aromatic* moiety on different metal surfaces such as Al and Au utilized for organizing nanoclusters of Ag. The carboxylic group of the mercaptoacetic acid binds to the Al surface rendering the SAM surface rich in thiol groups.[8a,b] The SAM is then immersed in the silver colloidal solution and the nanoparticles are expected to covalently coordinate to the thiol groups.

The effective utilization of functionalized interface of SAMs in two dimensional reactions for the solid state and biomimetic synthesis[10] is an active area of research along with the multilayer formation of zirconium phosphate and copper dithiol.[11] The final part of the present chapter demonstrates the effective use of SAM of 1,4-benzene dimethanethiol (BDT) to link Zr^{4+} from an aqueous solution of appropriate zirconium salt to subsequently form microcrystalline, monoclinic zirconia at room temperature by potentiodynamic cycling. As the preparation of zirconia is important due to different technological applications ranging from oxide fuel cells and oxygen sensors to catalysis,[12] this novel method is expected to profoundly influence many of these applications. Although particle size, texture, surface area and sintering characteristics etc. can be effectively controlled by other methods of zirconia preparation such as chemical vapor deposition, sputtering or sol-gel methods, almost all the methods invariably require a high temperature treatment for crystallization as the materials obtained in pure form or with additives, are amorphous.[13] Consequently, a room temperature method for preparation of crystalline zirconia will be interesting as well as extremely important considering all the possible applications of this material. XPS, CV and impedance measurement along with X-ray diffraction and SEM are used to characterize the monolayer formation from dithiols and subsequent attachment of zirconium leading to monoclinic ZrO_2 crystallites.

5.2. Experimental:

5.2.1. Materials:

ODT, DDS and BDT were purchased from Aldrich and were used as received. NDS[14] and 4-CTP[15] were synthesized according to the procedure detailed in literature. All the starting materials were obtained from Aldrich and were used as received. The desired compounds were purified by column chromatography followed by structure confirmation by NMR spectroscopy. The purity of the respective compound were better than 99.99% as determined by gas chromatography analysis. The Ag clusters were grown in colloidal form following the procedure of Vukovic and Nedeljkovic.[16] The method is basically a borohydride reduction of the Ag salt (10^{-4} M Ag_2SO_4) in aqueous solution. All the other compounds, namely, KF, Na_2SO_4, potassium ferro/ferricyanide and zirconium oxychloride octahydrate were of regent grade and were used without any purification. All the experiments were carried out using deionized water from Milli-Q system.

Vacuum deposited Au, Al and Cu on glass and single crystal (111 orientated) Si wafers and Cu-foils (99.99% purity) were used as substrates according to different experimental requirements. Thick films of Al and Au (purity 99.9 %) along with a Cr-buffer layer were deposited by thermal evaporation onto AT cut quartz crystals (6 MHz resonant frequency) for microbalance studies at a pressure of 1 x 10^{-7} Torr in an Edwards E306A vacuum coating unit equipped with a quartz crystal thickness monitor. On the other hand, Cu deposited on glass as well as copper foil were used for corrosion investigation and vacuum deposited Au on glass were used in case of ZrO_2 synthesis. In all the cases, a liquid nitrogen trap ensured deposition of metal films with minimum level of contamination. Prior to deposition of the metal films, the Si and glass substrates were cleaned by striking a glow discharge in the chamber which resulted in good adhesion of the metal film on the Si surface. The thickness of the metal films determined from the quartz microbalance was typically 200 nm. Since Cu is highly reactive to form an oxide layer, the substrates were freshly prepared whenever required. The

characterization of monolayer on Cu using XPS and electrochemical measurements were carried out using Cu-coated glass substrates.

For corrosion measurements, with impedance and different polarization techniques, a Cu-foil with total exposed area of one square centimeter was used. Prior to the derivatization with the respective disulfides and ODT, Cu-substrates were pretreated by HNO_3-etching. In this procedure, the substrates were first polished by SiC abrasive paper (for Cu foil only), followed by cleaning with absolute ethanol to remove hydrocarbon impurity. These samples were then subjected to etching in a 7 M HNO_3 solution for 30 s and rinsed first with distilled water and then with absolute ethanol. The samples were dried and then immediately transferred to a 1 mM solution of the respective disulfides in acetonitrile. Absolute ethanol was used as solvent for ODT. The exposure time was typically 30 minutes for all the monolayer formation as it gave reproducible results in electrochemical experiments. The substrates were removed after the specific time and rinsed with the solvent and absolute ethanol, then dried in a stream of Ar. All the monolayers were prepared at ambient conditions with no effort to remove oxygen.

For the organization of clusters, Al and Au coated Si wafers were cut into slides and cleaned through repeated exposures to sulfochromic acid as described in chapter 2. The substrates were rinsed with ethanol after cleaning and immediately transferred into the monomer containing solution. The kinetics of monolayer formation of the bifunctional molecule was followed by immersion of the quartz crystal in the monomer containing solution. For each monolayer deposition, a freshly prepared solution of the bifunctional molecule was used. Absolute ethanol was used as the solvent and a solution corresponding to a concentration of 1 mM of 4-CTP was used for derivatization. SAMs were formed by immersing the respective metal films into the ethanolic solution of respective thiols/disulfides at room temperature. Metal nanoparticle incorporation was accomplished by immersion of the SAM covered surface in the hydrosol. These films were washed with copious amounts of ethanol and dried in N_2 prior to further studies.

For ZrO_2 synthesis, self-assembled monolayer of BDT was formed on the Au film from a 1 mM ethanolic solution of the respective compounds for 24 hours following

established methods.[17] The different steps involved in the formation of microcrystalline ZrO_2 on SAM surface are summarized in Scheme 5.1. In the first step, dithiol SAM was formed on Au surface from 1 mM ethanolic solution of dithiol. Substrates were kept for 12 hours to obtain an equilibrium organization. In the next step, the SAM covered gold surface was introduced in a 5 mM aqueous $ZrOCl_2$. $8H_20$ solution to covalently link Zr^{4+} ion on the SAM surface with pendent -SH group at ambient temperature. Samples were kept for 24 hours to ensure complete attachment and after removal, the substrate was washed copiously with de-ionized water and dried under the flow of Ar. The variation of the immersion time in $ZrOCl_2$ solution between 1 to 24 hours gave indistinguishable results. In the final step, samples obtained from the second step were used as working electrode in a 1 M aqueous KCl solution and the potential was cycled between -1.1 V to + 0.7 V Vs SCE at a scan rate of 200 mV/s. After performing at least ten such cycles the sample was removed and washed with a gentle flow of de-ionized water and dried under Ar prior to characterization.

5.2.2. Electrochemical Experiments:

Linear polarization was carried out in 0.5 M aerated Na_2SO_4 solution both for bare Cu and the respective monolayer coated electrodes. Potentials were increased from the rest potential value upto a limit of 10 mV both at cathodic and anodic directions. Similarly, Tafel polarization was carried out in the same electrolyte solution after keeping the electrodes for a period of one hour. Both cathodic and anodic Tafel plots were separately recorded. In both the polarization measurements Hg/Hg_2SO_4 reference was used.

Impedance and cyclic voltammetric measurements were performed as described in chapter 2 (section 2.2.6). For understanding the monolayer formation, impedance response of bare Cu and respective monolayer coated electrodes were measured in a 0.1 M KF solution with SCE as the reference electrode. Corrosion of Cu was followed by measuring impedance of bare Cu and monolayer coated Cu in 0.5 M air saturated Na_2SO_4 solution after immersion of the electrode in the solution for one hour with Hg/Hg_2SO_4 as reference electrode in a frequency range of 100 KHz to 0.1 Hz. Double

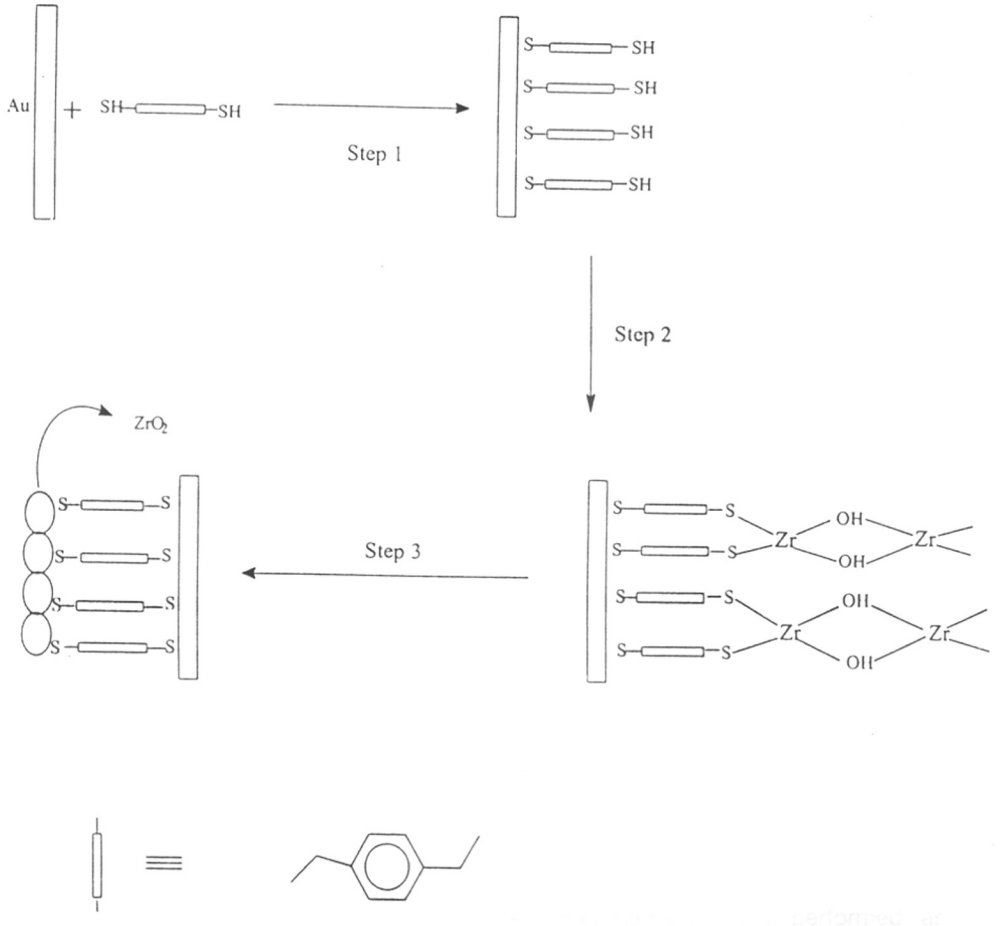

Scheme 5.1. Different Steps Involved During the Formation of Microcrystalline ZrO_2 on BDT SAM surface.

layer capacitance values were calculated from impedance plots by extrapolating the linear portions of the plots of log(absolute impedance) vs log (ω) = 0.

Cyclic voltammetry was carried out with bare and monolayer coated electrode in 0.1 M KF at a potential range of + 0.4 to -1.3 V with a scan rate of 200 mv/s. All the experiments were carried out at room temperature (298 ±0.1 K).

5.2.3. Other Measurements:

Optical absorption spectroscopy of the colloidal solution was performed using a HP 8452A diode array spectrophotometer (2 nm spectral resolution). The colloidal particles were then analyzed for size distribution and crystallinity by evaporating off the aqueous component of drops placed on carbon coated electron microscope grids.

Transmission Electron Microscopy (TEM) was done on a Jeol Model 1200EX, operated at an accelerating voltage of 120 KV together with selected area electron diffraction.

Scanning Electron Microscopy (SEM) of the SAMs was done on a Leica Stereoscan S-440 model microscope, operated at 20 KV accelerating voltage and 25 pA current.

Contact angle measurements were made using a Rame-Hart, Inc. contact angle goniometer on a sessile drop at different points on the sample surface to determine the surface inhomogeneity. These measurements were performed during formation of the SAM as well as during adsorption of the Ag nanoparticles.

The phase contents of the zirconia sample were analyzed at room temperature using Philip's 1730 X-ray diffractometer.

XPS and Quartz crystal microbalance measurements were performed as described in chapter 2 (section 2.2.5) and chapter 3 (section 3.2.2) respectively.

5.3. Results and Discussion:

5.3.1. SAM of NDS and DDS for Corrosion Protection of Cu:

The formation of SAMs from NDS, DDS and ODT have been followed by measuring time dependent impedance response of the copper electrodes modified with respective compounds in a 0.1 M KF solution. Copper electrode in these solutions can be described by a simple equivalent circuit with a series combination of a capacitor and the solution resistance since no faradaic process is possible. The value of capacitance can be calculated using the procedure described in chapter 2 (section 2.2.6). The value of capacitance of bare copper electrode in the above solution is calculated to be 54.5 $\mu F/cm^2$, which decreases appreciably with the respective monolayer formation. Impedance response of the various monolayer covered electrode have been monitored with time and it is observed that modification time of 30 minutes for all the molecules can give rise to equilibrium monolayer formation. During this time, interfacial capacitance has been decreased gradually for all the monolayer modified electrodes. Table 5.1 shows the double layer capacitance values obtained for different electrodes after the specified monolayer formation time. Impedance response was not reproducible if the time of modification increased. It may be possible that the electrode surface has undergone an irreversible change due to surface reaction with disulfides and thiols.

Figure 5.1 shows the gradual change in the double layer capacitance of different monolayer coated Cu-electrodes with time. The decrease in the double layer capacitance values are almost similar for the DDS and NDS unlike the case of ODT where a steeper decrease is observed. This difference in trend is understandable as dimension of the two sets of molecules are different (DDS and NDS ~ 0.7 nm and ODT ~ 2.1 nm) and it is known that the double layer capacitance values are strongly dependent on the thickness of the monolayer forming molecule. The equilibrium double layer capacitance values of NDS and DDS are comparable which can be attributed to the smaller size and presence of π-electron in the molecules. Moreover, these values are comparable to that obtained for the monolayer on Au surface with same molecules. On the other hand, for ODT, the value is in good agreement with the value obtained in

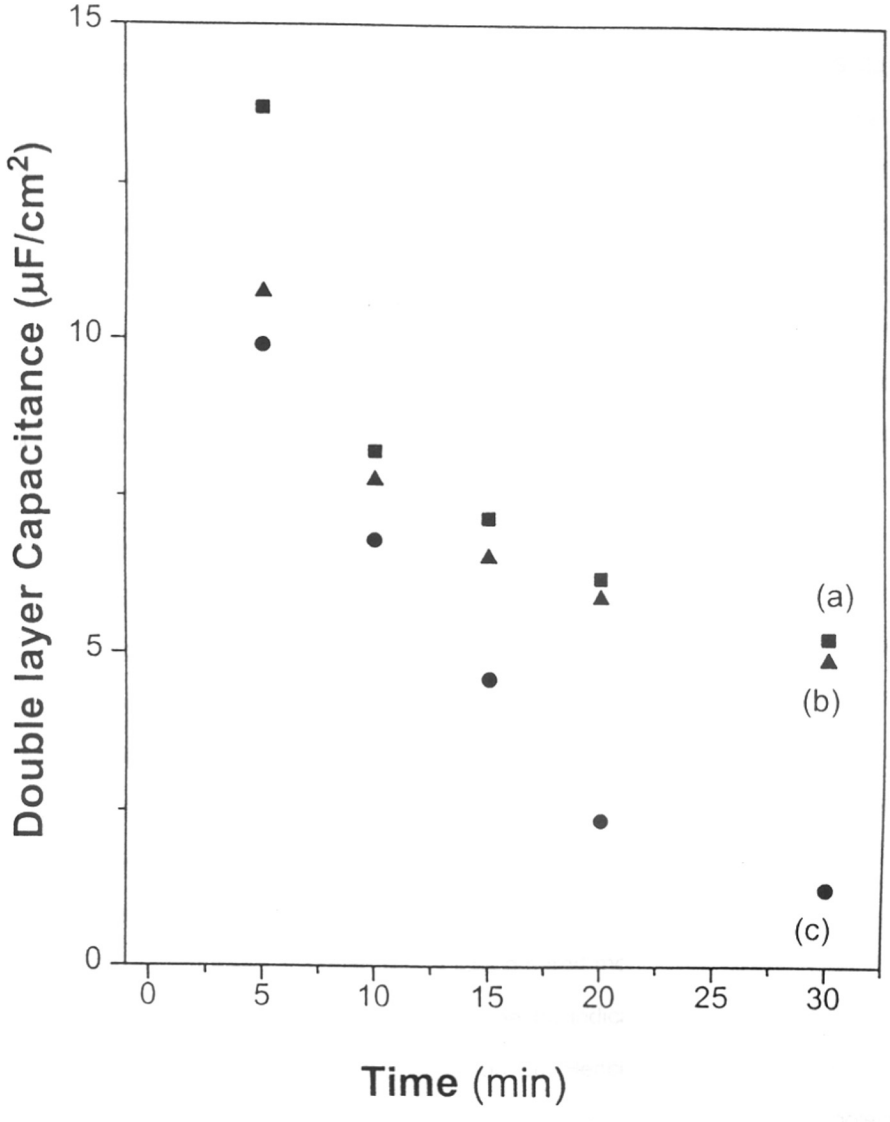

Figure 5.1. Change in double layer capacitance of Cu electrode modified with the monolayer of (a) NDS, (b) DDS and (C) ODT in 0.1 (M) KF solution measured from the time dependent impedance response.

case of ODT monolayer on Au surface.[18] In addition, Aramaki *et. al*[5] has observed a similar type of decrease in double layer capacitance for ODT monolayer on copper from an impedance measurement in an 0.1(M) $LiClO_4$ solution in acetonitrile. All these results strongly suggest the formation of organized molecular assemblies on the copper surface. The observed decrease in the double layer capacitance values are slightly more for DDS which suggests more compact organization compared to NDS.

Figures 2.12 and 5.2 (a, b) show the x-ray photoelectron spectra of S 2p for copper surface covered with NDS, DDS and ODT monolayers respectively. Table 5.1 shows the binding energy values of S 2p core level spectra for different monolayers on copper surface. Binding energy value obtained for ODT is similar to that obtained by Laibinis *et. al* and is attributed to the formation of a metal thiolate.[4a] On the other hand, the spectra for DDS and NDS also indicate the formation of a metal-thiolate bond with oxidative dissociation of the S-S bond. Both the spectra are similar to that obtained for monolayer on Au surface as discussed in chapter 3. The spectra of NDS monolayer modified Cu surface is different from the other two monolayers. In case of both DDS and ODT, single component sulfur signal is obtained. The spectra for DDS can be fitted to a doublet of S $2p_{3/2}$ and S $2p_{1/2}$ at 162.8 and 164 eV. On the contrary, there is an evidence of two types of sulfur environment for the NDS monolayer with two peaks observed at higher and lower binding energy values. The lower binding energy peak corresponds to the normal metal- thiolate species and that at a higher binding energy is possibly due to the oxidized form of sulfur.[19] Similar type of spectrum is also obtained for NDS on Au surface as discussed in chapter 2. The oxidized form of the sulfur (possibly sulfonate moiety) can be formed from the X-ray beam induced oxidation of the monolayer.[8a] This type of oxidation has been observed with a less ordered monolayer, having a number of defects. Therefore, this difference in the XPS spectra indicate more compact nature for ODT and DDS compared to NDS monolayer on Cu. Hence from the binding energy of NDS, DDS and ODT monolayers on copper, it can be concluded that, all the molecules form organized molecular assemblies.

Impedance measurement can also be applied to evaluate the corrosion resistance of different monolayer-coated copper in 0.5 (M) Na_2SO_4 solution. It is known

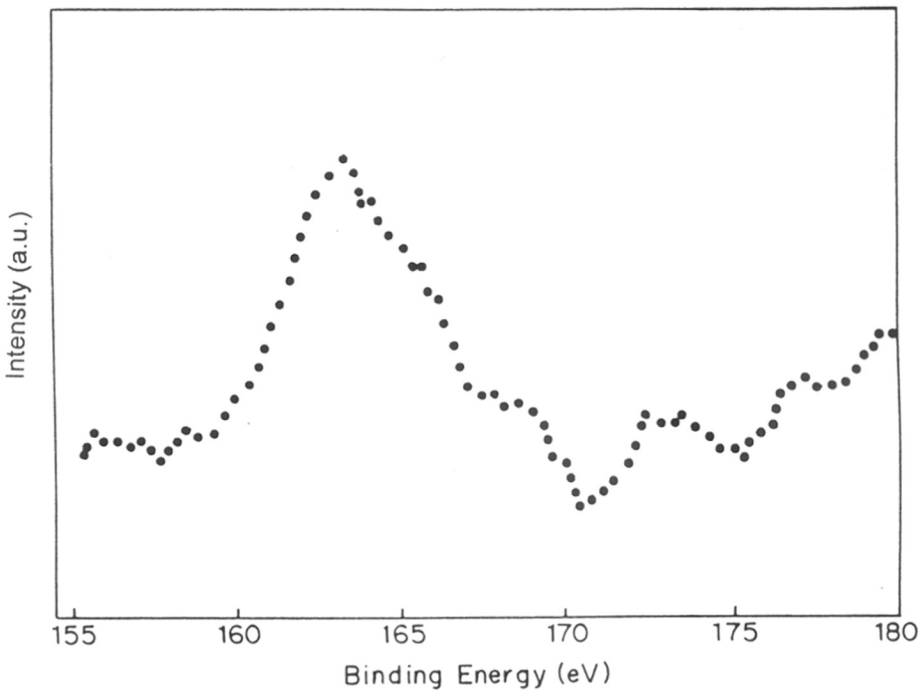

Figure 5.2. (a) S 2p core level spectrum of the DDS monolayer on copper surface.

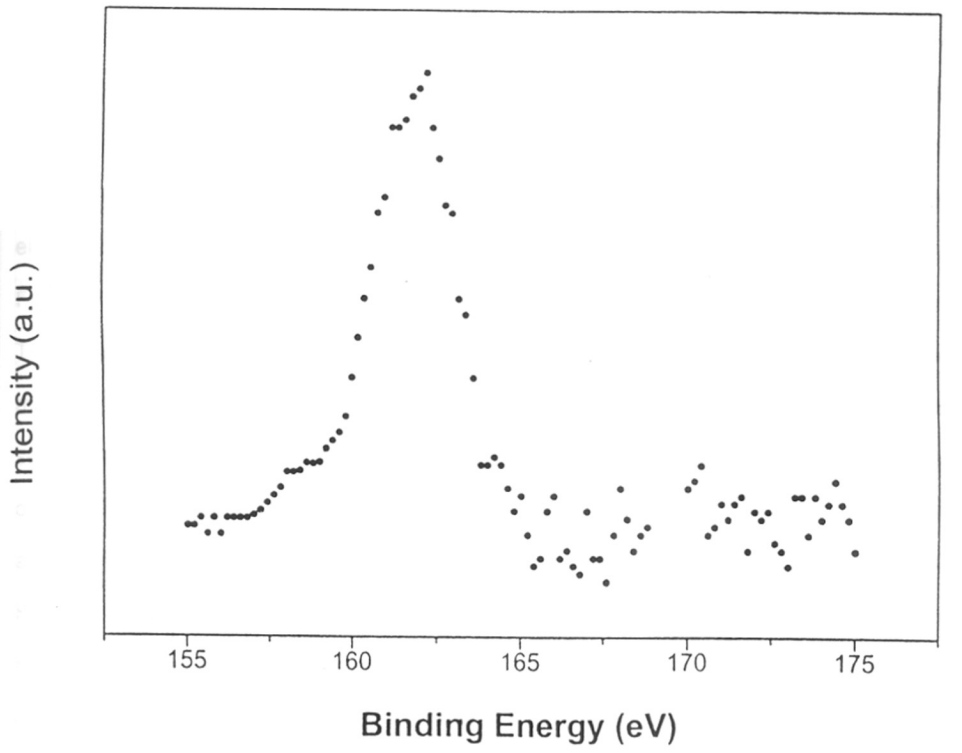

Figure 5.2. (b) S 2p core level spectrum of the ODT monolayer on copper surface.

that, at the copper surface in aerated 0.5 (M) Na_2SO_4 solution, the reaction mainly comprises of anodic dissolution of copper and cathodic oxygen reduction.[20] Superimposed impedance plot in Figure 5.3 of bare Cu and Cu electrode modified with NDS, DDS and ODT monolayer shows that charge transfer resistance R_{ct} is increased from bare to monolayer modified electrode. The semicircle observed in all the impedance response of monolayer modified electrode from high to low frequencies are indicative of charge-transfer controlled process due to the formation of respective monolayer. In all the cases, the low frequency region (Warburg impedance) due to diffusional process is absent which suggests that the corrosion is solely controlled by charge-transfer. Accordingly, an equivalent circuit can be proposed to represent the electrode/electrolyte interface with the respective monolayer as shown in the inset of Figure 5.3; R_{ct} is the charge-transfer resistance and C is the double layer capacitance. The quality of the monolayer can be estimated from R_{ct}, double layer capacitance and maximum phase angle (θ_{max}) of the impedance response. Since the diameter of the semicircle is a measure of the R_{ct}, the increase in the diameter of the semicircle and decrease in the capacitance can suggest high monolayer quality. The maximum phase angle should be 90° for a parallel R-C equivalent circuit representation when R_s = 0. However, the depressed semicircle which is generally obtained in the actual impedance response for the electrode/electrolyte interface can be attributed to the roughness of the electrode surface. A less depressed (with θ close to 90°) semicircle indicates better quality of the monolayer. In all cases, the impedance measurements are conducted after keeping the respective monolayer coated electrode in aerated 0.5 M Na_2SO_4 solution for one hour.

Table 5.1 shows different parameters obtained from the impedance plots in Figure 5.3 after fitting the impedance response to the proposed equivalent circuit. It is evident that in all the cases double layer capacitance value has been decreased from bare Cu electrode (25.4 $\mu F/cm^2$). For example, the value of double layer capacitance is decreased to 1.6 $\mu F/cm^2$ for ODT monolayer, which is in good agreement with the results obtained by previous studies.[5,21] This corresponds to a high value of charge-transfer resistance, indicating the high protection efficiency of the ODT monolayer. On

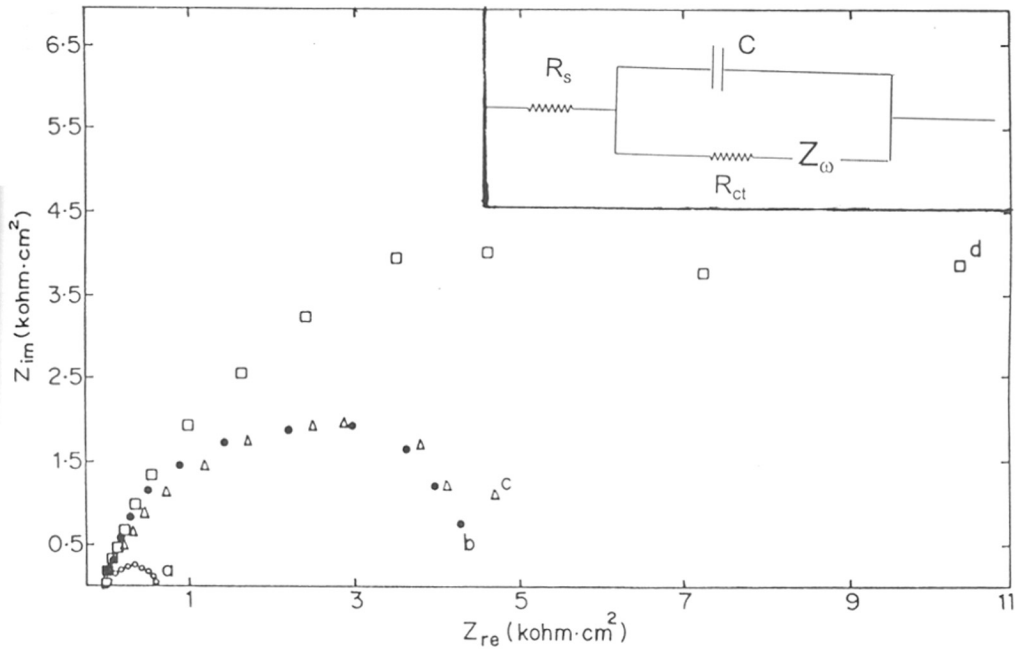

Figure 5.3. Impedance response at the open circuit potential E_{oc} vs Hg/Hg_2SO_4 in 0.5 M aqueous Na_2SO_4 solution for (a) bare copper electrode; copper electrodes with (b) NDS (c) DDS and (d) ODT SAM after keeping the respective electrodes for one hour in the solution. Frequency range used is 100 KHz to 100 mHz with a 5 mV rms signal at 5 steps per decade at 298 K. Inset shows the proposed equivalent circuit to represent the corrosion interface of monolayer-covered in the same solution. R_s is the solution resistance, R_{ct} is the charge-transfer resistance, C is the double layer capacitance, and Z_ω is the Warburg impedance appearing in the lower frequency region.

Table 5.1

Parameters obtained from XPS, Impedance and Polarization measurements for bare and different monolayers modified Cu surfaces

Electrode	Capacitance# ($\mu F/cm^2$)	XPS Binding Energy S 2p (eV)	Capacitance* ($\mu F/cm^2$)	P%	Corrosion current (i_{corr})	R_{ct}* ($ohm.cm^2$)
Cu	54.40	-----	25.4	---	2.1×10^{-5}	593
Cu/NDS	5.26	159 167.5	13.2	70	2.4×10^{-6}	5330
Cu/DDS	5.11	162.8	13.4	85	2.8×10^{-6}	4533
Cu/ODT	1.2	162	1.6	92	1.2×10^{-6}	10590

Double layer capacitance measured during monolayer formation in 0.1 M KF solution.

* Double layer capacitance measured in 0.5 M Na_2SO_4 solution.

the other hand, the decrease in the double layer capacitance is not much in case of DDS and NDS along with lower R_{ct} values. This can be attributed to the smaller dimension of the two molecules, which inturn indicates low protection efficiency than ODT. Moreover, corrosion current calculated from the corresponding R_{ct} values from impedance plot of respective bare and monolayer covered electrodes (Table 5.1) show decrease in the corrosion current for all the monolayers from the bare one, with the reduction being more for the ODT monolayer. In addition, NDS and DDS show a comparable corrosion current which is possible due to their nearly equal dimension. So, impedance response shows that the corrosion protection efficiency is lower for NDS and DDS compared to ODT monolayer on Cu.

Figure 5.4 shows the Tafel polarization curves of (a) bare Cu, (b) NDS, (c) DDS and (d) ODT monolayer covered Cu-electrodes in 0.5 M Na_2SO_4 after one hour of immersion. For the bare Cu-electrode, from the anodic portion of the Tafel curve an apparent Tafel slope of 50 mV/decade is obtained. However, this value is slightly lower than that reported in the literature.[22] For the electrodes treated with NDS, DDS and

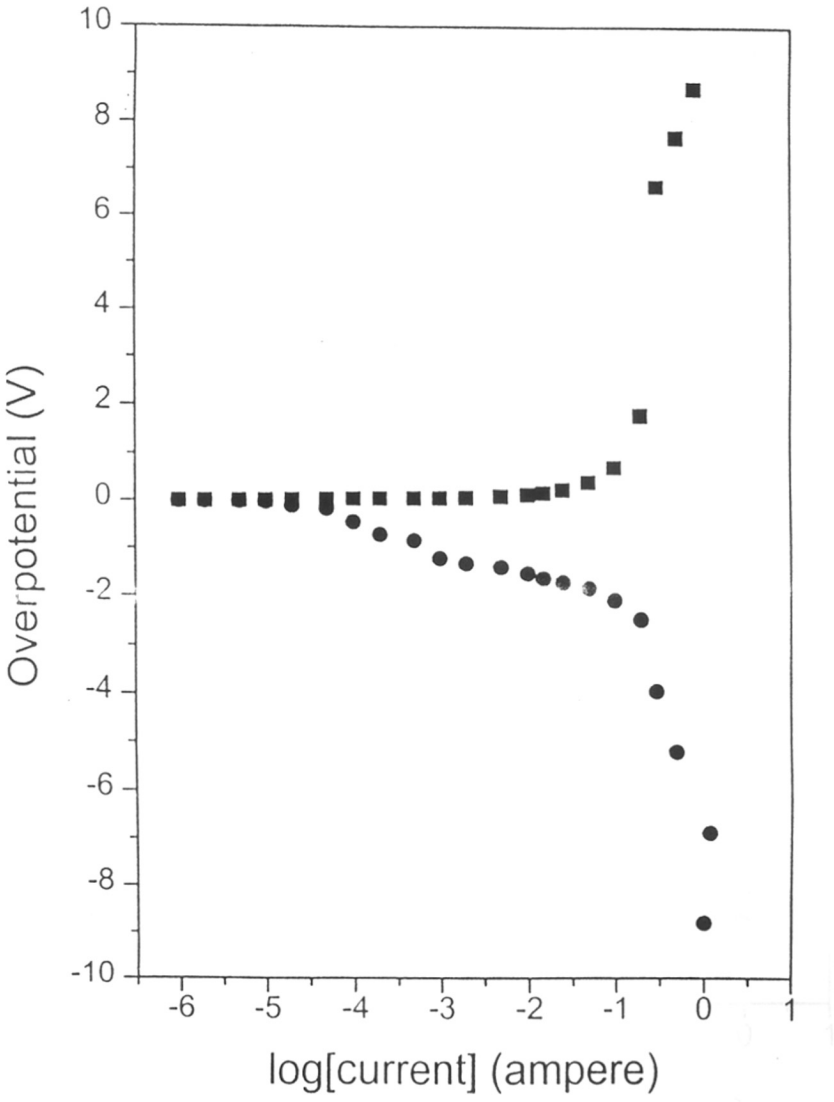

Figure 5.4 (a) Galvanostatic Tafel polarization curve for bare Cu electrode in 0.5 M aqueous Na_2SO_4 solution after keeping the electrode for one hour. Anodic (x) and cathodic (y) polarization curves are separately recorded using Hg/Hg_2SO_4 as reference electrode. Corrosion current (i_{corr}) is determined from the polarization curves by extrapolating the Tafel lines to corrosion potentials.

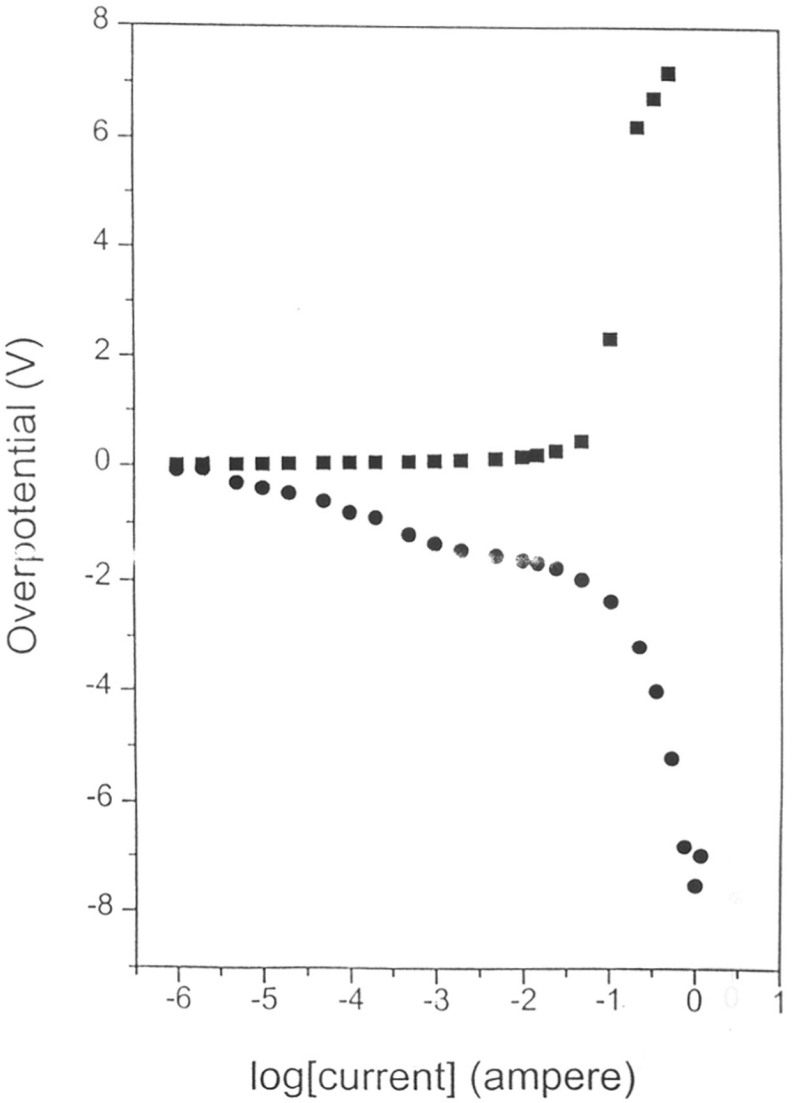

Figure 5.4 (b) Galvanostatic Tafel polarization curve for Cu electrode modified with NDS SAM in 0.5 M aqueous Na_2SO_4 solution after keeping the electrode for one hour. Anodic (x) and cathodic (y) polarization curves are separately recorded using Hg/Hg_2SO_4 as reference electrode. Corrosion current (i_{corr}) is determined from the polarization curves by extrapolating the Tafel lines to corrosion potentials.

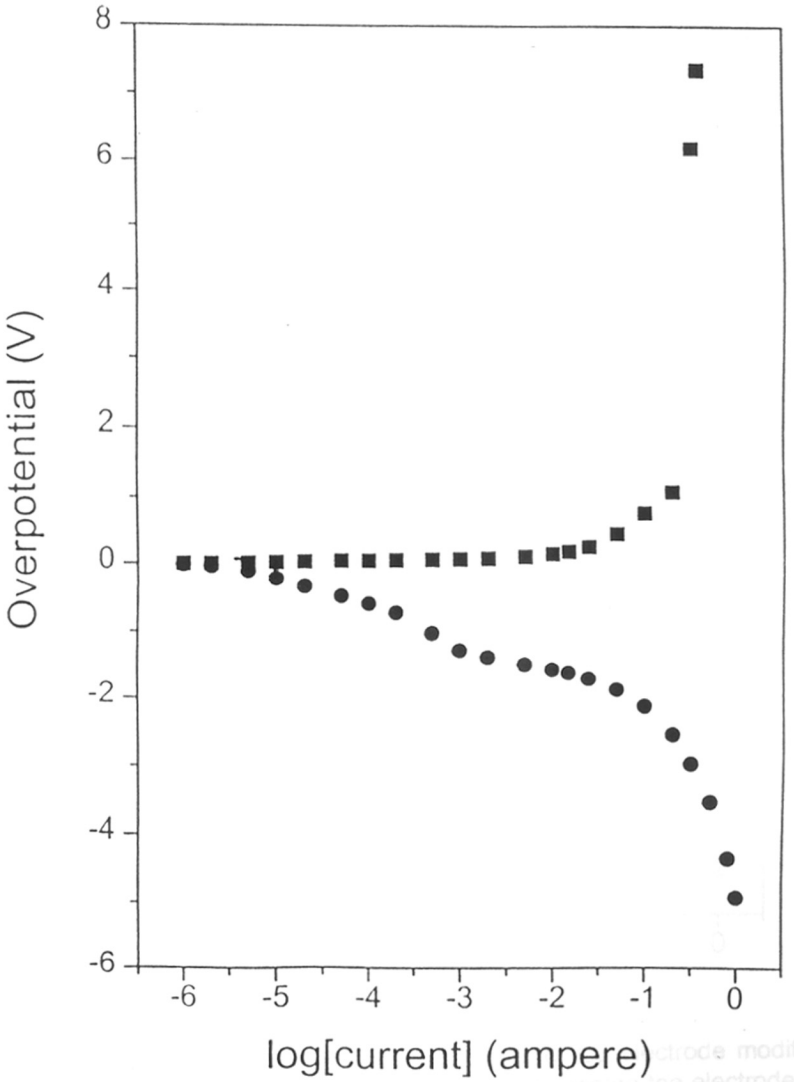

Figure 5.4 (c) Galvanostatic Tafel polarization curve for Cu electrode modified with DDS SAM in 0.5 M aqueous Na_2SO_4 solution after keeping the electrode for one hour. Anodic (x) and cathodic (y) polarization curves are separately recorded using Hg/Hg_2SO_4 as reference electrode. Corrosion current (i_{corr}) is determined from the polarization curves by extrapolating the Tafel lines to corrosion potentials.

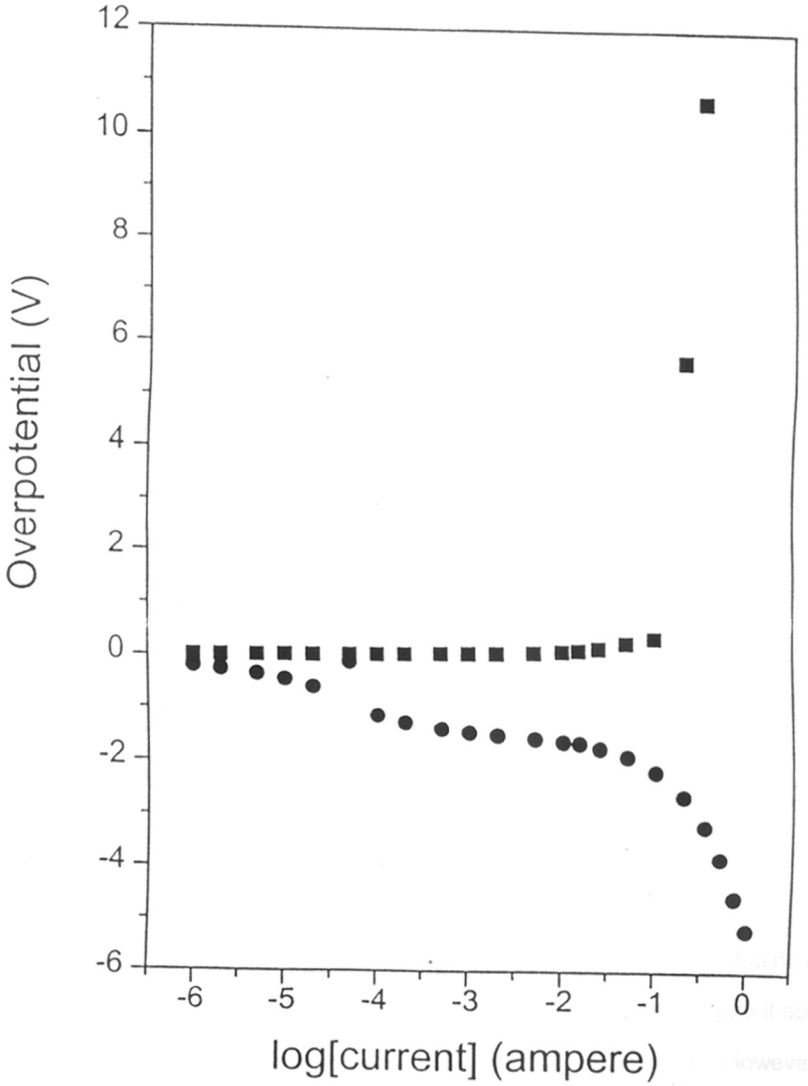

Figure 5.4 (d) Galvanostatic Tafel polarization curve for Cu electrode modified with ODT SAM in 0.5 M aqueous Na_2SO_4 solution after keeping the electrode for one hour. Anodic (x) and cathodic (y) polarization curves are separately recorded using Hg/Hg_2SO_4 as reference electrode. Corrosion current (i_{corr}) is determined from the polarization curves by extrapolating the Tafel lines to corrosion potentials.

ODT, both anodic as well as cathodic currents are inhibited which indicate that, all the monolayers are capable of retarding the reduction of dissolved oxygen and inhibiting the anodic dissolution of copper. Corrosion current densities (i_{corr}) can be estimated from the polarization curves by extrapolating the Tafel lines to the corrosion potentials. For bare Cu sample, i_{corr} is around 3.04 $\mu A/cm^2$ while for SAM containing electrodes, values of 0.92, 0.46 and 0.85 corresponding to NDS, DDS and ODT are obtained which are in good agreement with the values obtained by Aramaki *et. al.*[5] The protective efficiency (P%) can be calculated from these i_{corr} value using the equation:

$$P\% = 100\ [1-(i_{corr}/i^{\circ}_{corr})] \qquad (5.1)$$

where i_{corr} and i°_{corr} are the current at the bare and respective monolayer modified electrode. The observed efficiency values are listed in the Table 5.1 which shows that DDS is more effective among the two disulfides in protecting Cu from corrosion. This observation independently supports the conclusion drawn from impedance measurements.

5.3.2. Two Dimensional Organization of Metal Cluster from Solution:

The size distribution of the Ag particles synthesized in the hydrosol has been determined from TEM measurements. Figure 5.5 shows the electron micrograph obtained for the Ag colloidal deposited on an electron microscope grid from colloidal solution. A fairly uniform distribution of well dispersed particles is seen. The statistics of the size distribution as determined from the above and other micrographs obtained from many different regions of the surface are shown in Figure 5.6. From the figure it appears that, the distribution is bimodal, with peaks at roughly 10 and 38 nm. However, the distribution is mainly peaked around 10 nm cluster diameter and we have attempted to fit the lower diameter size range to a Gaussian, which is shown by the continuous line in the figure. The average cluster size from the above fit is 10.3 nm while the standard deviation was determined to be 4.4 nm.

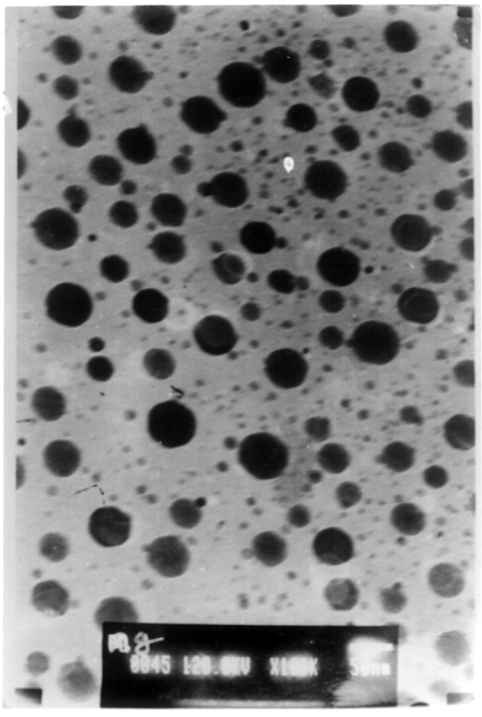

Figure 5.5. Transmission electron micrograph of the Ag nanoparticle film formed from solution. Micrograph has been recorded after evaporating off the aqueous component of drops placed on carbon-coated electron microscope grids.

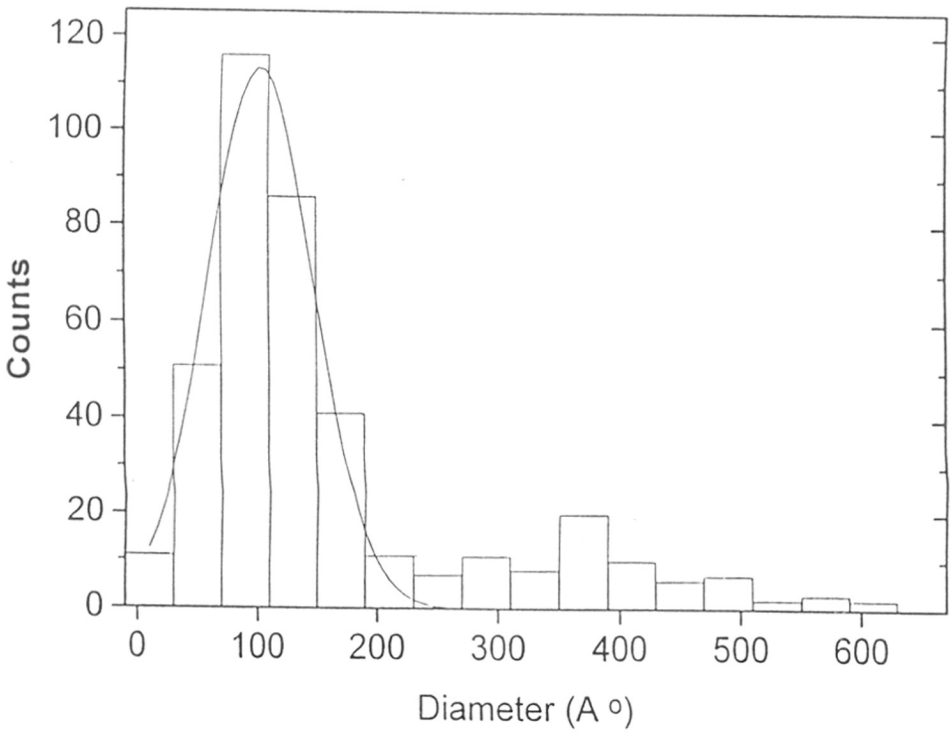

Figure 5.6. Histogram of the Ag colloidal particle size distribution with a fit using a log-normal distribution function.

Quartz crystal microgravimetry, due to its sensitivity towards mass loading (12 ng/cm^2 is the sensitivity of the instrument employed in this study), is a technique suitable for determining optimum conditions for formation of a compact monolayer of 4-CTP as has been shown before for other molecules.[23] The kinetics of SAM formation of 4-CTP is followed at room temperature for monomer concentrations varying from 10^{-2} to 10^{-7} M for both Al and Au surfaces. The surface roughness of the thermally evaporated Al and Au films on the quartz crystals are determined from cyclic voltammetry to be 2.2 and 2.5 respectively and this factor has been taken into account in the QCM calculations reported below.

From the kinetics of SAM formation it is found that, 10^{-3} M solution gives the largest frequency change which is found to stabilize within 12 hours of immersion for both the surfaces. A higher concentration (10^{-2} M) of monomer solution also gives comparable mass change but considerable fluctuations in the quartz crystal resonant frequency is noticed over long time intervals. Figure 5.7a shows the variation in mass loading of the Al (■) and Au (●) covered quartz crystals measured *ex-situ* as a function of time for crystals immersed in 10^{-3} M monomer. A sigmoidal curve (continuous line in the figure) is found to fit the growth kinetics of the SAM on the Al surface. The maximum mass loading in case of the Al surface is ~ 100 ng/cm^2 and corresponds to an average surface area/molecule of ~ 2.5 nm^2. The growth of the SAM on Au is quite different with an initial increase followed by a fall and stabilization at a mass coverage of ~ 75 ng/cm^2 (average area/molecule = 3.2 nm^2). While the exact reason for this behavior is not clear, a possible explanation could be in terms of an initial multilayer formation which equilibrates with time to a monolayer structure. Such behavior has been observed for alkane thiols chemisorbed on gold surfaces.[24] In the absence of the exact crystallographic information on the structure of the solid phase 4-CTP on Al and Au surfaces, we cannot comment on differences in molecular packing observed or whether the 4-CTP molecules are tilted etc. based solely on the QCM data .

While information regarding packing of molecules in the SAM is derived indirectly from QCM which only senses a mass loading, further characterization of the monolayer

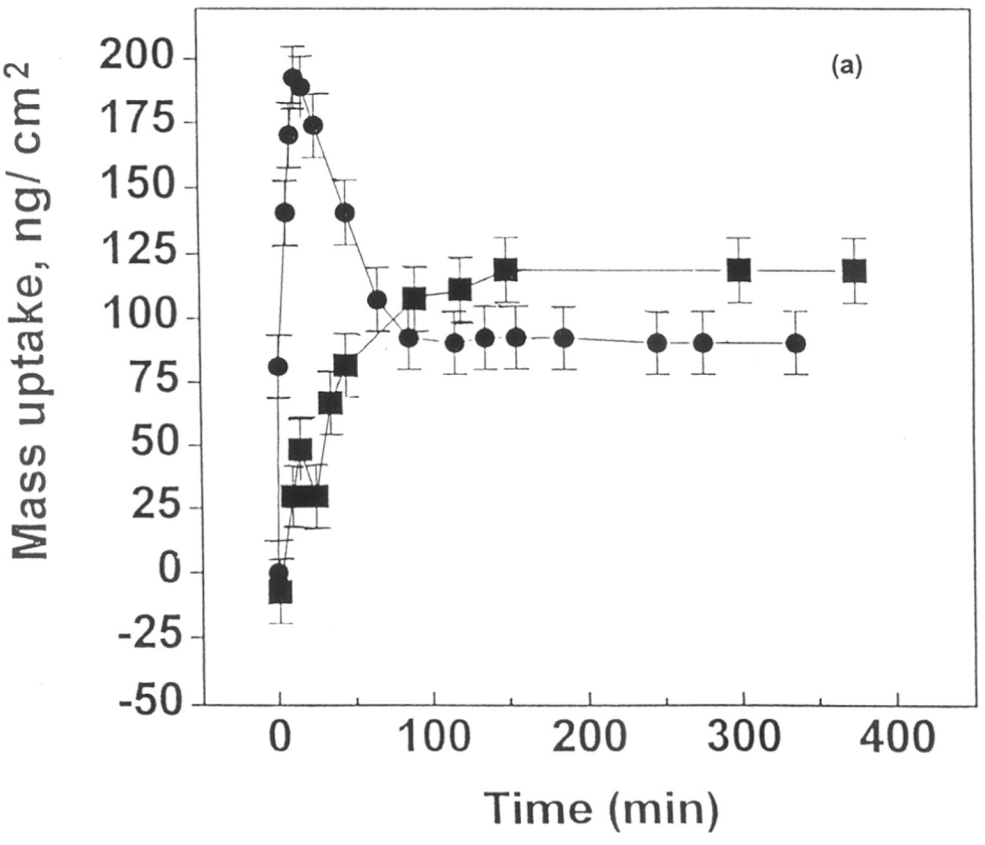

Figure 5.7. (a) Quartz crystal microbalance measurements of mass change with time for 4-CTP adsorbed on Al (filled squares) and Au (filled circles). A sigmoidal curve has been fit to the SAM growth on the Al surface (solid curve).

packing is important, especially in the light of different mass loading observed for the SAM on Al and Au surfaces. It is well known that, for an electrical double layer, the differential capacity decreases with increasing separation between the electrode surface and the plane of closest approach for the ionic charges.[25] Hence, double layer capacitance studies can give additional insight into the average structure of the self-organized assemblies. In the present case double layer capacitance values for both Al and Au surfaces have been calculated from impedance measurements in 0.1 M tetrabutylammoninum tetrafluoroborate in acetonitrile in the presence of 1 mM of ferrocene. The impedance plots of log(total impedance) with frequency on extrapolation to angular frequency (ω) = 1 gives a double layer capacitance value[26] of 6.29 and 1.7 $\mu F/cm^2$ for gold and aluminium respectively. The value obtained for the gold electrode is comparable to the values obtained in case of SAMs with dimensionally similar small aromatic disulfides on gold at ~ 99% surface coverage.[27] Hence, the measured double capacitance values indicate that, the surface coverage of the monolayer on gold and aluminium are high and more in case of Al surface which correlates well with the results obtained from QCM studies.

Once the SAM of 4-CTP is formed, Ag particle adsorption from the colloidal solution is also followed using *ex-situ* QCM measurements. Figure 5.7b shows the mass change with time of immersion for the SAMs on Al (■) and Au (●) surfaces. It is seen that adsorption of the clusters is extremely rapid for the SAM on Al with most of the mass change occurring within a couple of minutes. The frequency is however, found to stabilize only after an hour of immersion. Very little frequency change is noted for the SAM/Au system even after prolonged immersion (~ 60 minutes) indicating that the Ag clusters do not coordinate to the carboxylic acid groups. This result is in variance with the findings of Natan *et al*[8f] who observed that both Au and Ag clusters are bound to carboxylic acid groups. We believe this difference can be attributed to the borohydride reduced silver clusters having modified surfaces which inhibit binding with the carboxylic acid groups, an aspect discussed by Natan *et al.*[8f] It may be mentioned that our results are in agreement with Li *et al*[28] who observed that *n*-alkylamines and carboxylic acids do not self-assemble on silver nanostructures. For the SAM/Al surface, the mass change of

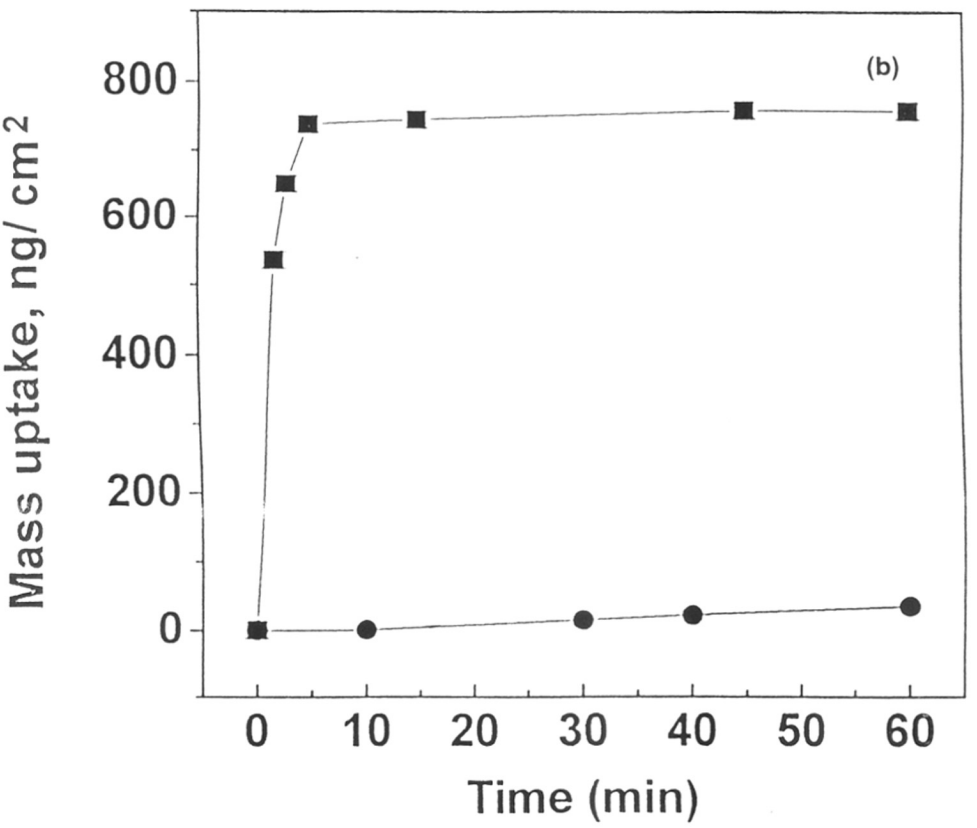

Figure 5.7. (b) Quartz crystal microbalance measurements of mass change with time for Ag colloidal particles adsorbed on SAM covered Al (filled squares, continuous line) and SAM covered Au (filled circles, dashed line). A sigmoidal curve has been fit to Ag particle adsorption on the SAM covered Al surface (solid curve).

~ 730 ng/cm^2 obtained from immersion in the Ag colloidal solution corresponds to a particle surface coverage of 5.8 x 10^{10} clusters/cm^2, assuming 10 nm diameter for the particles (TEM results) and 1.6 nm^3 per silver atom. This corresponds to a surface coverage of ~ 10 %. The small surface coverage is close to the value of 15% obtained by Natan *et al* for self-assembled gold colloidal particle films [8g] and may be rationalized in terms of strong interparticle repulsive interactions.

Based on the above results, the expected structure of the SAM formed using the aromatic bifunctional molecule on Au and Al surfaces and the adsorption of Ag clusters on the thiol rich SAM surface is illustrated in Schemes 5.2 (a, b). There is a reversal in the orientation of the molecule which leads to a SAM surface rich in thiol when organized on the Al surface which is then used to adsorb the Ag nanoparticles (Scheme.5.2a) while the SAM surface is carboxylate rich for the SAM organized on Au (Scheme.5.2b). The latter surface is inefficient in adsorbing the Ag nanoparticles as discussed earlier. A possible reason for the carboxylic acid surface not coordinating to the silver colloidal particles could be that the SAM on gold is disordered, a conclusion supported by QCM measurements.

SEM experiments were performed on the SAMs on both Au and Al film surfaces after immersion in the Ag hydrosol. Figure 5.8 shows the scanning electron micrograph of the SAM formed on the Al film after immersion in the Ag hydrosol. The adsorbed clusters can clearly be seen indicating that the terminal thiol groups provide efficient adsorption sites for the Ag nanoparticles. It appears that there is a large increase when compared to the cluster size distribution in the colloidal solution (Figures 5.5 and 5.6). This may be due to electron beam induced aggregation of the silver particles observed for gold clusters in the TEM.[29] We would like to note here that no Ag nanoparticle adsorption was seen using SEM on the SAM formed on the Au surface on immersion in the hydrosol in agreement with the QCM results.

XPS studies were performed on the SAM rich in thiol terminal groups (SAM formed on the Al surface) and the SAM on which Ag adsorption had taken place and which had been characterized in detail by the earlier mentioned techniques. The S 2p

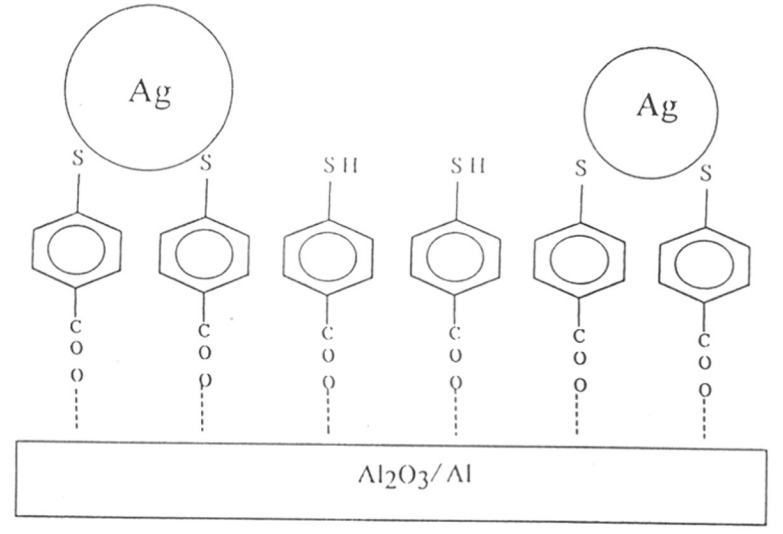

(a)

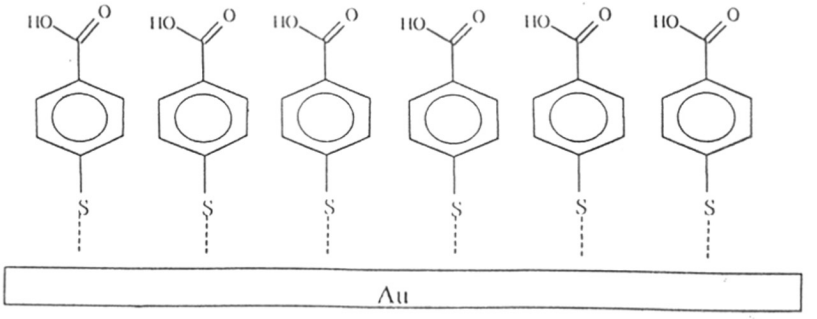

(b)

Scheme 5.2. Schematic Representation of the (a) SAM Formation on Al Films Showing the Surface Thiol Functionality of the SAM to Which Ag particles are Covalently Coordinated and (b) the 4-CTP SAM Formed on Au Films Showing the Surface Carboxylic acid Functionality of the SAM.

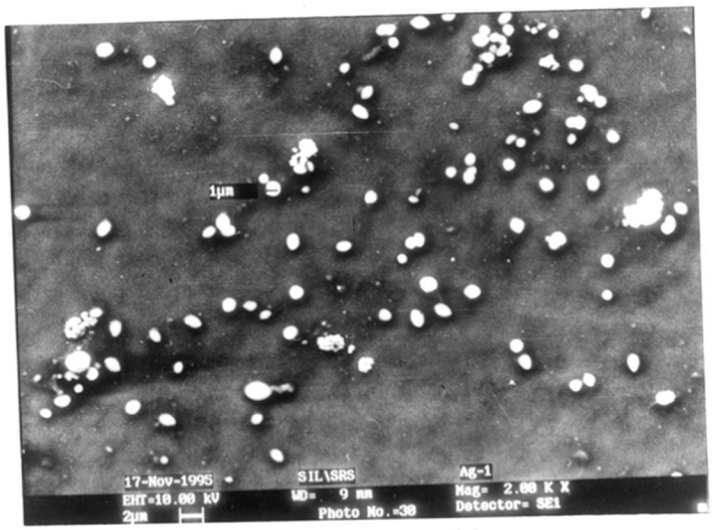

Figure 5.8. Scanning electron micrograph of Ag colloidal particles adsorbed onto a 4-CTP SAM formed on the Al surface.

and C 1s spectra of the uncovered SAM are shown in Figures 5.9a and 5.10a respectively. Fits to the above spectra yielded one spin-orbit pair for the S 2p core level (spin orbit splitting = 1.15 eV and $2p_{3/2}$ / $2p_{1/2}$ intensity ratio = 2)[4a] while three components constitute the C 1s core level signal. The BE of the S $2p_{3/2}$ signal is 163.9 eV and is characteristic of uncoordinated thiol sulfur.[4a] The three C 1s components at 285 eV, 286.9 eV and 288.6 eV are tentatively assigned to aromatic carbons, carbon coordinated to the thiol group and carboxylic acid carbon respectively.

Figures 5.9b and 5.10b show the S 2p and C 1s spectra for the Ag covered SAM surface. An additional component is observed in the S 2p spectrum at a BE of 161.8 eV which agrees well with reported BE for thiolate bonds with Ag.[4a] Growth of the low BE component is therefore a clear indication of covalent Ag particle attachment to the SAM surface. Comparison of the C 1s spectra before and after cluster adsorption (Figures 5.10 a and b respectively) reveals no changes in the component BEs. The attenuation factor for the C 1s and S 2p signals on adsorption of the Ag clusters were 3.3 and 2 respectively. The difference in the attenuation factors could be due to the fact that the S 2p electrons have higher kinetic energy than the C 1s electrons (1088 and 968 eV respectively) with a corresponding larger attenuation length.[30]

From the intensity ratios of the S 2p components in Figures 5.10a, we infer that roughly 30% of the surface thiol groups take part in the linkage with the Ag colloidal particles. From QCM studies, the surface coverage was determined to be ~ 10 %, assuming a spherical metal particle of diameter 10 nm. The reason for the discrepancy is not clear but may have to do with the fact that the clusters adsorbed on solid surfaces are not spheres but ellipsoids. The projected area onto the SAM surface may then account for the disparity observed. The Ag 3d spectrum recorded from the colloidal particle covered surface is shown in Figure 5.11. The spectrum clearly shows the presence of only one component [BE (Ag $3d_{5/2}$) = 368 eV ; spin-orbit splitting = 6.1 eV and Ag $3d_{5/2}$/Ag $3d_{3/2}$ intensity ratio = 1.5]. The fact that an additional component due to thiolate linkage of silver atoms is not seen is in agreement with the findings of Brust *et*

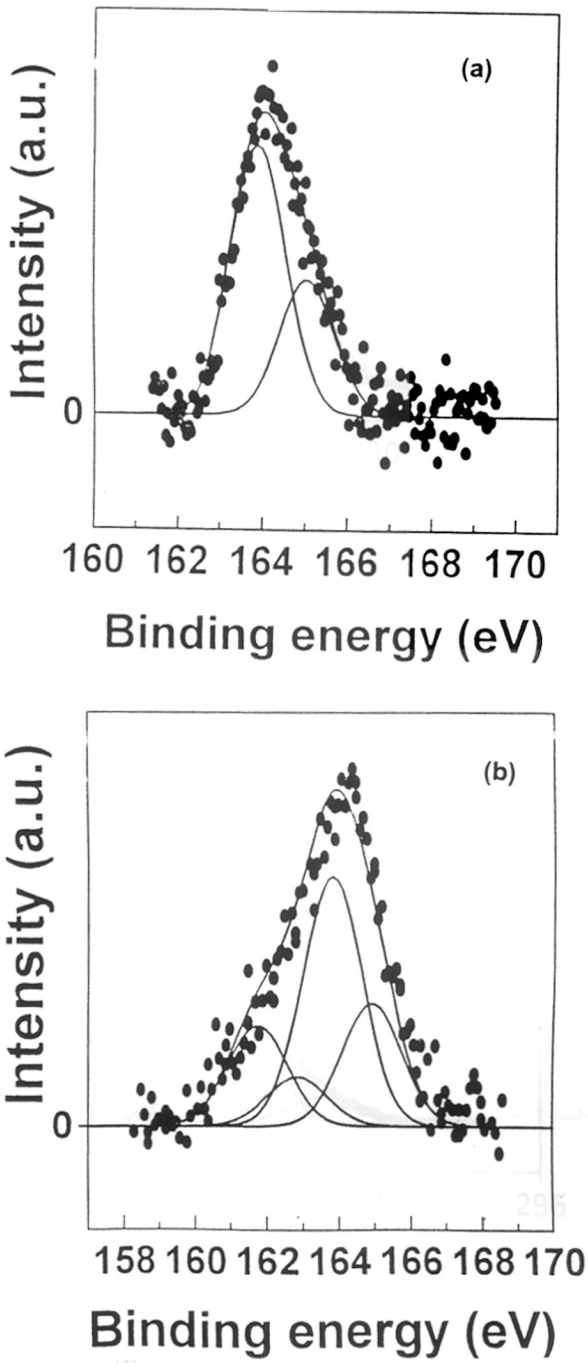

Figure 5.9. (a) S 2p core level spectrum of the bare 4-CTP SAM on Al together with the spin-orbit components. (b) S 2p core level spectrum from the Ag colloidal particle covered 4-CTP SAM on Al. The curve is stripped into two spin-orbit components.

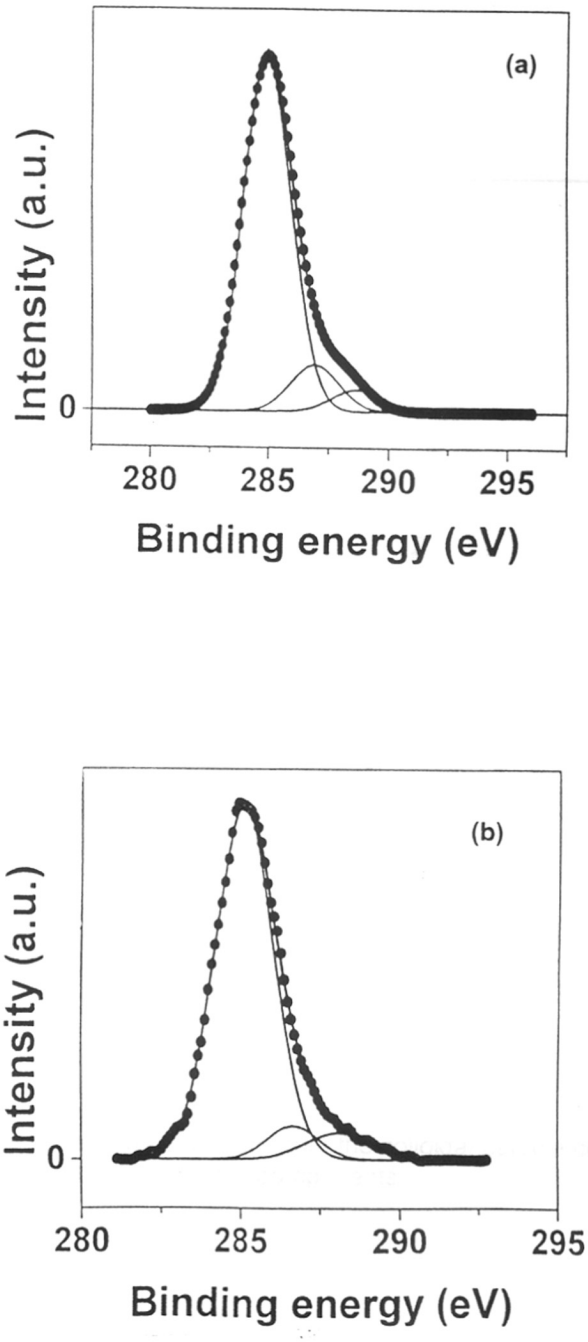

Figure 5.10. (a) C 1s core level spectrum from the 4-CTP SAM formed on Al together with Chemically shifted components. Assignments are indicated in the text. (b) C 1s core level spectrum from the Ag colloidal particle covered 4-CTP SAM formed on Al together with chemically shifted components.

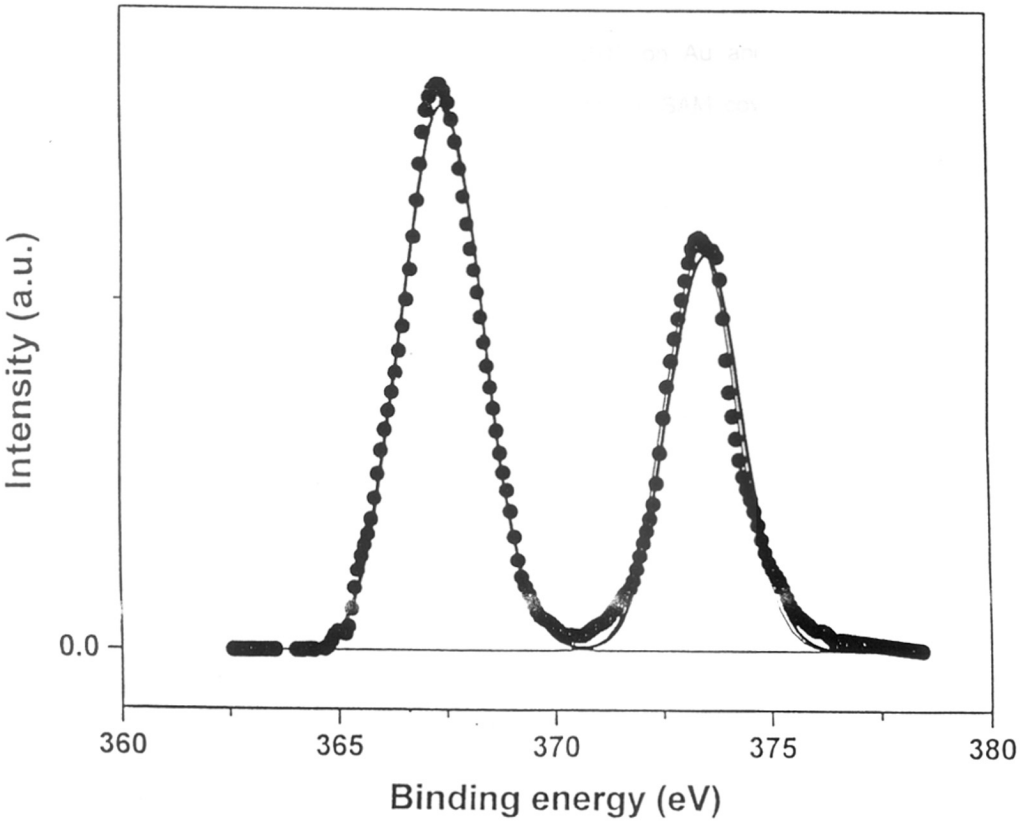

Figure 5.11. Ag 3d core level spectrum from the colloidal particle covered 4-CTP SAM on Al together with the spin-orbit components.

al[31] who found no evidence for chemically shifted peaks in dodecanethiol stabilized gold colloidal particles.

5.3.3. Formation of Microcrystalline ZrO_2 on the Functionalized Interface of SAM:

The process of monolayer formation from BDT on Au and the subsequent covalent attachment of Zr^{4+} from aqueous solution to the SAM covered surface was followed by XPS and cyclic voltammetry in aqueous 1 M KCl solution and also by impedance measurements in presence of redox active probe like $Fe(CN)_6^{4-/3-}$ couple. ZrO_2 synthesis has also been performed on bare gold surface to understand the importance of SAM on the nucleation and growth. XP spectrum of the monolayer coated electrode in Figure 5.12 shows a broad and asymmetric peak at lower binding energy side and a peak at higher binding energy for sulfur core level spectra. Although the relative cross section of sulfur is comparatively small, the binding energy values are particularly sensitive to the chemical environment of sulfur. Deconvulation of the lower binding energy peak indicates two sulfur components one at ~161 eV and another at ~ 164 eV. These are consistent with the metal-sulfide species and free thiol on the surface respectively,[19] thus pointing to the orientation and availability of the pendant -SH groups for Zr^{4+} linkage. The value of the sulfur peak at 170 eV is due to sulfate or sulfonic acid moiety,[32] since it is possible that the monolayer undergo beam-induced damages from X-ray source,[33] thus getting oxidized. XPS analysis after the formation of ZrO_2 on the surface shows a broad peak ~ 183 eV which is characteristic of Zr coordinated with highly electronegative group like oxygen as in this case.[34] Moreover, sulfur core level spectra indicate a peak at higher binding energy region with very low intensity. This demonstrates that underlying dithiol monolayer is stable under potential cycling.

Figure 5.13 shows a superimposed impedance plot of BDT monolayer coated gold and after adsorption of Zr^{4+} on the SAM surface. It is known that at higher frequency, the semicircle corresponds to a parallel RC equivalent circuit for the electrode impedance.[27] The total impedance plot for the dithiol monolayer coated electrode (Figure 5.13a) shows the behavior similar to a strongly blocking monolayer.[27] This is further

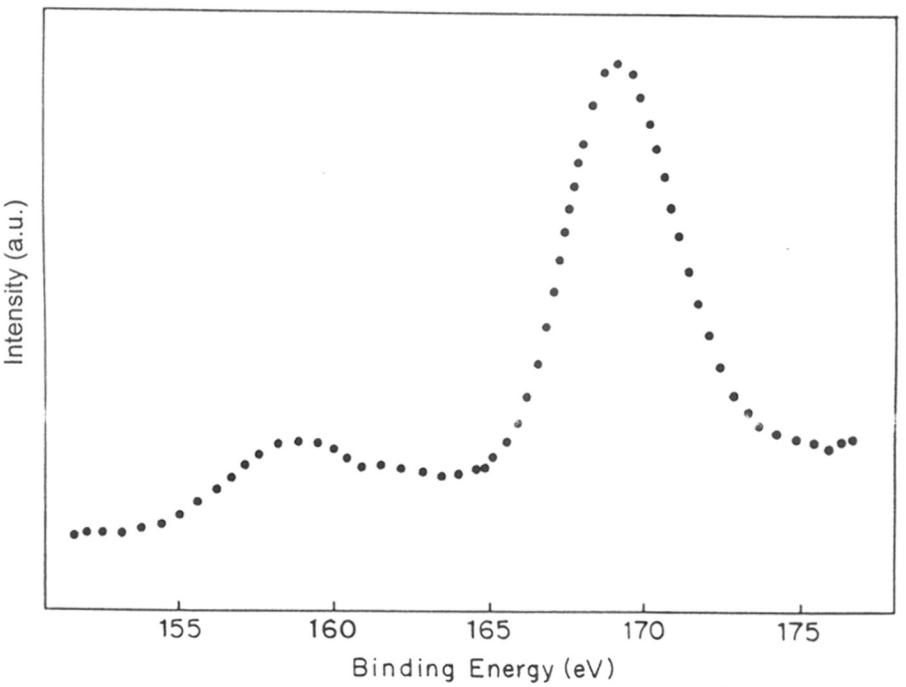

Figure 5.12. S 2p core level spectrum of the BDT monolayer on Au surface.

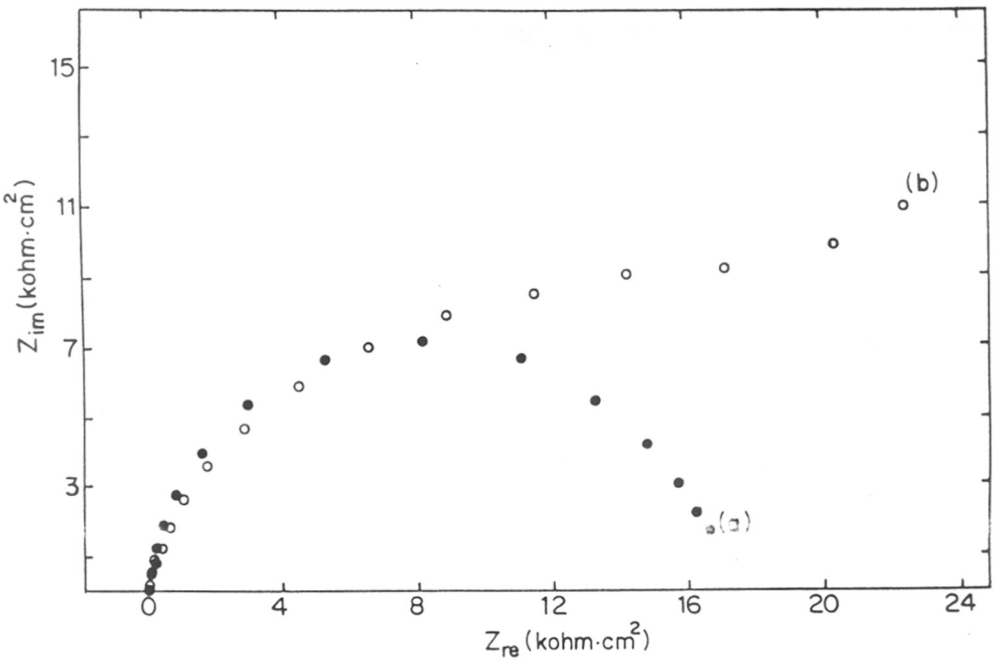

Figure 5.13. Superimposed impedance plot of (a) gold electrode with BDT SAM at a dc bias of 0.22 V vs SCE in 5 mM $K_3Fe(CN)_6$ + 5 mM $K_4Fe(CN)_6$ in 0.5 M aqueous KF solution. (b) gold electrode after Zr^{4+} attached on the BDT SAM surface from 5 mM aqueous solution of $ZrOCl_2$. $8H_2O$. Frequency range used is 100 KHz to 100 mHz with a 5 mV rms signal at 5 steps per decade.

confirmed from Figure 5.14 where the same impedance data for the monolayer is plotted vs $\omega^{-1/2}$ after converting to faradaic impedance by subtracting the interfacial capacitance and solution resistance. As discussed by Finklea *et al*,[35] this faradaic impedance plot of dithiol coated Au electrode behaves similar to a microarray electrode with two nearly linear domain at higher and lower frequencies.[35] From the slope of this curve at higher frequency, a surface coverage value of 0.99 can be obtained under some approximation, using a known value of Warburg coefficient measured with a bare electrode of same geometry in the same solution. This result demonstrates that the dithiol has formed a highly compact and organized monolayer assembly on Au surface thus acting like an ideal platform for further adsorption of Zr^{4+} from solution. The complex impedance plot of Au/SAM in Figure 5.13b shows a more dispersed impedance response and the expected semicircle at higher frequencies is not well-defined. This drastic difference in impedance response of the two electrodes can be attributed to the attachment of Zr^{4+} from solution to dithiol SAM covered surface.

The process of adsorption of dithiol, and the subsequent Zr^{4+} attachment can be understood following the cyclic voltammetric response of these modified electrodes in 1 M aqueous KF solution. Figure 5.15 shows a superimposed cyclic voltammogram of bare gold, gold electrode modified with dithiol and after adsorption of Zr^{4+} ion. It is clearly evident that, after the dithiol SAM formation, the nonfaradaic current is decreased significantly followed by a further reduction after Zr^{4+} attachment on the surface. An approximate estimation of double layer capacitance value from this response taken at 500 mV/s scan rate indicates a capacitance change from 25 $\mu F/cm^2$ for bare gold to 6.4 $\mu F/cm^2$ for dithiol modified gold electrode and finally to 2.6 $\mu F/cm^2$ after Zr^{4+} is attached to the surface.

Thus, XPS measurements together with cyclic voltammetric and impedance response of the surface modified dithiol monolayer and zirconium adsorption clearly demonstrate that a reasonably compact monolayer has been formed with surface thiol group so that tetrameric zirconium ion[36] can be hooked up on it from solution. The use of dithiol with short chain length to form the initial monolayer needs some comment. Most of the investigators have used much longer chain hydrocarbons (C_{10} or longer) for the

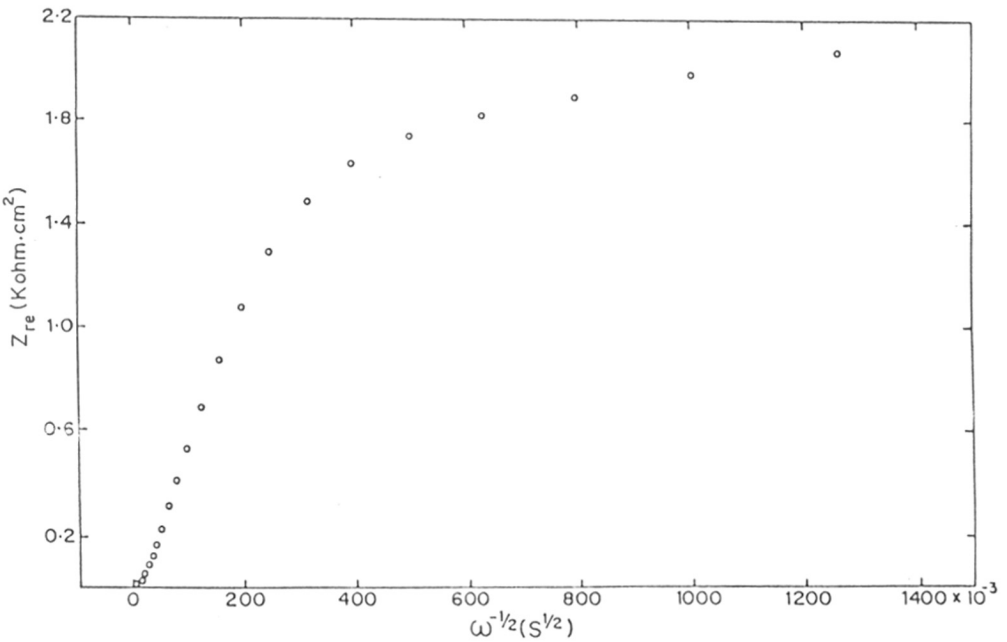

Figure 5.14. Plot of real part of Faradaic impedance (Z_{re}) vs $\omega^{-1/2}$ in 5 mM $K_3Fe(CN)_6$ + $K_4Fe(CN)_6$ in 0.5 M aqueous KF for gold electrode with BDT SAM.

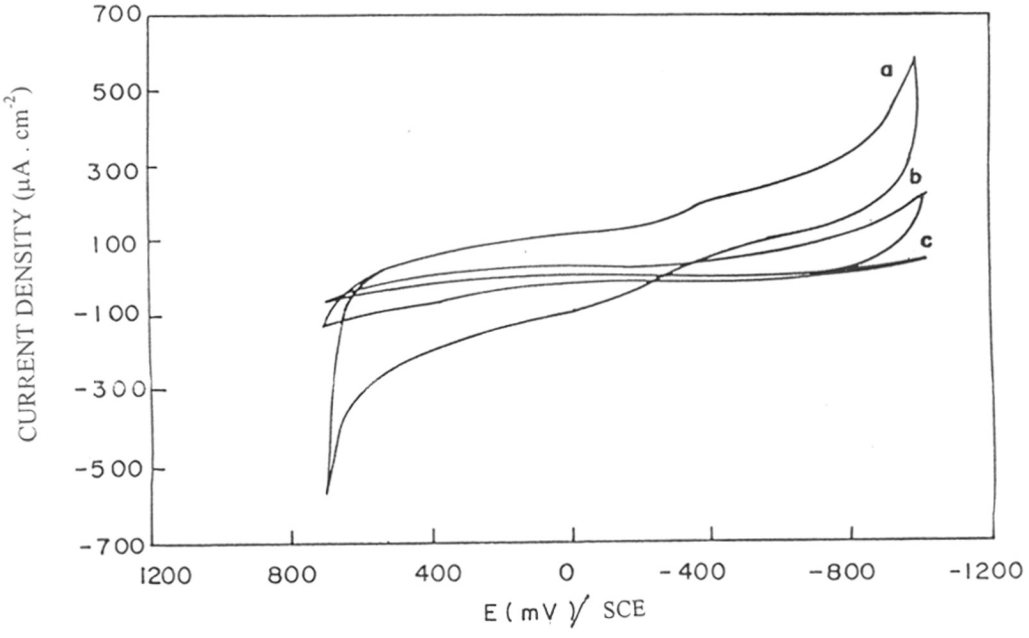

Figure 5.15. Superimposed cyclic voltammogram of (a) bare gold electrode; (b) gold electrode modified with SAM of BDT and (c) after attachment of Zr^{4+} from 5 mM $ZrOCl_2$. $8H_2O$ on the SAM surface in 1 M KF solution with a typical scan rate of 200 mV/s.

formation of crystalline monolayer since the lateral interaction between long chains are responsible for the organization of these systems, Such ordered system have lot of advantages with less pinhole but use of long chain thiol is not an essential prerequisite for these type of surface derivatization applications, since more important is the availability of free thiol on the surface to anchor the zirconium ions. Indeed, the short chains possibly avoid the problem of dithiol looping on gold surface as suggested by Bain *et al.*[37] But in a number of studies involving rigid conjugated dithiol as well as sufficiently long (C_{12}) α,ω-alkanedithiols, it is found that, these molecules are attached via only one thiol functionality.[38] Moreover, the species such as BDT cannot bind by both ends to the Au surface since it will introduce unfavorable steric interactions between the hydrogen and the benzene group. The success of these dithiol coated surface in binding solution Zr^{4+} species indicates the presence of available free thiol end on the surface.

Figure 5.16 shows a comparison of the SEM image of a section of microcrystalline ZrO_2 formed on both on (a) Au/dithiol functionalized and (b) bare gold surface after ten potentiodynamic cycles at room temperature. The distinct particles seen in the micrograph (Figure 5.16a) possess an average size of 7-15 μm with a large interparticle distance (17 μm). The unexpected effect is the presence of uniform and sharp-edged crystals suggesting the possibility of topographic control by SAM. These features are completely absent in the SEM image of ZrO_2 on bare gold where, a distribution of ZrO_2 particles is seen. with an average interparticle distance of 5 μm. The shape contrast suggests incomplete growth for this, in comparison with the crystal nucleation and growth onto functionalized (i.e. dithiol/Au) interfaces. These observations strongly suggest the importance of SAM in nucleation and growth of the solid materials at the interface. This is specially significant for biomimetic processing of materials since several reports have recently shown that the manipulation of the surface energies can be possible through SAM formation to favor the heterogeneous growth and nucleation.[39] In this respect, it can be suggested that, SAM can play a key role in decreasing the free energy process related to the interfacial nucleation.

The powder diffraction pattern of the microcrystalline zirconia on (a) bare gold surface and on (b) dithiol SAM modified Au surface is shown in Figure 5.17. In both the

(a)

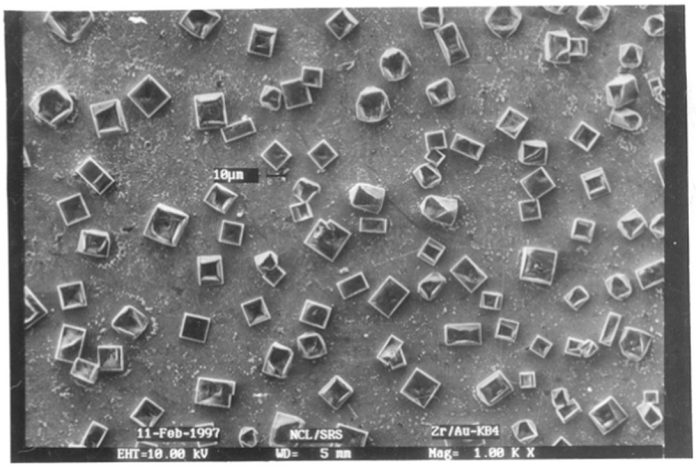

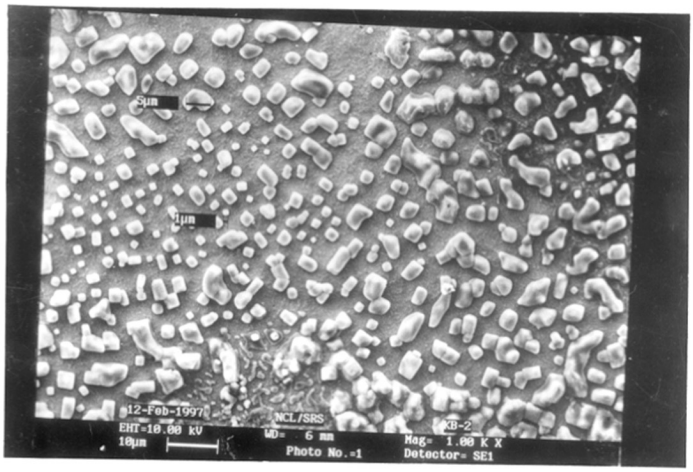

Figure 5.16. SEM micrograph of microcrystalline zirconia on (a) gold substrates derivatized with SAM of BDT and on (b) bare gold substrate. Samples were prepared by potentiodynamic cycling at a scan rate of 200 mV/s in a potential range of + 0.7 V to -1.1 V vs SCE.

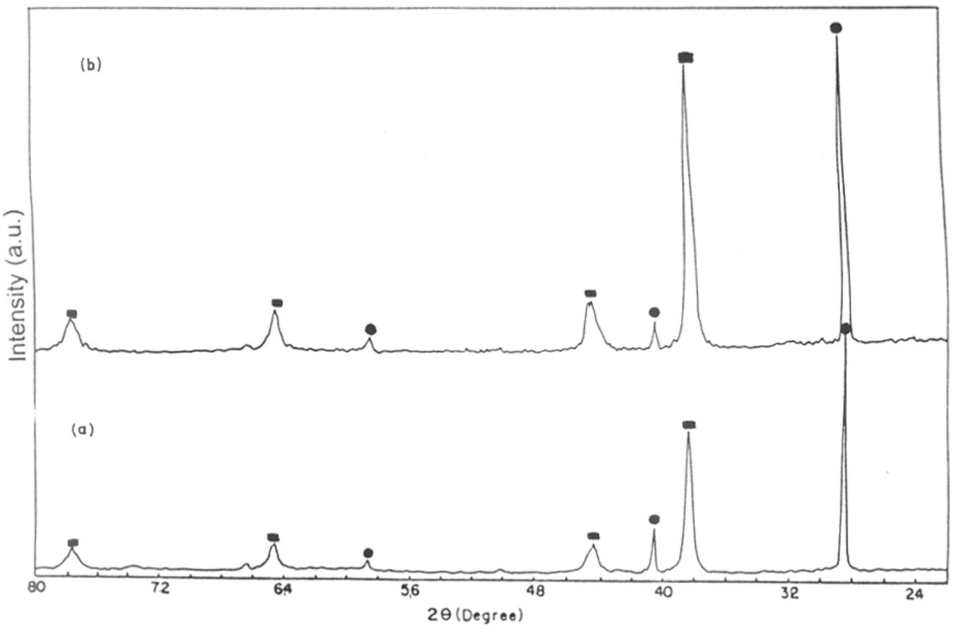

Figure 5.17. XRD patterns of zirconia prepared on (a) bare gold surface and on (b) BDT SAM coated gold surface by potentiodynamic cycling (as mentioned in the text). The peaks corresponding to underlying gold substrate are marked by (■) while that of zirconia by (●).

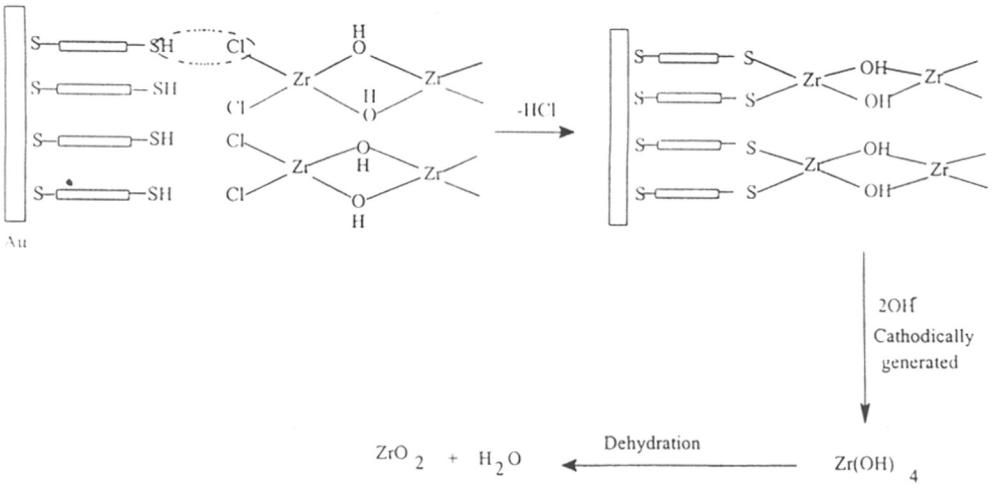

Scheme 5. 3. A Tentative Scheme for Different Steps Involved in the Proposed Mechanism of the ZrO_2 Formation on the BDT SAM Surface.

cases, there are sharp peaks (●) due to the underlying gold surface while three major peaks are distinctly observed for ZrO_2 (O) corresponding to [111], [112] and [222] planes of monoclinic zirconia. The intensity of the peak corresponding to the ZrO_2 are higher in case of SAM modified gold surface, indicating more orientated nature of the ZrO_2 formed onto functionalized interface - an observation in conformity with the SEM images in Figure 5.16. This also underlines the importance of functionalized interface of SAM to favor the orientation of the crystals. This is further supported by the experimental observation that even a continuous potentiostatic cathodic polarization at -1.1 V for several minutes does not yield a smooth and continuous ZrO_2 film. Use of different single crystal surface of Au with SAM of the same molecule may provide further confirmation for this.

At present, the exact mechanism of the ZrO_2 formation on the surface of SAM is not clear. It is reasonable to believe that the covalent linkage of zirconium ion to the surface can be formed by the reaction between the pendant surface -SH and tetrameric zirconium ion in solution by the elimination of HCl which is common for other surface modification schemes.[40] In the next step, the surface bound Zr reacts with cathodically generated OH^- to produce $Zr(OH)_4$ on the surface, which can form ZrO_2 crystals upon dehydration,[41] as represented in Scheme 5.3. Although XPS results show the retention of atleast some of the thiol molecules on Au surface, several questions related to the nucleation and growth of the ZrO_2 phases and more importantly the reorganization of the monolayers, need futher investigation.

5.4. Conclusion:

In this chapter, three specific applications of SAM of small aromatic thiol/disulfides are demonstrated. Protection efficiency of disulfide SAMs in Cu corrosion are studied and the result are compared with long chain thiol (ODT) monolayer. Characterization of monolayer on Cu surface by impedance and XPS measurements suggest that NDS monolayer is comparatively less ordered and suffer x-ray beam induced damage. It is observed that an equivalent circuit with parallel combination of resistance and capacitor can be used to understand the interfacial impedance response.

Impedance response shows comparable protection efficiency for both the disulfides. In contrast, Tafel polarization clearly shows a high suppression of the corrosion current for DDS compared to NDS which inturn suggests a high protection efficiency. The comparison of all the results with different molecules suggest that, the SAM of these dimensionally small molecules can provide an effective protection to the Cu corrosion. The difference in the monolayer organization and efficiency of protection for the two disulfides monolayer can be explained on the basis of their structural rigidity which is responsible for the equilibrium monolayer organization on the surface.

The investigation of two dimensional organization of metal cluster has shown that close packed SAMs can be formed from 4-CTP on both Al and Au surfaces. Depending on the metal surface, the molecule packs with different surface functionality and this aspect has been used to self-assemble Ag nanoparticles from colloidal solution by forming a covalent linkage with the thiol groups. SAMs formed on Au surfaces with carboxylic acid surface functionality are inefficient in adsorbing Ag clusters from solution.

It is also demonstrated that a two dimensional reaction between zirconyl oxychloride in solution and self-assembled monolayers of BDT on Au surface, followed by a simple potentiodynamic cycling leads to the formation of microcrystalline, monoclinic ZrO_2 at room temperature. The innovations that are likely to develop from this surface modification strategy have promising applications in a wide range of fields including electrochemical sensors, catalysis and toughened ceramics. Moreover, this process could possibly be extended to stabilize tetragonal or cubic zirconia at room temperature, by controlling the electrolyte composition and potentiodynamic cycling conditions, leading to successful well-known applications of the materials.

5. 5. References:

1. (a) Ulman, A. *An introduction to ultrathin organic films from Langmuir-Blodgett to self-assembly*: Academic Press: San Diego, CA, 1991. (b) Ulman, A. *Chem. Rev.* **1996**, *96*, 1533.

2. (a) Putvinski, T. M; Schilling, M. L.; Katz, H. E.; Chidsey, C. E. D.; Mujsce, A. M.; Emerson, A. B. *Langmuir* **1990**, *6*, 1567. (b) Kumar, A.; Abboh, N. L.; Kim, E.; Biebuyck, H. A.; Whitesides, G. M. *Acc. Chem. Res.* **1995**, *28*, 219. (c) Berggren, K. K.; Bard, A.; Wilbur, J. L.; Gillaspy, J. D.; Heig, A. G.; Mc. Clelland, J. J.; Rolston, S. L.;Philips, W. D.; Prentiss, M.; Whitesides, G. M. *Science* **1995**, *269*, 1255. (d) Kumar, A.; Biebuyck, H. A.; Whitesides, G. M. *Langmuir* **1994**, *10*, 1498. (e) Rubinstein, I.; Steinberg, S.; Tor, Y.; Shanzer, A.; Sagiv. J. *Nature* **1988**, *332*, 426. (f) Rojas, M. T.; Königer, R.; Stoddart, J. F.; Kaifer, A. E. *J. Am. Chem. Soc.* **1995**, *117*, 336.

3. Nuzzo, R. G., Zegarski, B. R., Dubois, L. H. *J. Am. Chem. Soc.* **1987**, *109*, 733. (b) Nuzzo, R. G., Fusco, F.A., Allara, D. L., *J. Am. Chem. Soc.* **1987**, *109*, 2358. (c) Offord, D. A., Jhon, C. M., Griffin, J. H. *Langmuir* **1994**, *10*, 761. (d) Porter, M. D., Brish, T. B., Allara, D. L., Chidsey, C. E. D. *J. Am. Chem. Soc.* **1987**, *109*, 3559. (e) Miller, C.,Cuendent. P., Gratzel, M. *J. Phys. Chem.* **1991**, *95*, 877. (f) Takami, T.,Delamarche, B. M.; Gerber. Q. *Langmuir* **1995**, *11*, 3876. (g) Bain, C. D.; Biebuyck, H. A.; Whitesides, G. M. *Langmuir* **1989**, *5*, 723.

4. (a) Laibinis, P. E.; Whitesides, G. M.; Allara, D. L.; Tao, Y. T.; Parikh, A. N.; Nuzzo, R. G. *J. Am. Chem. Soc.*, **1991**, *113*, 7152. (b) Laibinis, P. E.; Whitesides, G. M. *J. Am. Chem. Soc.* **1992**, *114*, 1990. (c) Laibinis, P. E.; Whitesides, G. M. *J. Am. Chem. Soc.* **1992**, *114*, 9022. (c) Freeman, T. L.; Evans, S. D.; Ulman, A. *Thin Solid Films* **1994**, *244*, 784.

5. Yamamoto, Y.; Nishihara, H.; Aramaki, K. *J. Electrochem. Soc.* **1993**, *140*, 436.

6. Jennings, G. K.; Laibinis, P. E. *Colloids Surf. A* **1996**, *116*, 105.

7. Feng, Y.; Teo, W. -K.; Siow, K.-S.; Gao, Z.; Tan, K.-L.; Hsieh, A.-K. *J. Electrochem. Soc.* **1997**, *144*, 55.

8. (a) Colvin, V. L.; Goldstein, A. N.; Alivisatos, A. P. *J. Am. Chem. Soc.* **1992**, *114*, 5221. (b) Colvin, V. L.; Alivisatos, A. P.; Tobin, J. G., *Phys. Rev. Lett.* **1991**, *66*, 2786. (c) Henglein, A.; *J. Phys. Chem.* **1993**, *97*, 5457. (d) Meldrum, F. C.; Kotov, N. A.; Fendler, J. H., *Langmuir* **1994**, *10*, 2035. (e) Chumanov, G.; Sokolov, K.; Gregory, B. W.; Cotton, T. M., *J. Phys. Chem.* **1995**, *99*, 9466. (f) Grabar, K. C.; Freeman, R. G.; Hommer, M. B.; Natan, M. J., *Anal. Chem.* **1995**, *67*, 735. (g) Grabar, K. C.; Allison, K. J.; Baker, B. E.; Bright, R. M.; Brown, K. R.; Freeman, R. G.; Fox, A. P.; Keating, C. D.; Musick, M. D.; Natan, M. J. *Langmuir* **1996**, *12*, 2353.

9. (a) See the editorial and accompanying articles on clusters in the *Science* **1996**, *271*. (b) Kotov, N. A.; Meldrum, F. C.; Wu, C.; Fendler, J. H., *J. Phys. Chem.* **1994**, *98*, 2735. (c) Meldrum, F. C.; Kotov, N. A.; Fendler, J. H., *J. Phys. Chem.* **1994**, *98*, 4506. (d) Kotov, N. A.; Meldrum, F. C.; Fendler, J. H., *J.Phys.Chem.* **1994**, *98*, 8827.

10. (a) Rieke, P. C.; Marsh, B. D.; Wood, L. L; Tarsevich, B. J.; Liu, J.; Song, L.; Fryxell, G. E. *Langmuir* **1995**, *11*, 318. (b) Bunker, B. C.; Rieke, P. C.; Tarasevich, B. J.; Campbell, A. A.; Fryxell, G. E.; Graf, G. L.; Song, L.; Liu, J.; Virden, J.W.; McVay, G.

L. *Science* **1994**, *264*, 48. (c) Meldrum, F. C.; Flath, J.; Knoll, W. *Langmuir* **1997**, *13*, 2033. (d) Agarwal, M.; De Guire, M. R.; Heuer, H. *J. Am. Ceram. Soc.* **1997**, *80*, 2967.

11. (a) Lee, H.; Kepley, L. J.; Hong, H.-G.; Mallouk, T. E. *J. Am. Chem. Soc.* **1988**, *110*, 618. (b) Brust, M.; Blass, P. M.; Bard, A. J. *Langmuir* **1997**, *13*, 5602.

12. (a) Logothetis, E. M.; *Automative oxygen sensors,* in N. Yamazoe (Ed.) Chemical Sensor Thechnology, Vol 3, Kodansha, Tokyo/ Elsevier, Amsterdam, 1991, 83. (b) Kendall, K. *Ceramic Bulletin* **1990**, *70,* 1159.

13. Ramamurthi, S. D.; Xu, Z.; Payne, D. A. *J. Am. Ceram. Soc.* **1990**, *73,* 2760.

14. Gamage. S. A.; Smith, R. A. J. *Tetrahedron* **1990**, *46*, 2111.

15. Kamiyama, T.; Enomoto, S.; Inoue, M. *Chem. Pharm. Bull.* **1985**, *33*, 5184.

16. Vukovic, V. V.; Nedeljkovic, J. M. *Langmuir* 1993, **9**, 980.

17. (a) Bain, C. D.; Troughton, E. B.; Tao, Yu-Tai, Evall, J.; Whitesides, G. M.; Nuzzo, R. G. *J. Am. Chem. Soc.* **1989**, *111*, 321. (b) Bain, C. D.; Evall, J.; Whitesides, G. M. *J. Am. Chem. Soc.* **1989**, *111*, 7155.

18. Porter, M. D.; Bright, T. B.; Allara, D. L.; Chidsey, C. E. D. *J. Am. Chem. Soc.* **1987**, *109*, 3559.

19. Castner, D. G.; Hinds, K.; Grainger, D. W. *Langmuir* **1996**, *12*, 5083.

20. Itoh, M.; Nishihara, H.; Aramaki, K. *J. Electrochem. Soc.* **1995**, *142*, 1839.

21. Scherer, J.; Vogt, M. R.; Magnussen, O. M.; Behm, R. J. *Langmuir* **1997**, *13*, 7045.

22. Lee, H. P.; Nobe, K. *J. Electrochem. Soc.* **1986**, *133*, 2035.

23. (a) Hahner, G.; Woll, C.; Buck, M.; Grunze, M., *Langmuir* **1993**, *9*, 1955. (b) Frubose, C.; Doblhofer, K., *J. Chem. Soc. Faraday Trans.* **1995**, *91*, 1949.

24. Schneider, T. W.; Buttry, D. A. *J. Am. Chem. Soc.* **1993**, 115, 12391.

25. Delahay, P. In *Double layer and electrode kinetics*; Interscience Publishers: New York,1965.

26. Application Note AC-1, EG & G Princeton Applied Research.

27. Sabatani, E.; Cohen-Boulakia, J.; Bruening, M.; Rubinstein, I. *Langmuir* **1993**, *9*, 2974.

28. Li, W.; Virtanen, J. A.; Penner, R. M. *Langmuir* **1995**, *11*, 4361.

29. Duff, D. G.; Baiker, A.; Gameson, I.; Edwards, P. P. *Langmuir* **1993**, *9*, 2310.

30. Sastry, M.; Badrinarayanan, S.; Ganguly, P. *Phys.Rev.B.* **1992**, *45,* 9320.

31. Brust, M.; Walker, M.; Bethell, D.; Schiffrin, D. J.; Whyman, R. *J. Chem. Soc., Chem. Commun.* 1994, 801.

32. Mekhalif, Z.; Riga, J.; Pireaux, J. -J.; Delhalle, J. *Langmuir* **1997**, *13*, 2285.

33. Henglein, A. *Top. Curr. Chem.* **1988**, *143*, 113.

34. Sharma, D. D.; Rao, C. N. R. *J. Electron Spectroscopy and Rel. Phenomenon* ***1980***, 20, 25. (b) Parmigiani, F.; Depero. L. E.; Sangaletti, L.; Samoggia, G. *J. Elec. Spec. Rel. Pheno.* **1993**, *63*, 1.

35. Finklea, H. O.; Sinder, D. A.; Fedyk, J.; Sabatani, E.; Gafni, Y.; Rubinstein, I.; *Langmuir* **1993**, *9*, 3660.

36. Wells, A. F. *Structural Inorganic Chemistry 4*; Clarendon Press: Oxford, 1975.

37. Bain, C. D.; Biebuycky, H. A.; Whitesides, G. M. *Langmuir* **1989**, *5*, 723.

38. (a) Brust, M.; Blass, P. M.; Bard, A. J. *Langmuir* **1997**, *13*, 5602. (b) Tour, J. M.; Jones, L., II; Person, D. L.; Lamba, J. J. S.; Burgin, T. P.; Whitesides, G. M.; Allara, D. L.;Parikh, A. N.; Atre, S. V. *J. Am. Chem. Soc.* **1995**, *117*, 9529. (c) Nakamura, T.; Kondoh, H.; Matsumoto, M.; Nozoye, H. *Langmuir* **1996**, *12*, 5977.

39. (a) Bunker, B. C.; Rieke, P. C.; Tarasevich, B. J.; Campbell, A. A.; Fryxell, G. E.; Graff, G. L.; Song, L.; Liu, J.; Virden, J. W.; McVay, G. L. *Science* **1994**, *264*, 48. (b) Agarwal, M.; Guire, M. R.; Heuer, A. H. *J. Am. Ceram. Soc.* **1997**, *80*, 2967. (c) Liu, J.; Feng, X.; Fryxell, G. E.; Wang, -Q.; Kim, A. Y.; Gong, M. *Adv. Mater.* **1998**, *10*, 161.

40. Murray, R. W. in *Electroanalytical Chemistry*. Edited by A. J. Bard., Vol. 13, 1984, Marcel and Dekker Inc. New york and Brasel.

41. Or-Gal, L.; Silberman, Chaim, R. *J. Electrochem. Soc.* **1991**, *138*, 1939.

PUBLICATIONS

1. Formation of Redox Active Self-Assembled Monolayer: Naphtho[1,8-*cd*]-1,2-dithiol on Gold.
   Krisanu Bandyopadhyay, Murali Sastry, Vincent Paul and Kunjukrishna Vijayamohanan ***Langmuir*** 1997, *13*, 866.

2. Adsorption of Silver Colloidal Particles through Covalent Linkage to Self-Assembled Monolayers.
   Krisanu Bandyopadhyay, V. Patil, K. Vijayamohanan and Murali Sastry ***Langmuir*** 1997, *13*, 5244.

3. Synthesis And Characterization of Hydrophobic, Approtically-Dispersible, Silver Nanoparticles in Winsor II Type Microemulsions.
   Abhijit Manna, B. D. Kulkarni, **Krisanu Bandyopadhyay** and K. Vijayamohanan ***Chem. Mater.*** 1997, *9*, 3032.

4. Spontaneously organized molecular assembly of an aromatic disulfide on silver/platinum alloy surfaces: an angle dependent X-ray photoemission investigation.
   K. Bandyopadhyay, K. S. Mayya, K. Vijayamohanan and Murali Sastry ***J. Electron. Spectrosc. Relat. Phenom.*** 1997, *87*, 101.

5. pH Dependent changes in the optical properties of carboxylic acid derivatized silver colloidal particles.
   Murali Sastry, K. S. Mayya and **K. Bandyopadhyay** ***Colloid. and Surfaces A.*** 1997, *127*, 221.

6. Role of Surfactants in the Synthesis of Poly(*p*-phenylene) Film in Microemulsions.
   Abhijit Manna, **Krisanu Bandyopadhyay**, K. Vijayamohanan P. R. Rajmohanan. S. Sainkar and B. D. Kulkarni. ***Langmuir*** 1998, *14*, 84.

7. Formation of a Self-Assembled Monolayer of Diphenyl Diselenide on Polycrystalline Gold.
   Krisanu Bandyopadhyay and K. Vijayamohanan. ***Langmuir*** 1998, *14*, 625.

8. Impedance Analysis of Self-Assembled Naphthalene Disulfide Monolayer on Gold using External Redox probes.
   Krisanu Bandyopadhyay, K. Vijayamohanan, G. S. Shekhawat and Ram P. Gupta ***J. Electroanal. Chem.*** (in press)

9. Effect of Geometric Constraints on the Self-Assembled Monolayer Formation of Aromatic Disulfides on Polycrystalline Gold.
   Krisanu Bandyopadhyay, Vijaya Patil, Murali Sastry and K. Vijayamohanan. ***Langmuir,*** accepted.

10. A Novel Room Temperature Synthesis of Microcrystalline Zirconia.
Krisanu Bandyopadhyay, S. R. Sainkar and K. Vijayamohanan. ***J. Ame. Ceramic. Soc.***, accepted.

11. Effect of Co-adsorbed Surfactant on the Structure of Self-Assembled Monolayer of Thiol on Polycrystalline Gold.
Krisanu Bandyopadhyay, K. Vijayamohanan, Abhijit Manna and B. D. Kulkarni. ***J. Colloid and Interface. Sc.***, accepted.

12. Formation of Microcrystalline Zirconia using Functionalized Interface of Self-Assembled Monolayer of Dithiol on Polycrystalline Gold at Room Temperature.
Krisanu Bandyopadhyay and K. Vijayamohanan. Communicated to *Langmuir*.

13. Corrosion Protection of Copper by Self-Assembled Monolayer of Small Aromatic Disulfides.
Krisanu Bandyopadhyay and K. Vijayamohanan. Communicated to *Corrosion. Sc.*

14. Self-assembled Monolayers of Small Aromatic Disulfide and Diselenide Molecules on Polycrystalline Gold Films: A Comparitive Study of the Geometrical Constraint Using Temperature Dependent Surface Enhanced Raman Spectroscopy, X-ray Photoelectron Spectroscopy and Electrochemistry.
Krisanu Bandyopadhyay, K. Vijayamohanan, M. Venkataramanan and T. Pradeep. Communicated to *J. Phys. Chem.*